



HAL
open science

Solvants ioniques biosourcés et CO₂ supercritique : conception des processus durables pour la synthèse de molécules cibles (BISCO₂)

Garima Garg

► **To cite this version:**

Garima Garg. Solvants ioniques biosourcés et CO₂ supercritique : conception des processus durables pour la synthèse de molécules cibles (BISCO₂). Génie des procédés. Institut National Polytechnique de Toulouse - INPT, 2019. Français. NNT : 2019INPT0085 . tel-04169290

HAL Id: tel-04169290

<https://theses.hal.science/tel-04169290v1>

Submitted on 24 Jul 2023

HAL is a multi-disciplinary open access archive for the deposit and dissemination of scientific research documents, whether they are published or not. The documents may come from teaching and research institutions in France or abroad, or from public or private research centers.

L'archive ouverte pluridisciplinaire **HAL**, est destinée au dépôt et à la diffusion de documents scientifiques de niveau recherche, publiés ou non, émanant des établissements d'enseignement et de recherche français ou étrangers, des laboratoires publics ou privés.



Université
de Toulouse

THÈSE

En vue de l'obtention du

DOCTORAT DE L'UNIVERSITÉ DE TOULOUSE

Délivré par :

Institut National Polytechnique de Toulouse (Toulouse INP)

Discipline ou spécialité :

Génie des Procédés et de l'Environnement

Présentée et soutenue par :

Mme GARIMA GARG

le lundi 21 octobre 2019

Titre :

Solvants ioniques biosourcés et CO₂ supercritique: conception des processus durables pour la synthèse de molécules cibles (BISCO₂)

Ecole doctorale :

Mécanique, Energétique, Génie civil, Procédés (MEGeP)

Unité de recherche :

Laboratoire de Génie Chimique (LGC)

Directeur(s) de Thèse :

MME YAOCIHUATL MEDINA GONZALEZ

MME MONTSERRAT GOMEZ

Rapporteurs :

Mme MARGARIDA COSTA GOMES, CNRS

M. SAMUEL MARRE, CNRS AQUITAINE

Membre(s) du jury :

M. JEAN STEPHANE CONDORET, TOULOUSE INP, Président

M. DANIEL PLA, CNRS TOULOUSE, Invité

Mme ANNA MASDEU BULTO, UNIVERSITAT ROVIRA I VIRGILI TARRAGONA, Membre

Mme MONTSERRAT GOMEZ, UNIVERSITE TOULOUSE 3, Membre

Mme SOPHIE GALINAT, SOLVAY PESSAC, Invité

Mme YAOCIHUATL MEDINA GONZALEZ, UNIVERSITE BORDEAUX 1, Membre

This Thesis is dedicated to my parents

Acknowledgements

I would like to present my sincere thanks to the reviewers, the examiners and invited members of the jury for my Thesis defense, Dr. Samuel Marre, Dr. Margarida Costa Gomes, Dr. Jean-Stephane Condoret, Dr. Anna Maria Masdeu-Bultó, Dr. Daniel Pla and Dr. Sophie Galinat. Thank you for reading, correcting and helping me to improve my manuscript with your positive criticism. I am grateful for the time and efforts you devoted for my Thesis.

I would like to show my gratitude to the two women who made this PhD possible; my supervisors Dr. Yaocihuatl Medina-Gonzalez and Prof. Montserrat Gómez. Thank you for these years of my PhD, without you this would have never been possible. I am grateful for your continuous support, patience, motivation, and immense knowledge. All the comments, remarks, criticism that I received from you not only helped me finish my thesis successfully but also made me a better person.

I am also grateful to the funding of this project: IDEX Recherche – Edition 2015 – Actions Thématiques Stratégiques – Université Fédérale Toulouse Midi Pyrénées.

During my three years of the PhD, I have shared my time between two labs: Laboratoire de Génie Chimique and Laboratoire Hétérochimie Fondamentale et Appliqué. I would like to thank the directors of both the labs Pierre Aimar and Didier Bourissou. Thank you for giving me this great opportunity. It was an honor to be a part of LGC and LHFA.

I would also like to thank the administrative staff of both the labs Daniele Bouscary, Patricia Uliana and Jean-Luc Labeyrie at LGC and Maryse Beziat, Sérah Noel and Olivier Volpato at LHFA, thank you for your kindness and availability, the infinite help and your smiles. At the technical platform, Alec, Jean-Louis and Bruno from LGC and Olivier Thillaye du Boullay, Romaric, Sonia, Nathalie and Julien Babinot from LHFA, thank you for simplifying the work while being our colleagues, sharing the laughter as well as the scientific discussions. Last but not least, Alain, you are one of the people with the best heart I have ever met. Always keep your smile on.

I would also like to say thank you to Service Analyses et Procédés at LGC especially Christine Rey-Rouch and Marie-Line Pern for helping with the DSC and Rheometer analyses. Also, Caroline Toppan for NMR, Sonia Mallet-Ladeira for XRD, Isabelle Fabing for HPLC, Guillaume Sauthier for XPS, Alain Moreau for ICP analysis.

During my PhD, I also had the honor to work with Dr. Anna Maria Masdeu-Bultó at University Rovira I Virgili in Tarragona, Spain. Thank you, Anna, for having me in your lab. It was a truly a great experience working with you.

It was great being a part of LGC, especially team STPI. Thank you Séverine for helping with extractions and sharing your insights. Emanuel, Claire, Han bin, Benoit, Robbie, Hassan, Mei, Peter it was a great pleasure getting to know you all. Hélène (aka Sheriff) and Astrid (aka French Garima), thank you girls for being a part of my life and sharing my emotions whenever I will knock at your office door complaining about things. Alexandre (aka Bibi) and Emilien

(aka Gandu) thanks for making me laugh. Our soirée STPI could not be the same without you. Marco you are one of the kindest people I know, never change. Also, thank you for being my translator whenever I failed to understand French. I can never forget the UNO community Sid, Yosra, Thomas...I made a very special friend at LGC, Melisa, thank you for making these three years so memorable.

At LHFA, it was a joy, being a part of the SYMAC team. We shared a lot of moments in and out of the lab that I will always cherish, the birthday celebrations, Christmas lunch, picnic and calçots are few of the many. Daniel, thank you for sharing your ideas on my work and helping me see through my problems, they were always valuable. You are truly a brilliant chemist. Thank you, Christian, for doing all the TEM analyses with utmost patience. A special shout-out to Isabelle Favier for being my lab-saver. You have always been there to help me through the experiments with a great smile. I knew I could always knock your door whenever I was in doubt. I will miss all your jokes and our time together in the lab. Thank you, Isabelle, you are the best.

I started my journey in LHFA with the two best officemates anyone can ever get Antonio and Trung. Antonio, you were not only my colleague but also a dear friend. You have always given me wonderful advices and helped and motivated me through difficult times. Trung, you are a true gift as a friend. I can never forget how you used to make me laugh, care about me and tease me. Having you was like having a big brother. Lorena, my bella, meeting you was one of the best things that happened to me during these three years. The moments that we have shared are incredible. You have taken care me like I am a little girl of yours. I will miss you much, love you. Marc and Alejandro, I regret that I didn't get to spend a lot of time with you, having you in the team had been fun. All the best for your own PhD journeys. Tais, it was a joy knowing you. Stay cool, hope to see you in Brazil someday. Of course, I can't forget all the occasional visitors in the team. Jesica, Marie-Lou, Tiago, Alejandro Serrano and Alejandro Leal. It has been a pleasure to have you in the team. Tiago, I hope I will be able to fulfill my promise of visiting you in Portugal someday. Jesica, you know that you very special to me. Thank you for coming to Toulouse and introducing me to the coolest gal I know.

Finally, I would like to express my gratitude for my parents, my sister Kritika and my brother Divyam, you are my motivation and strength. I could not have done it without your love and faith. Shorya, my love, thank you for standing by me and believing in me.

Index

| | |
|--|-----------|
| General Introduction Objectives and Layout..... | 1 |
| Chapter 1: Solvent Engineering aspects of Supercritical Carbon dioxide and Metal Nanoparticles..... | 7 |
| 1. Solvent engineering aspects of Supercritical Carbon Dioxide..... | 9 |
| 1.1. What is a solvent?..... | 9 |
| 1.2. Supercritical Fluids..... | 11 |
| 1.2.1. Physiochemical Properties of Supercritical Carbon Dioxide..... | 12 |
| 1.2.2. Supercritical Carbon Dioxide as Tunable Media..... | 16 |
| 1.3. Gas-expanded Liquids (GXLs)..... | 17 |
| 1.3.1. CO ₂ -expanded Liquids (CXLs)..... | 18 |
| 1.4. Ionic Liquids (ILs)..... | 19 |
| 1.4.1. Properties of Ionic Liquids | 21 |
| 1.4.2. Mass Transfer in Ionic Liquids..... | 23 |
| 1.4.3. Heat Transfer in Ionic Liquids..... | 25 |
| 1.5. Deep Eutectic Solvents (DESs)..... | 28 |
| 1.5.1. Ionic Liquids versus Deep Eutectic Solvents..... | 29 |
| 1.5.2. Properties of Deep Eutectic Solvents..... | 30 |
| 1.5.3. Glycerol-based DESs..... | 33 |
| 2. Metal Nanoparticles..... | 34 |
| 2.1. Synthesis of Metal Nanoparticles..... | 35 |
| 2.1.1. Polyol Methodology..... | 36 |
| 2.2. Metal Nanoparticles in Glycerol..... | 37 |
| 2.3. Metal Nanoparticles in Ionic Liquids..... | 38 |
| 2.3.1. Interaction between Ionic Liquids and Metal Nanoparticles..... | 38 |
| 2.3.2. Stabilization of Metal Nanoparticles by Ionic Liquids..... | 40 |
| 2.4. Catalytic Activity of Metal Nanoparticles..... | 42 |
| 2.4.1. Catalytic Hydrogenation Application of Metal Nanoparticles under Carbon Dioxide.... | 44 |
| 3. Conclusions..... | 46 |
| 4. References..... | 46 |

| | |
|--|------------|
| Chapter 2: Viscosity Measurements using Molecular Rotors..... | 61 |
| 2.1 Introduction..... | 63 |
| 2.2 Molecular Rotors..... | 65 |
| 2.3 Experimental Section..... | 70 |
| 2.4 Results and Discussion..... | 72 |
| 2.5 Conclusions..... | 77 |
| 2.6 References..... | 77 |
| | |
| Chapter 3: Synthesis and Characterization of Palladium Nanoparticles Stabilized by Novel Choline- based Ionic Liquids in Glycerol applied in Hydrogenation Reactions..... | 83 |
| 3.1 Palladium Nanoparticles..... | 85 |
| 3.1.1 Introduction..... | 85 |
| 3.1.2 Synthesis of palladium Nanoparticles..... | 86 |
| 3.1.3 Characterization of Palladium Nanoparticles..... | 91 |
| 3.2 Pd-catalyzed Hydrogenation Reactions..... | 93 |
| 3.2.1 Introduction..... | 93 |
| 3.2.2 Results and Discussion..... | 95 |
| 3.3 Experimental Section..... | 102 |
| 3.4 Conclusions..... | 105 |
| 3.5 References..... | 105 |
| | |
| Chapter 4: Catalytic Hydrogenation under Carbon Dioxide and Extraction of Products using Supercritical Carbon Dioxide..... | 113 |
| 4.1 Pd-catalyzed hydrogenation reactions under sub and supercritical carbon dioxide..... | 115 |
| 4.1.1 Introduction..... | 115 |
| 4.1.2 Results and Discussion..... | 119 |
| 4.2 Extraction of organic products using supercritical carbon dioxide..... | 124 |
| 4.2.1 Introduction..... | 124 |
| 4.2.2 The Extractor..... | 126 |
| 4.2.3 Results and Discussion..... | 128 |
| 4.3. Synthesis of palladium nanoparticles under scCO₂ and their catalytic activity..... | 134 |
| 4.3.1. Results and discussion..... | 134 |
| 4.3 Experimental Section..... | 137 |
| 4.4 Conclusions..... | 138 |
| 4.5 References..... | 138 |

Summary, Conclusions and Perspectives.....147
Annex 1.....151
Annex 2.....155

General Introduction, Objectives and Layout

There is a growing concern regarding the development of greener chemical processes as the implementation of more sustainable production processes is a prerequisite for a more sustainable world. Long-term environmental, social and economic viability of chemical processes must be developed by creating greener technologies based either on currently available feedstock or by replacing fossil-based raw materials with renewable ones such as those derived from biomass.¹⁻³ One of the main issues is the implementation of green bio-sourced solvents. Solvents define a major part of the environmental performance of a process, impacting cost, safety, and health issues, generating waste and pollution and demanding important energy consumption.⁴

The project developed in the present thesis represents an effort to develop green versatile catalytic systems based on the coupling of green bio-sourced ionic liquids including deep eutectic solvents (DESs), with supercritical CO₂ (scCO₂) in a biphasic system. Green bio-sourced DESs can be obtained from renewable materials and are considered as environmentally benign solvents because of their negligible vapor pressure, non-flammability and high thermal and chemical stability together with their excellent solubility properties, biodegradability and biocompatibility compared to traditional ionic liquids, including conventional DESs.⁵⁻⁷ DESs are now widely acknowledged as a new class of ionic liquids (IL) because they share many characteristics and properties with ILs.⁸ DESs contain ionic compounds that have low lattice energy and hence low melting points. They can usually be obtained by the combination of a quaternary ammonium salt with a metal salt or hydrogen bond donor.^{9,10} The charge delocalization occurring through hydrogen bonding between for example a halide ion and the hydrogen-donor moiety (such as urea, polyols) is responsible for the decrease in the melting point of the mixture relative to the melting points of the individual components, *i.e.* donor and acceptor hydrogen bond partners.

However, one of the major challenges in bio-sourced DESs is their high viscosity, which leads to hindrance in mass transfer. Solvent Engineering can be used to overcome this challenge. It allows triggering changes in physicochemical properties of the solvent (such as viscosity, density, polarity, etc.) and permits to couple two or more steps of a given chemical process, increasing efficiency and decreasing energy and raw materials wastage. Development of a biphasic system containing scCO₂ and bio-sourced DESs represents a strategy to perform Solvent Engineering and to incorporate these solvents into industrial applications by prevailing

General Introduction, Objectives and Layout

separation issues, because scCO₂ may allow the extraction of organic products from DES phase at the same time as tuning their properties (like viscosity, polarity etc.).^{11–15} This strategy allows the intensification of the reaction process.

The DESs used in this study are amino-acid based cholinium salts as hydrogen bond acceptor and glycerol as hydrogen bond donor. Choline-based ILs are environmentally friendly with good biocompatible properties and presenting interesting solvent properties: non-inflammability, negligible vapor pressure at ambient conditions and high solubility.¹⁶ In this context, glycerol also represents an innovative solvent coming from biomass and produced in high amounts as a by-product in the production of biodiesel.¹⁷ Its low-cost, non-toxicity, high boiling point (290 °C), negligible vapor pressure (< 1 mmHg at 293 K), high solubilizing ability for organic (except those completely apolar) and inorganic compounds, and low miscibility with other organic solvents such as ethers and alkanes, constitute striking properties that make it especially interesting for applications in catalysis.¹⁸

Choline-based DESs are expected to interact strongly with CO₂ due to the presence of the ammonium group, which is a CO₂-philic group.¹⁹ These strong interactions may result in a high uptake of CO₂ by choline-based derivatives, which allows the modulation of properties such as polarity, hydrogen bonding, density and viscosity across a very large range of values only by controlling the pressure of the system.

It is known that metal-based nanoparticles are efficiently prepared in ionic liquids for catalytic purposes.²⁰ The use of glycerol allows the efficient immobilization of the catalyst leading to metal-free organic compounds by simple extraction, as previously proven in the group.^{21–24} Furthermore, CO₂ can play an important role in the catalytic hydrogenation by increasing the solubility of hydrogen in the medium.

Additionally, due the higher solubility of organic compounds in scCO₂, the extraction of organic compounds can be done by using scCO₂, avoiding use of volatile organic solvents and promoting a greener method for extraction. The above-mentioned data lead to the following objectives of the thesis:

- Synthesis of deep eutectic solvent from amino-acid based cholinium salt and glycerol; and to study the tunability of its viscosity with changing pressure of carbon dioxide.
- Synthesis of palladium nanoparticles stabilized by amino-acid based cholinium salts in glycerol as solvent.

General Introduction, Objectives and Layout

- Application of palladium nanoparticles for catalytic hydrogenation reactions.
- Use of sub and supercritical carbon dioxide to enhance the catalytic activity of palladium nanoparticles.
- Use of supercritical carbon dioxide for the extraction of organic products after catalysis.

This manuscript is divided into **4** parts, as described in following paragraphs.

In **Chapter 1**, firstly, the physiochemical properties of supercritical fluids (especially supercritical carbon dioxide), ionic liquids and deep eutectic solvents are discussed. One of the major challenges of DESs is to overcome their viscosity issues. Supercritical fluids (SCFs) and gas-expanded liquids used as tunable media for various catalytic reactions are also described. Secondly, synthesis of metal nanoparticles in various media focusing especially on ionic liquids and glycerol has been reported. Catalytic activity of various nanoparticles in hydrogenation is discussed. Metal-catalyzed hydrogenation reactions using metal nanoparticles under sub- and super-critical CO₂ are also studied.

In **Chapter 2**, the synthesis of DES from choline tosylalaninate and glycerol is reported. Study of viscosity of DES in the presence of scCO₂ is also reported. An innovative method for the measurement of viscosity is described in this Chapter. Molecular rotors have been used as a probe to determine *in-situ* viscosity for DES/scCO₂ phases. A comparative study of different kinds of molecular rotors has been carried out.

In **Chapter 3**, the synthesis of palladium nanoparticles (PdNPs) stabilized by a mixture of choline tosylalaninate and glycerol is reported. PdNPs have been fully characterized in both liquid phase and solid state (PdNPs isolated by centrifugation from the corresponding colloidal solutions). The as-prepared metal nanoparticles have exhibited remarkable catalytic activity in hydrogenation processes for a significant variety of functional groups (alkenes, alkynes, nitro derivatives, benzaldehydes, aromatic ketones).

Hydrogenation reactions using PdNPs have been also carried out under CO₂. Extraction of the organic products was carried using scCO₂. **Chapter 4** reports the effect of CO₂ on the catalytic activity of PdNPs in those hydrogenation reactions. The efficiency of scCO₂ to extract the product directly from the catalytic phase is also reported.

References

- (1) Anastas, P.; Eghbali, N. Green Chemistry: Principles and Practice. *Chem. Soc. Rev.* **2010**, *39* (1), 301–312. <https://doi.org/10.1039/b918763b>.
- (2) Cole-Hamilton, D. J. Asymmetric Catalytic Synthesis of Organic Compounds Using Metal Complexes in Supercritical Fluids. *Adv. Synth. Catal.* **2006**, *348* (12–13), 1341–1351. <https://doi.org/10.1002/adsc.200606167>.
- (3) Anastas, P. T.; Kirchhoff, M. M.; Williamson, T. C. Catalysis as a Foundational Pillar of Green Chemistry. *Appl. Catal. A Gen.* **2001**. [https://doi.org/10.1016/S0926-860X\(01\)00793-1](https://doi.org/10.1016/S0926-860X(01)00793-1).
- (4) Medina-Gonzalez, Y.; Camy, S.; Condoret, J. S. ScCO₂/Green Solvents: Biphase Promising Systems for Cleaner Chemicals Manufacturing. *ACS Sustain. Chem. Eng.* **2014**, *2* (12), 2623–2636. <https://doi.org/10.1021/sc5004314>.
- (5) Mamilla, J. L. K.; Novak, U.; Grilc, M.; Likozar, B. Natural Deep Eutectic Solvents (DES) for Fractionation of Waste Lignocellulosic Biomass and Its Cascade Conversion to Value-Added Bio-Based Chemicals. *Biomass and Bioenergy* **2019**. <https://doi.org/10.1016/j.biombioe.2018.12.002>.
- (6) Schweiger, A. K.; Ríos-Lombardía, N.; Winkler, C. K.; Schmidt, S.; Morís, F.; Kroutil, W.; González-Sabín, J.; Kourist, R. Using Deep Eutectic Solvents to Overcome Limited Substrate Solubility in the Enzymatic Decarboxylation of Bio-Based Phenolic Acids. *ACS Sustain. Chem. Eng.* **2019**, *7* (19), 16364–16370. <https://doi.org/10.1021/acssuschemeng.9b03455>.
- (7) Zhang, Q.; De Oliveira Vigier, K.; Royer, S.; Jérôme, F. Deep Eutectic Solvents: Syntheses, Properties and Applications. *Chem. Soc. Rev.* **2012**, *41* (21), 7108–7146. <https://doi.org/10.1039/c2cs35178a>.
- (8) Ruesgas-Ramón, M.; Figueroa-Espinoza, M. C.; Durand, E. Application of Deep Eutectic Solvents (DES) for Phenolic Compounds Extraction: Overview, Challenges, and Opportunities. *J. Agric. Food Chem.* **2017**, *65* (18), 3591–3601. <https://doi.org/10.1021/acs.jafc.7b01054>.
- (9) Smith, E. L.; Abbott, A. P.; Ryder, K. S. Deep Eutectic Solvents (DESs) and Their Applications. *Chem. Rev.* **2014**, *114* (21), 11060–11082.

<https://doi.org/10.1021/cr300162p>.

- (10) Abbott, A. P.; Boothby, D.; Capper, G.; Davies, D. L.; Rasheed, R. K. Deep Eutectic Solvents Formed between Choline Chloride and Carboxylic Acids: Versatile Alternatives to Ionic Liquids. *J. Am. Chem. Soc.* **2004**, *126* (29), 9142–9147. <https://doi.org/10.1021/ja048266j>.
- (11) Mukhopadhyay, M. Extraction and Processing with Supercritical Fluids. *J. Chem. Technol. Biotechnol.* **2009**, *84* (1), 6–12. <https://doi.org/10.1002/jctb.2072>.
- (12) Daintree, L. S.; Kordikowski, A.; York, P. Separation Processes for Organic Molecules Using SCF Technologies. *Advanced Drug Delivery Reviews.* 2008. <https://doi.org/10.1016/j.addr.2007.03.024>.
- (13) Camy, S.; Condoret, J. S. Modelling and Experimental Study of Separators for Co-Solvent Recovery in a Supercritical Extraction Process. *J. Supercrit. Fluids* **2006**. <https://doi.org/10.1016/j.supflu.2005.03.005>.
- (14) Reverchon, E.; De Marco, I. Supercritical Fluid Extraction and Fractionation of Natural Matter. *Journal of Supercritical Fluids.* 2006. <https://doi.org/10.1016/j.supflu.2006.03.020>.
- (15) Demirbaş, A. Supercritical Fluid Extraction and Chemicals from Biomass with Supercritical Fluids. *Energy Convers. Manag.* **2001**. [https://doi.org/10.1016/S0196-8904\(00\)00059-5](https://doi.org/10.1016/S0196-8904(00)00059-5).
- (16) Hou, X. D.; Li, N.; Zong, M. H. Facile and Simple Pretreatment of Sugar Cane Bagasse without Size Reduction Using Renewable Ionic Liquid/water Mixtures. *ACS Sustain. Chem. Eng.* **2013**, *1* (5), 519–526. <https://doi.org/10.1021/sc300172v>.
- (17) Díaz-Álvarez, A.; Cadierno, V. Glycerol: A Promising Green Solvent and Reducing Agent for Metal-Catalyzed Transfer Hydrogenation Reactions and Nanoparticles Formation. *Appl. Sci.* **2013**, *3* (1), 55–69. <https://doi.org/10.3390/app3010055>.
- (18) Chahdoura, F.; Favier, I.; Gómez, M. Glycerol as Suitable Solvent for the Synthesis of Metallic Species and Catalysis. *Chem. - A Eur. J.* **2014**, *20* (35), 10884–10893. <https://doi.org/10.1002/chem.201403534>.
- (19) Sarmad, S.; Mikkola, J. P.; Ji, X. Carbon Dioxide Capture with Ionic Liquids and Deep Eutectic Solvents: A New Generation of Sorbents. *ChemSusChem* **2017**, *10* (2), 324–

352. <https://doi.org/10.1002/cssc.201600987>.
- (20) Favier, I.; Madec, D.; Gómez, M. Metallic Nanoparticles in Ionic Liquids - Applications in Catalysis. *Nanomater. Catal. First Ed.* **2012**, 203–249. <https://doi.org/10.1002/9783527656875.ch5>.
- (21) Favier, I.; Pla, D.; Gómez, M. Metal-Based Nanoparticles Dispersed in Glycerol: An Efficient Approach for Catalysis. *Catal. Today* **2018**, 310 (June 2017), 98–106. <https://doi.org/10.1016/j.cattod.2017.06.026>.
- (22) Dang-Bao, T.; Pla, D.; Favier, I.; Gómez, M. Bimetallic Nanoparticles in Alternative Solvents for Catalytic Purposes. *Catalysts* **2017**, 7 (7). <https://doi.org/10.3390/catal7070207>.
- (23) Reina, A.; Pradel, C.; Martin, E.; Teuma, E.; Gómez, M. Palladium Nanoparticles Stabilised by Cinchona-Based Alkaloids in Glycerol: Efficient Catalysts for Surface Assisted Processes. *RSC Adv.* **2016**, 6 (95), 93205–93216. <https://doi.org/10.1039/c6ra19230k>.
- (24) Chahdoura, F.; Pradel, C.; Gómez, M. Copper(I) Oxide Nanoparticles in Glycerol: A Convenient Catalyst for Cross-Coupling and Azide-Alkyne Cycloaddition Processes. *ChemCatChem* **2014**, 6 (10), 2929–2936. <https://doi.org/10.1002/cctc.201402214>.

Chapter 1

Solvent Engineering aspects of
Supercritical Carbon dioxide
and

Metal Nanoparticles

1. Solvent Engineering aspects of Supercritical Carbon dioxide

Solvents define a major part of the environmental performance of a process, impacting cost, safety, and health issues, generating waste and pollution and demanding important energy consumption for its recycling, reuse and/or eventual disposal. However, choosing the right type of solvent can be tricky. For instance, in recent years, replacement of highly pollutant solvents by more environmentally friendly, less toxic solvents is needed; however, a solvent can be biodegradable but be volatile and ozone depleting. It can have an extremely low impact on health and the environment but needs a great amount of energy to be manufactured.¹ The choice of a better solvent is then a difficult task and needs different solutions depending on the application.

1.1. What is a solvent?

A solvent is defined as any liquid, gas, solid, gas expanded liquid, or supercritical fluid in which a solute is dissolved, either partially or completely. Solvents are usually categorized in two broad groups: polar and non-polar.² The role of solvent in chemical processes is quite evident. Usages of solvents as a reaction medium, in separation procedures, purifications, analyses and/or as diluters are widely known in various industrial processes. It can also act as a means of temperature control in a reaction. A solvent is determined by many physicochemical properties, such as, its dielectric constant, dipole moment, refractive index, hydrogen bonding capacity, among others, these properties have been described through several descriptors such as solvatochromic parameters, dispersion, induction-polarizability.³

The choice of the solvent is always an important factor not only as a reaction medium, but also from the environmental, safety and economical perspectives. As reaction medium, solvents are prescribed to bring reactants and/or catalyst together and to deliver energy. Also, its chemical and physical nature may affect the activity and selectivity in a reaction.^{4,5} As Clark *et al.* has defined, an ideal solvent is a compound which is environmentally benign, low cost and would be a right brew of solvation properties (like hydrogen bonding, polarizability, ion binding, etc.) to maximize the reaction process and at the same time being unreactive in the system while enabling easy separation and recycling after the reaction.⁶

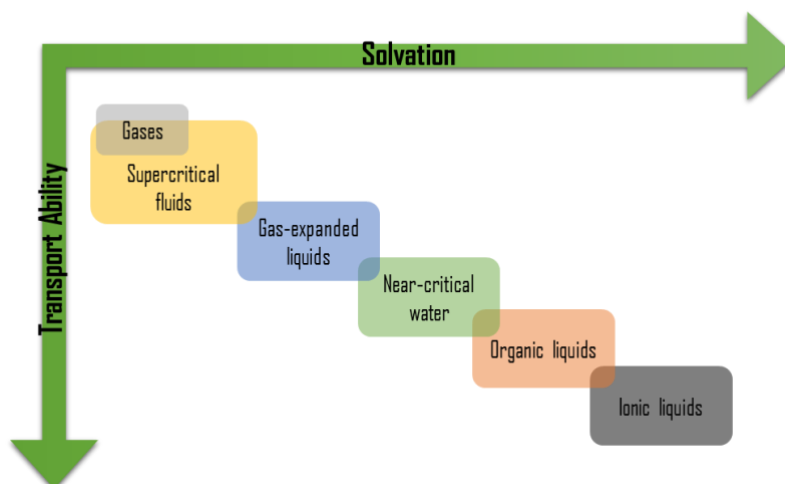


Figure 1.1. Compromise of transport ability and solvent power for various types of solvents. (Reproduced from Reference (2) with permission from the Royal Society of Chemistry)

Considering the above-mentioned points, water as solvent is the first choice; as a reaction solvent, it allows easy separation of homogeneous catalysts from reaction mixtures that allows them to be recycled and re-used, resulting in giving higher turnover numbers and reducing wastes.⁶ However, its low solubility of many organic compounds and organometallic complexes limits its use.⁴ Organic and petroleum-based solvents have, up to recent years, solved the problem of solubility, but they are usually a source of pollution of the environment and of toxicity for living organisms. Thus, in order to minimize the generation of volatile organic compounds (VOCs), the scientific community is continuously searching for new sustainable media or alternative solvents. In the last decades, some potential approaches for current solvent innovation have been polyethylene glycol, perfluorinated solvents, ionic liquids, supercritical fluids.⁶⁻⁹ Pollet *et al.* proposed that a compromise usually exists between transport properties (expressed, for instance, as diffusion coefficient, D_A) and solvation (expressed, as example, as Kamlet–Taft dipolarity/polarizability parameter, π^*) as shown in Figure 1.1. For instance, gases have high diffusion coefficients but low π^* which makes them poor solvents, on another hand, ionic liquids are good solvents with poor transport properties.² Other solvents like supercritical fluids (SCFs), gas-expanded liquids (GXLs), near-critical water and organic solvents that lie between the two extreme points can be wisely chosen according to the requirements, their properties being dependent of the temperature and of the pressure, two variables that are easily adjusted in chemical processes.

Supercritical fluids is the class of solvents that surpass the conventional solvents in terms of compressibility.¹⁰ SCFs possess viscosity like gases that allows easy mass transfer and diffusivity like liquids that gives them higher solvating power.^{2,11,12} Moreover, SCFs provides a platform for a type of tunable solvents because their physicochemical properties can be tuned by changing parameters like temperature and pressure.^{11–13} The ability for SCFs to dissolve in many organic solvents like alcohols, ketones, ethers, esters and as well in ionic liquids provides flexibility to alter the physicochemical properties (like polarity, dielectric constant, density etc.) of the liquid solvent.^{14–18}

In the next section, we discuss in details the properties of SCFs especially supercritical carbon dioxide (scCO_2). The next part also describes how solvent engineering can be applied to these solvents for them to serve as tunable media for various chemical reaction, extraction and separation processes.

1.2. Supercritical Fluids

Supercritical fluids are substances that are above their critical pressures (P_c) and temperatures (T_c) (Figure 1.2).¹⁰ If a substance is in equilibrium with its vapor in a closed vessel and heated to a temperature above its critical temperature, making the pressure go over its critical pressure, the interface between the two phases diminishes, and only one phase remains filling the entire space of the vessel that is technically the SCF phase. In fact, in SCF state, liquid and vapor phases do not exist.¹⁹

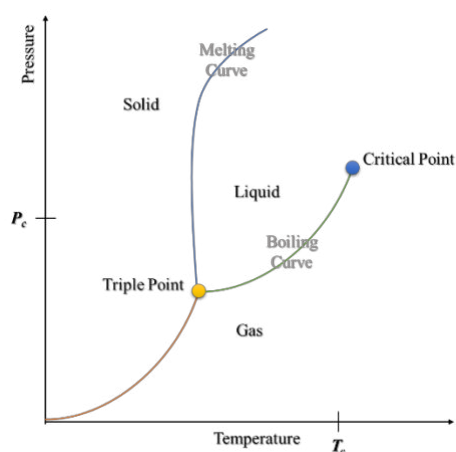


Figure 1.2. Phase diagram showing the different states of matter

The critical point of a SCF represents the highest temperature and pressure at which the substance can exist as a vapor and liquid in equilibrium.¹⁰ Table 1.1 shows critical temperature

and critical pressure for some compounds.¹⁹ In this Thesis, the focus is on supercritical carbon dioxide (scCO₂). Supercritical carbon dioxide (scCO₂), in this context, attracts a lot of attention due to its green properties and easy availability. ScCO₂ is relatively chemically inert (for example, it is resistant to free radical chemistry) and exhibits a low-toxicity aprotic solvent power.^{20–22}

Table.1.1 Critical points and critical density for a selection of fluids. (Data taken from reference (19))

| Supercritical Fluid | Critical Temperature (°C) | Critical Pressure (MPa) |
|---------------------|---------------------------|-------------------------|
| Carbon dioxide | 31 | 7.4 |
| Water | 374 | 22.1 |
| Ethane | 32 | 4.9 |
| Propane | 97 | 4.3 |
| Ethylene | 9 | 5.0 |
| Methanol | 239 | 8.1 |
| Ethanol | 241 | 6.1 |
| Toluene | 319 | 4.1 |
| Sulfur hexafluoride | 46 | 3.8 |
| Dinitrogen monoxide | 33 | 7.4 |
| Ammonia | 132 | 11.3 |

1.2.1. Physiochemical Properties of Supercritical Carbon Dioxide

ScCO₂ ($P_c = 7.38$ bar and $T_c = 304$ K) (Table 1.1) is a nonpolar compound and has a large quadrupolar moment that enables dipole-quadrupole interactions with other molecules.²⁰ It has the relative static permittivity or dielectric constant similar to hexane and therefore, can easily solubilize nonpolar low molecular weight compounds.^{23,24} In scCO₂, a small change in pressure can lead to a large change in its volume and density. This property gives us a huge opportunity to tune the physiochemical properties of scCO₂.²⁵

1.2.1.1. Density

Density is an important property in any SCF as the solubility of many compounds depends on the density of SCFs. Near the critical point, a small increase in the temperature decreases the solvent density and consequently the solubilizing ability. At lower pressure, there is a large

negative change in the density of SCFs with the increasing temperature resulting in the decrease of solubility. On the other hand, at higher pressures, the change in density is not significant with increasing temperature, thus, the solubility increases with increasing temperature.²⁵

The density of scCO₂ can be calculated by an *equation of state* (EOS). For example, Soave-Redlich-Kwong equation^{26,27} or Peng-Robinson EOS.^{28,29} Wang *et al.* used an apparatus to accurately measure the density of scCO₂ over a wide range of temperature and pressures.³⁰ They evaluated the error between the experimentally calculated density and various EOS proposed in the literature. They showed that when the increase in density with pressure presents a linear behavior, the predicted densities using EOS was accurate. However, in the high-pressure areas, the increase in density is dramatic and the calculated densities varies with the experimental densities in these areas. They introduced an error of correction (Equation 1.1) and proposed a new method for calculating the density of scCO₂ for a known density and temperature (Equation 1.2).³⁰

$$\varepsilon_r = \frac{\rho_{cal} - \rho}{\rho} \times 100\% \approx \frac{\rho_{cal} - \rho_{exp}}{\rho} \times 100\% \quad \text{Equation 1.1}$$

where, ε_r is the relative error of the CO₂ density at a fixed temperature and pressure calculated using EOS, ρ_{cal} is the CO₂ density computed from the EOS, ρ_{exp} is the CO₂ density measured using the experimental apparatus and ρ is the true density of CO₂.

$$R^2 = 1 - \frac{\sum_i (\hat{\rho}_i - \bar{\rho})^2}{\sum_i (\rho_i - \bar{\rho})^2} \quad \text{Equation 1.2}$$

where R^2 is the non-dimensional coefficient of determination, ρ_i is the measured density, $\hat{\rho}_i$ is the density calculated by new formula and $\bar{\rho}$ is the mean value of density calculated by all the measured densities. The above-developed formula is for a temperature range of 303K - 473K and pressure range of 30 - 600 bar. In the equation, R^2 of the new correlation is 0.873, which means that the density of the supercritical CO₂ can be well described.

1.2.1.2. Viscosity and Mass Transfer

It is generally accepted that viscosity and density of a supercritical fluid are similar to a gas and to a liquid respectively. Intuitively, a lower viscosity contributes to an enhancement of mass transport inside the system. This phenomenon is well described by the Fick's first and second law of diffusion (Equation 1.3 and 1.4).³¹

$$J = -D_{12} \frac{\partial C}{\partial x} \quad \text{Equation 1.3}$$

$$\frac{\partial C}{\partial t} = D_{12} \frac{\partial^2 C}{\partial x^2} \quad \text{Equation 1.4}$$

Where, J is the diffusion flux of the compound per area, D_{12} is the binary diffusion coefficient of the compound in the solvent, C is the concentration of the compound, x is the position and t is the time. Equation 1.4 is valid for constant diffusion coefficients. This equation has an exact solution for the simplest systems; for the others, a numerical solution is needed.

Diffusion coefficients in supercritical fluids are higher than in liquids. Cunico *et al.* have reviewed self-diffusion of scCO_2 as a function of temperature and pressure.¹⁹ Some methods to calculate self-diffusion and binary diffusion coefficients can be used, such as the Stokes-Einstein equation (Equation 1.5).

$$D_i = \frac{\kappa_B T}{6 \pi \eta_s r}$$

Equation 1.5

Where, κ_B is the Boltzmann constant, T is the temperature, r is the hydrodynamic radius of the particle, η_s is the shear viscosity of the solvent.

Other similar equations to the Stokes-Einstein relation have been derived and compared to experimental results with good accuracy.³² Diffusion coefficients for solutes in supercritical fluids reported in the literature and the correlation methods applied by the authors for modelling their experimental data have been published by I. Medina,³³ where mostly equations based on Stokes-Einstein model and on the Rough-Hard-Sphere model are represented. Shenai *et al.* have discussed the validity of some of the existing methods to correlate diffusivities when no experimental data exists.³⁴ Molecular Dynamics-based methods to calculate diffusion coefficients from the mean-square displacements of the molecules represent a valuable approach; this method is especially useful when the validity of the equations cited before is not proven.³⁵

It is to note that dynamic viscosity (η) of supercritical fluids is comparable to that of a gas but the density (ρ) is similar to that of a liquid making kinematic viscosity (γ) very low near the supercritical point ($\gamma = \eta/\rho$). This phenomenon enhances mass transfer, because natural convection depends on kinematic viscosity. It is important to say here that natural convection

plays a non-negligible role in the mechanism of transfer in systems involving supercritical fluids as the kinematic viscosities of supercritical fluids are very small, and therefore the role of buoyancy forces may be predominant in mass transfer in systems involving such fluids.³⁶

1.2.1.3. Dielectric properties

The solvent and the solute intermolecular interaction is determined by the dielectric properties of the solvent, which indeed determines the solubility.¹⁹ As stated above, scCO₂ has the relative static permittivity or dielectric constant similar (even lower) than hexane and therefore, can easily solubilize nonpolar low molecular weight compounds. Hourri *et al.* were the firsts to determine the solubility of solids in SCFs using dielectric constant of saturated supercritical solution solvent–solute and the supercritical solvent as a function of pressure at varying temperatures.³⁷ Later, Abbott *et al.* studied the solubility of aromatic hydrocarbons in supercritical difluoromethane showing that the dielectric constant method is capable of determining the solubility of a range of solutes in supercritical medium. They stated that pressure, solvent polarity, number of polar interaction sites, and their relative substitution position affect the solubility of a particular solute.^{38,39} Leeke *et al.* also determined the solubility of various aromatic compounds in scCO₂ using relative permittivity. Their technique allowed obtaining solubility data *in situ*.⁴⁰

Onsager and Kirkwood-Frohlich is one the most used equation for the determination of dielectric constant (Equation 1.6).^{41,42}

$$\frac{(\epsilon_r - \epsilon_\infty)(2\epsilon_r + \epsilon_\infty)}{(2\epsilon_r + 2)^2 \epsilon_r} \frac{M}{\rho} = \frac{4\pi N_A}{9k_B T} g \mu^2 \quad \text{Equation 1.6}$$

where, ϵ_∞ is the infinite relative permittivity, M is the molecular weight, ρ is the density, N_A is Avogadro's number, k_B is Boltzmann's constant, T is the temperature of the system, μ is the dipole moment of the fluid molecule in the vacuum, and g is the Kirkwood parameter. The parameter g measures the local order among molecules (nearest neighbors) and can be calculated as:

$$g = 1 - z \langle \cos \varphi \rangle$$

where, z is the coordinator number and φ is the angle between the test dipole and the neighbor.

W. Schröder reported that the first analysis of Onsager and Kirkwood-Frohlich equation ignores the free ion yields Kirkwood- g -factor of 0.05, which is much smaller than any value found in dipolar fluids.⁴³ Therefore, they laid out a macroscopic theory that could be applied to the dielectric properties in ILs. The model proposed by W. Schröder by a factor of g from the classic model of Onsager and Kirkwood-Frohlich equation. As a result, they derived a correction for g that could be applied to Onsager and Kirkwood-Frohlich theories (Equation 1.7).

$$g = \frac{1}{1 + \frac{\epsilon_r - \epsilon_\infty}{2\epsilon_r + \epsilon_\infty} \frac{3(1 + k_B r)}{k_B^2 r^2 + k_B^2 r^2}} \quad \text{Equation 1.7}$$

Ionic liquids have tunable polarity and hydrophilicity that can be used to enhance the miscibility with solvents of medium or low polarity.⁴⁴

1.2.2. Supercritical CO₂ as Tunable Media

As said above, scCO₂ has the ability to dissolve in many organic compounds like alcohols, ketones, ethers, esters and ionic liquids, which provides the ability to alter the physiochemical properties (like polarity, dielectric constant, density etc.) of these organic compounds by modulating the concentration of CO₂, which can be easily performed from a processes point of view, through control of pressure (Figure 1.3).⁴⁵

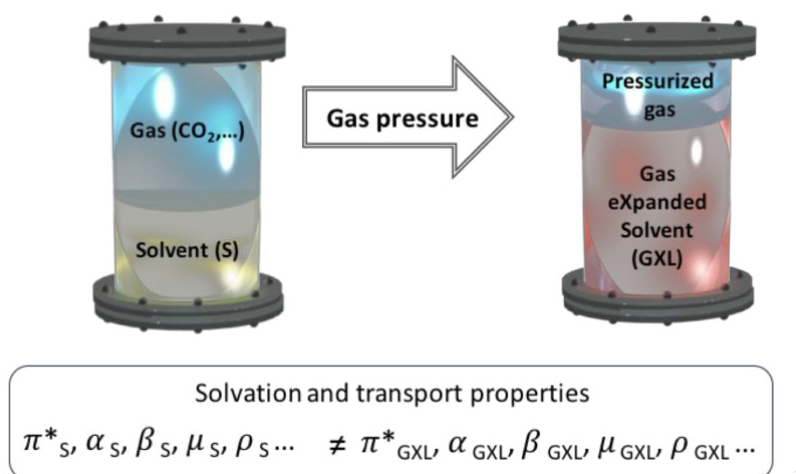
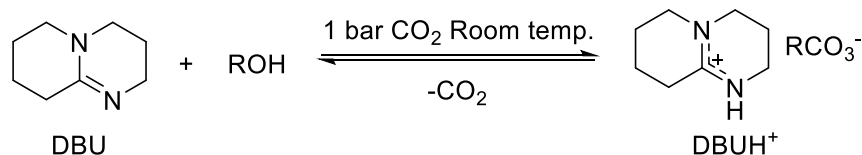


Figure 1.3. Change in physiochemical properties of a solvent on dissolution of carbon dioxide. (Reprinted (adapted) with permission from (45). Copyright (2018) American Chemical Society)

A tunable/switchable solvent is a solvent that can be switched from one form to another by tuning its physiochemical properties like (dielectric constant, acidity, basicity, density, polarity,

degree of polymerization etc.) upon application of a trigger like CO₂.^{13,19,46} The group of Jessop in collaboration with Eckert and Liotta were the firsts to develop switchable polarity solvents.^{46,47} They use CO₂ to switch from lower to higher polarity solvent. They found that in the presence of just 1 bar of CO₂ at room temperature, when two non-ionic solvents (1,8-diazabicyclo-[5.4.0]-undec-7-ene and 1-hexanol) were converted to ionic species resulting in a high polarity solvent. The system could promptly be converted back to the original form by bubbling nitrogen or argon (Scheme 1.1).



Scheme 1.1. Protonation of 1,8- diazabicyclo-[5.4.0]-undec-7-ene (DBU) in the presence of an alcohol and carbon dioxide.⁴⁶

Tunable solvents are important media for organic reactions because in this case, a reaction can be performed in one form of solvent and then it can be switched to the other form and if the product or catalyst is not soluble in the converted, medium it will just precipitate.⁴⁸ The same principle of tunability can also be applied to extraction.⁴⁶

1.3. Gas-expanded liquids

Over a decade, interest in gas-expanded liquids (GXLs) has rapidly increased. They are promising alternative media for performing separations, extractions, reactions, and other applications. However, a precise definition of GXLs has not been given out; so far, GXL can be defined as a liquid whose volume is increased when pressurized with a condensable gas such as CO₂ or ethane.¹⁸ In addition, one of the more recent definitions was proposed by Jessop *et al.* where a GXL was defined as “a mixed solvent composed of a compressible gas dissolved in an organic solvent”.⁴⁹

Since, different liquids behave differently with expanding gases, Jessop *et al.* have proposed a classification:⁴⁹

- Class I GXL is one where the expanding gas has a low solubility in the liquid, and which does not expand much (such as CO₂+water).
- Class II GXL is one where the solubility of the expanding gas is high and the expansion is large, e.g. CO₂+THF.

- Class III GXLs are liquids where the gas is moderately soluble, but the expansion is small (*e.g.* CO₂+ILs or liquid polymers). Figure 1.4 shows the solubility of CO₂ in different classes of liquids.

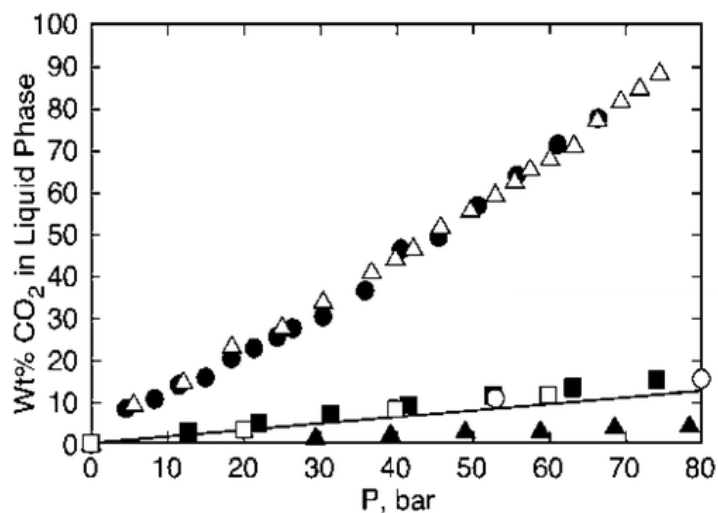


Figure 1.4. The mass fraction solubility of CO₂ in Class I (water (▲)), Class II (ethyl acetate (●) and MeCN (Δ)), and Class III liquids ([bmim]BF₄ (■), crude oil (UOPK factor= 11.7, assuming molar weight of 350 gmol⁻¹, shown as a line), PEG (○), and PPG (□)). bmim = 1-n-butyl-3-methylimidazolium; PEG = Polyethylene glycol; PPG = Polypropylene glycol. (Reprinted (adapted) with permission from reference (49). Copyright (2007) American Chemical Society.)

1.3.1. CO₂ - expanded liquids (CXLs)

Because of the safety and economic advantages of CO₂, CXLs are the most commonly used class of GXLs. By varying the CO₂ composition, a continuum of liquid media ranging from the neat organic solvent to scCO₂ is generated, the properties of which can be adjusted by tuning the operating pressure; for example, a large amount of CO₂ favors mass transfer and, in many cases, gas solubility, and the presence of polar organic solvents enhances the solubility of solid and liquid solutes. CXLs have been shown to be optimal solvents in a variety of roles including inducing separations, precipitating fine particles, and facilitating polymer processing, and serving as reaction media for catalytic reactions.⁵⁰ Process advantages include ease of removal of the CO₂, enhanced solubility of reagent gases (compared to liquid solvents), fire suppression capability of the CO₂, and milder process pressures (tens of bars) compared to scCO₂ (hundreds of bars). Reaction advantages include higher gas miscibility compared to organic solvents at ambient conditions, enhanced transport rates due to the properties of dense CO₂.⁵¹ The typical

expansion behavior of a class II GXL is shown in Figure 1.5, using CO₂+THF.⁵¹ The expansion increases with pressure, rising almost exponentially towards the critical point. When the expansion is plotted against the CO₂ mole fraction in the liquid phase, it is largely independent of the pressure or temperature. This expansion changes both the solvent character and the physical properties of the liquid.

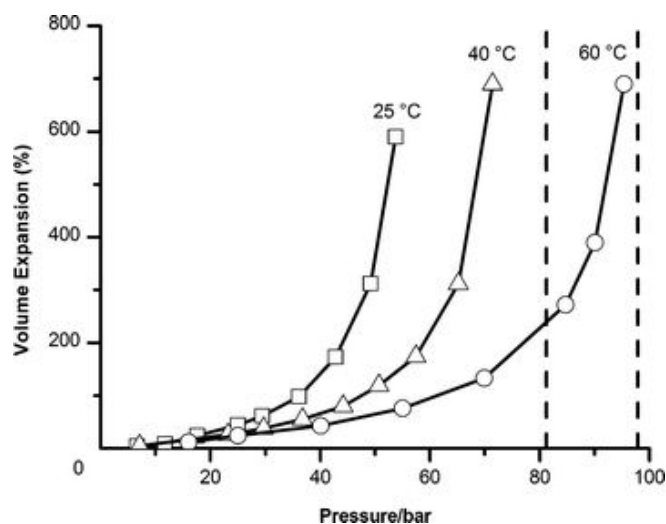


Figure 1.5. Volume expansion of THF with varying CO₂ pressure at different temperatures, as measured visually in a Jerguson view cell. (Reproduced from reference (51) with permission of Royal Society Of Chemistry in the format Thesis/Dissertation via Copyright Clearance Center)

When CO₂ dissolves into the liquid, it reduces both the polarity and the hydrogen-bonding abilities of the expanded liquid. However, the solvent power is maintained for longer than expected, compared to simple dilution by CO₂, since the polar solvent molecules can cluster dynamically around the solute. This leads to both an increase in the proportion of solvent molecules in the cybotactic region (part of a solution near a solute molecule in which the ordering of the solvent molecules is modified by the presence of the solute molecule), but also an increase in the local density.^{52,53}

1.4. Ionic Liquids (ILs)

It was 1914 that the first report was made on ionic liquid (ILs) by Paul Walden.⁵⁴ He reported the physical properties of ethylammonium nitrate (EAN) that was formed by neutralization of ethylamine with concentrated nitric acid.⁵⁵ He found that its physical properties were similar to water except that EAN possessed higher viscosity. However, its ionic

conductivity struck a remarkable property to Walden.⁵⁶ Ionic liquids are molten salts, that are generally liquid at room temperature, whose enormous potential arises from particular characteristics of these liquids, namely, their physicochemical properties (viscosity, density, hydrophilicity, and solubility), which can be tuned by the combination of different cations and anions.^{57–59} Figure 1.6 shows a various examples of cations and anions that have the ability to form ILs.⁶⁰ Ionic liquids can participate in a variety of interactions; they can participate from the weak, nonspecific, and isotropic forces like van der Waals, solvophobic, dispersion to specific, anisotropic, strong Coulombic forces like hydrogen bonding, halogen bonding, dipole-dipole, magnetic dipole, electron pair donor/acceptor interactions.⁵⁷

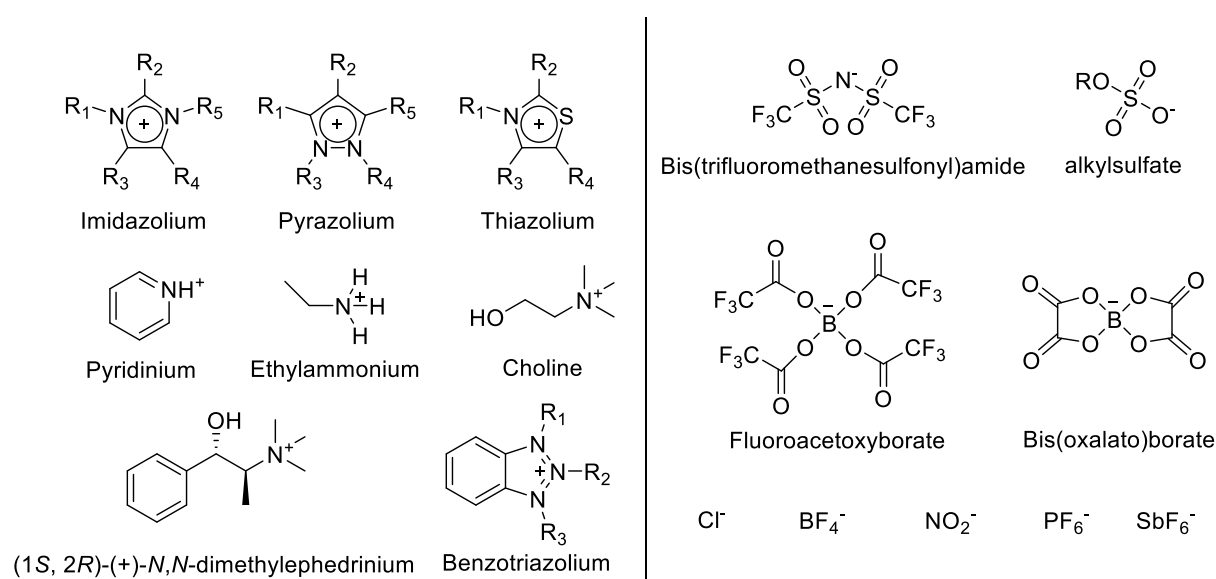


Figure 1.6. Various examples of cations and anions that have the ability to form ILs.

Ionic liquids serve as up-and-coming solvents for various reasons like: (1) they can solubilize wide variety of both organic and inorganic materials; (2) they are composed of poorly coordinated ions, thus, they can be polar without being highly coordinating solvents; (3) they are immiscible with organic solvents and therefore can provide biphasic medium, which can come useful in extraction and separation processes; (4) they are non-volatile and can be used under high-vacuum environment. ⁶¹

1.4.1. Properties of Ionic Liquids

Ionic liquids are often referred to as “designer liquids” since their physical and chemical properties can be altered by changing the type of cations and anions.⁶² Ionic liquids are generally non-volatile, non-flammable, and showing high viscosity.⁵⁷ In the section below, some of the important properties of ILs are discussed.

1.4.1.1. Melting points

Melting point of ILs is one of their key identifying features. ILs are defined as salts with melting points below 100 °C.⁶⁰ Seddon *et al.* has showed that the melting point of alkali metal chlorides is much higher than the chlorides with organic cations.⁶³ Wasserschied *et al.* showed how the melting point of 1-ethyl-3-methylimidazolium (emim) based ILs changes as the anion is changed.^{53,64} They also showed how the melting point can also vary just by varying the molar ration of the cation and anion for [emim]Cl/AlCl₃ system (Figure 1.7).⁵³ They concluded that in this ILs the presence of several anions decreases the melting point. Wasserscheild *et al.* reported that melting points of ILs containing symmetrical cation are higher than ILs with asymmetrical cations.⁵³

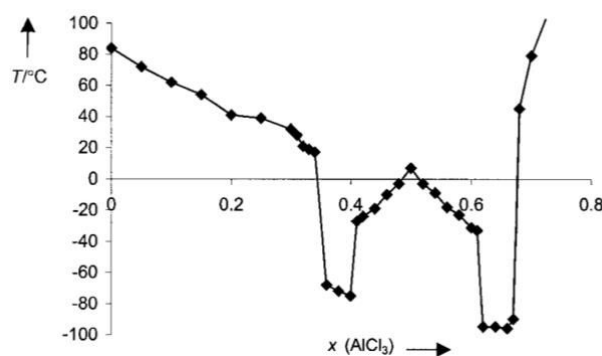


Figure 1.7. Experimental phase diagram for the [EMIM]Cl/AlCl₃ system.

(emim = 1-ethyl-3-methylimidazolium) (Reproduced from reference (53) with permission of WILEY via Copyright Clearance Center. Year of copyright (2000))

1.4.1.2. Vapor Pressure

ILs are considered to have no vapor pressure due its non-volatility.⁵³ ILs have reduced Columbic interactions between ions, this energetically restricts the ion-pair formation required for volatization of salts resulting in lower vapor pressure.⁶⁵ Due to lack of vapor pressure, ILs

serve as better solvent as compared to VOCs; after a reaction, the product recovery can be carried out in some systems by distillation.⁵³ In fact, even if most of the ILs have negligible vapor pressure and therefore they lack the ability to be distilled,^{57–59,63} Earle *et al.* demonstrated the volatility and the distilling ability of some ILs.⁶⁶ They showed a range of pure, aprotic ILs that can be vaporized at 200–300 °C under vacuum and then recondensed at lower temperatures. It is true that there are sets of ILs that possess zero vapor pressure, however, they reported the distillation of pure 1-alkyl-3-methylimidazolium bis-((trifluoromethyl)-sulphonyl)amide ([C_nmim][NTf₂]). According to them, ILs were volatilized as neutral molecular species by proton transfer mechanism instead of being transferred as ionic species into gas phase.⁶⁷ This method can be useful for purification of ILs. Nevertheless, the vapor pressure of ILs remains negligible near ambient temperature, which allow ILs to continue serving as the phenomenal solvents.

1.4.1.3. Viscosity

ILs have higher viscosities than conventional solvents.⁶⁰ ILs viscosities at room temperature range from a low of around 10 cP to values in excess of 500 cP (Viscosities of water, ethylene glycol and glycerol are 0.890, 16.1, and 934 cP, respectively).⁵³ In an IL, viscosity is determined by their hydrogen bond ability and the strength of van der Waals interaction.⁶⁸ Bonhôte *et al.* compared the viscosities of 1-alkyl-3-methylimidazolium based ILs. In Figure 1.8, they show that the increase of the van der Waals attraction dominates over the H-bonding from triflate (TfO⁻) to nonaflate (NfO⁻) and from trifluoroacetate (TA⁻) to heptafluorobutanoate (HB⁻). However, from TfO⁻ to NfO⁻ complete H-bonding suppression slightly dominates over the van der Waals attraction increase. On the other hand, in the case of TA⁻ and acetate (AcO⁻) opposite trend is observed as much stronger H-bonding overcompensates for smaller anion weight. TA⁻ and bis-((trifluoromethyl)-sulphonyl)amide (Tf₂N⁻) salts combine minimal anion weight with moderate basicity and minimal basicity with moderate anion weight respectively and hence, present the lowest viscosities. The cation also influences the viscosity. It was observed that alkyl chain lengthening increases the viscosity due to increased van der Waals interaction. Additionally, from butyl to isobutyl the ILs become more viscous due to the hindrance in the freedom of rotation.⁶⁸

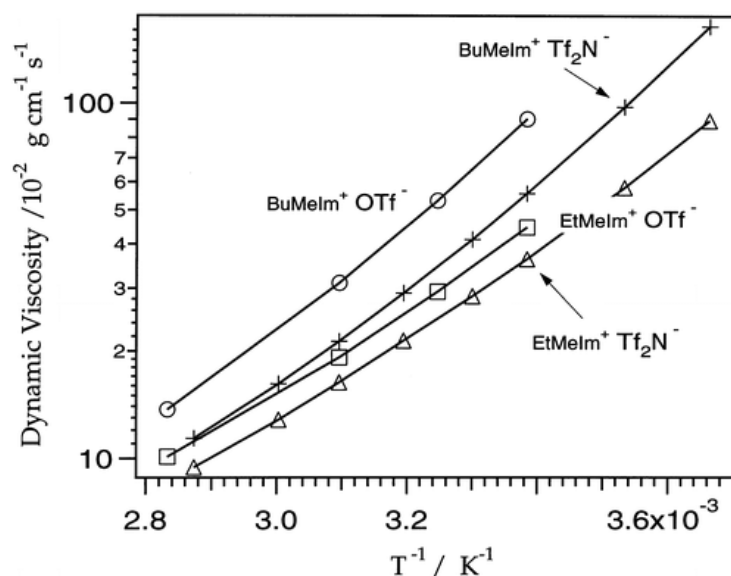


Figure 1.8. Plot of dynamic viscosity (η , estimated error: (5%)) of some ambient temperature molten salts as function of reciprocal absolute temperature (T^{-1}). BuMeIm = 1-butyl-3-methylimidazolium, EtMeIm = 1-ethyl-3-methylimidazolium (Reprinted (adapted) with permission from (68). Copyright (1996) American Chemical Society)

The dynamic viscosity of ILs can be calculated using the same empirical equation that is used for unassociated liquid electrolytes (Equation 1.8).⁶⁹

$$\eta = \eta_{\infty} \exp(-E_a/RT) \quad \text{Equation 1.8}$$

where, η is the dynamic viscosity, η_{∞} is the viscosity at the infinite temperature E_a is the activation energy for viscous flow, R is the gas constant and T is the temperature.

1.4.2. Mass Transfer in Ionic Liquids

Viscosity is an important mass transfer property; it is inversely proportional to the diffusion coefficient.^{19,25} Viscosity is also an important property for the prediction of pressure drops and heat transfer rates in processes. Additionally, low solubility of gaseous reactants like H_2 , CO , CO_2 , etc. in ionic liquids (ILs) can reduce reaction efficiency.^{65,70} Zhang *et al.* has provided an insight of gas-liquid mass-transfer properties in CO_2 absorption with ILs.⁷¹ In their contribution, they have determined the liquid-side mass transfer coefficient of CO_2 (k_L) in ILs- H_2O system by pressure drop method in a stirrer cell reactor. The coefficient was also evaluated and analyzed with respect to several parameters like type of IL, absorption temperature, stirrer speed and IL concentration. They derived the equation 1.9 for the determination of k_L .

$$k_L at = \frac{\beta}{1+\beta} \ln \left[\frac{P_{CO_2}^0}{(1+\beta)P_{CO_2}^0 - \beta P_{CO_2}^0} \right] \quad \text{Equation 1.9}$$

where, $a = A/V_L$ and $\beta = \frac{V_G K_H}{ZRTV_L}$, a is specific gas-liquid interfacial area (m^{-1}), A is gas-liquid interfacial area (m^2), $P_{CO_2}^0$ is the initial pressure of CO_2 in kPa and t is time in seconds. For equation 1.9, the volumetric mass-transfer coefficient within the time interval $[0,t]$ can be determined by the linear fitting method. In the study, it was concluded that k_L is influenced by the viscosity and the molecular structure of ILs. k_L decreases while CO_2 solubility increases with the increase of IL concentrations (Figure 1.9). They also found that a higher stirrer speed could result in a higher speed of pressure drop in the reactor, which can be attributed to a greater k_L .

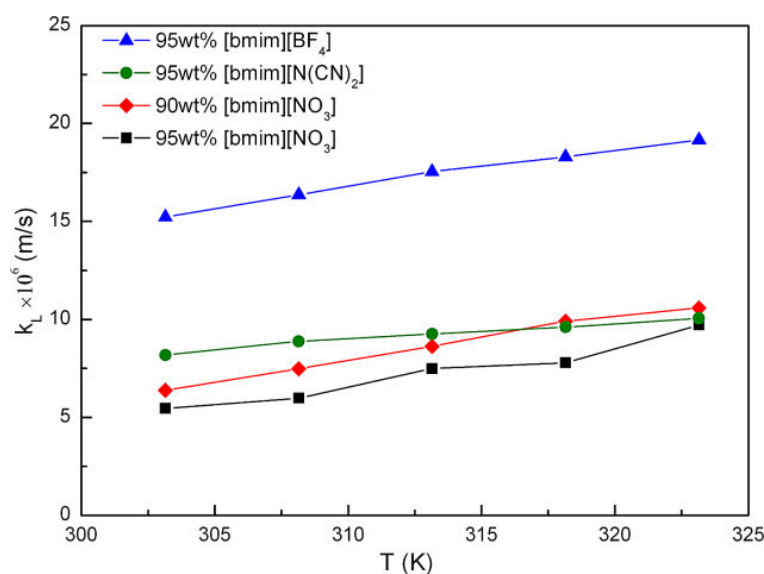


Figure 1.9. k_L in different IL-H₂O systems over the temperature range from 303 - 323 K. bmim = 1-n-butyl-3-methylimidazolium (Reproduced from reference (71) with permission of WILEY via Copyright Clearance Center. Year of copyright (2014))

Solinas *et al.*, described how the combination of ILs and scCO₂ could not only increase the mass transfer but also increase the solubility of H₂ in the system.⁷² This behavior is clearly beneficial for the effective hydrogenation reactions in ILs.

Kian *et al.* measured the dynamic viscosity for three binary alkane mixtures of n-hexane, n-decane, or n-tetradecane saturated with CO₂, at three different isotherms (25, 40, and 55 °C) and pressures from 0 to 107 bar (Figure 1.10).⁷³ They reported that the viscosity decreases considerably with the pressure of the CO₂. According to them, it is not a pressure effect but the

large increase in CO₂ solubility in the liquid phase that decreases the viscosity. For example, the system of n-tetradecane/CO₂ shows the largest absolute and relative drop in viscosity due to the dissolution of CO₂ in the liquid phase. For this system at 25 °C, 40 °C and 50 °C, the viscosity of liquid phase drops by 65%, 76% and 87% respectively compared to the ambient pressure viscosity, at about 55% mole CO₂ solubility. Similarly, Sih *et al.* determined the viscosity of CO₂ in methanol as a function of temperature from 25 to 40 °C, from 0 to 0.85 mole fraction CO₂ and from 1 to 76.7 bar. They reported that the liquid viscosity of the system decreased with CO₂ enrichment and decreased with increasing liquid density.⁷⁴ From this data, it is pertinent to say that, in general, CO₂ provides an easy knob for decreasing mass transfer and viscosity in gas-expanded liquids. Jacquemin *et al.* determined the solubility of eight different gases (carbon dioxide, ethane, methane, oxygen, nitrogen, hydrogen, argon and carbon monoxide) in [Bmim][PF₆].⁷⁵ They found out that CO₂ is the most soluble and hydrogen is the least soluble of the gases. Shannon *et al.* demonstrated that as the alkyl chain length on the cation increases the amount of CO₂ decreases.⁷⁶

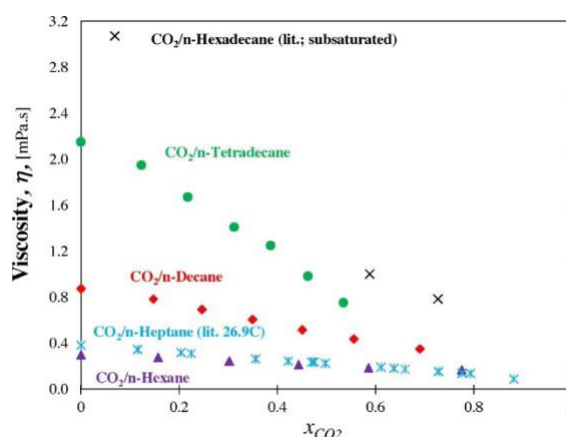


Figure 1.10. Comparison of viscosity of saturated CO₂/n-alkane mixtures at 25 °C. (Reprinted from reference (73), Copyright (2017), with permission from Elsevier)

1.4.3. Heat Transfer in Ionic Liquids

Applications of heat transfer fluid is numerous in both industrial and consumer applications. They are used in refrigerators at low temperature, solar energy collection and storage at high temperature etc.²¹ It has been reported that ILs have the high density and high heat capacity, and also good thermal and chemical stability making them promising candidates for heat transfer fluids in medium and high temperature heat transfer systems.⁷⁷ ILs are also known to be possessing large heat storage capacity (up to 50% larger than current heat transfer fluids).^{78,79} França *et al.*, compared the heat capacity of several ILs with commercial thermal fluids (data

for the density and heat capacity of the ILs chosen were taken from the IL Thermo database) (Figure 1.11). Heat capacity per unit volume of ILs between room temperature and 130 °C is 20 to 40% higher.⁷⁸

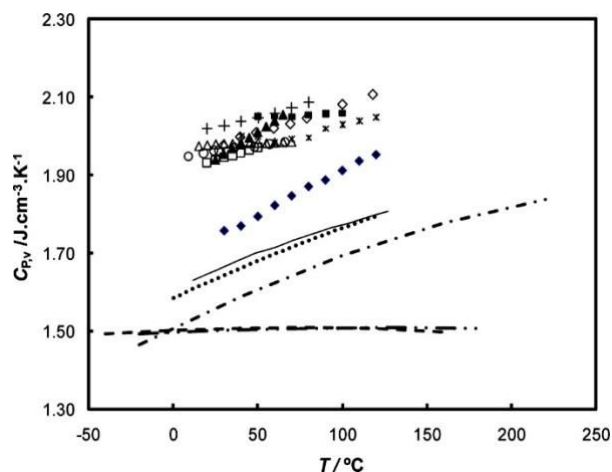


Figure 1.11. Heat capacity per unit volume of several ionic liquids. Data for the ionic liquids were taken from ref 10 and for the heat transfer fluids from their Material Safety Data Sheets available online.⁸ ◆, [C₆mim][PF₆]; ◇, [C₄mim][PF₆]; +, [C₂mim][BF₄]; ■, [C₆mim][(CF₃SO₂)₂N]; ▲, [C₄mim][C₁₈O₁₇SO₄]; *, [C₄mim][CF₃SO₃]; ●, [C₄mim][(CF₃SO₂)₂N]; □, [C₂mim][PF₆]; ○, [C₂mim][(CF₃SO₂)₂N]; △, [C₂mim][C₂H₅SO₄]; - - -, Syltherm 800; - · - ·, Syltherm HF; —, Dowtherm A; - - - -, Dowtherm MX; ····, Paratherm HE. Reprinted (adapted) with permission from reference (78). Copyright (2009) American Chemical Society.

Nieto de Cartro *et al.* reported the thermal conductivity of ionic liquids with carbon nanotubes (CNTs) for alkylmethylimidazolium liquids.⁸⁰ They reported the variation of heat capacity with temperature, together with the results obtained by different authors (Figure 1.12). The heat capacity (C_P in Jmol⁻¹K⁻¹) measurements were done at a pressure of 0.1 MPa at temperatures (T) between 308 K and 423 K by using polynomial equation 1.10 as a function of temperature, where b is the coefficient of regression.

$$C_P = b_1 + b_2(T) + b_3(T)^2 \quad \text{Equation 1.10}$$

They reported the data by Rebelo *et al.*,⁸¹ Kim *et al.*,⁸² Fredlake *et al.*,⁸³ Waliszewski *et al.*,⁸⁴ Van Valkenburg *et al.*,⁸⁵ Garcia-Miaja *et al.*⁸⁶ and Garcia-Miaja *et al.*⁸⁷ The data reported by Nieto de Cartro *et al.* in figure 1.12 agrees with the other published data by an estimated uncertainty of 1%. Since ILs are fluid at room temperature and they disperse CNTs by

themselves, they give a gelatinous substance also known as “bucky gels”.⁸⁸ This allow the design of soft composite material directly from the gels by modifying their physical properties, incorporating certain functionalities and/or transfer them into other fluid media or solid matrices.⁸⁹

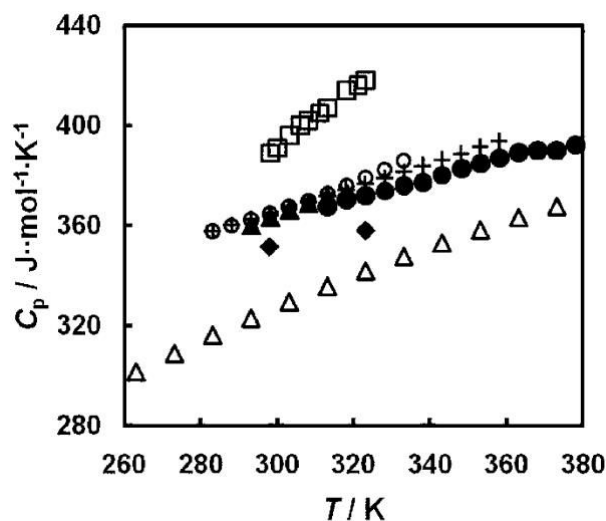


Figure 1.12. Heat capacity C_p of [bmim][BF₄] as a function of temperature T . Data from other authors are also shown. ●, Nieto de Cartro *et al.*;⁸⁰ ○, Rebelo *et al.*;⁸¹ □, Kim *et al.*;⁸² ◆, Fredlake *et al.*;⁸³ +, Waliszewski *et al.*;⁸⁴ Δ, Van Valkenburg *et al.*;^{85*} Garcia-Miaja *et al.*;⁸⁶ ▲, Garcia-Miaja *et al.*⁸⁷ Reprinted (adapted) with permission from reference (80). Copyright (2010) American Chemical Society.

Tenney *et al.* studied the heat transfer properties of nine different ILs both computationally and experimentally.⁹⁰ They showed the experimental Prandtl number (the ratio of the heat capacity multiplied by the viscosity to the thermal conductivity) versus temperature for each (Figure 1.13). The values they obtained for Prandtl number ranged from 1,000 or higher at the lowest temperatures to 100 at the higher temperatures.⁹⁰

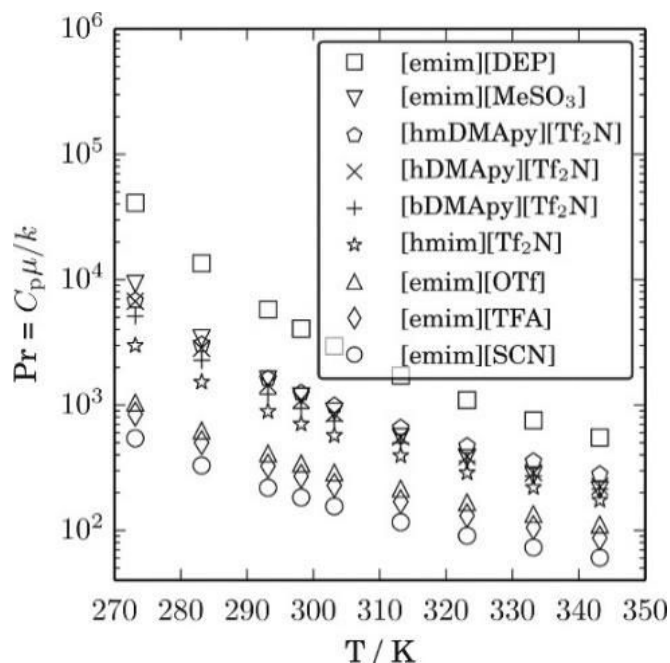


Figure 1.13. Prandtl number versus temperature calculated from experimental measurements of the present study. Ionic liquids in the legend are listed roughly in order of decreasing Prandtl number. emim = 1-ethyl-3-methylimidazolium; hmim = 1-hexyl-3-methylimidazolium; hmDMApy = 1-Hexyl-3-methyl-4-(dimethylamino)pyridinium; hDMApy = 1-hexyl-4-(dimethylamino)pyridinium; bDMApy = 1-butyl-4-(dimethylamino)pyridinium. Reprinted (adapted) with permission from reference (90). Copyright (2014) American Chemical Society.

Unfortunately, no heat transfer studies could be found concerning CO₂-ionic liquid systems. It is also note to worth the lack of reports describing heat transfer in catalytic hydrogenation reactions in GXLs.

1.5. Deep Eutectic Solvents (DESs)

Over the last decade, DESs has appealed the interest of researchers as designer solvents for various electrochemical and material applications such as metal electrodeposition, gas adsorption, metal extraction and the processing of metal oxides.⁹¹ DESs are also promising green solvents that present properties like high viscosity, high thermal stability and low vapor pressure. The term “deep eutectic solvent” was first laid in 2003 by Abbott *et al.*⁹², they defined DES as a mixture of two or more components that form a eutectic mixture, the melting point of this mixture being lower than both the individual components. DESs usually contain a mixture of hydrogen bond acceptor and a hydrogen bond donor (HBD). The first DESs reported by

Abbott *et al.* were constituted by a mixture of a salt based on quaternary ammonium cation and a hydrogen donor (amines, imides, and carboxylic acids).⁹³ This eutectic phenomenon was first observed through a mixture of urea and choline chloride with a 2:1 molar ratio. The result was a eutectic mixture that melts at 12 °C (melting points of urea and choline chloride are 133 °C and 302 °C, respectively).

As mentioned in section 1, DESs are now widely acknowledged as a new class of ionic liquids because they share many characteristics and properties with ILs such as low volatility, non-flammability, low melting points, low vapor pressure, dipolar nature, chemical and thermal stability. However, the increasing interest in DESs as compared to traditional ILs is due to their potential to even more environmentally benign as compared to latter. DESs are superior in terms of the availability of raw materials, the ease of storage and synthesis, and the low cost of their starting materials.⁹⁴ Besides having almost similar solvation properties, DESs put forward many potential applications in various fields of chemistry and electrochemistry. So far and due to economic reasons, the cases of using DESs at a commercial scale are still in finite amounts. The advantages of DESs over ILs are discussed in next section.

1.5.1. Ionic Liquids versus Deep Eutectic Solvents

ILs have been used for a variety of purposes like non-conventional solvents, performance additives, and for immobilizing of catalysts.⁶² However, ILs costs are a barrier for practical uses, therefore, in order to combine sustainability and promising benefits of ILs, a new generation of solvents “deep eutectic solvents” is quite appealing. DESs are sometimes referred to as analogues of ILs and are often produced by heating and stirring two salts (*e.g.* choline chloride and urea). A DES may also has an ionic character, but consists of a mixture of organic compounds. A major advantage of DESs over ILs is the facility and versatility to prepare these solvents. DES can be prepared from the mixture of concentrated aqueous solutions containing each compound, from a melt of a first component in which the second is dissolved or from the solid mixture of the two components heated to a predetermined temperature.⁹⁵

There are unlimited methods to prepare various DESs due to their high flexibility to choose their individual components as well as their compositions. DESs production provides different properties and numerous applications can be envisaged especially in high-tech production and process that demand low costing materials. Recently, bio-based DES have been developed and attracted great attention due to their low-cost, easy recyclability and environment friendly

nature.⁹⁶ They are non-volatile, biocompatible and biodegradable solvents.⁹⁷ Chlorine chloride has become one the most famous choice for the hydrogen bond acceptor moiety whereas urea and glycerol are some of the choices as hydrogen bond donor.⁹⁸

1.5.2. Properties of Deep Eutectic Solvents

Through a wisely chosen combination of salts and HBD task-specific DESs can be produced, which can fulfill the desired requirements in terms of physicochemical properties for various applications. For example, solubility of a material in DES can be tuned by the choice of HBD. DESs are characterized by high conductivity, viscosity and surface tension. Additionally, they show lower vapor pressures as compared to other solvents.

1.5.2.1. Density

The density is one of the most important physical properties for a solvent. Generally, densities of DESs are determined by means of a specific gravity meter. Table 1.2 lists the density data of common DESs. Most of DESs exhibit higher densities than water.⁹⁸ For instance, ZnCl₂ - HBD eutectic mixtures have densities higher than 1.3 g cm⁻³. Among them, density of ZnCl₂ - urea (1:3.5) and ZnCl₂ acetamide (1:4) are different (1.63 and 1.36 g cm⁻³, respectively). This notable difference of density might be attributed to a different molecular organization or packing of the DES.

Table 1.2. Densities of common DESs at 25 °C. (Data taken from reference 98)

| Salt | HBD | Salt : HBD (mol : mol) | Density (ρ , g cm ⁻³) |
|----------------------|-----------------------------------|---------------------------|--|
| EtNH ₃ Cl | CF ₃ CONH ₂ | 1:1.5 | 1.273 |
| EtNH ₃ Cl | Acetamide | 1:1.5 | 1.014 |
| EtNH ₃ Cl | Urea | 1:1.5 | 1.140 |
| ChCl | CF ₃ CONH ₂ | 1:2 | 1.342 |
| ChCl | Urea | 1:2 | 1.25 |
| ZnCl ₂ | Urea | 1:3.5 | 1.63 |
| ZnCl ₂ | Acetamide | 1:4 | 1.36 |
| ZnCl ₂ | Ethylene glycol | 1:4 | 1.45 |
| ZnCl ₂ | Hexanediol | 1:3 | 1.38 |
| ChCl | Glycerol | 1:2 | 1.18 |

| | | | |
|------|-----------------|-----|------|
| ChCl | Glycerol | 1:3 | 1.20 |
| ChCl | Glycerol | 1:1 | 1.16 |
| ChCl | Glycerol | 1:3 | 1.20 |
| ChCl | Ethylene glycol | 1:2 | 1.12 |
| ChCl | Ethylene glycol | 1:3 | 1.12 |
| ChCl | Malonic acid | 1:2 | 1.25 |

1.5.2.2. Viscosity

DESs have high viscosity, which is an important issue that needs to be addressed. Except for ChCl–ethylene glycol eutectic mixture, most of the DESs exhibit relatively high viscosities (>100 cP) compared to water (0.890 cP) or ethanol (1.095 cP) at room temperature. The high viscosity of DESs is often attributed to the presence of an extensive hydrogen bond network between each component, which results in a lower mobility of free species within the DES. The large ion size and very small void volume of most DESs, but also other forces such as electrostatic or van der Waals interactions may contribute to the high viscosity of DESs. Owing to their potential applications as green media, the development of DESs with low viscosities is highly desirable. In general, viscosities of eutectic mixtures are mainly affected by the chemical nature of the DES components (type of the ammonium salts and HBDs, organic salt/HBD molar ratio, etc.), the temperature, and the water content. As discussed above, viscosity of DES is also dependent on the free volume. Hence, this theory can also be used to design DESs with low viscosities. For instance, the use of small cations or fluorinated hydrogen-bond donors can lead to the formation of DES with low viscosity.

Hydrogen bonds, van der Waals and electrostatic interactions effectively control the viscosity of binary eutectic mixtures. For instance, ChCl/ethylene glycol (1:4) DES exhibits the lowest viscosity (19 cP at 20 °C).⁹⁹ In contrast, the use of sugar-based derivatives (*e.g.* xylitol, sorbitol) or carboxylic acids (*e.g.* malonic acid) as HBDs led to DESs exhibiting high viscosities (*e.g.* 12,730 cP at 20 °C for ChCl/sorbitol), due to the presence of a more robust 3D intermolecular hydrogen-bond network.¹⁰⁰

In the case of a ChCl/glycerol DES, an increase of the ChCl/glycerol molar ratio results in a decrease of the DES viscosity (Figure 1.14). For example, at 20 °C, viscosities of ChCl–glycerol mixtures with a molar ratio of 1:4, 1:3, 1:2 were 503, 450, and 376 cP, respectively.⁹⁸ Glycerol has a strong cohesive energy due to the presence of an important intermolecular

hydrogen bond network.^{4,101} This drastic decrease of the glycerol viscosity upon addition of ChCl was attributed to the partial rupture of this hydrogen bond network.¹⁰²

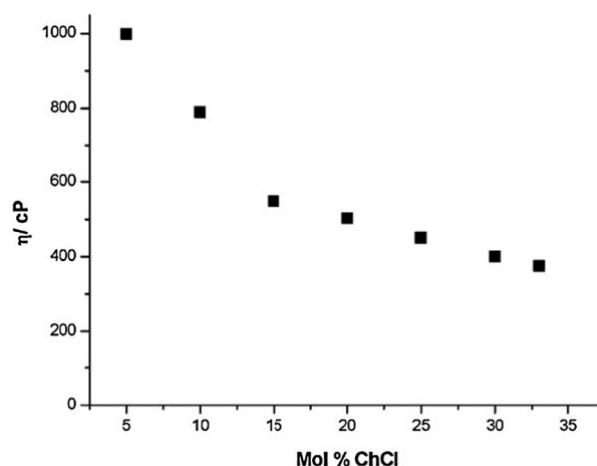


Figure 1.14. Effect of ChCl on the viscosity of glycerol as a function of composition at 298 K. (Republished with permission of Royal Society of Chemistry, from reference (98); permission conveyed through Copyright Clearance Center, Inc)

In addition, viscosity of most of the eutectic mixtures follows an Arrhenius like behavior, that is, as the temperature increases, the viscosity decreases.

1.5.2.3. Polarity

Polarity of a solvent is a term used commonly in the context of the capacity of a solvent for solvating dissolved charged or neutral (polar or apolar) species.¹⁰³ In other words, modifying the polarity of the solvent initially miscible compounds are likely to become immiscible even at moderate pressures. Generally, polarity scale $\{E_T(30)\}$ is used to evaluate the polarity of a solvent, which is defined as the electronic transition energy of a probe dye (*e.g.* Reichardt's Dye 30) in a solvent.⁹⁸ By means of UV-vis technology and using Reichardt's Dye 30, $E_T(30)$ can be calculated according to equation 1.11.

$$E_T(30) = h_{CU_{max}}N_A = (2.8591 \times 10^{-3})U_{max} = 28591/\lambda_{max} \quad \text{Equation 1.11}$$

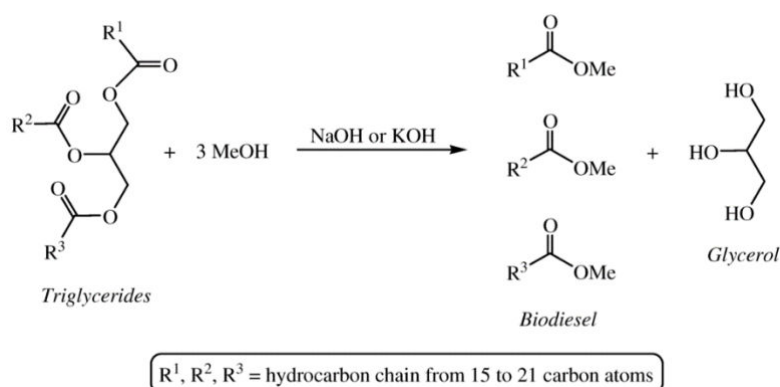
where, h is Plank's constant, C is the speed of light, U_{max} is the concentration and λ_{max} is the wavelength.

Table 1.3. Solvent polarity parameter of various ChCl-glycerol mixtures. (Data taken from reference 98)

| Solvent | Molar ratio of ChCl:Glycerol | $E_T(30)/\text{kcal mol}^{-1}$ |
|---------------|------------------------------|--------------------------------|
| Glycerol | — | 57.17 |
| ChCl:Glycerol | 1:3 | 57.96 |
| ChCl:Glycerol | 1:2 | 58.28 |
| ChCl:Glycerol | 1:1.5 | 58.21 |
| ChCl:Glycerol | 1:1 | 58.49 |

1.5.3. Glycerol-based DESs

About 100 kg of glycerol is formed as byproduct per ton of biodiesel (Scheme 1.2).¹⁰⁴ World-wide production of glycerol had reached 2 million tons in 2010 and it is expected to grow in the near future due to the increasing demand for biodiesel, as well as the emergence of other large-scale processes based on the conversion of cellulose and lignocelluloses, where glycerol is also a concomitant product.



Scheme 1.2. Overall reaction in the production of biodiesel from triglycerides.¹⁰⁴

Thus, glycerol is considered as green reaction medium for synthetic chemistry due to its properties like renewable origin and unique combination of physicochemical properties, such as high polarity, low toxicity and flammability, high boiling point, ability to form strong hydrogen bonds and to dissolve both organic and inorganic compounds (salts, acids, bases, transition metal complexes).^{104,105}

In the section 1.5.2.2, it was discussed how the viscosity of glycerol can be tuned by forming a DES where glycerol acts as HBD with different molar ratio of ChCl/glycerol. Its common use stems in part from its simple manufacture, an efficient gas phase reaction between

trimethylamine, ethylene oxide and HCl. This means that the E factor (defined as the mass ratio of waste to desired product and the atom efficiency) for this salt is close to zero because almost no waste products are formed during this reaction.¹⁰⁶ Abbott *et al.* concluded that the 3D intermolecular H-bond interactions in glycerol get broken on addition of ChCl resulting in a less ordered system is the cause for decrease in viscosity.⁹⁹ This conclusion was backed up by the density data they recorded, that is, the density also decreased as ChCl was added. Additionally, the conductivity of the system increased as a function of ChCl addition due to more charge carrying species being available in an increasingly more fluid solvent.

In the next, synthesis of metal nanoparticles in alternative solvents is discussed in details. The reactivity of metal nanoparticles depends on size and shape of the nanoparticles.^{107,108} Synthesis of metal nanoparticles in liquid phase provides a better control on the morphology from a thermodynamical and kinetic provision.¹⁰⁹

2. Metal Nanoparticles

Approximately 150 years ago, on in 1857, Michael Faraday presented a lecture “Experimental Relations of Gold (and other Metals) to Light” to the Royal Society of London. Intrigued by the ruby color of colloidal gold, Faraday investigated the interaction of light in metal particles.^{110–112} Ruby glass had been used as for stained glass window since 17th century; however, it was the discovery by Faraday that led to a breakthrough in the field of nanoscience and nanotechnology. He prepared a biphasic aqueous solution of a gold salt and a solution of phosphorus in carbon disulfide. After some time, the bright yellow color of the Na[AuCl₄] solution turned into a ruby color characteristic of gold nanoparticles.¹¹⁰ Although, the solution prepared by Faraday was a colloidal gold dispersions, it is to be noted that the term “colloid” was not be coined until 1861 by T. Graham.¹¹³

Nanoparticles are assemblies of hundreds to thousands of atoms and a size in the range of 1-50 nm that can be considered at first approximation as a state of matter intermediate between single atoms or molecules and bulk bodies.¹¹⁴ Depending on the structure, nanoparticles can be 0D (like quantum dots), 1D (like nanotubes, nanoribbons, nanowires), 2D (nanoplates, nanowalls, nanodisks) or 3D (like nanocoils, nanoflowers, nanoballs).¹¹⁵ The sizes, shapes, dimensionality and morphologies of nanoparticles are key factors to define their performance and application and thus, can be exploited to tune their activity.^{115,116} Depending upon the

morphology, size, physical and chemical properties, nanoparticles can be classified into various categories (Figure 1.14).¹¹⁷ In this Chapter, with the context of this Thesis, the focus is given to metal nanoparticles (MNPs).

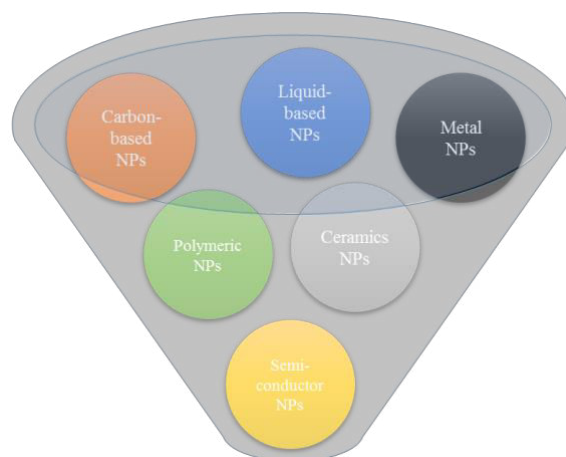


Figure 1.14. Different categories of nanoparticles based on their morphology, size, physical and chemical properties.

2.1. Synthesis of Metal Nanoparticles

There are two well-known general approaches for the synthesis of metal nanoparticles; top-down and bottom-up methodologies.¹¹⁸ The top-down approach is breaking down of bulk metal into nanoparticles by physical processes. Some of the most commonly used top-down processes are sputtering, laser ablation, and lithography or spray drying.¹¹⁸ However, it is often very difficult to synthesize or fabricate uniformly shaped materials or achieve perfection in the surface structure using these processes. Moreover, these processes have a high-energy consumption or expensive equipments leading to high cost. On the other hand, in the bottom-up approach, the atoms/molecules are brought together to form nanostructures. Chemical vapor deposition, photochemical and sonochemical deposition, chemical reduction and electrodeposition are some of the most well-known bottom-up techniques.¹¹⁰ Unlike the top-down approach, bottom-up processes yields better results when it comes to controlling the size, shape and morphology of the nanoparticles. One of the most popular method is chemical reduction. The idea is to take a metal precursor and reduce it into naked atoms that spontaneously starts to nucleate eventually forming metal nanoparticles. It is very important to highlight that this process takes place in the presence of a stabilizer.¹¹⁹

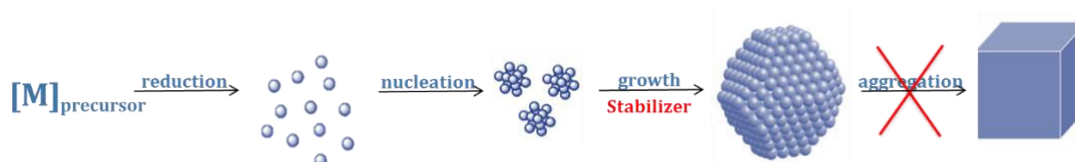


Figure 1.15. Schematic diagram showing the mechanism of formation of metal nanoparticles by chemical reduction of a metal precursor (salt, organometallic compound etc.)

The presence of stabilizer plays an essential role in the synthetic route, not only it inhibits aggregation of nanoparticles into bulk method, it also helps to control the size and shape of the nanoparticles. In addition to the type of stabilizer used, nature of metallic precursor, reaction conditions, reducing agents and the choice of solvents are also very relevant in governing the morphology and surface-state of the metal nanoparticles.¹⁰⁶⁻¹¹⁴

2.1.1. Polyol Methodology

The polyol methodology was first reported by Fiévet *et al.* in 1989.¹²⁰ They synthesized Co and Ni particles, and Co-Ni and Fe-Ni bimetallic particles of various compositions.¹²⁰⁻¹²² In this process, liquids polyols like ethylene glycol and diethylene glycol are used as solvent and as reducing agents for the preparation of metallic powder from various inorganic precursors like copper acetate.^{123,124}

Hachani *et al.* synthesized superparamagnetic iron oxide nanoparticles using polyol process.¹²⁵ The size and magnetic properties could be finely tuned by modifying the solvent, reaction time and concentration of iron precursor iron (III) acetylacetonate. They reported that NPs synthesized by this method had a narrow size distribution as compared to conventional methods such as thermal decomposition or co-precipitation. Dong *et al.* wrote in a review that the most important feature of the polyols is that they can be considered as water-equivalent but with high boiling points. They can allow synthesis temperature as 200-320 °C.¹²⁶ Carroll *et al.* used an experimental and theoretical approach to interpret the interaction of the polyols with metal surface (Cu and Ni nanoparticles) giving an insight of the mechanism of reduction and the shape of the resulting metal nanoparticles.¹²⁷ However, it should be noted that the polyol methodology is restricted by the reducing power of the solvent and low solubility of non-polar metal surfaces that can result in insufficient stabilization in polar polyol.¹²⁶

2.2. Metallic Nanoparticles in Glycerol

In the field of metal-mediated reactions, glycerol plays an enormous role for both molecular- and colloidal-based catalyst.^{128–130,131} It has a negligible vapor pressure (0.003 mmHg at 50 °C) and high ability to solubilize both organic and inorganic polar compounds, and also its immiscibility with low polar solvents.¹³¹ Nanoparticles prepared in glycerol with/without stabilizing agent exhibit excellent catalytic properties. Chahdoura *et al.* well-defined and small Cu₂O nanoparticles stabilized by poly(vinylpyrrolidone) in neat glycerol were synthesized and applied to C-heteroatom bond formation and azide–alkyne cycloaddition processes, obtaining high isolated yields. In the desired products, the catalytic phase could be recycled at least ten times whilst retaining the activity and selectivity of the Cu₂ONPs.¹²⁸ PdNPs dispersed in neat glycerol and stabilized by TPPTS (triphenylphosphine-3,3',3''-trisulfonic acid trisodium salt) have been efficiently applied in a large panel of reactions, leading to the synthesis of heterocyclic compounds: (na)phthalimides, isoindole-1-ones, tetrahydroisoquinolin-1,3-diones, (Z)-3-(arylmethylene)isoindolin-1-one and (Z)-1-methylene-1,3-dihydroisobenzofurans.¹²⁸ The desired products were obtained by one-pot tandem and/or sequential methodologies without the isolation of the generated intermediates. Furthermore, isolation of compounds containing two heterocycles, even using in the same medium two different catalysts, Pd and Cu₂O based nanoparticles was possible.¹²⁸ Lately, palladium nanoparticles capped by cinchona-based ligands were also synthesized in neat glycerol and successfully applied in dihydrogen-based processes, such as hydrogenation of unsaturated functional groups (alkenes, alkynes, imines, and nitro-based substrates) and hydrodehalogenation of halo-aromatic compounds by Reina *et al.*¹³²

Based on the review published Chahdoura *et al.*, glycerol accelerates reactions, immobilizes the catalyst mainly in the case of nanoparticles systems, allows the recycling of the catalytic phase, and yields metal-free target compounds.¹³³ Contrary to the most organic solvents, glycerol favors the stabilization of metallic nanoparticles, thus recovering nanoparticles at the end of the organic transformations that helps in better immobilization of the nanometallic species in the liquid phase during the products extraction procedure. The supramolecular network in glycerol leads to favors the dispersiom of nanoparticles than in conventional organic solvents and therefore the catalytic phase is preserved.¹³³ It is to be noted that in the above examples H₂ acts as a reducing agent whereas glycerol is only used as solvent.

In its pure anhydrous condition, glycerol has a density of 1.261 gmL⁻¹, a melting point of 18.2 °C and a boiling point of 290 °C under normal atmospheric pressure, accompanied by decomposition. At low temperatures, glycerol may form crystals that melt at 17.9 °C. Overall, it possesses a unique combination of physical and chemical properties, which are utilized in many thousands of commercial products. 105

2.3. Metal Nanoparticles in Ionic Liquids

Metallic Nanoparticles (MNPs) synthesized in ILs applied have applications in catalysis. Some ILs also act as reducing agents (*e.g.* hydroxylated imidazolium derivatives), even leading to the oxidation of the imidazolium cation by the metal precursor, as observed in the formation of gold nanoparticles (AuNPs) starting with Au(III) species.¹³⁴

2.3.1. Interactions between Ionic Liquids and Metal Nanoparticles

Quaternary ammonium salts are the most widespread model that can explain the stabilization of metallic nanoparticles by salt effect. A well-established stabilization mode consists in the interstitial layer constituted by the anions between the metal core and the surfactant shell. However, depending on the electronegativity of the metal, the literature describes a direct interaction of the ammonium cation to the metal surface (Figure 1.16).¹³⁵

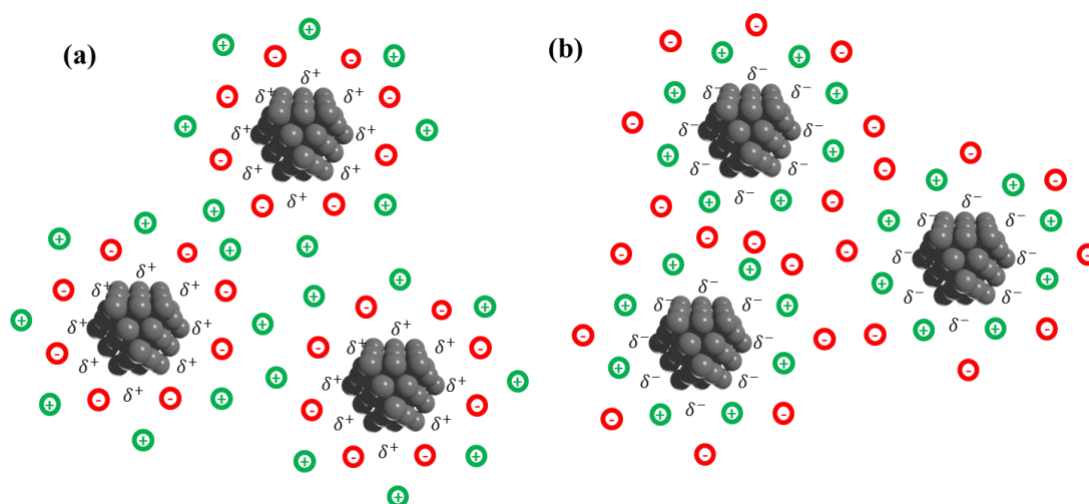


Figure 1.16. Representation of ionized MNPs at the surface: (a) positively and (b) negatively charged MNPs, surrounded by the corresponding shells of ionic species (black cluster denotes a metallic nanoparticle)

All these interactions generate channel-like molecular assemblies. Depending on the anion and cation nature, the interaction energies can be very different as well as the organization of the ILs. The ionic liquid cations are attracted to the surface of a negative charged nanoparticle to form a positive ion layer, and then counter ions form a second layer on the nanoparticle surface by electrostatic attraction. This electrical double layer efficiently keeps nanoparticles from aggregating.¹³⁵

Van der Waals interactions are also present in almost all the colloidal systems. The van der Waals force, arising from correlations between electrons motions in two neighboring molecules, is a short-range unidirectional force that is relatively weak compared to electrostatic interactions.

The Derjaguin–Landau–Verwey–Overbeek (DLVO) theory can be applied to quantitatively calculate the stability of colloidal dispersions.¹³⁶ It considers a combination of electrostatic double layer repulsion (Coulomb forces) and van der Waals attraction to examine the colloidal stability. The total particle–particle interaction energy potential (V_{total}) is calculated by addition of the van der Waals potential (V_{vdw}) and the electrostatic potential (V_{ele}):

$$V_{\text{total}} = V_{\text{vdw}} + V_{\text{ele}} \quad \text{Equation 1.6}$$

In an example of DLVO theory utilization, the potential between two gold NPs (with a diameter of 6 nm) dispersed in 1-butyl-3-methylimidazolium bis(trifluoromethylsulfonyl)imide ([bmim][NTf₂]) was calculated by adding the electrostatic potential and the van der Waals potential. A negative total potential over the whole distance range resulted, indicating an unstable colloidal system.¹³⁷

An approximate expression (when $\kappa R \gg 1$) for the electrostatic repulsion potential $V_{\text{ele}}(d)$ is:¹³⁸

$$V_{\text{ele}} = 2\pi R \epsilon_0 \epsilon_r \psi_0 \ln[1 + \exp(-\kappa d)] \quad \text{Equation 1.7}$$

where, ψ_0 is the surface potential. The Debye reciprocal length parameter κ can be calculated from:¹³⁸

$$\kappa = \left(\frac{\sum_i (z_i e)^2 c_{i0}^*}{\epsilon_0 \epsilon_r kT} \right)^{1/2} \quad \text{Equation 1.8}$$

where z_i stands for ion valence, e is the elementary charge, c_{i0}^* is the bulk concentration of ions (at a reference point where the potential equals zero), ϵ_r is the solvent dielectric constant,

ϵ_0 is the permittivity of free space, k is the Boltzmann constant and T is the absolute temperature. The thickness of the Debye layer ($1/k$) can be utilized as a measure of colloidal electrostatic stability.¹³⁸ The colloidal particles are more stable with a thicker Debye layer because it expands the distance between nanoparticles, reducing the chance for nanoparticle agglomeration. Moreover, a wider separation between nanoparticles reduces van der Waals interactions, which further discourages nanoparticle aggregation.

2.3.2. Stabilization of Metal Nanoparticles by Ionic Liquids

Metallic nanoparticles stabilized by ILs are generally considered as core-shell systems, mainly involving electrostatic and steric repulsion forces. Electrostatic stabilization is often based on Derjaguin, Landau, Verwey and Overbeek (DLVO) theory, which describes a balance between repulsive columbic forces opposed to attractive van der Waals ones as discussed in section 2.3.1. The anions interact with the electrophilic surface of the nanoparticles, forming a layer at the surface of the MNP. The thickness of the counter ions surrounding the MNP (Debye layers) affects the stability of the MNP. In general, the thinner the layers are, the greater is the interparticle distance. However, this anionic stabilization mode cannot explain all the reported observations.

Apart from DLVO interaction, other interactions can govern the stability of nanoparticles in ILs. The next sections discuss some these non-DLVO interactions.

2.3.2.1. Structural Aspects

In colloidal systems, the motion of the solvent molecules surrounding the particle surface is constrained within a narrow range. Solvation shells are built by proton-donors and proton-acceptors forming hydrogen bonds, and by electrostatic interactions attracting counterions. For aqueous colloidal systems, this orientation restriction is indicated as hydration pressure and the solvation shell is referred as a hydration shell. In dispersions of nanoparticles in ionic liquids, ion shells are built around nanoparticles to effect stabilization through structural forces. The nanoparticles can be viewed as encapsulated in constraining nano-regions of ionic liquids. The solvation layers are squeezed out of the closing gap when two solid surfaces approach each other, thus providing structural repulsion to prevent nanoparticles from agglomerating. The constraining effect on solvent molecules/ ions and the attractive interactions between the nanoparticle surface and solvent molecules/ions hence generate solvation forces between neighboring nanoparticles.

2.3.2.2. *Solvophobic Interactions*

The hydrophobic force is another non-DLVO force acting on aqueous colloidal systems that is considered as a factor affecting colloidal stability. In the case of ionic liquid-based colloidal systems, we refer to this as solvophobic force. Analogous to polymers in a bad solvent, the nanoparticles tend to aggregate to reduce the contact area with the ionic liquid in the case where the nanoparticle surface is solvophobic relative to the ionic liquid medium.

A better dispersibility indicated by Newtonian fluid-like rheological behavior in the hydrophilic ionic liquid at room temperature and at 100 °C, even at higher nanoparticle concentrations, implied that the hydrophilic silica nanoparticles with silanol groups were more stable under solvophilic conditions. To further confirmation, the silica nanoparticles were surface functionalized to render them hydrophobic. The hydrophobic silica nanoparticles in the hydrophobic ionic liquid behaved like Newtonian fluids, indicating better dispersibility.

Besides the direct influence of solvophobic forces, the relative solvophobicities of ionic liquids and nanoparticles having surface-grafted polymers can affect the colloidal stability through steric interactions

2.3.2.3. *Steric Interactions*

When two nanoparticles with polymers adsorbed on their surface approach each other, the polymer layers may undergo some compression resulting in a strong repulsion that is referred to as steric interaction. The physical basis of steric repulsion is a combination of entropic and osmotic contributions. The entropic contribution is due to a volume restriction effect that decreases possible configurations in the region between two surfaces. The osmotic effect arises from a difference in concentration of the adsorbed polymers in the region between the two surfaces as they approach closer. In ionic liquid-based colloidal systems, steric forces can emerge from bulky groups within a molecule and/or from the addition of macromolecules, both of which hinder nanoparticles from physically contacting each other and/or from forming chemical bonds.¹³⁹

Compared to structural forces, which originate from the solvation layer being squeezed out of the closing gap when two solid nanoparticles approach each other, steric forces originate from polymers or side chains attached at the solid–liquid interface dangling out into the solution where they remain thermally mobile. In the cases of nanoparticles in pure ionic liquid without polymer addition, the ionic liquid provides structural forces through forming solvation layers. However, if the ionic liquid comprises a long alkyl side chain, *e.g.* from imidazolium- or

pyrazolium-based cations, the cations being attracted near nanoparticle surfaces can provide steric forces by stretching out their bulky side-chains, thus hindering the nanoparticles from approaching each other. This effect is steric rather than structural.

The difference in polarity and the hydrogen-bonded supramolecular structure with cation and anion aggregates engender microheterogeneity in ionic liquids. The semi-organized ionic liquid-based nanostructure that extends beyond the electrostatic double layer also leads to steric forces that stabilize the embedded nanoparticles.¹³⁹

2.3.2.4. *Hydrogen Bonding Interactions*

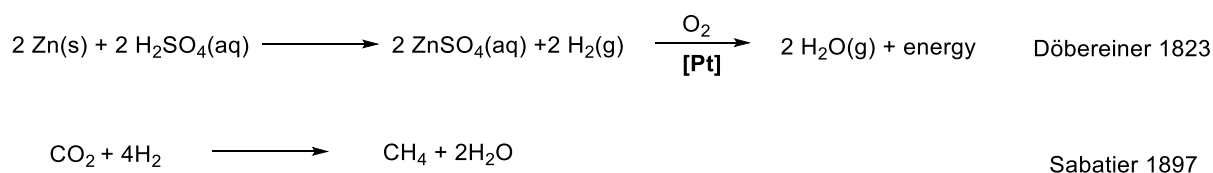
Hydrogen bond interactions are necessary to be considered in ionic liquid-based colloidal systems in addition to the classic electrostatic and van der Waals interactions. Several ionic liquids are highly hydrogen bonded to form supramolecular structures. In such ionic liquids, the cations contain one or more proton donors, which could form X–HY hydrogen bonds with halogen containing anions, *e.g.* $[\text{BF}_4]^-$, $[\text{PF}_6]^-$. Some nanoparticles possess hydroxy- and/or oxy-moieties on their surface, *e.g.* silica nanoparticles have silanol groups ($-\text{Si}-\text{OH}$), which can also hydrogen bond with ionic liquids.⁵³ The cation–anion hydrogen bond and NP–IL hydrogen bond compete with each other and contribute to nanoparticle stabilization in ionic liquids.

2.4. Catalytic Activity of Metal Nanoparticles

Nanoparticles have electronic properties intermediate between molecules and bulk metals.¹⁴⁰ The activity of nanoparticles depend hugely on their size and surface state; as the size decreased the exposed surface atoms increase leading to more area for the surface reactant interaction.¹⁴⁰ C. R. Henry presented a study of supported nanometer-sized particles that are used in heterogeneous catalysis *via* the reactivity of size selected and soft-landed small metal clusters containing 2 to 50 atoms called as molecular approach and the reactivity of extended single crystal surfaces called as surface science approach.¹⁴¹ He reported that the intrinsic heterogeneities (like the presence of different types of facets, the presence of edges and the presence of the support) encounter to the peculiarity of the nanometer-sized supported clusters.¹³¹ Therefore, the compositional and structural complexity of these catalyst allows the chemical and adsorption properties in order to optimize their performance in a specific reaction.¹⁴² MNPs have been very popular for their catalytic properties in a variety of reactions, for example, as a surfactant for water-soluble polymer, resins, vesicles etc, including

Fischer-Tropsch, isomerization, and hydroformylation, etc which uses Rh, Pt, Ir, Au, and Pd nanoparticles as catalysts.¹⁴³ Fisher-Tropsch is an important industrial process to convert feedstock like coal and biomass into clean diesel.¹⁴⁴ In this process, nanocatalysts of Fe and Co of size 0-15 nm are used in slurry reactors to improve the production of high molecular waxes. These waxes then hydrocracked to generate green diesel.¹⁴⁵ Kang *et al.* reported the selective conversion of synthesis gas to diesel fuel using Ru nanoparticles supported on carbon nanotubes.¹⁴⁶ They said that both selectivity and turnover frequency (TOF) for CO conversion depend on the mean size of Ru particles. As already said above, reactivity of MNPs highly depends on its size. Bezemer *et al.* reported that the TOF for CO conversion over Co supported on carbon nanofibers increased with Co size up to roughly 8 nm and then remained almost unchanged with further size increases.¹⁴⁵

One of the most popular catalytic reaction by MNPs is hydrogenation, which has been investigated since 19th century when Paul Sabatier discovered hydrogenation of unsaturated hydrocarbons using Ni as catalyst.¹⁴⁷ The Sabatier process to hydrogenate carbon dioxide to form methane and water was the reason he was awarded Nobel Prize in Chemistry in 1912. Until date, hydrogenation reaction based on his work as well as the work of Döbereiner have been investigated.



Scheme 1.3. The Döbereiner and Sabatier reactions

Recently, Han *et al.* fabricated hexahedral Ni nanoparticles confined in mixed domains of Al₃₊-doped NiO and tested the catalytic hydrogenation reduction of *p*-nitrophenol to *p*-aminophenol.¹⁴⁸ Qu *et al.* also synthesized bimetallic AuPd nanoparticles supported on TiO₂ for solvent-free selective hydrogenation of nitroarenes.¹⁴⁹ The catalyst showed a good selectivity for the chemoselective hydrogenation of 4-chloronitrobenzene to 4-chloroaniline. They compared the reactivity of these bimetallic nanoparticles with monometallic (Au and Pd) nanoparticles and found the reactivity of former to be 54% more than the latter under identical reaction conditions, evidencing the synergy between metals.¹⁵⁰

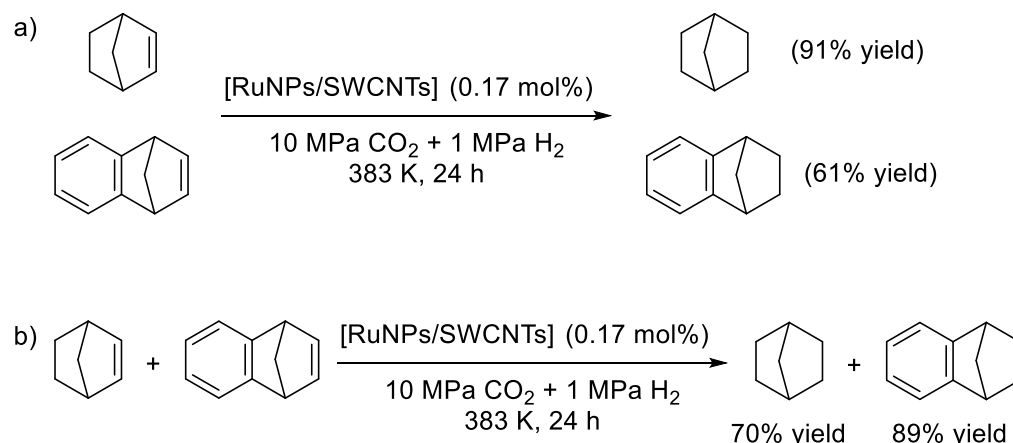
F. Zaera studied the surface chemistry of transition metal-based heterogeneous catalysts for hydrogenation.¹⁵¹ He discussed the state-of-the-art of hydrogenation catalysis using the example of olefin hydrogenation to study the adsorption of the organic reactants, the role that

the strongly adsorbed carbonaceous deposits that form during reaction play in defining the catalytic kinetics, the mechanistic details of the hydrogen dissociative uptake and surface mobility during reaction, and the dynamic changes of the structure of the surface induced by the catalytic conditions. They also discussed the issue of selectivity in connection with the hydrogenation of alkynes, dienes, trienes, and aromatics; unsaturated aldehydes and imines; and cases where hydrogenation competes with other types of reactions such as dehydrogenations, skeletal rearrangements, cyclizations, and hydrogenolysis.

2.4.1. Catalytic Hydrogenation Applications of Metal Nanoparticles under Carbon dioxide

Hydrogenation reactions are often limited due to the low solubility of hydrogen in the solvents currently used. Application of supercritical fluids (SCFs) during hydrogenation can serve as a promotor for transporting hydrogen into the liquid phase and thus enhance the equilibrium concentrations of both reactants and products in the gaseous phase. Supercritical reaction media have been investigated for completely solubilizing hydrogen and thereby eliminating gas–liquid transport resistances in heterogeneous-catalyzed hydrogenations. Cyclohexene hydrogenation is often used as benchmark for both optimization of reaction parameters and comparative purposes of different catalysts. Howdle *et al.* prepared PdNPs on silica aerogels in scCO₂.¹⁵² The as-synthesized catalytic material was successfully applied in the hydrogenation of cyclohexene under flow conditions using scCO₂, without observing sintering or coking on the metal surface after catalysis. Later, Knez's group reported the synthesis of PdNPs on organic modified silica aerogels (AEROMOSIL), prepared following one-pot methodology from tetramethoxysilane, polydimethylsiloxane, formic acid and the Pd(II) precursor under scCO₂ conditions (313 K, 50 MPa CO₂).¹⁵³ This catalyst was applied in the hydrogenation of 2,5-dihydro-2,5-dimethoxyfurane both under batch and continuous flow scCO₂, being the latter reactor much more efficient: under comparable conditions, batch reactor led to 60% conversion, while flow reactor achieved 99%. RuNPs supported on carbon-based solids (Single Walled Carbon Nanotubes, SWCNTs; hollow Graphitized Nanofibers, GNFs) applied on hydrogenation of alkenes, evidenced the essential role of scCO₂ in the transport of reactants to the metallic surface, in particular for RuNPs/SWCNTs (mean size: 0.74 ± 0.18 nm).¹⁵⁴ Actually, RuNPs/GNFs were less active under the same conditions (10 MPa CO₂, 1 MPa H₂, 383 K, 0.17 mol% Pd, 24 h), for the hydrogenation of both substrates norbornene and benzonorbornadiene (Scheme 1.4). For both catalysts, RuNPs were confined inside the carbon

material (proven by STEM and HRTEM analyses). For commercial Ru/C catalyst, where the Ru nanoparticles are located at the support surface, the activity was lower than for RuNPs/SWCNTs. The affinity of the aromatic substituents for the interior of carbon supports could be demonstrated by the competitive reaction between both substrates, which altered the selectivity of the reactions.



Scheme 1.4. Ru-based nanocatalysts on SWCNTs catalyzed the hydrogenation of the non-aromatic C=C bond: a) independent reactions of norbornene and benzonorbornadiene; b) competitive reactions of norbornene and benzonorbornadiene

The design of catalysts for selective hydrogenation processes without additives represents a challenging and sustainable approach. For the hydrogenation of alkenes containing a benzyl group, hydrogenolysis process can also take place (deprotection reaction), which is often precluded modifying the catalyst by additives.¹⁵⁵ Lee *et al.* prepared a selective catalyst based on PdNPs supported on mesoporous silica SBA-15 by palladium confinement on the pores, which was applied in the chemoselective hydrogenation of 4-methoxycinnamic acid benzyl ester in $scCO_2$.^{156,157} Comparing with other heterogeneous catalysts (Pd/C, Pd/Al₂O₃), PdNPs/SBA-15 was the most selective giving up to 97% selectivity for full conversion (for Pd/C and Pd/Al₂O₃, 38% (100% conversion) and 64% (92% conversion) of selectivity, respectively).

In gas-liquid heterogeneous catalytic systems several steps can be identified: 1) transfer of gaseous reactants from bulk gas phase to gas/liquid interface by diffusion, 2) transfer from this interface to the bulk of the liquid phase through adsorption and diffusion, 3) transfer of both reactants from bulk liquid to the catalytic surface by diffusion through the stagnant film at the surface of the catalyst, 4) transfer of the reactants inside the pores of the catalyst through internal diffusion, 5) adsorption of reactants, 6) reaction at the surface, 7) desorption and transfer of the

products by internal and external diffusion to bulk liquid or gas phase. It is clear here that diffusion plays a key role in the transfer of substrates, hydrogen and products. At the interface, mass transfer is a non-equilibrium process. Transport phenomena that occur outside of the catalyst particle are commonly referred to as *external* or *interphase* transport effects or resistances. The phenomena occurring inside the pores of the catalyst are called *internal* or *intraparticle* effects.

3. Conclusions

To summarize, in the first part of this we have described the physiochemical properties of supercritical fluids (especially supercritical carbon dioxide), ionic liquids and deep eutectic solvents at length. Furthermore, we have described how SCFs and gas-expanded liquids can be used as tunable media for various reactions. We have discussed how these solvents are a smart choice over the volatile organic solvents. We have also discussed the limitations of mass transfer in the ILs and DES and the use of scCO₂ to overcome these limitations.

In the next part, we have talked about synthesis of metal nanoparticles in various media focusing especially on ionic liquids and glycerol. Catalytic activity of various nanoparticles in hydrogenation have been discussed. Special focus has been given to hydrogenation reaction using metal nanoparticles under sub and supercritical CO₂.

4. References

- (1) Medina-Gonzalez, Y.; Camy, S.; Condoret, J. S. ScCO₂ Green Solvents: Biphasic Promising Systems for Cleaner Chemicals Manufacturing. *ACS Sustain. Chem. Eng.* **2014**, *2* (12), 2623–2636. <https://doi.org/10.1021/sc5004314>.
- (2) Pollet, P.; Davey, E. A.; Ureña-Benavides, E. E.; Eckert, C. A.; Liotta, C. L. Solvents for Sustainable Chemical Processes. *Green Chem.* **2014**, *16* (3), 1034–1055. <https://doi.org/10.1039/c3gc42302f>.
- (3) Laffort, P. Updated Definition of the Three Solvent Descriptors Related to the Van Der Waals Forces in Solutions. *Open J. Phys. Chem.* **2018**, *08* (01), 1–14. <https://doi.org/10.4236/ojpc.2018.81001>.
- (4) Wolfson, A.; Dlugy, C. Palladium-Catalyzed Heck and Suzuki Coupling in Glycerol. *Chem. Pap.* **2007**, *61* (3), 228–232. <https://doi.org/10.2478/s11696-007-0026-3>.

- (5) Xi, D.; Zhou, R.; Zhou, R.; Zhang, X.; Ye, L.; Li, J.; Jiang, C.; Chen, Q.; Sun, G.; Liu, Q.; et al. Mechanism and Optimization for Plasma Electrolytic Liquefaction of Sawdust. *Bioresour. Technol.* **2017**. <https://doi.org/10.1016/j.biortech.2017.05.132>.
- (6) Clark, J. H.; Tavener, S. J. Alternative Solvents: Shades of Green. *Org. Process Res. Dev.* **2007**, *11* (1), 149–155. <https://doi.org/10.1021/op060160g>.
- (7) Byrne, F. P.; Jin, S.; Paggiola, G.; Petchey, T. H. M.; Clark, J. H.; Farmer, T. J.; Hunt, A. J.; Robert McElroy, C.; Sherwood, J. Tools and Techniques for Solvent Selection: Green Solvent Selection Guides. *Sustain. Chem. Process.* **2016**, *4* (1), 1–24. <https://doi.org/10.1186/s40508-016-0051-z>.
- (8) Díaz-Álvarez, A. E.; Francos, J.; Lastra-Barreira, B.; Crochet, P.; Cadierno, V. Glycerol and Derived Solvents: New Sustainable Reaction Media for Organic Synthesis. *Chem. Commun.* **2011**, *47* (22), 6208–6227. <https://doi.org/10.1039/c1cc10620a>.
- (9) DeSimone, J. M. Practical Approaches to Green Solvents. *Science* (80-.). **2002**, *297* (5582), 799–803. <https://doi.org/10.1126/science.1069622>.
- (10) Jain, A.; Panchal, S.; Sharma, S.; Ameta, R. *Supercritical Fluids*; 2013. <https://doi.org/10.1201/b15500>.
- (11) Subramaniam, B.; Chaudhari, R. V.; Chaudhari, A. S.; Akien, G. R.; Xie, Z. Supercritical Fluids and Gas-Expanded Liquids as Tunable Media for Multiphase Catalytic Reactions. *Chem. Eng. Sci.* **2014**, *115*, 3–18. <https://doi.org/10.1016/j.ces.2014.03.001>.
- (12) Eckert, C. A.; Liotta, C. L.; Bush, D.; Brown, J. S.; Hallett, J. P. Sustainable Reactions in Tunable Solvents. *J. Phys. Chem. B* **2004**, *108* (47), 18108–18118. <https://doi.org/10.1021/jp0487612>.
- (13) Herrero, M.; Mendiola, J. A.; Ibáñez, E. Gas Expanded Liquids and Switchable Solvents. *Curr. Opin. Green Sustain. Chem.* **2017**, *5*, 24–30. <https://doi.org/10.1016/j.cogsc.2017.03.008>.
- (14) Elizalde-Solis, O.; Galicia-Luna, L. A.; Sandler, S. I.; Sampayo-Hernández, J. G. Vapor-Liquid Equilibria and Critical Points of the CO₂ + 1-Hexanol and CO₂ + 1-Heptanol Systems. *Fluid Phase Equilib.* **2003**, *210* (2), 215–227. [https://doi.org/10.1016/S0378-3812\(03\)00170-5](https://doi.org/10.1016/S0378-3812(03)00170-5).
- (15) Silva-Oliver, G.; Galicia-Luna, L. A.; Sandler, S. I. Vapor-Liquid Equilibria and Critical Points for the Carbon Dioxide +1-Pentanol and Carbon Dioxide +2-Pentanol Systems at Temperatures from 332 to 432 K. *Fluid Phase Equilib.* **2002**. [https://doi.org/10.1016/S0378-3812\(02\)00024-9](https://doi.org/10.1016/S0378-3812(02)00024-9).
- (16) Kazarian, S. G.; Briscoe, B. J.; Welton, T. Combining Ionic Liquids and Supercritical Fluids: In Situ ATR-IR Study of CO₂ Dissolved in Two Ionic Liquids at High Pressures. *Chem. Commun.*

- 2000, No. 20, 2047–2048. <https://doi.org/10.1039/b005514j>.
- (17) Blanchard, L. a; Hancu, D. Scientific Correspondence A Stimulatory Phalloid Organ in a Weaver Bird Green Processing Using Ionic Liquids and CO₂ Long-Distance Transport of Pollen into the Arctic. *Nature* **1999**, *399* (May), 28–29. <https://doi.org/10.1038/19887>.
- (18) Kordikowski, A.; Schenk, A. P.; Van Nielen, R. M.; Peters, C. J. Volume Expansions and Vapor-Liquid Equilibria of Binary Mixtures of a Variety of Polar Solvents and Certain near-Critical Solvents. *J. Supercrit. Fluids* **1995**. [https://doi.org/10.1016/0896-8446\(95\)90033-0](https://doi.org/10.1016/0896-8446(95)90033-0).
- (19) Cunico, L. P.; Turner, C. *Supercritical Fluids and Gas-Expanded Liquids*; Elsevier Inc., 2017. <https://doi.org/10.1016/B978-0-12-805297-6.00007-3>.
- (20) Budisa, N.; Schulze-Makuch, D. Supercritical Carbon Dioxide and Its Potential as a Life-Sustaining Solvent in a Planetary Environment. *Life* **2014**, *4* (3), 331–340. <https://doi.org/10.3390/life4030331>.
- (21) Mayadevi, S. Ijca 51a(9-10) 1298-1305. **2012**, *51*, 1298–1305.
- (22) Jessop, P. G.; Ikariya, T.; Noyori, R. Homogeneous Catalysis in Supercritical Fluids Homogeneous Catalysis in Supercritical Fluids. *Technology* **1999**, *99* (January), 475–494. <https://doi.org/10.1021/cr970037a>.
- (23) Cabral, B. J. C.; Rivelino, R.; Coutinho, K.; Canuto, S. A First Principles Approach to the Electronic Properties of Liquid and Supercritical CO₂. *J. Chem. Phys.* **2015**, *142* (2). <https://doi.org/10.1063/1.4905256>.
- (24) van Itterbeek, A.; de Clippeleir, K. Measurements on the Dielectric Constant of Carbon Dioxide as a Function of Pressure and Temperature. *Physica* **1947**. [https://doi.org/10.1016/0031-8914\(47\)90033-5](https://doi.org/10.1016/0031-8914(47)90033-5).
- (25) Kopcak, U.; Mohamed, R. S. Caffeine Solubility in Supercritical Carbon Dioxide/Co-Solvent Mixtures. *J. Supercrit. Fluids* **2005**, *34* (2 SPEC. ISS.), 209–214. <https://doi.org/10.1016/j.supflu.2004.11.016>.
- (26) Soave, G. Equilibrium Constants from a Modified Redkh-Kwong EOS. *Chem. Eng. Sci.* **1972**, *27* (6), 1197–1203.
- (27) Redlich, O.; Kwong, J. N. S. On the Thermodynamics of Solutions. V. An Equation of State. Fugacities of Gaseous Solutions. *Chem. Rev.* **1949**, *44* (1), 233–244. <https://doi.org/10.1021/cr60137a013>.
- (28) Robinson, D. B.; Peng, D. Y.; Chung, S. Y. K. The Development of the Peng - Robinson

- Equation and Its Application to Phase Equilibrium in a System Containing Methanol. *Fluid Phase Equilib.* **1985**. [https://doi.org/10.1016/0378-3812\(85\)87035-7](https://doi.org/10.1016/0378-3812(85)87035-7).
- (29) Peng, D. Y.; Robinson, D. B. A New Two-Constant Equation of State. *Ind. Eng. Chem. Fundam.* **1976**, *15* (1), 59–64. <https://doi.org/10.1021/i160057a011>.
- (30) Wang, Z.; Sun, B.; Yan, L. Improved Density Correlation for Supercritical CO₂. *Chem. Eng. Technol.* **2015**, *38* (1), 75–84. <https://doi.org/10.1002/ceat.201400357>.
- (31) Lauffer, M. A. Theory of Diffusion in Gels. *Biophys. J.* **1961**, *1* (3), 205–213. [https://doi.org/10.1016/S0006-3495\(61\)86884-7](https://doi.org/10.1016/S0006-3495(61)86884-7).
- (32) Liu, H.; Ruckenstein, E. Predicting the Diffusion Coefficients in Supercritical Fluids. *Ind. Eng. Chem. Res.* **1997**, *36* (3), 888–895. <https://doi.org/10.1021/ie9604381>.
- (33) Medina, I. Determination of Diffusion Coefficients for Supercritical Fluids. *Journal of Chromatography A*. 2012. <https://doi.org/10.1016/j.chroma.2012.04.052>.
- (34) M. Shenai, V.; L. Hamilton, B.; A. Matthews, M. *Diffusion in Liquid and Supercritical Fluid Mixtures*; 2009. <https://doi.org/10.1021/bk-1992-0514.ch008>.
- (35) Palafox-Hernandez, J. P.; Mendis, C. H.; Thompson, W. H.; Laird, B. B. Pressure and Temperature Tuning of Gas-Expanded Liquid Structure and Dynamics. *J. Phys. Chem. B* **2019**, *123* (13), 2915–2924. <https://doi.org/10.1021/acs.jpcc.8b09826>.
- (36) Debenedetti, P. G.; Reid, R. C. Diffusion and Mass Transfer in Supercritical Fluids. *AIChE J.* **1986**, *32* (12), 2034–2046. <https://doi.org/10.1002/aic.690321214>.
- (37) Hourri, A.; St-Arnaud, J. M.; Bose, T. K. Solubility of Solids in Supercritical Fluids from the Measurements of the Dielectric Constant: Application to CO₂-Naphthalene. *Rev. Sci. Instrum.* **1998**, *69* (7), 2732–2737. <https://doi.org/10.1063/1.1149007>.
- (38) Abbott, A. P.; Corr, S.; Durling, N. E.; Hope, E. G. Solubility of Substituted Aromatic Hydrocarbons in Supercritical Difluoromethane. *J. Chem. Eng. Data* **2002**, *47* (4), 900–905. <https://doi.org/10.1021/je0155397>.
- (39) Abbott, A. P.; Eardley, C. A.; Tooth, R. Relative Permittivity Measurements of 1,1,1,2-Tetrafluoroethane (HFC 134a), Pentafluoroethane (HFC 125), and Difluoromethane (HFC 32). *J. Chem. Eng. Data* **1999**, *44* (1), 112–115. <https://doi.org/10.1021/je980130b>.
- (40) Leeke, G.; Santos, R.; Al-Duri, B.; Seville, J.; Smith, C.; Holmes, A. B. Solubilities of 4-Phenyltoluene, Phenylboric Acid, Biphenyl, and Iodobenzene in Carbon Dioxide from Measurements of the Relative Permittivity. *J. Chem. Eng. Data* **2005**, *50* (4), 1370–1374.

<https://doi.org/10.1021/je050075o>.

- (41) Kirkwood, J. G. The Dielectric Polarization of Polar Liquids. *J. Chem. Phys.* **1939**, *7* (10), 911–919. <https://doi.org/10.1063/1.1750343>.
- (42) Bordewijk, P. ON THE DERIVATION KIRKWOOD-FRÖHLICH. **1973**, *69*, 422–432.
- (43) Schröer, W. Generalization of the Kirkwood - Fröhlich Theory of Dielectric Polarization for Ionic Fluids. *J. Mol. Liq.* **2001**. [https://doi.org/10.1016/S0167-7322\(01\)00178-7](https://doi.org/10.1016/S0167-7322(01)00178-7).
- (44) Jiang, Y.; Nadolny, H.; Käshammer, S.; Weibels, S.; Schröer, W.; Weingärtner, H. The Ion Speciation of Ionic Liquids in Molecular Solvents of Low and Medium Polarity. *Faraday Discuss.* **2012**, *154*, 391–407. <https://doi.org/10.1039/c1fd00075f>.
- (45) Granero-Fernandez, E.; Machin, D.; Lacaze-Dufaure, C.; Camy, S.; Condoret, J. S.; Gerbaud, V.; Charpentier, P. A.; Medina-Gonzalez, Y. CO₂-Expanded Alkyl Acetates: Physicochemical and Molecular Modeling Study and Applications in Chemical Processes. *ACS Sustain. Chem. Eng.* **2018**, *6* (6), 7627–7637. <https://doi.org/10.1021/acssuschemeng.8b00454>.
- (46) Jessop, P. G.; Mercer, S. M.; Heldebrant, D. J. CO₂-Triggered Switchable Solvents, Surfactants, and Other Materials. *Energy Environ. Sci.* **2012**, *5* (6), 7240–7253. <https://doi.org/10.1039/c2ee02912j>.
- (47) Phan, L.; Chiu, D.; Heldebrant, D. J.; Huttenhower, H.; John, E.; Li, X.; Pollet, P.; Wang, R.; Eckert, C. A.; Liotta, C. L.; et al. Switchable Solvents Consisting of Amidine/Alcohol or Guanidine/Alcohol Mixtures. *Ind. Eng. Chem. Res.* **2008**, *47* (3), 539–545. <https://doi.org/10.1021/ie070552r>.
- (48) Jessop, P. G.; Jessop, D. A.; Fu, D.; Phan, L. Solvatochromic Parameters for Solvents of Interest in Green Chemistry. *Green Chem.* **2012**, *14* (5), 1245–1259. <https://doi.org/10.1039/c2gc16670d>.
- (49) Jessop, P. G.; Subramaniam, B. Gas-Expanded Liquids. *Chem. Rev.* **2007**, *107* (6), 2666–2694. <https://doi.org/10.1021/cr040199o>.
- (50) Subramaniam, B.; Akien, G. R. Sustainable Catalytic Reaction Engineering with Gas-Expanded Liquids. *Curr. Opin. Chem. Eng.* **2012**, *1* (3), 336–341. <https://doi.org/10.1016/j.coche.2012.02.005>.
- (51) Akien, G. R.; Poliakoff, M. A Critical Look at Reactions in Class I and II Gas-Expanded Liquids Using CO₂ and Other Gases. *Green Chem.* **2009**, *11* (8), 1083–1100. <https://doi.org/10.1039/b904097h>.

- (52) Culllck, A. S.; Mathis, M. L. Densities and Viscosities of Mixtures of Carbon Dioxide and N-Decane from 310 to 403 K and 7 to 30 MPa. *J. Chem. Eng. Data* **1984**, *29* (4), 393–396. <https://doi.org/10.1021/je00038a008>.
- (53) Bier, M.; Dietrich, S.; Bonafos, R. C.; Carles, R.; Britun, N.; Minea, T.; Konstantinidis, S.; Snyders, R.; Cha, I. Y.; Ahn, M.; et al. *Small-Angle X-Ray Scattering Study of Au Nanoparticles Dispersed in the Ionic Liquids 1-Alkyl-3-Methylimidazolium Tetrafluoroborate*; 2011; Vol. 8. <https://doi.org/10.5772/14646>.
- (54) Walden, P.; Molekulargr, U. *Math-Net . Ru.* **2019**, *8* (6), 405–422.
- (55) Plechkova, N. V.; Seddon, K. R. Applications of Ionic Liquids in the Chemical Industry. *Chem. Soc. Rev.* **2008**, *37* (1), 123–150. <https://doi.org/10.1039/b006677j>.
- (56) Kar, M.; Plechkova, N. V.; Seddon, K. R.; Pringle, J. M.; MacFarlane, D. R. Ionic Liquids-Further Progress on the Fundamental Issues. *Aust. J. Chem.* **2019**, *72* (2), 3–10. <https://doi.org/10.1071/CH18541>.
- (57) Hayes, R.; Warr, G. G.; Atkin, R. Structure and Nanostructure in Ionic Liquids. *Chem. Rev.* **2015**, *115* (13), 6357–6426. <https://doi.org/10.1021/cr500411q>.
- (58) Lei, Z.; Dai, C.; Chen, B. Gas Solubility in Ionic Liquids. *Chem. Rev.* **2014**, *114* (2), 1289–1326. <https://doi.org/10.1021/cr300497a>.
- (59) Keskin, S.; Kayrak-Talay, D.; Akman, U.; Hortaçsu, Ö. A Review of Ionic Liquids towards Supercritical Fluid Applications. *J. Supercrit. Fluids* **2007**, *43* (1), 150–180. <https://doi.org/10.1016/j.supflu.2007.05.013>.
- (60) They, C. *Room-Temperature Ionic Liquids and Eutectic Mixtures*; 2013. <https://doi.org/10.1039/9781849736824-00175>.
- (61) Welton, T. Room-Temperature Ionic Liquids . Solvents for Synthesis and Catalysis Room-Temperature Ionic Liquids . Solvents for Synthesis and Catalysis. *Chem. Rev.* **1999**, *99* (July), 2071–2084. <https://doi.org/10.1021/cr980032t>.
- (62) Vekariya, R. L. A Review of Ionic Liquids: Applications towards Catalytic Organic Transformations. *J. Mol. Liq.* **2017**, *227*, 44. <https://doi.org/10.1016/j.molliq.2016.11.123>.
- (63) Seddon, K. R. Ionic Liquids for Clean Technology. *J. Chem. Technol. Biotechnol.* **1997**, *68* (4), 351–356. [https://doi.org/10.1002/\(SICI\)1097-4660\(199704\)68:4<351::AID-JCTB613>3.0.CO;2-4](https://doi.org/10.1002/(SICI)1097-4660(199704)68:4<351::AID-JCTB613>3.0.CO;2-4).
- (64) Fannin, A. A.; Floreani, D. A.; King, L. A.; Landers, J. S.; Piersma, B. J.; Stech, D. J.; Vaughn,

- R. L.; Wilkes, J. S.; Williams, J. L. Properties of 1,3-Dialkylimidazolium Chloride-Aluminum Chloride Ionic Liquids. 2. Phase Transitions, Densities, Electrical Conductivities, and Viscosities. *J. Phys. Chem.* **1984**, *88* (12), 2614–2621. <https://doi.org/10.1021/j150656a038>.
- (65) Anthony, J. L.; Maginn, E. J.; Brennecke, J. F. Solubilities and Thermodynamic Properties of Gases in the Ionic Liquid 1-n-Butyl-3-Methylimidazolium Hexafluorophosphate. *J. Phys. Chem. B* **2002**, *106* (29), 7315–7320. <https://doi.org/10.1021/jp020631a>.
- (66) Earle, M. J.; Esperança, J. M. S. S.; Gilea, M. A.; Lopes, J. N. C.; Rebelo, L. P. N.; Magee, J. W.; Seddon, K. R.; Widegren, J. A. The Distillation and Volatility of Ionic Liquids. *Nature* **2006**, *439* (7078), 831–834. <https://doi.org/10.1038/nature04451>.
- (67) Halbritter, K.; Noe, R.; Bartsch, M.; Siegel, W.; Stegmann, V.; Flores, M.; Becker, M. (12) United States Patent. **2008**, 2 (12).
- (68) Bonhôte, P.; Dias, A. P.; Papageorgiou, N.; Kalyanasundaram, K.; Grätzel, M. Hydrophobic, Highly Conductive Ambient-Temperature Molten Salts. *Inorg. Chem.* **1996**, *35* (5), 1168–1178. <https://doi.org/10.1021/ic951325x>.
- (69) Liu, F.; Zhong, X.; Xu, J.; Kamali, A.; Shi, Z. Temperature Dependence on Density, Viscosity, and Electrical Conductivity of Ionic Liquid 1-Ethyl-3-Methylimidazolium Fluoride. *Appl. Sci.* **2018**, *8* (3). <https://doi.org/10.3390/app8030356>.
- (70) Jacquemin, J.; Costa Gomes, M. F.; Husson, P.; Majer, V. Solubility of Carbon Dioxide, Ethane, Methane, Oxygen, Nitrogen, Hydrogen, Argon, and Carbon Monoxide in 1-Butyl-3-Methylimidazolium Tetrafluoroborate between Temperatures 283 K and 343 K and at Pressures Close to Atmospheric. *J. Chem. Thermodyn.* **2006**. <https://doi.org/10.1016/j.jct.2005.07.002>.
- (71) Lim, E.; Yao, J. Modeling and Simulation of the Polymeric Nanocapsule Formation Process. *IFAC Proc. Vol.* **2009**, *7* (4), 405–410. <https://doi.org/10.1002/aic>.
- (72) Solinas, M.; Pfaltz, A.; Cozzi, P. G.; Leitner, W. Enantioselective Hydrogenation of Imines in Ionic Liquid/Carbon Dioxide Media. *J. Am. Chem. Soc.* **2004**, *126* (49), 16142–16147. <https://doi.org/10.1021/ja046129g>.
- (73) Kian, K.; Scurto, A. M. Viscosity of Compressed CO₂-Saturated n-Alkanes: CO₂/n-Hexane, CO₂/n-Decane, and CO₂/n-Tetradecane. *J. Supercrit. Fluids* **2018**, *133* (August 2017), 411–420. <https://doi.org/10.1016/j.supflu.2017.10.030>.
- (74) Sih, R.; Dehghani, F.; Foster, N. R. Viscosity Measurements on Gas Expanded Liquid Systems- Methanol and Carbon Dioxide. *J. Supercrit. Fluids* **2007**, *41* (1), 148–157. <https://doi.org/10.1016/j.supflu.2006.09.002>.

- (75) Jacquemin, J.; Husson, P.; Majer, V.; Gomes, M. F. C. Low-Pressure Solubilities and Thermodynamics of Solvation of Eight Gases in 1-Butyl-3-Methylimidazolium Hexafluorophosphate. *Fluid Phase Equilib.* **2006**, *240* (1), 87–95. <https://doi.org/10.1016/j.fluid.2005.12.003>.
- (76) Shannon, M. S.; Tedstone, J. M.; Danielsen, S. P. O.; Hindman, M. S.; Irvin, A. C.; Bara, J. E. Free Volume as the Basis of Gas Solubility and Selectivity in Imidazolium-Based Ionic Liquids. *Ind. Eng. Chem. Res.* **2012**, *51* (15), 5565–5576. <https://doi.org/10.1021/ie202916e>.
- (77) Liu, J.; Wang, F.; Zhang, L.; Fang, X.; Zhang, Z. Thermodynamic Properties and Thermal Stability of Ionic Liquid-Based Nanofluids Containing Graphene as Advanced Heat Transfer Fluids for Medium-to-High-Temperature Applications. *Renew. Energy* **2014**, *63*, 519–523. <https://doi.org/10.1016/j.renene.2013.10.002>.
- (78) Franç, J. M. P.; Nieto De Castro, C. A.; Lopes, M. M.; Nunes, V. M. B. Influence of Thermophysical Properties of Ionic Liquids in Chemical Process Design. *J. Chem. Eng. Data* **2009**, *54* (9), 2569–2575. <https://doi.org/10.1021/je900107t>.
- (79) Aparicio, S.; Atilhan, M.; Karadas, F. Thermophysical Properties of Pure Ionic Liquids: Review of Present Situation. *Ind. Eng. Chem. Res.* **2010**, *49* (20), 9580–9595. <https://doi.org/10.1021/ie101441s>.
- (80) De Castro, C. A. N.; Lourenço, M. J. V.; Ribeiro, A. P. C.; Langa, E.; Vieira, S. I. C.; Goodrich, P.; Hardacre, C. Thermal Properties of Ionic Liquids and IoNanoFluids of Imidazolium and Pyrrolidinium Liquids. *J. Chem. Eng. Data* **2010**, *55* (2), 653–661. <https://doi.org/10.1021/je900648p>.
- (81) Rebelo, L. P. N.; Najdanovic-Visak, V.; Visak, Z. P.; Nunes Da Ponte, M.; Szydłowski, J.; Cerdeiriña, C. A.; Troncoso, J.; Romaní, L.; Esperança, J. M. S. S.; Gliedes, H. J. R.; et al. A Detailed Thermodynamic Analysis of [C4mim][BF4] + Water as a Case Study to Model Ionic Liquid Aqueous Solutions. *Green Chem.* **2004**, *6* (8), 369–381. <https://doi.org/10.1039/b400374h>.
- (82) Kim, K. S.; Shin, B. K.; Lee, H.; Ziegler, F. Refractive Index and Heat Capacity of 1-Butyl-3-Methylimidazolium Bromide and 1-Butyl-3-Methylimidazolium Tetrafluoroborate, and Vapor Pressure of Binary Systems for 1-Butyl-3-Methylimidazolium Bromide + Trifluoroethanol and 1-Butyl-3-Methylimidazolium Te. *Fluid Phase Equilib.* **2004**, *218* (2), 215–220. <https://doi.org/10.1016/j.fluid.2004.01.002>.
- (83) Bhattacharjee, A.; Lopes-da-Silva, J. A.; Freire, M. G.; Coutinho, J. A. P.; Carvalho, P. J. Thermophysical Properties of Phosphonium-Based Ionic Liquids. *Fluid Phase Equilib.* **2015**,

- 400, 103–113. <https://doi.org/10.1016/j.fluid.2015.05.009>.
- (84) Waliszewski, D.; Stępnia, I.; Piekarski, H.; Lewandowski, A. Heat Capacities of Ionic Liquids and Their Heats of Solution in Molecular Liquids. *Thermochim. Acta* **2005**, *433* (1–2), 149–152. <https://doi.org/10.1016/j.tca.2005.03.001>.
- (85) Valkenburg, M. E. V.; Vaughn, R. L.; Williams, M.; Wilkes, J. S. Thermochemistry of Ionic Liquid Heat-Transfer Fluids. *Thermochim. Acta* **2005**, *425* (1–2), 181–188. <https://doi.org/10.1016/j.tca.2004.11.013>.
- (86) García-Miaja, G.; Troncoso, J.; Romani, L. Excess Properties for Binary Systems Ionic Liquid + Ethanol: Experimental Results and Theoretical Description Using the ERAS Model. *Fluid Phase Equilib.* **2008**, *274* (1–2), 59–67. <https://doi.org/10.1016/j.fluid.2008.09.004>.
- (87) García-Miaja, G.; Troncoso, J.; Romani, L. Excess Molar Properties for Binary Systems of Alkylimidazolium-Based Ionic Liquids + Nitromethane. Experimental Results and ERAS-Model Calculations. *J. Chem. Thermodyn.* **2009**, *41* (3), 334–341. <https://doi.org/10.1016/j.jct.2008.09.002>.
- (88) Fukushima, T.; Aida, T. Ionic Liquids for Soft Functional Materials with Carbon Nanotubes. *Chem. - A Eur. J.* **2007**, *13* (18), 5048–5058. <https://doi.org/10.1002/chem.200700554>.
- (89) Fukushima, T.; Kosaka, A.; Ishimura, Y.; Yamamoto, T.; Takigawa, T.; Ishii, N.; Aida, T. Molecular Ordering of Organic Molten Salts Triggered by Single-Walled Carbon Nanotubes. *Science (80-.)*. **2003**, *300* (5628), 2072–2074. <https://doi.org/10.1126/science.1082289>.
- (90) Tenney, C. M.; Massel, M.; Mayes, J. M.; Sen, M.; Brennecke, J. F.; Maginn, E. J. A Computational and Experimental Study of the Heat Transfer Properties of Nine Different Ionic Liquids. *J. Chem. Eng. Data* **2014**, *59* (2), 391–399. <https://doi.org/10.1021/je400858t>.
- (91) Smith, E. L.; Abbott, A. P.; Ryder, K. S.; Osch, V.; Kow, K. K.; Sirat, K. Eutectic Solvent.Pdf. *Chinese Chem. Lett.* **2014**, *26* (10), 1311–1314. <https://doi.org/10.1016/j.ccllet.2015.05.049>.
- (92) Abbott, A. P.; Capper, G.; Davies, D. L.; Rasheed, R. K.; Tambyrajah, V. Novel Solvent Properties of Choline Chloride/Urea Mixtures. *Chem. Commun.* **2003**, *9* (1), 70–71. <https://doi.org/10.1039/b210714g>.
- (93) Abbott, A. P.; Boothby, D.; Capper, G.; Davies, D. L.; Rasheed, R. K. Deep Eutectic Solvents Formed between Choline Chloride and Carboxylic Acids: Versatile Alternatives to Ionic Liquids. *J. Am. Chem. Soc.* **2004**, *126* (29), 9142–9147. <https://doi.org/10.1021/ja048266j>.
- (94) Mbous, Y. P.; Hayyan, M.; Hayyan, A.; Wong, W. F.; Hashim, M. A.; Looi, C. Y. Applications of Deep Eutectic Solvents in Biotechnology and Bioengineering—Promises and Challenges.

- Biotechnol. Adv.* **2017**, *35* (2), 105–134. <https://doi.org/10.1016/j.biotechadv.2016.11.006>.
- (95) Paiva, A.; Craveiro, R.; Aroso, I.; Martins, M.; Reis, R. L.; Duarte, A. R. C. Natural Deep Eutectic Solvents - Solvents for the 21st Century. *ACS Sustain. Chem. Eng.* **2014**, *2* (5), 1063–1071. <https://doi.org/10.1021/sc500096j>.
- (96) Mamilla, J. L. K.; Novak, U.; Grilc, M.; Likozar, B. Natural Deep Eutectic Solvents (DES) for Fractionation of Waste Lignocellulosic Biomass and Its Cascade Conversion to Value-Added Bio-Based Chemicals. *Biomass and Bioenergy* **2019**. <https://doi.org/10.1016/j.biombioe.2018.12.002>.
- (97) Schweiger, A. K.; Ríos-Lombardía, N.; Winkler, C. K.; Schmidt, S.; Morís, F.; Kroutil, W.; González-Sabín, J.; Kourist, R. Using Deep Eutectic Solvents to Overcome Limited Substrate Solubility in the Enzymatic Decarboxylation of Bio-Based Phenolic Acids. *ACS Sustain. Chem. Eng.* **2019**, *7* (19), 16364–16370. <https://doi.org/10.1021/acssuschemeng.9b03455>.
- (98) Zhang, Q.; De Oliveira Vigier, K.; Royer, S.; Jérôme, F. Deep Eutectic Solvents: Syntheses, Properties and Applications. *Chem. Soc. Rev.* **2012**, *41* (21), 7108–7146. <https://doi.org/10.1039/c2cs35178a>.
- (99) Abbott, A. P.; Harris, R. C.; Ryder, K. S. Application of Hole Theory to Define Ionic Liquids by Their Transport Properties. *J. Phys. Chem. B* **2007**, *111* (18), 4910–4913. <https://doi.org/10.1021/jp0671998>.
- (100) Maugeri, Z.; Domínguez De María, P. Novel Choline-Chloride-Based Deep-Eutectic-Solvents with Renewable Hydrogen Bond Donors: Levulinic Acid and Sugar-Based Polyols. *RSC Adv.* **2012**, *2* (2), 421–425. <https://doi.org/10.1039/c1ra00630d>.
- (101) Wolfson, A.; Dlugy, C.; Shotland, Y. Glycerol as a Green Solvent for High Product Yields and Selectivities. *Environ. Chem. Lett.* **2007**, *5* (2), 67–71. <https://doi.org/10.1007/s10311-006-0080-z>.
- (102) Ong, H. R.; Khan, M. M. R.; Ramli, R.; Du, Y.; Xi, S.; Yunus, R. M. Facile Synthesis of Copper Nanoparticles in Glycerol at Room Temperature: Formation Mechanism. *RSC Adv.* **2015**, *5* (31), 24544–24549. <https://doi.org/10.1039/c4ra16919k>.
- (103) Pandey, A.; Rai, R.; Pal, M.; Pandey, S. How Polar Are Choline Chloride-Based Deep Eutectic Solvents? *Phys. Chem. Chem. Phys.* **2014**, *16* (4), 1559–1568. <https://doi.org/10.1039/c3cp53456a>.
- (104) Díaz-Álvarez, A.; Cadierno, V. Glycerol: A Promising Green Solvent and Reducing Agent for Metal-Catalyzed Transfer Hydrogenation Reactions and Nanoparticles Formation. *Appl. Sci.*

- 2013, 3 (1), 55–69. <https://doi.org/10.3390/app3010055>.
- (105) Pagliaro, B. M.; Rossi, M.; Pagliaro, M. Glycerol: Properties and Production. *RSC Green Chem.* **2010**, 1–187.
- (106) Sheldon, R. A. Selective Catalytic Synthesis of Fine Chemicals: Opportunities and Trends. *J. Mol. Catal. A Chem.* **1996**, 107 (1–3), 75–83. [https://doi.org/10.1016/1381-1169\(95\)00229-4](https://doi.org/10.1016/1381-1169(95)00229-4).
- (107) Zahmakiran, M.; Özkar, S. Metal Nanoparticles in Liquid Phase Catalysis; From Recent Advances to Future Goals. *Nanoscale* **2011**, 3 (9), 3462–3481. <https://doi.org/10.1039/c1nr10201j>.
- (108) Tao, A. R.; Habas, S.; Yang, P. Shape Control of Colloidal Metal Nanocrystals. *Small* **2008**, 4 (3), 310–325. <https://doi.org/10.1002/sml.200701295>.
- (109) Nong-Moon Hwang, Jae-Soo Jung and Dong-Kwon Lee (October 3rd 2012). Thermodynamics and Kinetics in the Synthesis of Monodisperse Nanoparticles, Thermodynamics - Fundamentals and Its Application in Science, Ricardo Morales-Rodriguez, IntechOpen, DOI: 10.5772/50324.
- (110) Heiligtag, F. J.; Niederberger, M. The Fascinating World of Nanoparticle Research. *Mater. Today* **2013**, 16 (7–8), 262–271. <https://doi.org/10.1016/j.mattod.2013.07.004>.
- (111) Edwards, P. P.; Thomas, J. M. Gold in a Metallic Divided State - From Faraday to Present-Day Nanoscience. *Angew. Chemie - Int. Ed.* **2007**, 46 (29), 5480–5486. <https://doi.org/10.1002/anie.200700428>.
- (112) Thompson, D. T. Michael Faraday's Recognition of Ruby Gold: The Birth of Modern Nanotechnology. *Gold Bull.* **2008**, 40 (4), 267–269. <https://doi.org/10.1007/BF03215598>.
- (113) Diffusion, L. C 183]. **1861**.
- (114) Kraynov, A.; E., T. Concepts for the Stabilization of Metal Nanoparticles in Ionic Liquids. *Appl. Ion. Liq. Sci. Technol.* **2011**. <https://doi.org/10.5772/22111>.
- (115) Tiwari, J. N.; Tiwari, R. N.; Kim, K. S. Zero-Dimensional, One-Dimensional, Two-Dimensional and Three-Dimensional Nanostructured Materials for Advanced Electrochemical Energy Devices. *Prog. Mater. Sci.* **2012**, 57 (4), 724–803. <https://doi.org/10.1016/j.pmatsci.2011.08.003>.
- (116) Kreyling, W. G.; Semmler-Behnke, M.; Chaudhry, Q. A Complementary Definition of Nanomaterial. *Nano Today* **2010**, 5 (3), 165–168. <https://doi.org/10.1016/j.nantod.2010.03.004>.
- (117) Khan, I.; Saeed, K.; Khan, I. Nanoparticles: Properties, Applications and Toxicities. *Arab. J. Chem.* **2017**. <https://doi.org/10.1016/j.arabjc.2017.05.011>.

- (118) Iravani, S. Green Synthesis of Metal Nanoparticles Using Plants. *Green Chem.* **2011**, *13* (10), 2638–2650. <https://doi.org/10.1039/c1gc15386b>.
- (119) Asensio, J. M.; Tricard, S.; Coppel, Y.; Andrés, R.; Chaudret, B.; de Jesús, E. Knight Shift In¹³C NMR Resonances Confirms the Coordination of N-Heterocyclic Carbene Ligands to Water-Soluble Palladium Nanoparticles. *Angew. Chemie - Int. Ed.* **2017**, *56* (3), 865–869. <https://doi.org/10.1002/anie.201610251>.
- (120) Fievet, F.; Lagier, J. P.; Figlarz, M. Preparing Monodisperse Metal Powders in Micrometer and Submicrometer Sizes by the Polyol Process. *MRS Bull.* **1989**, *14* (12), 29–34. <https://doi.org/10.1557/S0883769400060930>.
- (121) Viau, G.; Ravel, F.; Fiket, F. Preparation and Microwave Characterization of s and Monodisperse Co-Ni Particles. *J. Magn. Magn. Mater.* **1995**, *140–144* (94), 377–378.
- (122) Viau, G.; Fiévet-Vincent, F.; Fiévet, F. Nucleation and Growth of Bimetallic CoNi and FeNi Monodisperse Particles Prepared in Polyols. *Solid State Ionics* **1996**, *84* (3–4), 259–270. [https://doi.org/10.1016/0167-2738\(96\)00005-7](https://doi.org/10.1016/0167-2738(96)00005-7).
- (123) Fievet, F.; Fievet-Vincent, F.; Lagler, J. P.; Dumont, B.; Figlarz, M. Controlled Nucleation and Growth of Micrometre-Size Copper Particles Prepared by the Polyol Process. *J. Mater. Chem.* **1993**, *3* (6), 627–632. <https://doi.org/10.1039/jm9930300627>.
- (124) Fievet, F.; Ammar-Merah, S.; Brayner, R.; Chau, F.; Giraud, M.; Mammeri, F.; Peron, J.; Piquemal, J. Y.; Sicard, L.; Viau, G. The Polyol Process: A Unique Method for Easy Access to Metal Nanoparticles with Tailored Sizes, Shapes and Compositions. *Chem. Soc. Rev.* **2018**, *47* (14), 5187–5233. <https://doi.org/10.1039/c7cs00777a>.
- (125) Hachani, R.; Lowdell, M.; Birchall, M.; Hervault, A.; Mertz, D.; Begin-Colin, S.; Thanh, N. T. B. D. K. Polyol Synthesis, Functionalisation, and Biocompatibility Studies of Superparamagnetic Iron Oxide Nanoparticles as Potential MRI Contrast Agents. *Nanoscale* **2016**, *8* (6), 3278–3287. <https://doi.org/10.1039/c5nr03867g>.
- (126) Dong, H.; Chen, Y. C.; Feldmann, C. Polyol Synthesis of Nanoparticles: Status and Options Regarding Metals, Oxides, Chalcogenides, and Non-Metal Elements. *Green Chem.* **2015**, *17* (8), 4107–4132. <https://doi.org/10.1039/c5gc00943j>.
- (127) Carroll, K. J.; Reveles, J. U.; Shultz, M. D.; Khanna, S. N.; Carpenter, E. E. Preparation of Elemental Cu and Ni Nanoparticles by the Polyol Method: An Experimental and Theoretical Approach. *J. Phys. Chem. C* **2011**, *115* (6), 2656–2664. <https://doi.org/10.1021/jp1104196>.
- (128) Chahdoura, F.; Mallet-Ladeira, S.; Gómez, M. Palladium Nanoparticles in Glycerol: A Clear-

- Cut Catalyst for One-Pot Multi-Step Processes Applied in the Synthesis of Heterocyclic Compounds. *Org. Chem. Front.* **2015**, 2 (4), 312–318. <https://doi.org/10.1039/c4qo00338a>.
- (129) Chahdoura, F.; Pradel, C.; Gómez, M. Copper(I) Oxide Nanoparticles in Glycerol: A Convenient Catalyst for Cross-Coupling and Azide-Alkyne Cycloaddition Processes. *ChemCatChem* **2014**, 6 (10), 2929–2936. <https://doi.org/10.1002/cctc.201402214>.
- (130) Chahdoura, F.; Pradel, C.; Gómez, M. Palladium Nanoparticles in Glycerol: A Versatile Catalytic System for C-X Bond Formation and Hydrogenation Processes. *Adv. Synth. Catal.* **2013**, 355 (18), 3648–3660. <https://doi.org/10.1002/adsc.201300753>.
- (131) Favier, I.; Pla, D.; Gómez, M. Metal-Based Nanoparticles Dispersed in Glycerol: An Efficient Approach for Catalysis. *Catal. Today* **2018**, 310 (June 2017), 98–106. <https://doi.org/10.1016/j.cattod.2017.06.026>.
- (132) Reina, A.; Pradel, C.; Martin, E.; Teuma, E.; Gómez, M. Palladium Nanoparticles Stabilised by Cinchona-Based Alkaloids in Glycerol: Efficient Catalysts for Surface Assisted Processes. *RSC Adv.* **2016**, 6 (95), 93205–93216. <https://doi.org/10.1039/c6ra19230k>.
- (133) Chahdoura, F.; Favier, I.; Gómez, M. Glycerol as Suitable Solvent for the Synthesis of Metallic Species and Catalysis. *Chem. - A Eur. J.* **2014**, 20 (35), 10884–10893. <https://doi.org/10.1002/chem.201403534>.
- (134) Gao, Y.; Voigt, A.; Zhou, M.; Sundmacher, K. Synthesis of Single-Crystal Gold Nano- and Microprisms Using a Solvent-Reductant-Template Ionic Liquid. *Eur. J. Inorg. Chem.* **2008**, No. 24, 3769–3775. <https://doi.org/10.1002/ejic.200800467>.
- (135) Favier, I.; Madec, D.; Gómez, M. Metallic Nanoparticles in Ionic Liquids - Applications in Catalysis. *Nanomater. Catal. First Ed.* **2012**, 203–249. <https://doi.org/10.1002/9783527656875.ch5>.
- (136) Konakom, K.; Kittisupakorn, P.; Mujtaba, I. M. Neural Network-Based Controller Design of a Batch Reactive. *2011 Int. Symp. Adv. Control Ind. Process.* **2011**, No. March, 361–377. <https://doi.org/10.1002/apj>.
- (137) Dash, P.; Miller, S. M.; Scott, R. W. J. Stabilizing Nanoparticle Catalysts in Imidazolium-Based Ionic Liquids: A Comparative Study. *J. Mol. Catal. A Chem.* **2010**, 329 (1–2), 86–95. <https://doi.org/10.1016/j.molcata.2010.06.022>.
- (138) Carnie, S. L.; Chan, D. Y. C. Interaction Free Energy between Plates with Charge Regulation: A Linearized Model. *Journal of Colloid And Interface Science.* 1993, pp 260–264. <https://doi.org/10.1006/jcis.1993.1464>.

- (139) Wittmar, A.; Ruiz-Abad, D.; Ulbricht, M. Dispersions of Silica Nanoparticles in Ionic Liquids Investigated with Advanced Rheology. *J. Nanoparticle Res.* **2012**, *14* (2), 1–10. <https://doi.org/10.1007/s11051-011-0651-1>.
- (140) Shapter, J. *Nanoscale Materials in Chemistry*(Ed. Kenneth J. Klabunde); 2002; Vol. 55. https://doi.org/10.1071/ch02005_br.
- (141) Henry, C. R. ChemInform Abstract: Catalytic Activity of Supported Nanometer-Sized Metal Clusters. *ChemInform* **2010**, *31* (44), no-no. <https://doi.org/10.1002/chin.200044276>.
- (142) Schauermaun, S.; Nilius, N.; Shaikhutdinov, S.; Freund, H. J. Nanoparticles for Heterogeneous Catalysis: New Mechanistic Insights. *Acc. Chem. Res.* **2013**, *46* (8), 1673–1681. <https://doi.org/10.1021/ar300225s>.
- (143) Alshammari, A.; Kalevaru, V. N.; Martin, A. Metal Nanoparticles as Emerging Green Catalysts. *Green Nanotechnol. - Overv. Furth. Prospect.* **2016**. <https://doi.org/10.5772/63314>.
- (144) Abatzoglou, N.; Dalai, A. K.; Gitzhofer, F. Green Diesel from Fischer–Tropsch Synthesis: Challenges and Hurdles. *Proc. 3rd IASME/ ...* **2007**, 223–232.
- (145) Bezemer, G. L.; Bitter, J. H.; Kuipers, H. P. C. E.; Oosterbeek, H.; Holewijn, J. E.; Xu, X.; Kapteijn, F.; Van Diilen, A. J.; De Jong, K. P. Cobalt Particle Size Effects in the Fischer-Tropsch Reaction Studied with Carbon Nanofiber Supported Catalysts. *J. Am. Chem. Soc.* **2006**, *128* (12), 3956–3964. <https://doi.org/10.1021/ja058282w>.
- (146) Kang, J.; Zhang, S.; Zhang, Q.; Wang, Y. Ruthenium Nanoparticles Supported on Carbon Nanotubes as Efficient Catalysts for Selective Conversion of Synthesis Gas to Diesel Fuel. *Angew. Chemie - Int. Ed.* **2009**, *48* (14), 2565–2568. <https://doi.org/10.1002/anie.200805715>.
- (147) Rönsch, S.; Schneider, J.; Matthischke, S.; Schlüter, M.; Götz, M.; Lefebvre, J.; Prabhakaran, P.; Bajohr, S. Review on Methanation - From Fundamentals to Current Projects. *Fuel.* 2016. <https://doi.org/10.1016/j.fuel.2015.10.111>.
- (148) Han, J.; Jia, H.; Yang, Z.; Fan, Q.; Zhang, F. Confined Hexahedral Nickel Nanoparticle Catalyst for Catalytic Hydrogenation Reaction. *J. Mater. Sci.* **2018**, *53* (7), 4884–4896. <https://doi.org/10.1007/s10853-017-1934-4>.
- (149) Qu, R.; Macino, M.; Iqbal, S.; Gao, X.; He, Q.; Hutchings, G. J.; Sankar, M. Supported Bimetallic AuPd Nanoparticles as a Catalyst for the Selective Hydrogenation of Nitroarenes. *Nanomaterials* **2018**, *8* (9). <https://doi.org/10.3390/nano8090690>.
- (150) Dang-Bao, T.; Pradel, C.; Favier, I.; Gómez, M. Making Copper(0) Nanoparticles in Glycerol: A Straightforward Synthesis for a Multipurpose Catalyst. *Adv. Synth. Catal.* **2017**, *359* (16),

- 2832–2846. <https://doi.org/10.1002/adsc.201700535>.
- (151) Zaera, F. The Surface Chemistry of Metal-Based Hydrogenation Catalysis. *ACS Catal.* **2017**, *7* (8), 4947–4967. <https://doi.org/10.1021/acscatal.7b01368>.
- (152) Morley, K. S.; Licence, P.; Marr, P. C.; Hyde, J. R.; Brown, P. D.; Mokaya, R.; Xia, Y.; Howdle, S. M. Supercritical Fluids: A Route to Palladium-Aerogel Nanocomposites. *J. Mater. Chem.* **2004**, *14* (7), 1212–1217. <https://doi.org/10.1039/b311065f>.
- (153) Jespersen, H. T.; Štandeker, S.; Novak, Z.; Schaumburg, K.; Madsen, J.; Knez, Ž. Supercritical Fluids Applied to the Sol-Gel Process for Preparation of AEROMOSILS/Palladium Particle Nanocomposite Catalyst. *J. Supercrit. Fluids* **2008**, *46* (2), 178–184. <https://doi.org/10.1016/j.supflu.2008.04.013>.
- (154) Aygün, M.; Stoppiello, C. T.; Lebedeva, M. A.; Smith, E. F.; Gimenez-Lopez, M. D. C.; Khlobystov, A. N.; Chamberlain, T. W. Comparison of Alkene Hydrogenation in Carbon Nanoreactors of Different Diameters: Probing the Effects of Nanoscale Confinement on Ruthenium Nanoparticle Catalysis. *J. Mater. Chem. A* **2017**, *5* (40), 21467–21477. <https://doi.org/10.1039/c7ta03691d>.
- (155) Sajiki, H.; Hattori, K.; Hirota, K. The Formation of a Novel Pd/C-Ethylenediamine Complex Catalyst: Chemoselective Hydrogenation without Deprotection of the o-Benzyl and ZV-Cbz Groups. *J. Org. Chem.* **1998**, *63* (22), 7990–7992. <https://doi.org/10.1021/jo9814694>.
- (156) Lee, B. Il; Bae, D.; Kang, J. K.; Kim, H.; Byeon, S. H. Synthesis of SBA-15 Supported Rh Nanoparticles with High Loading Density and Its Catalytic Hydrogenation of Phenol in Supercritical Carbon Dioxide. *Bull. Korean Chem. Soc.* **2009**, *30* (8), 1701–1702. <https://doi.org/10.5012/bkcs.2009.30.8.1701>.
- (157) Lee, S. S.; Park, B. K.; Byeon, S. H.; Chang, F.; Kim, H. Mesoporous Silica-Supported Pd Nanoparticles; Highly Selective Catalyst for Hydrogenation of Olefins in Supercritical Carbon Dioxide. *Chem. Mater.* **2006**, *18* (24), 5631–5633. <https://doi.org/10.1021/cm061060s>.

Chapter 2

Viscosity Measurements using Molecular Rotors

2.1. Introduction

Viscosity is a measure of a fluid's resistance to flow. It describes the internal friction of a moving fluid. Viscosity is the property of a fluid that offers resistance to the movement of one layer of fluid over an adjacent layer.

Viscosity of fluids used in a chemical process is crucial from processes design and optimization points of view as it defines the mass transfer properties of a substance. Liquids, for example, ionic liquids and polyols (such as glycerol), possess in general high viscosity (2-3 times higher than usual organic solvents),¹ which decreases mass transfer efficiency (Table 2.1). In 1980, Manger and Ponters published results showing the decreasing of mass transfer coefficient (k_La) with increasing viscosity of carbon dioxide into pure water and aqueous glycerol mixtures.² The rate of mass transfer is proportional to the concentration difference of the compound and the interfacial transfer area, the proportionality constant in equation 2.1 is defined as mass transfer coefficient (k_La).³

$$N_1 = k_La(c_{1i} - c_1) \quad \text{Equation 2.1}$$

where, N_1 is the rate of transferred mass per area at the interface, c_{1i} is the concentration at the interphase of the phase and c_1 is the concentration at the bulk of phase. Chen *et al.* proposed a correlation for mass transfer coefficient for both Newtonian⁴ and non-Newtonian fluids.⁴ Mass transfer coefficient k_La defined by is:⁵

$$k_La = \frac{Q_L}{\pi(r_o^2 - r_i^2)} \frac{\ln\left[\left(1 - \frac{1}{S}\right)\frac{x_i + \frac{1}{S}}{x_o + \frac{1}{S}}\right]}{1 - \frac{1}{S}} \quad \text{Equation 2.2}$$

where, Q_L is the liquid flow rate, r_o and r_i are the outer and inner radius (respectively) of the packed bed, S is the stripping factor defined as $S = (HQ_G)/Q_L$ with H as Henry's constant and Q_G as gas flow rate. x_o and x_i are mole fractions of solute in the outlet and inlet liquid stream respectively. Based on equation 2.2, they stated that an increase in liquid viscosity would lead to a slower flow of the liquid, a smaller degree of liquid mixing at the packing junction, and thicker liquid films, which causes the decrease in mass transfer efficiency.⁶

As stated above, it is important to overcome the viscosity issues in order to solve the problems of mass transfer. In this context, gas-expanded liquids (GXLs) have emerged as an innovative solution because it is possible to change the viscosity of GXLs by changing the operating pressure of the gas dissolved. The definition of GXLs is well reported in the review

by B. Subramaniam and P. G. Jessop.⁷ When gases, such as carbon dioxide, and light hydrocarbons (propylene, ethylene) are mildly compressed at ambient temperatures, they attain liquid-like densities and can be dissolved in most conventional solvents creating a GXL phase.⁷

Table 2.1. Viscosities of some selected solvents at 25 °C.

| Solvent | Viscosity (mPa.s) |
|---|-------------------|
| Acetone | 0.32 |
| Benzene | 0.56 |
| Dichloromethne | 0.79 |
| Water | 1.00 |
| Ethylene glycol | 19.83 |
| Choline hydroxide | 25.30 |
| 1-Decyl-3-methylimidazolium bis(trifluoro- methylsulfonyl)imide | 90.06 |
| Glycerol | 1412 |

Maroncelli *et al.* have simulated the transport properties of CO₂-expanded liquids. They reported translational diffusion coefficients, rotational correlation times and shear viscosities of the liquids as function of CO₂ mole fraction.^{8–10} Granero-Fernandez *et al.* have performed a physicochemical and molecular study on CO₂-expanded alkyl acetates.¹¹ Both teams found a significant decrease in the viscosity with increasing amounts of CO₂. This decrease in viscosity at the expanded state improves the mass transport for these alkyl acetates as compared to other organic liquids. Water does not have ability to dissolve sufficient CO₂; hence, no viscosity change is observed and on the other hand, viscosity of methanol can be varied from 0.6 cP to less than 0.1 cP (at 25 °C) by increasing the amount of CO₂.^{7,12,13} Similar results were reported by Lin *et al.* for the measurement of the diffusion coefficient of benzonitrile in the CO₂-expanded ethanol. They found that the diffusion coefficient increased with increasing the amount of CO₂. This indicated that as the amount of CO₂ increases, more CO₂ is dissolved in ethanol. This leads to reduction of collision between molecules and decrease in viscosity and density, favoring the diffusion of benzonitrile in liquid.¹⁴

As it has been stated, the study of viscosity is key in highly viscous systems. In this context, the conventional methods to measure viscosity from the beginning of the 20th century until date includes the use of instrumentations like capillary viscometer, the falling ball viscometer, rheometer among others, which are mechanical methods.^{15–17} As stated by Haidekker and Theodorakis, all mechanical methods have in common that the fluid is subjected to shear forces, and the resistance of the fluid to these forces (internal friction) is measured.¹⁸ The internal friction of a fluid is proportional to the dynamic viscosity and the velocity gradient (*i.e.*, the shear rate) between layers of different velocities.¹⁸ In 1936, Bacon reported the measurement of absolute viscosity by the falling sphere viscometer,¹⁹ and on the other hand, Topham in 1972 reported a rising sphere rheometer;²⁰ both of them working on the same principle of determining viscosity of viscous Newtonian fluids by measuring the rate of fall of a sphere through the liquid. However, these conventional methods are focused on measuring the bulk macroscopic viscosity. The microscopic viscosity is one of the key parameters that controls the diffusion rate of molecular species and hence affects the reaction rates of diffusion-controlled processes on the microscopic level.²¹

Molecular rotors have emerged as one the most innovative methods to measure the viscosity at the micro-scale.^{21–23} Molecular rotors are in general fluorophores that form twisted intramolecular charge transfer (TICT) states upon photoexcitation. Thus, depending upon the viscosity of the system, they can exhibit two de-excitation pathways: (1) fluorescence emission and (2) non-radiative de-excitation.¹⁸

2.2. Molecular rotors

In 1973, Rotkiewicz, Grellmann and Grabowski formulated a structural hypothesis for “inner-charge transfer” for the reinterpretation of the anomalous fluorescence of *p-N,N*-dimethylamino-benzonitrile.²⁴ Later, based on various studies by Mataga *et al.*²⁵ Grabowski coined the term twisted intramolecular charge transfer or TICT for electronic structures in which an electron transfer occurs upon photoexcitation in molecules constituted by a donor (D) and an acceptor (A) moiety linked by a single bond.^{24,26,27}

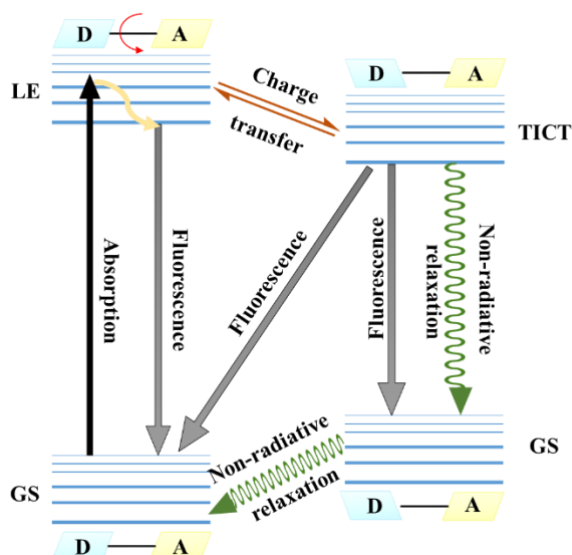


Figure 2.1. Jablonski diagram of electron donor-acceptor (D–A) system for TICT dynamics. GS = ground state; LE = locally excited state. Reproduced from Ref. (28) with permission from the Royal Society of Chemistry.

TICT governs the phenomena of fluorescence in fluorophores. The electron transfer is accompanied by intramolecular D-A twisting around the single bond (Figure 2.1) and produces a relaxed perpendicular structure. The equilibration between a relaxed perpendicular conformer and a coplanar conformer often results in dual fluorescence, *i.e.* from a high-energy band through relaxation of the locally excited (LE) state and from a lower energy band due to emission from the TICT state.²⁸

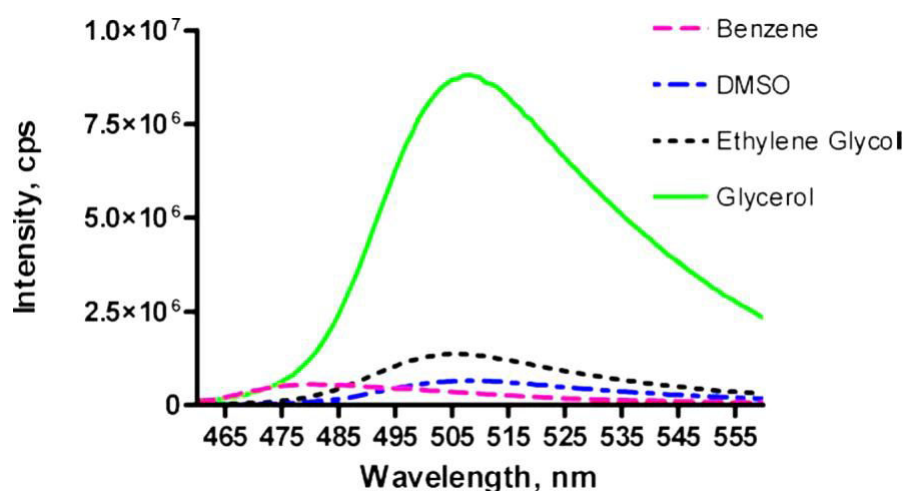


Figure 2.2. Emission spectra of 9-(dicyanovinyl)julolidine (DCVJ) in some selected solvents. Reprinted from reference (29), Copyright (2005), with permission from Elsevier.

Since the relaxation pathways can easily be modulated by substituents, local polarity and steric restrictions, the TICT process can be exploited for novel design strategies of functional molecules.^{30–32} One of the major applications and our focus of interest, however, is molecular rotors. As mentioned above, molecular rotors are fluorophores that exhibit TICT on photoexcitation consequently giving fluorescence or non-radiative emission on de-excitation. One of the most commonly known molecular rotor is 9-(dicyanovinyl)julolidine (DCVJ). Reed *et al.* have described DCVJ as a fluorescent dye whose intramolecular rotational relaxation depends on the nature of the solvent.^{33,34} Figure 2.2 shows the emission spectra of DCVJ in different solvents.²⁹ In the case of DCVJ, on photoexcitation, the electron pair on the julolidine nitrogen is transferred to one of the nitrile group that induces TICT in the molecule (Figure 2.3). The intermolecular rotation caused within the molecule is governed by the molecular-free volume of the solvent. This implies that when the solvent is viscous the molecule is sterically hindered to rotate, in this case, the relaxation shifts towards higher radiative rates.²⁸ In other words, we can say that more is the viscosity, less is the molecular-free volume hence more is the fluorescence intensity.

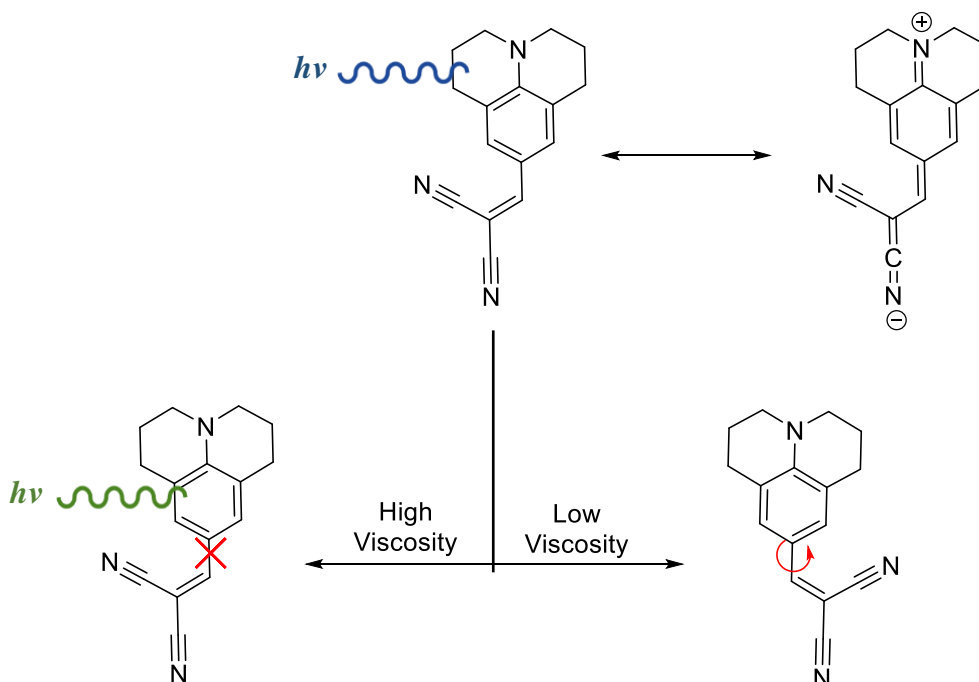


Figure 2.3. Schematic diagram showing how DCVJ works under irradiation.

Many scientists are now working on the development of synthetic molecular rotors. Ibarra-Rodríguez *et al.* have synthesized molecular rotors of organoboron compounds from Schiff

bases (Figure 2.4) and have successfully proven that the fluorescence quantum yield increases strongly with increasing solvent viscosity (Figure 2.5).³⁵

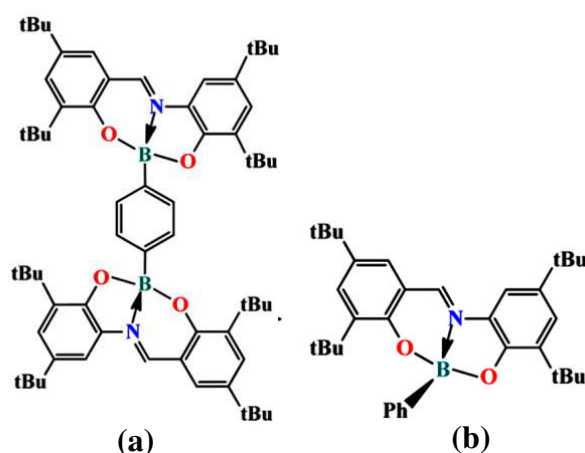


Figure 2.4. Organoboronic molecular rotors synthesized from Schiff bases. Adapted with permission from reference (35). Copyright (2017) American Chemical Society.

The observed increase in fluorescence intensity is consistent with the restricted rotation of the phenyl bonded to the boron atom in the medium of high viscosity and dissipated energy by intramolecular rotation, and the photoactivated molecule may relax by a non-radiative decay process.³⁵

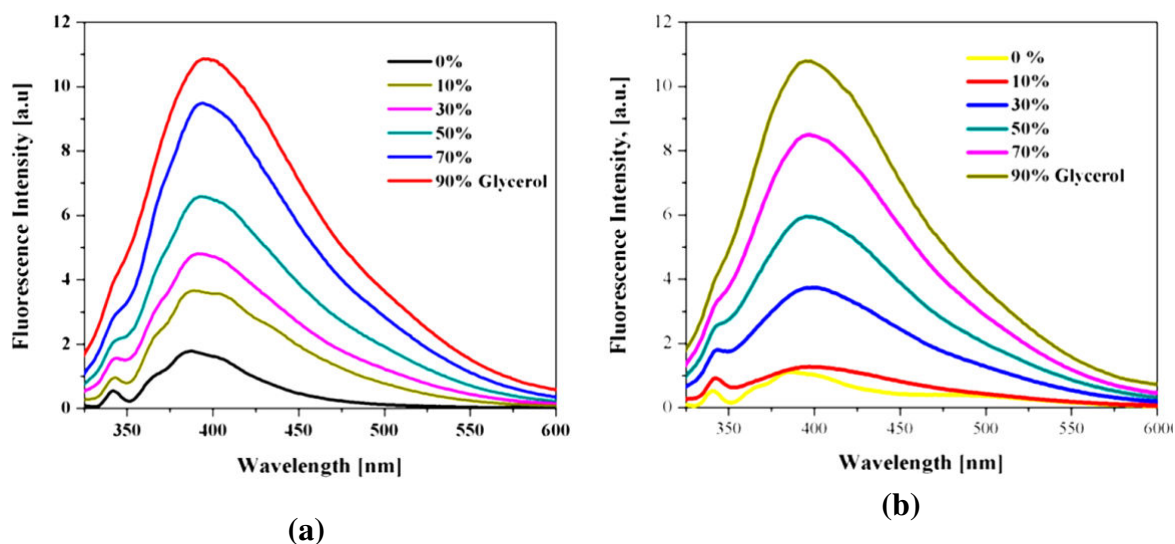


Figure 2.5. Fluorescence spectra exhibited by molecular rotors (a, left) and (b, right) shown in Figure 2.4, synthesized from Schiff bases in binary mixtures of methanol and glycerol in different ratios. Adapted with permission from reference (35). Copyright (2017) American Chemical Society.

Very recently, Jin *et al.* used tetraphenylethylene (TPE) derivatives with different-length alkyl chains for viscosity measurements of hydrocarbon and silicone oil fluids (Figure 2.6). They successfully determined the viscosity using these molecular rotors.³⁶

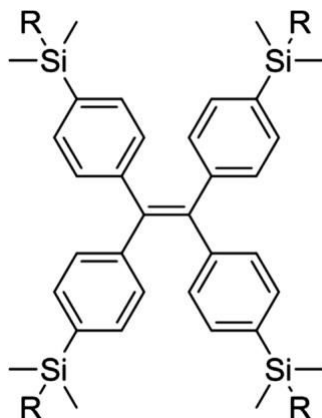


Figure 2.6. Chemical structures of TPE derivatives (R = *n*-octadecyl, *n*-octyl and methyl).

Reprinted from reference (35), Copyright (2019), with permission from Elsevier.

In the next section, we present the study on the viscosity measurement of DES synthesized using choline-based amino acid and glycerol. The viscosity was measured at different temperatures and different pressures of CO₂ by using DCVJ and 4,4'-difluoro-4-bora-3a,4a-diaza-*s*-indacene (BODIPY) - based molecular rotors (Figure 2.7). In other words, we discuss in detail the changes in viscosity of DES with changing amounts of CO₂. An $x - y$ equation obtained from a calibration curve has been used to calculate the viscosity using the fluorescence intensity (Equation 2.3).³²⁻³⁷

$$\log y = \log k + m \log x \quad \text{or} \quad y = kx^m \quad \text{Equation 2.3}$$

where, y is the fluorescence intensity obtained from the molecular rotor and x is the calculated viscosity. The plot of $\log y$ as a function of $\log x$ yields a straight line with a slope of m . The straight line, typically observed only in the intermediate range of viscosities (15-1000 cP), serves as a calibration plot for molecular rotors. The intercept of the line gives information about the radiative rate constant, k for the molecule.

In the context of our work, Lu *et al.* investigated the solvent properties of mixtures of 1-butyl-3-methylimidazolium hexafluorophosphate ([bmim][PF₆]) and CO₂ as functions of temperature (range: 35-50 °C) and CO₂ pressure (range: 0-230 bar). They concluded that the effect of added CO₂ on the microviscosity might be significant for promoting mass transport and facilitating separation for viscous room temperature ionic liquids.³⁷

2.3. Experimental Section

2.3.1. Materials and methods

Unless otherwise stated, all chemical reagents were obtained from commercial suppliers and used without further purification. 9-(2,2-Dicyanovinyl)julolidine was taken from Sigma-Aldrich with 97% purity. All manipulations were performed using Schlenk techniques under argon atmosphere. Glycerol was dried under vacuum at 80 °C for 18 h prior to use. Choline tosylalaninate was prepared following reported methodology.³⁸ TA INSTRUMENTS DSC Q2000 was used for Differential scanning calorimetry to measure the melting point of the DES. Bulk viscosity was measured using the Rheometer AR2000Ex from TA Instruments. Three molecular rotors were tested: commercial rotor DCVJ (to complete,); and 2 BODIPY-derived rotors which were synthesized by the group of Pr. Norberto Farfan, at the Facultad de Química of the Universidad Nacional Autónoma de México (UNAM).^{35,39–41} Details on the characterization of these compounds are given in Annex 1. Synthesis details are out of the scope of this thesis, where the purpose is the utilization of these rotors as microviscosity probes (Figure 2.7); for convenience, molecular rotors are called **MR1** and **MR2**.

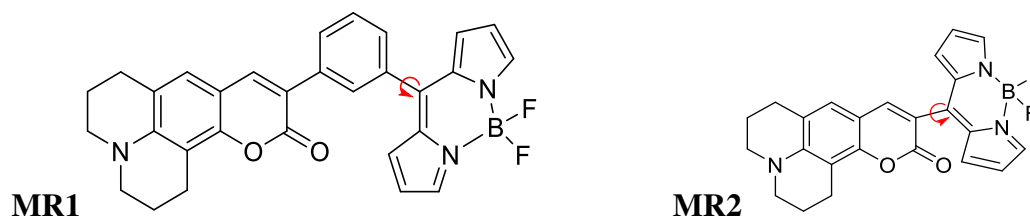


Figure 2.7. Structures of BODIPY-based molecular rotors.

2.3.2. Synthesis of choline *N*-tosylalaninate (ChTs-ala)

Choline hydroxide (103 mg, 0.85 mol, 46 wt.% in H₂O) was stirred with an aqueous solution of *N*-tosylalanine (206 mg, 0.85 mmol) at 60 °C for 12 h. After the ion exchange reaction, water was evaporated under vacuum at 80 °C, obtaining a brownish viscous oil (294.1 mg, 99.9%). ChTs-ala was obtained as a racemic mixture. ¹H NMR (300 MHz, DMSO-*d*₆) δ 7.72 – 7.61 (m, 2H), 7.35 – 7.22 (m, 2H), 4.08 – 3.96 (m, 2H), 3.69 – 3.60 (m, 1H), 3.50 – 3.44 (m, 2H), 3.19 – 3.12 (m, 9H), 2.29 (s, 3H), 1.20 (d, *J* = 7.2 Hz, 3H). ¹³C NMR (75 MHz, DMSO-*d*₆) δ 172.6, 142.4, 137.8, 129.5, 126.6, 67.0, 67.0, 66.9, 55.1, 53.2, 53.1, 53.1, 52.1 20.9, 19.6. HR-MS (ESI+) for C₅H₁₄NO⁺: theoretical = 104.1075, experimental = 104.1072; HR-MS (ESI-) for

$C_{10}H_{12}NO_4S^-$: theoretical = 242.0487, experimental = 242.0483. IR (ATR, cm^{-1}): 3256, 3045, 2954, 2922, 2866, 2853, 2427, 1718, 1598, 1456, 1397, 1324, 1221, 1093, 958, 884, 816, 708, 662. Viscosity 3054 Pa.s at 25 °C and 2.973 Pa.s at 80 °C.

2.3.3. Preparation of Deep Eutectic Solvent (DES)

20 mL of glycerol was mixed with 3.4 mmol (1.17 g) of choline tosylalaninate in a Schleck at 80 °C for 1 h under inert atmosphere. A light brownish viscous liquid was formed. Differential scanning calorimetry was done to determine the melting point of the DES. Unfortunately, the melting point could not be determined as the melting point expected for this kind of DES was out of range from the DSC instrument used.

2.3.4. Determination of Viscosity of the DES at increasing pressure of CO₂

A stainless steel cell of 5 mL with four sapphire windows was used for fluorescence spectroscopy determinations. The windows were sealed with Teflon gasket joints capable of withstanding pressures exceeding 350 bar. The temperature control unit for the cell consisted of heating cartridges inserted into the body, probes, and a temperature controller. A magnetic stirrer was used to agitate the contents in the cell throughout measurements to facilitate equilibrium. The cell was completely filled with the above prepared DES and the molecular rotor solution depending on the experiment (concentration of DCVJ, **MR1** and **MR2**: $1.12 \times 10^{-4} \text{ mmolL}^{-1}$, $1.12 \times 10^{-4} \text{ mmolL}^{-1}$ and $1.12 \times 10^{-4} \text{ mmolL}^{-1}$ respectively), then the cell was tightly closed. A UV-source and a fluorescent detector were placed on adjacent windows of the cell making them orthogonal to each other (Figure 2.8). A StellarInc spectrophotometer was used to record the detected fluorescence on a computer. This experiment was done at three different temperatures: 40 °C, 60 °C and 80 °C. Each time, the cell was filled with a certain pressure of CO₂ and rested until an equilibrium between DES and CO₂ was achieved. A calibration curve was used to determine the viscosity from the fluorescence measurements described in next section (see Annex 2).

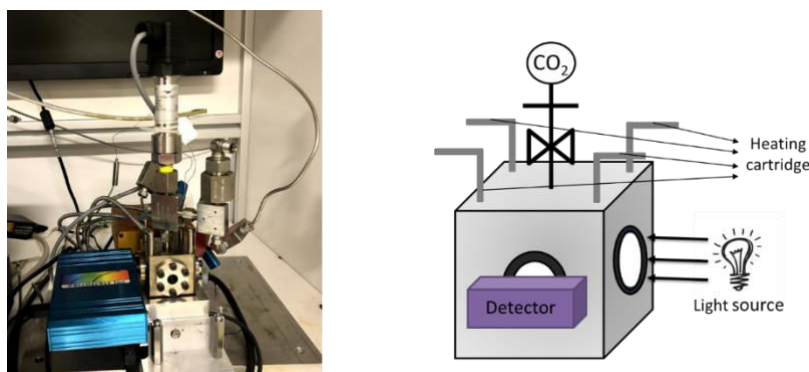


Figure 2.8. Set-up (actual (left); schematic (right)) of the high-pressure cell for the measurement of the fluorescence

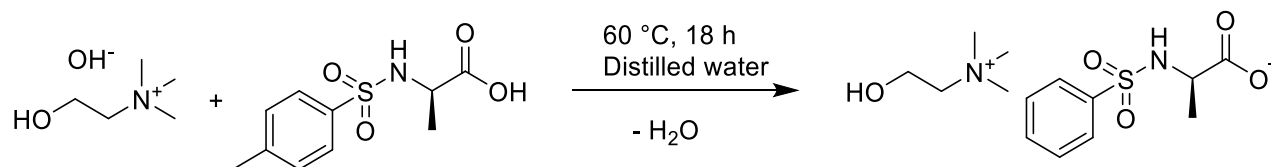
2.3.5. Calibration of molecular rotors

Four solutions of different viscosity were prepared using mixtures of glycerol:ethylene glycol in the ratio of 1:0, 8:2, 6:4 and 4:6. The viscosities of these four solutions were measured using a rheometer at 40 °C, 60 °C and 80 °C. Molecular rotors (concentration of DCVJ, **MR1** and **MR2**: $1.12 \times 10^{-4} \text{ mmolL}^{-1}$, $1.12 \times 10^{-4} \text{ mmolL}^{-1}$ and $1.12 \times 10^{-4} \text{ mmolL}^{-1}$ respectively) were added to each one of these solutions and then fluorescence was recorded using the procedure mentioned in section 2.5.4 (see below) at 40 °C, 60 °C and 80 °C. A $x - y$ graph was plotted for the three different temperatures using the viscosity from the rheometer measurements to the corresponding fluorescence obtained from the molecular rotors. The calibration curves of DCVJ, **MR1** and **MR2** are reported in Annex 2 Part 1, Part 2 and Part 3 respectively.

2.4. Results and Discussion

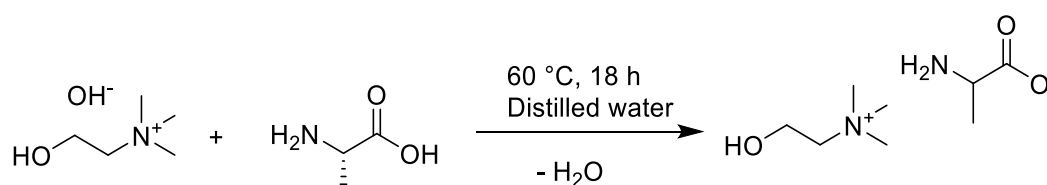
2.4.1. Synthesis of Choline tosylalaninate (ChTs-ala)

The ionic liquid choline tosylalaninate (ChTs-ala) was prepared based on the reported methodology for the preparation of choline carboxylate ionic liquids (see Experimental section 2.3.2) (Scheme 2.1).³⁸ After the ion exchange reaction, water was evaporated under vacuum at 80 °C, obtaining a brownish viscous oil of ChTs-ala was obtained as a racemic mixture, as proven by the optical activity obtained; $[\alpha]_D = +0.002$. The ChTs-ala was dissolved in glycerol in a ratio of 1:100, in order to synthesize the corresponding Deep Eutectic Solvent (DES). It was important to wash the resulting solution with dichloromethane in order to remove any insoluble IL from glycerol phase.

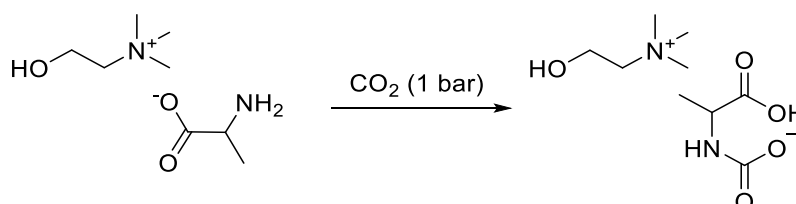


Scheme 2.1. Synthesis of choline tosylalaninate (ChTs-ala).

The use of choline alaninate was envisaged (Scheme 2.2),⁴² instead of the protected anion *N*-tosylalaninate; however, choline alaninate became unstable under atmospheric conditions, due to its high reactivity with carbon dioxide, giving the corresponding carbamate (Scheme 2.3).⁴³



Scheme 2.2. Synthesis of choline alaninate.



Scheme 2.3. Formation of choline *N*-alanine carbamate from choline alaninate in the presence of CO₂.

2.4.2. Determination of viscosity using DCVJ

Viscosity of the above-prepared DES was determined using DCVJ. The procedure to determine the viscosity using DCVJ has been described in the experimental section 2.3.4 and 2.3.5 Figure 2.9 gives the value of viscosity measured by using DCVJ as molecular rotors at 40 °C, 60 °C and 80 °C.

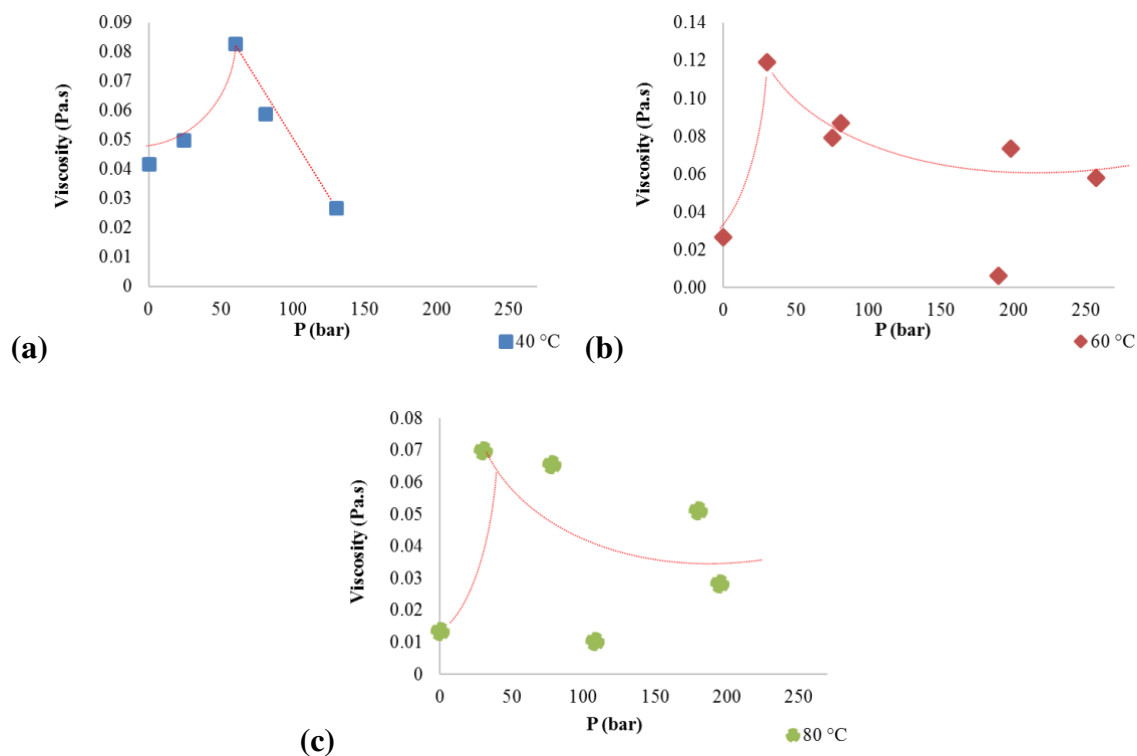


Figure 2.9. Determination of viscosity using DCVJ as molecular rotor at (a) 40 °C, (b) 60 °C and (c) 80 °C.

As reported in literature, it would be expected that with increasing pressure of CO₂ the viscosity of the DES should decrease. However, in this case we observe an initial increase in the viscosity before the viscosity decrease at higher pressure. The reasoning proposed behind this was that initially when CO₂ is added in the system, it starts to fill up the space between the molecules making the mass transfer more difficult. However, as the pressure is increased these spaces starts to expand resulting in a viscosity decrease.^{10,44} It is to note the second increase in viscosity observed at around 200 bar could probably due to experimental error. This behaviour was reproducible when different experiments where performed at different temperatures.

2.4.3. Determination of viscosity using BODIPY-based molecular rotors

MR1 was tested for the measurement of viscosity of the DES in the similar fashion as above. The viscosity measurement was first carried out at 80 °C and the results were compared with that of DCVJ and **MR2** (see below). Figure 2.11 gives the value of viscosity measured by using **MR1** as molecular rotors at 80 °C. As can be seen in this figure, the viscosity trend of **MR1** does not correlate with that of DCVJ and **MR2**. Additionally, the calibration curve obtained for

MR1 was also not linear; hence, the results obtained from **MR1** cannot be quantified (Annex 2, part 2). The possible reason for this error might be the experimental set-up.

Additionally, from ^{19}F and ^{11}B NMR spectra of **MR1**, it was seen that this molecular rotor contains 12% of BF_4^- salt as impurity (probably NaBF_4) (Figure 2.10). However, this impurity is not fluorescent then it is expected that is not affecting the fluorescence from **MR1**.

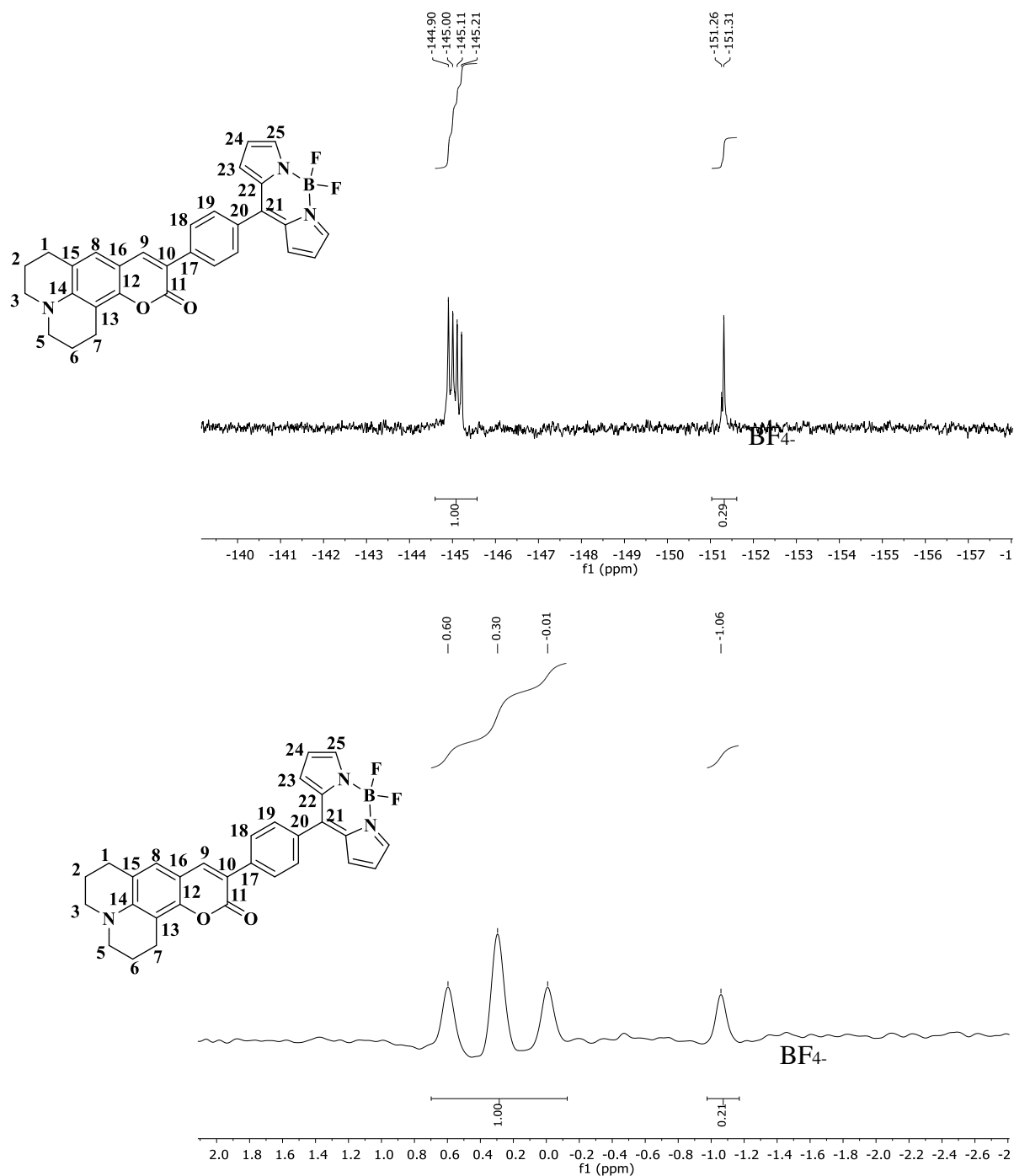


Figure 2.10. ^{19}F NMR (282 MHz, CDCl_3) spectrum of **MR1** showing BF_4^- salt impurity (top). ^{11}B NMR (96 MHz, CDCl_3) spectrum of **MR1** showing BF_4^- salt impurity (bottom).

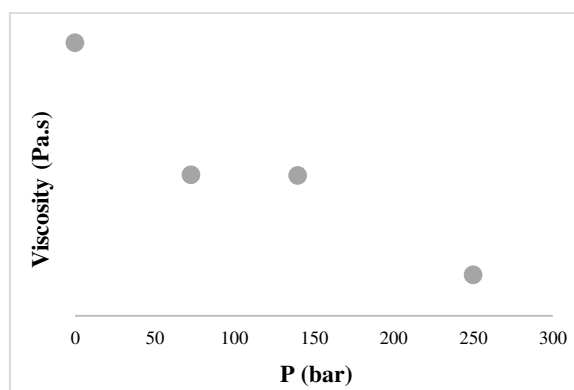


Figure 2.11. Determination of viscosity using **MR1** as molecular rotor at 80 °C.

In the next step, viscosity of the DES has been measured using **MR2** (Figure 2.12). The behavior is similar to that obtained with DCVJ; it means an initial increase in the viscosity before going on to viscosity decrease at higher pressure. These observations verify that BODIPY-based molecular rotors can be used as a tool to measure viscosity.

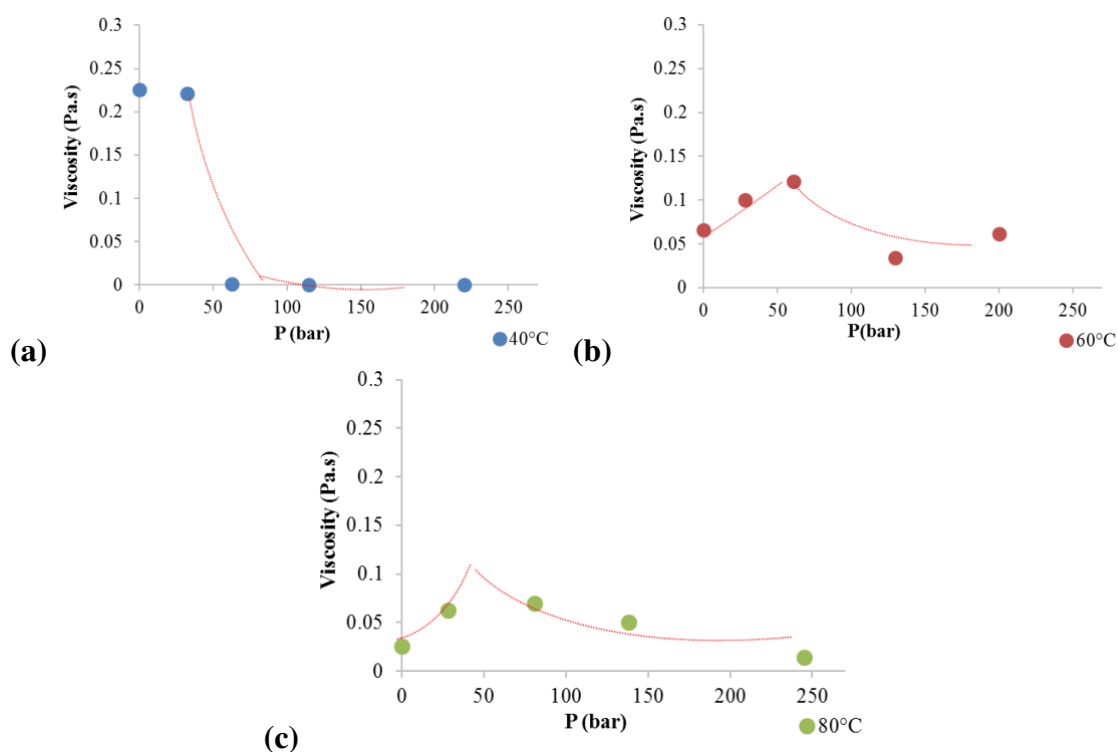


Figure 2.12. Determination of viscosity using **MR2** as molecular rotor at (a) 40 °C, (b) 60 °C and (c) 80 °C.

In the above results, it has been demonstrated that the viscosity of the DES can be decreased with increasing the pressure of CO₂. These results help us to understand the viscosity behavior of the DES and hence can be exploited for further applications.

2.5. Conclusions

From the above results and discussion, it can be concluded that molecular rotors may represent an innovative method to determine the *in-situ* viscosity for a determined system. In addition, it minimizes the use of expensive instruments. DCVJ and BODIPY-based molecular rotors can be used as probe for the viscosity measurements. On another hand, accurate determinations of the emission spectra are needed, and some experimental error may be originated from manipulating the set-up during changes in pressure and sample, which can lead to important errors in acquisition of the spectra because the spectrometer and the light source may not be well collimated. Use of lifetime decay of the rotor instead of its fluorescence intensity would be more accurate, as it is independent of the concentration of the rotor and viscosity-dependant property; a more sophisticated set-up is needed for these determinations.

It has been proven that the viscosity of the DES prepared from glycerol (as hydrogen bond donor) and choline tosylalaninate (as hydrogen bond acceptor) could be tuned using supercritical CO₂. It was observed that the viscosity of the DES first increases with the pressure and then decreases at higher pressures. In this context, we report how the viscosity of highly viscous DES can be decreased with increasing pressure of carbon dioxide, which can help in better mass transport properties of these solvents and envisage many applications.

2.6. References

1. Bai L, Zhao S, Fu Y, Cheng Y. Experimental study of mass transfer in water/ionic liquid microdroplet systems using micro-LIF technique. *Chem Eng J*. 2016;298:281-290. doi:10.1016/j.cej.2016.04.034
2. Mangers RJ, Ponter AB. Effect of Viscosity on Liquid Film Resistance to Mass Transfer in a Packed Column. *Ind Eng Chem Process Des Dev*. 1980;19(4):530-537. doi:10.1021/i260076a005
3. Okubo A. Diffusion: Mass Transfer in Fluid Systems. E. L. Cussler . *Q Rev Biol*. 1987;62(1):131-131. doi:10.1086/415398
4. City WG. T h e h y d r o d y n a m i c s o f n o n - N e w t o n i a n f l u i d s . I. 1947;(November):260-281.

5. Liu HS, Lin CC, Wu SC, Hsu HW. Characteristics of a rotating packed bed. *Ind Eng Chem Res.* 1996;35(10):3590-3596. doi:10.1021/ie960183r
6. Chen YS, Lin CC, Liu HS. Mass transfer in a rotating packed bed with viscous newtonian and non-Newtonian fluids. *Ind Eng Chem Res.* 2005;44(4):1043-1051. doi:10.1021/ie0499409
7. Jessop PG, Subramaniam B. Gas-expanded liquids. *Chem Rev.* 2007;107(6):2666-2694. doi:10.1021/cr040199o
8. Jin H, O'Hare B, Dong J, et al. Physical properties of ionic liquids consisting of the 1-butyl-3-methylimidazolium cation with various anions and the bis(trifluoromethylsulfonyl)imide anion with various cations. *J Phys Chem B.* 2008;112(1):81-92. doi:10.1021/jp076462h
9. Li H, Arzhantsev S, Maroncelli M. Solvation and solvatochromism in CO₂-expanded liquids. 2. Experiment-simulation comparisons of preferential solvation in three prototypical mixtures. *J Phys Chem B.* 2007;111(12):3208-3221. doi:10.1021/jp067916y
10. Li H, Maroncelli M. Solvation and solvatochromism in CO₂-expanded liquids. 1. Simulations of the solvent systems CO₂ + cyclohexane, acetonitrile, and methanol. *J Phys Chem B.* 2006;110(42):21189-21197. doi:10.1021/jp064166j
11. Granero-Fernandez E, Machin D, Lacaze-Dufaure C, et al. CO₂-Expanded Alkyl Acetates: Physicochemical and Molecular Modeling Study and Applications in Chemical Processes. *ACS Sustain Chem Eng.* 2018;6(6):7627-7637. doi:10.1021/acssuschemeng.8b00454
12. Turner C. From supercritical carbon dioxide to gas expanded liquids in extraction and chromatography of lipids. *Lipid Technol.* 2015;27(12):275-277. doi:10.1002/lite.201500060
13. Diamond LW, Akinfiev NN. Solubility of CO₂ in water from -1.5 to 100°C and from 0.1 to 100 MPa: Evaluation of literature data and thermodynamic modelling. *Fluid Phase Equilib.* 2003;208(1-2):265-290. doi:10.1016/S0378-3812(03)00041-4
14. Lin IH, Tan CS. Diffusion of benzonitrile in CO₂-expanded ethanol. *J Chem Eng Data.* 2008;53(8):1886-1891. doi:10.1021/je800211x

15. Maheshwar M. a Review Article on Measurement of Viscosity. *Ijrpc*. 2018;8(1):69-77. <http://www.ijrpc.com/files/13-01-18/08.pdf>.
16. Mackley MR, Hassell DG. The multipass rheometer a review. *J Nonnewton Fluid Mech*. 2011;166(9-10):421-456. doi:10.1016/j.jnnfm.2011.01.007
17. Barnes HA, Nguyen QD. Rotating vane rheometry-a review. *J Nonnewton Fluid Mech*. 2001;98(1):1-14. doi:10.1016/S0377-0257(01)00095-7
18. Haidekker MA, Theodorakis EA. Molecular rotors - Fluorescent biosensors for viscosity and flow. *Org Biomol Chem*. 2007;5(11):1669-1678. doi:10.1039/b618415d
19. Bacon LR, Co PQ, Stokes T. au. 1935;XI(1322).
20. Topham JD. A rising sphere rheometer. *J Pharm Sci*. 1972;61(5):783-787. doi:10.1002/jps.2600610524
21. Shimolina LE, Izquierdo MA, López-Duarte I, et al. Imaging tumor microscopic viscosity in vivo using molecular rotors. *Sci Rep*. 2017;7(December 2016):1-11. doi:10.1038/srep41097
22. Vyšniauskas A, Kuimova MK. A twisted tale: Measuring viscosity and temperature of microenvironments using molecular rotors. *Int Rev Phys Chem*. 2018;37(2):259-285. doi:10.1080/0144235X.2018.1510461
23. Kuimova MK. Mapping viscosity in cells using molecular rotors. *Phys Chem Chem Phys*. 2012;14(37):12671-12686. doi:10.1039/c2cp41674c
24. Grabowski ZR, Rotkiewicz K, Siemiarczuk A. Dual fluorescence of donor-acceptor molecules and the Twisted Intramolecular Charge Transfer (TICT) states. *J Lumin*. 1979;18-19(PART 1):420-424. doi:10.1016/0022-2313(79)90153-4
25. Okada T, Fujita T, Kubota M, et al. Intramolecular electron donor-acceptor interactions in the excited state of (anthracene)-(CH₂)_n-(N,N-dimethylaniline) systems. *Chem Phys Lett*. 1972;14(5):563-568. doi:10.1016/0009-2614(72)87208-7
26. Siemiarczuk A, Grabowski ZR, Krówczyński A, Asher M, Ottolenghi M. Two emitting states of excited p-(9-anthryl)-n,n-dimethylaniline derivatives in polar solvents. *Chem Phys Lett*. 1977;51(2):315-320. doi:10.1016/0009-2614(77)80411-9

27. Herbich J, Salgado FP, Rettschnick RPH, Grabowski ZR, Wójtowicz H. "Twisted" intramolecular charge-transfer states in supercooled molecules: Structural effects and clustering with polar molecules. *J Phys Chem.* 1991;95(9):3491-3497. doi:10.1021/j100162a011
28. Sasaki S, Drummen GPC, Konishi GI. Recent advances in twisted intramolecular charge transfer (TICT) fluorescence and related phenomena in materials chemistry. *J Mater Chem C.* 2016;4(14):2731-2743. doi:10.1039/c5tc03933a
29. Haidekker MA, Brady TP, Lichlyter D, Theodorakis EA. Effects of solvent polarity and solvent viscosity on the fluorescent properties of molecular rotors and related probes. *Bioorg Chem.* 2005;33(6):415-425. doi:10.1016/j.bioorg.2005.07.005
30. Ren M, Deng B, Kong X, et al. A TICT-based fluorescent probe for rapid and specific detection of hydrogen sulfide and its bio-imaging applications. *Chem Commun.* 2016;52(38):6415-6418. doi:10.1039/c6cc00966b
31. Oesch D, Luedtke NW. Fluorescent chemosensors of carbohydrate triols exhibiting TICT emissions. *Chem Commun.* 2015;51(63):12641-12644. doi:10.1039/c5cc03857j
32. Zhang P, Dou W, Ju Z, et al. A 9,9'-bianthracene-cored molecule enjoying twisted intramolecular charge transfer to enhance radiative-excitons generation for highly efficient deep-blue OLEDs. *Org Electron physics, Mater Appl.* 2013;14(3):915-925. doi:10.1016/j.orgel.2012.12.040
33. Kung CE, Reed JK. Microviscosity Measurements of Phospholipid Bilayers Using Fluorescent Dyes That Undergo Torsional Relaxation. *Biochemistry.* 1986;25(20):6114-6121. doi:10.1021/bi00368a042
34. Kung CE, Reed JK. Fluorescent Molecular Rotors: A New Class of Probes for Tubulin Structure and Assembly. *Biochemistry.* 1989;28(16):6678-6686. doi:10.1021/bi00442a022
35. Ibarra-Rodríguez M, Muñoz-Flores BM, Dias HVR, et al. Fluorescent Molecular Rotors of Organoboron Compounds from Schiff Bases: Synthesis, Viscosity, Reversible Thermochromism, Cytotoxicity, and Bioimaging Cells. *J Org Chem.* 2017;82(5):2375-2385. doi:10.1021/acs.joc.6b02802
36. Jin YJ, Choi YG, Kwak G. Molecular rotors with long alkyl chains as fluorescent

- viscosity sensors for hydrocarbon and silicone oil fluids. *J Mol Liq.* 2019;276:1-6. doi:10.1016/j.molliq.2018.11.158
37. Lu J, Liotta CL, Eckert CA. Spectroscopically probing microscopic solvent properties of room-temperature ionic liquids with the addition of carbon dioxide. *J Phys Chem A.* 2003;107(19):3995-4000. doi:10.1021/jp0224719
38. Tao D, Cheng Z, Chen F, Li Z, Hu N, Chen X. Synthesis and Thermophysical Properties of Biocompatible Cholinium-Based Amino Acid Ionic Liquids. 2013. doi:10.1021/je301103d
39. Chaari M, Gaztelumendi N, Cabrera-González J, et al. Fluorescent BODIPY-Anionic Boron Cluster Conjugates as Potential Agents for Cell Tracking. *Bioconjug Chem.* 2018;29(5):1763-1773. doi:10.1021/acs.bioconjchem.8b00204
40. Xochitiotzi-Flores E, Jiménez-Sánchez A, García-Ortega H, et al. Optical properties of two fluorene derived BODIPY molecular rotors as fluorescent ratiometric viscosity probes. *New J Chem.* 2016;40(5):4500-4512. doi:10.1039/c5nj03339j
41. Jastrzebska I, Pawlak T, Arcos-Ramos R, et al. Synthesis, Structure, and Local Molecular Dynamics for Crystalline Rotors Based on Hecogenin/Botogenin Steroidal Frameworks. *Cryst Growth Des.* 2016;16(10):5698-5709. doi:10.1021/acs.cgd.6b00726
42. Liu QP, Hou XD, Li N, Zong MH. Ionic liquids from renewable biomaterials: Synthesis, characterization and application in the pretreatment of biomass. *Green Chem.* 2012;14(2):304-307. doi:10.1039/c2gc16128a
43. Yang Q, Wang Z, Bao Z, et al. New Insights into CO₂ Absorption Mechanisms with Amino-Acid Ionic Liquids. *ChemSusChem.* 2016;9(8):806-812. doi:10.1002/cssc.201501691
44. Sih R, Dehghani F, Foster NR. Viscosity measurements on gas expanded liquid systems- Methanol and carbon dioxide. *J Supercrit Fluids.* 2007;41(1):148-157. doi:10.1016/j.supflu.2006.09.002

Chapter 3

Synthesis and Characterization
of Palladium Nanoparticles
Stabilized by Novel Choline-
based Ionic Liquids in Glycerol
applied in Hydrogenation
Reactions

3.1. Palladium Nanoparticles

3.1.1. Introduction

Palladium nanoparticles (PdNPs), due to their high efficiency, selectivity and their ability to perform various kinds of catalytic reactions, have emerged as an important tool in organic synthesis. PdNPs are one of the most used and efficient catalysts to build C–C bonds and to perform other chemical transformations such as carbon-heteroatom bond formation, hydrogenation, carbonylation and oxidation processes.^{1–4} Well-defined PdNPs are appropriate catalysts for hydrogen activation and hydrogen spillover.^{5,6} PdNPs can be synthesized *via* chemical and electrochemical routes.⁷

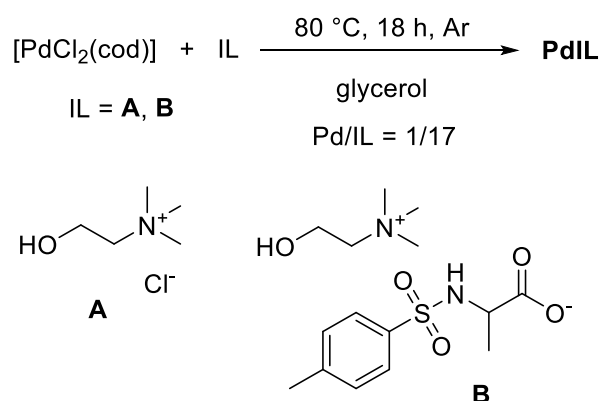
PdNPs dispersed in neat glycerol and stabilized by TPPTS have been efficiently applied in a large panel of reactions, leading to the synthesis of heterocyclic compounds: (na)phthalimides, isoindole-1-ones, tetrahydroisoquinolin-1,3-diones, (*Z*)-3-(arylmethylene)isoindolin-1-one and (*Z*)-1-methylene-1,3-dihydroisobenzofurans.⁸ The desired products were obtained by one-pot tandem and/or sequential methodologies without the isolation of the generated intermediates. Furthermore, isolation of compounds containing two heterocycles, even using in the same medium two different catalysts, Pd and Cu₂O based nanoparticles was possible.⁸ Lately, palladium nanoparticles capped by cinchona-based ligands were also synthesized in neat glycerol and successfully applied in dihydrogen-based processes, such as hydrogenation of unsaturated functional groups (alkenes, alkynes, imines, and nitro-based substrates) and hydrodehalogenation of halo-aromatic compounds by Reina *et al.*⁹

Dupont *et al.* have reported numerous work on catalysis by PdNPs for hydrogenation and selective hydrogenation.^{10–14} In a recent publication, they worked structural, electronic and support effect on PdNPs prepared by sputtering deposition and chemical reduction of a Pd(II) precursor in/on a poly(ionic liquid) for selective hydrogenation of α,β -unsaturated carbonyl compounds and dienes.¹⁰ Hu *et al.* also reported the IL stabilized PdNPs for the selective hydrogenation C=C double bonds of various functionalized alkenes.¹⁵

3.1.2. Synthesis of palladium nanoparticles

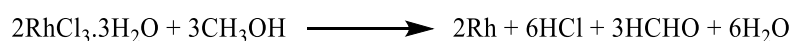
In this work, we prepared palladium nanoparticles (**PdA**, **PdB**) by thermal decomposition of $[\text{PdCl}_2(\text{cod})]$ (cod = 1,5-cyclooctadiene) in the presence of a choline-based ionic liquid [choline chloride (**A**); choline *N*-tosylalaninate (**B**)], using glycerol as solvent (Scheme 3.1). The preparation of ionic liquid **B** is described in Chapter 2 (Experimental section 2.3.2). The synthesis of nanoparticles followed polyol methodology where the water present in the ionic liquids act as the reducing agent.¹⁶

In both cases, we obtained black colloidal solutions, constituted by spherical small nanoparticles (for **PdA**, 1.4 ± 0.6 nm; for **PdB**, 1.7 ± 0.6 nm), exhibiting a very well-dispersion mainly thanks to the supramolecular structure of glycerol which avoids agglomeration, as evidenced in previous works using ligands and polymers as stabilizers reported by our group (Figure 3.2).^{8,9,17–19} It is important to highlight that these reaction conditions did not trigger any deprotection of choline *N*-tosylalaninate.²⁰



Scheme 3.1. Synthesis of palladium nanoparticles in glycerol using choline-based ionic liquids (**A**, **B**) as stabilizers.

Control tests proved that the water present on the IL (for **A**, 0.25%; for **B**, 1.70%; determined by Karl-Fischer titration) is the responsible of the reduction of Pd(II) into Pd(0); $[\text{PdCl}_2(\text{cod})]$ in dry glycerol under the same conditions used in the synthesis of PdNPs was stable and did not exhibit decomposition. This is in agreement with the work carried out by Hirai and coworkers, proving the unsuccessful synthesis of zero-valent rhodium nanoparticles in anhydrous alcohols.²¹



They synthesized rhodium nanoparticles stabilized by polyvinyl alcohol. They found out that in the absence of polyvinyl alcohol, rhodium(III) chloride was not reduced to the zero valence state in anhydrous methanol but to a black precipitate of rhodium metal in methanol-

water. They concluded that the presence of water is indispensable for both dissolution of polyvinyl alcohol and reduction of rhodium(III) chloride to the zero valence state.

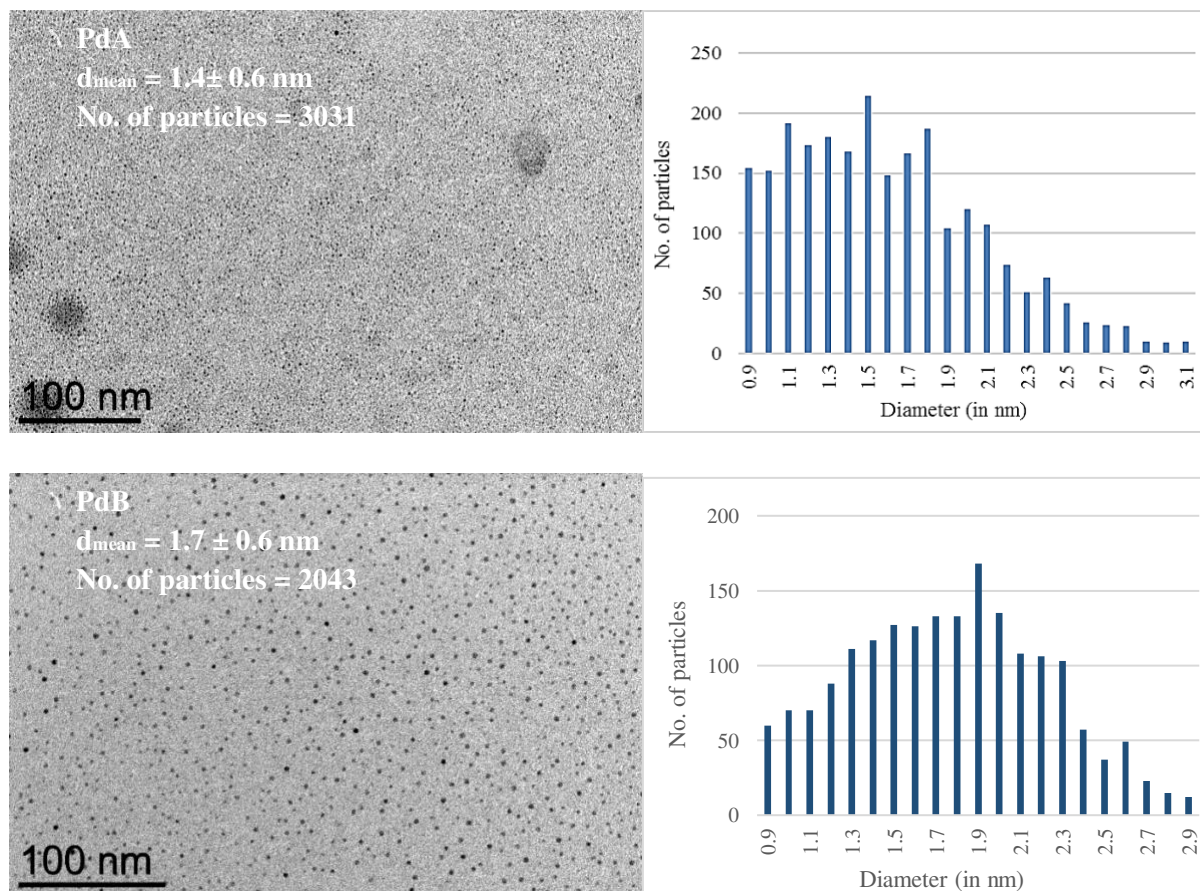
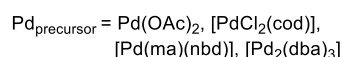
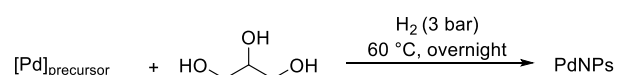


Figure 3.2. TEM images of **PdA** and **PdB** in glycerol with the corresponding size distribution diagrams.

When PdNPs were synthesized in the absence of any stabilizer and under hydrogen atmosphere using wet glycerol and different palladium precursors, Pd(0) agglomerates were formed (Figure 3.3).¹⁸



cod = cyclooctadiene
 ma = maleic anhydride
 nbd = norbornadiene
 dba = dibenzylideneacetone

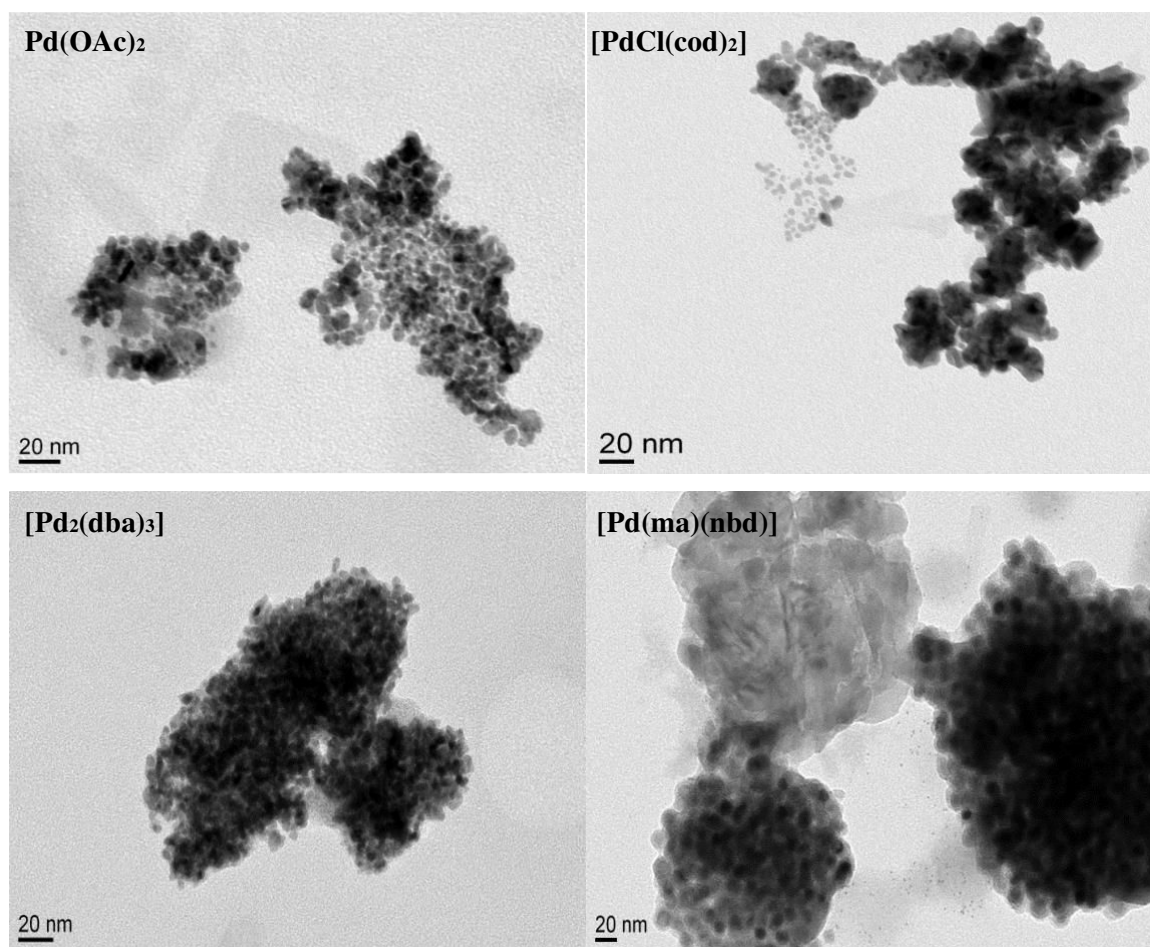
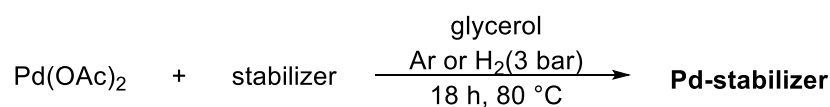


Figure 3.3. Synthesis of palladium nanoparticles in neat glycerol in the absence of any other stabilizer and the corresponding TEM images.¹⁸

We also tried palladium acetate as starting metal precursor with the two choline derivatives (**A** and **B**), obtaining in both cases aggregates; for choline chloride, anisotropic nano-objects were observed probably due to the presence of halides at the metal surface (see Figure 3.4(a,b)).²² We then added polyvinylpyrrolidone (mean molecular weight = 10000 g.mol⁻¹), in order to improve the dispersion, but in this case very few nanoparticles could be detected by TEM (see Figure 3.4(c,d)). Curiously, when dihydrogen was used as reducing agent, an immediate precipitation of bulk palladium took place. Venkatesan *et al.* observed a similar behavior when trying to synthesize Pd(0) nanoparticles stabilized by ILS.¹³ In their case, very much like ours, the reactions employed show that the simple thermal treatment of palladium acetate provides the best results towards the formation of well-dispersed and immobilized nanoparticles. Instead, other reducing agents provoke those nanoparticles formation that was followed by metal precipitation. In most cases it can be assumed that the reduction with

hydrogen as the reductant is too fast, therefore the local concentration of Pd(0) is too high which provokes fast agglomeration and metal precipitation.^{12,13}



Stabilizer = (a)-(d)

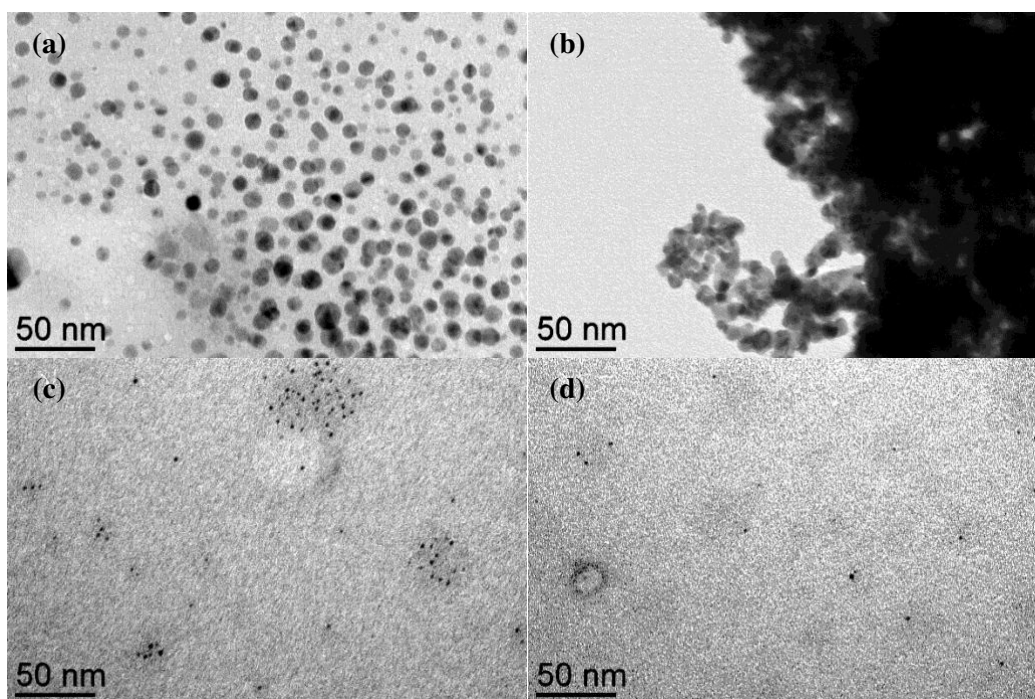
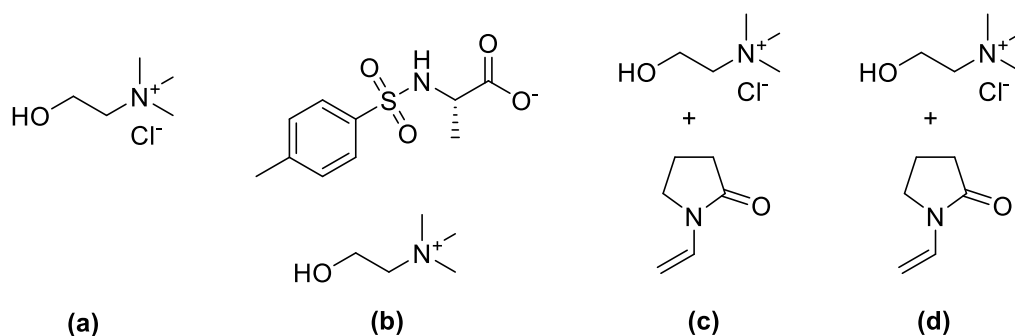


Figure 3.4. TEM analyses recorded in glycerol of palladium nanoparticles, starting from Pd(OAc)₂, using (a) choline chloride; (b) choline tosylalaninate; and (c) polyvinylpyrrolidone (ChCl:PVP molar ratio = 1:2) as stabilizers and synthesized by thermal heating under argon; (d) synthesized under 3 bar dihydrogen pressure with polyvinylpyrrolidone (ChCl:PVP molar ratio = 1:2).

We envisaged the use of choline alaninate²³ as, instead of the protected anion *N*-tosylalaninate; however, choline alaninate, however, choline alaninate became unstable under atmospheric conditions, due to its high reactivity with carbon dioxide, giving the corresponding

carbamate (See Chapter 2 Section 2.4.1 Scheme 2.3).²³ Moreover, we also studied the effect of the solvent on the synthesis of colloidal PdNPs, using water and ethanol instead of glycerol under the same conditions than those described in Scheme 1. In both cases, fast precipitation of black palladium was observed, proving that glycerol avoids the agglomeration of metal-based nanoparticles probably due to its supramolecular structure.^{24–26}

3.1.3. Characterization of palladium nanoparticles

Given the better catalytic behavior of **PdB** (see below Table 3.1), we selected this catalyst for its full characterization. Palladium nanoparticles at solid state were isolated by centrifugation (4500 rpm for 1 h). Powder X-ray diffraction (PXRD) analysis showed the presence of crystalline nanoparticles exhibiting face cubic center Pd(0) structure (Fig. 3.5). The crystallite size found from the X-ray diffraction peaks (calculated by the Scherrer equation) is *ca.* 3.7 nm.²⁷ Differences in size between TEM and XRD are frequently observed because the average crystallite size (PXRD) is not necessarily the same as the particle size (TEM).^{28,29} As mentioned by Jensen *et al.*, nanopowders often consist of primary particles arranged in a larger macroscopic structure. The primary particle size is defined to be the smallest size of individual particles. The primary particles can be made up of several crystals or consist of a crystalline core with an amorphous shell. The size of the primary particles can be determined by for example SAXS and electron microscopy, TEM and SEM. The primary particle size is not necessarily equal to the crystallite size determined by XRD where only the crystalline part is detected. Furthermore, powders are normally not monodisperse but consist of a size distribution. The polydispersity of nanopowders is not taken into account in Scherrer's formula.³⁰

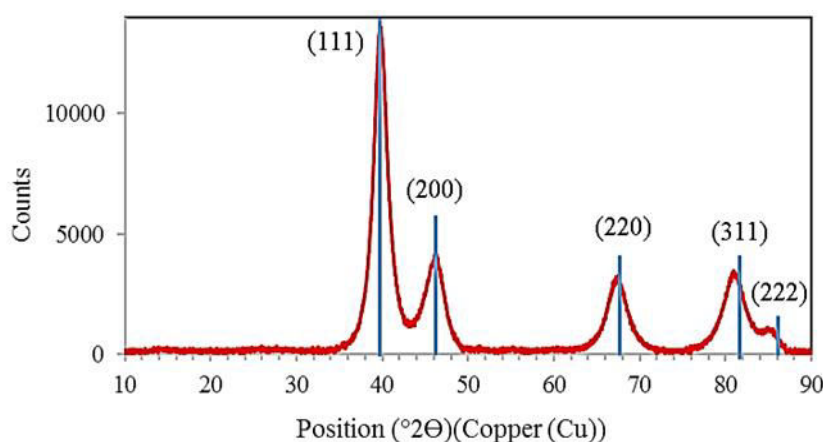


Figure 3.5. PXRD diffractogram of **PdB** at solid state (sharp blue lines correspond to the diffraction pattern of bulk fcc Pd(0)).³⁰

XPS analysis corroborated the absence of any oxidized palladium species (Fig. 3.6 and Fig. 3.7); XPS showed the presence of carbon, oxygen and nitrogen that confirms the presence of the ionic liquid at solid state; the presence of chloride probably comes from the metal precursor (Figure 3.7 (e)). The metal precursor used in the synthesis is $[\text{PdCl}_2(\text{cod})]$, where the oxidation state of palladium is +2. On reduction of Pd(II) to Pd(0), chlorides are released that can be detected by XPS analysis.³¹

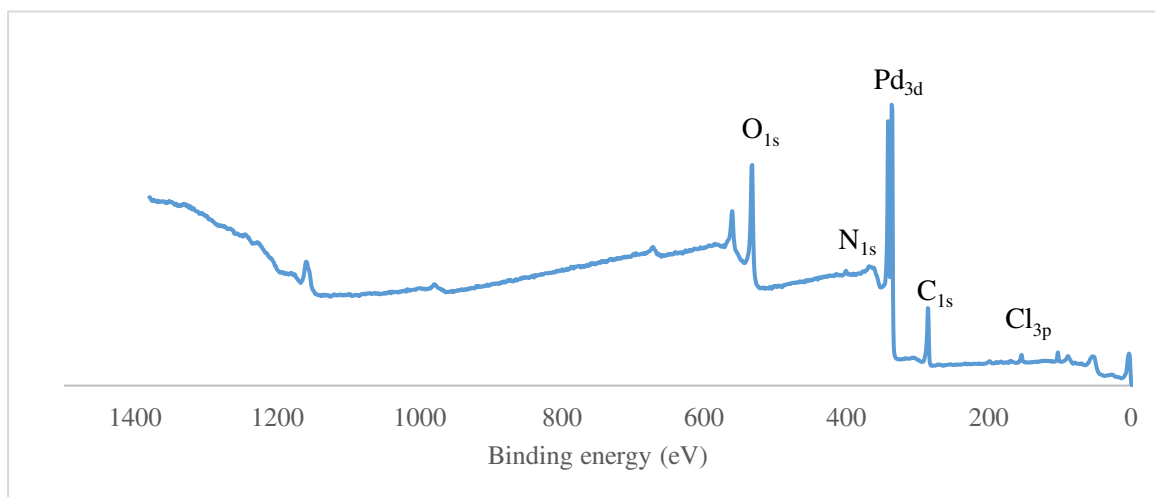
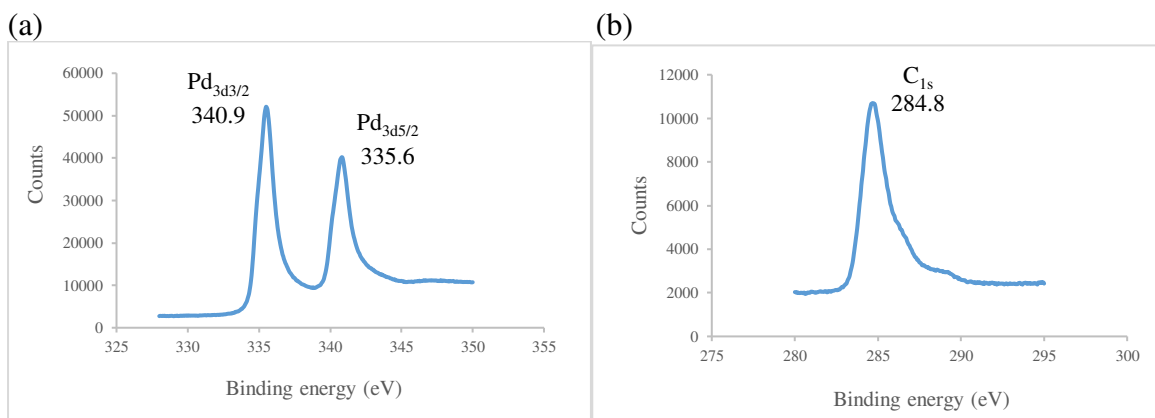


Figure 3.6. XPS survey spectrum of **PdB** at solid state.

Figure 3.7 shows the HR-XPS of **PdB** at solid state. Figure 3.7(a) only showed the corresponding binding energies for palladium ($\text{Pd } 3d_{3/2}$ and $\text{Pd } 3d_{5/2}$) which concludes the presence of only Pd(0) and absence of amorphous phases of palladium oxides. This result compensates the drawback of powder-XRD, which can only confirm the presence of Pd(0) in crystalline form and not give us any information about the amorphous phase. Even though there are peaks of carbon and oxygen (Figure 3.7(a & b) respectively) in the HR-XPS survey, it is the spectrum of nitrogen (Figure 3.7(d)) that truly confirms the presence of IL on the surface of palladium even in solid state.



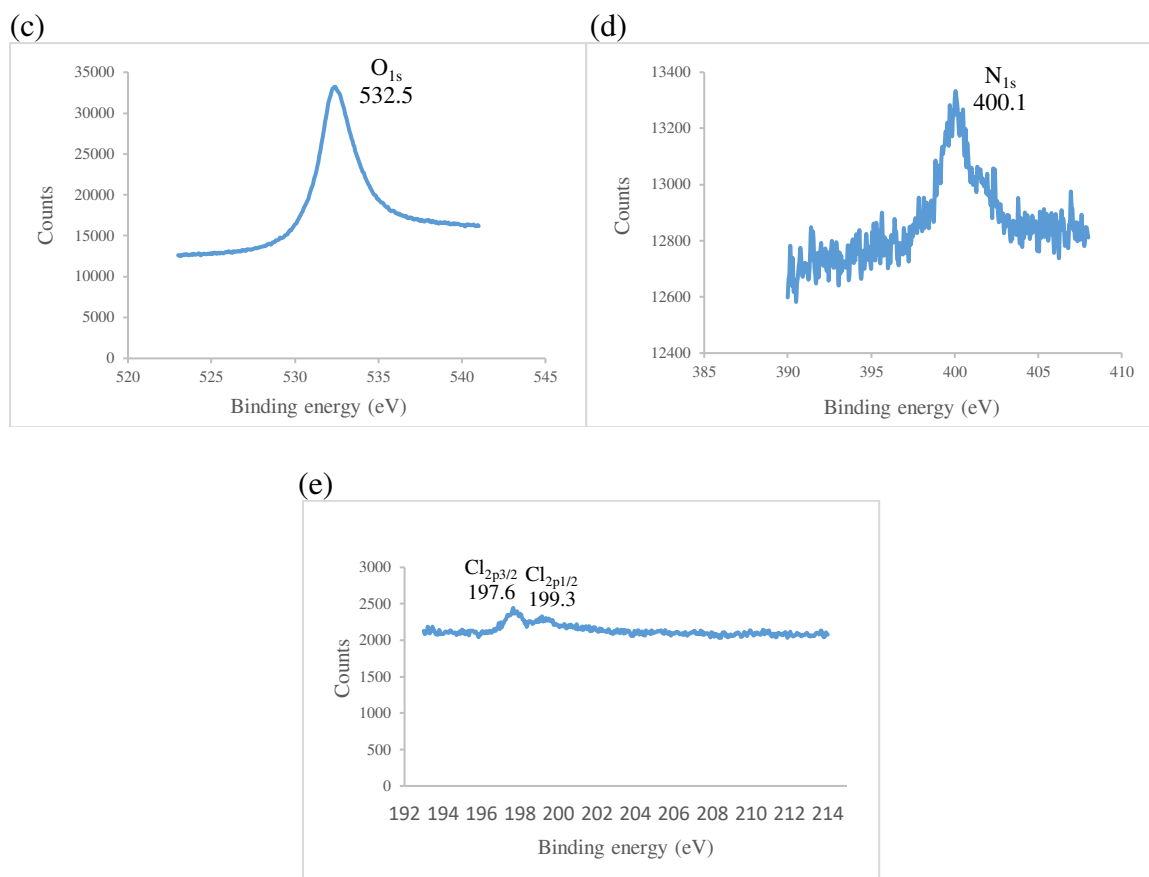


Figure 3.7. HR-XPS spectra of **PdB** at solid state for (a) Pd(0), (b) carbon, (c) oxygen and (d) nitrogen.

In this context, it is important to highlight that **PdB** at solid state could be re-dispersed in glycerol without formation of aggregates (Figure 3.8).

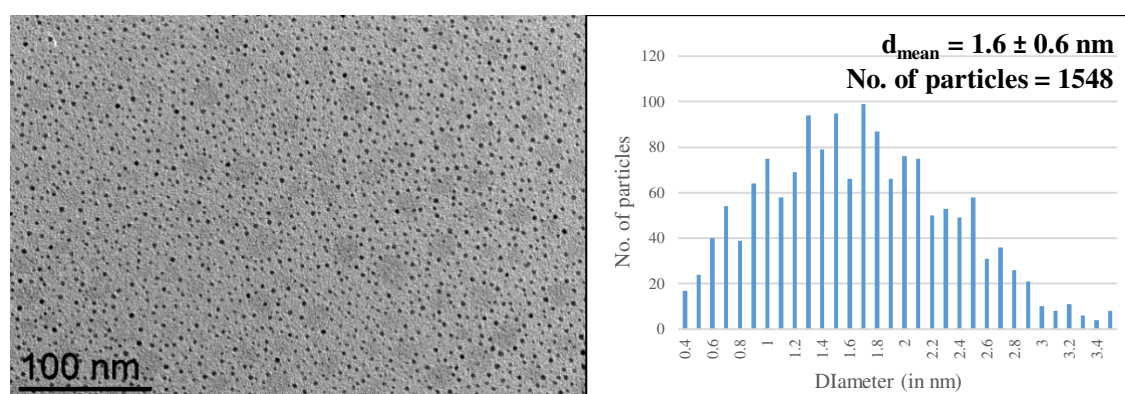


Figure 3.8. TEM analyses (left) and mean size distribution (right) of **PdB** after centrifugation (isolation of PdNPs at the solid state) and re-dispersion in glycerol.

3.2. Pd-catalyzed Hydrogenation Reactions

3.2.1. Introduction

Hydrogenation is a fundamental process in organic chemistry to add elemental hydrogen to unsaturated bonds.³² In fact, a process that has been used and explored for centuries. One of the best well-known example dates as early as 1823, Johann W. Döbereiner a German scientist who observed that when a stream of hydrogen mixed with air is passed over porous platinum; it is ignited. This was the observation that the great Swedish chemist, Jöns Jacob Berzelius, coined as “catalysis.”³³ Interestingly, it is Döbereiner’s lamp forms the basis of lighters (Figure 3.9).³⁴

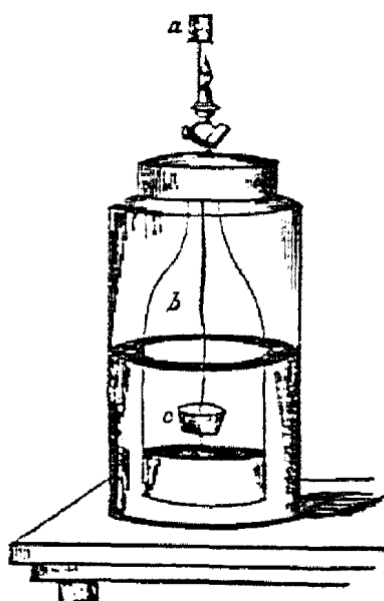
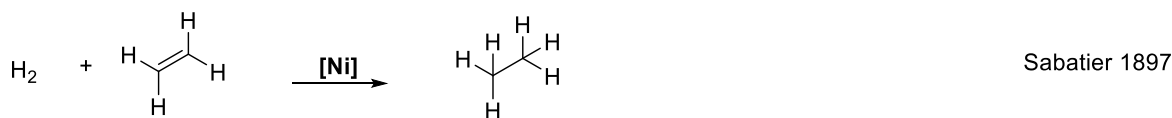
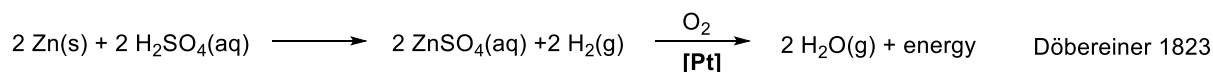


Figure 3.9. Döbereiner hydrogen Lamp ³⁴

In late 19th century, Paul Sabatier discovered hydrogenation of unsaturated hydrocarbons using Ni as catalyst.³⁵ The Sabatier process to hydrogenate carbon dioxide to form methane and water was the reason he was awarded Nobel Prize in Chemistry in 1912. Until date, hydrogenation reaction based on his work as well as the work of Döbereiner are been investigated. The Sabatier reaction, Haber-Bosch³⁶ and Fischer-Tropsch³⁷ processes have provided a significant platform of research for industrial applications.



Scheme 3.4. The Döbereiner and Sabatier reactions

The mechanism of hydrogenation was proposed by Horiuti and Polyani in 1934 (Figure 3.10). The mechanism is very aptly described by Mattson *et al.* in three steps: (i) alkene adsorption on the surface of the hydrogenated metal catalyst, (ii) hydrogen migration to the β -carbon of the alkene with formation of a σ -bond between the metal and α -C, and finally (iii) reductive elimination of the free alkane.³⁸ In their paper, they describe the investigation of gas-phase reactions between deuterium and 1-butene using a supported palladium catalyst under ambient laboratory conditions and how the results are consistent with the Horiuti–Polanyi mechanism.³⁸

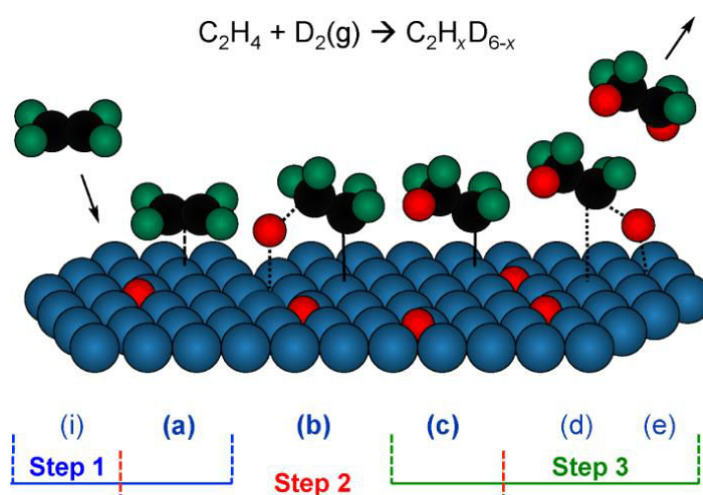


Figure 3.10. Profile of Horiuti–Polanyi mechanism. Step 2, (a) \rightarrow (b) \rightarrow (c), is reversible. Pd atoms are blue, carbon atoms are black, hydrogen atoms are green, and deuterium atoms are red. Reprinted (adapted) with permission from (38). Copyright 2013 American Chemical Society.

On the other hand, Yang *et al.* has investigated the prevalence of the non-Horiuti–Polanyi mechanism over the Horiuti–Polanyi mechanism on a series of metals for hydrogenation of acrolein.³⁹ Ohno *et al.* has described the mechanism of olefin hydrogenation catalysis driven by palladium dissolved hydrogen. They had characterized the hydrogen and butene co-adsorption system on Pd(110) through temperature programmed desorption (TPD), high

resolution electron energy loss spectroscopy (HREELS) and nuclear reaction analysis (NRA) measurements and discussed the individual roles of Pd-dissolved hydrogen, of surface chemisorbed hydrogen, and of the butene adsorbate in the catalytic hydrogenation reaction.⁴⁰

Palladium nanoparticles, as mentioned above, due to their high efficiency, selectivity and their ability to perform various kinds of catalytic reactions have been widely investigated. Reduction of unsaturated hydrocarbons and various functional groups like nitro-compounds and carbonyls can be achieved using palladium nanoparticles. The group Dupont has long since been working on palladium nanoparticles stabilized by different kind of ionic liquids catalytically active for hydrogenation.^{10,12-14}

Our team has synthesized PdNPs in both solution and solid state, using tris(3-sulfophenyl)phosphinetrisodium salt (TPPTS);¹⁸ thioether-phosphine ligands;⁴¹ naturally occurring cinchona-based alkaloids,⁹ applied in dihydrogen-based processes, such as hydrogenation of unsaturated functional groups. In the next section, we describe the catalytic behavior exhibited by the palladium nanoparticles synthesized in glycerol using choline tosylalaninate as the stabilizer.

3.2.2. Results and discussion

We chose the hydrogenation of 4-phenylbut-3-en-2-one as benchmark reaction to study the catalytic activity of PdNPs. 4-phenylbut-3-en-2-one provides a scope to study the reactivity and selectivity of the PdNPs, since it contains an unsaturated C-C bond, a carbonyl group and an aromatic ring; all three of them are subject to reduction. Both catalysts, **PdA** and **PdB**, behave likewise, giving exclusively 4-phenylbutan-2-one (entries 1-2, Table 3.1), interesting skeleton present in fragrances.⁴² Both systems were also highly active at low Pd load (0.1 mol%, entries 3-4, Table 3.1). However, at shorter times (1 h reaction), only **PdB** preserved the activity (entry 5 vs 6, Table 3.1), probably due to the non-innocent effect of the chloride anions present in **PdA**, which can trigger a poison effect due to the adsorption of chloride ions at the surface.⁴³

Table 3.1. Hydrogenation of 4-phenylbut-3-en-2-one catalyzed by PdNPs in glycerol stabilized by ChCl (**A**) and ChTsAla (**B**).^a

| Entry | Catalyst | Conv. (yield) ^b (%) |
|------------------|------------|--------------------------------|
| 1 | PdA | >99 (96) |
| 2 | PdB | >99 (93) |
| 3 ^c | PdA | 50 (49) |
| 4 ^c | PdB | >99 (91) |
| 5 ^{c,d} | PdB | 96 (92) |
| 6 ^{c,d} | PdA | 55 (51) |

^a Results from duplicated experiments. Reaction conditions: 1 mmol of **1** and 1 mL of the corresponding catalytic glycerol solution of PdNPs (10⁻² mol L⁻¹, 0.01 mmol of total Pd). ^b Determined by GC and GC/MS using decane as internal standard. ^c 0.1 mol% Pd load. ^d Reaction time 1 h.

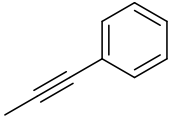
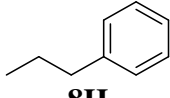
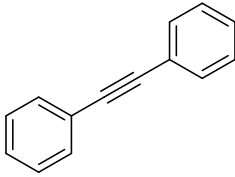
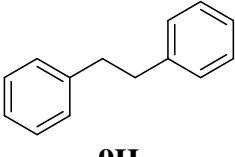
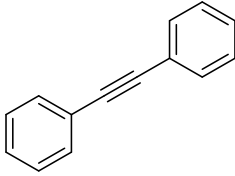
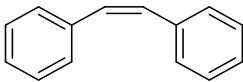
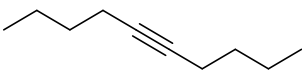
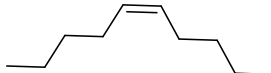
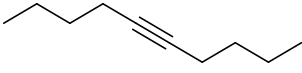
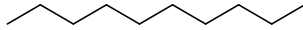
With the aim of carrying out a scope related to functions to be reduced by **PdB**, we firstly analyzed the behavior of **PdB** in the hydrogenation of alkenes and alkynes (Table 3.2). The terminal alkene 1-dodecene (**2**) was fully converted into dodecane and internal alkenes in a ratio of 54/46 respectively under smooth conditions (3 bar H₂ and 2 h of reaction; entry 1, Table 3.2). Similar results were obtained when the reaction was carried out under higher pressure (20 bar; entry 1, Table 3.2). Under harsher conditions (20 bar H₂, 18 h), (-)- β -pinene (**3**) was mainly isomerized, giving only 18% of hydrogenated product (entry 2, Table 3.2); **PdB** was not active enough to reduce (+)- α -pinene (entry 3, Table 3.2). However, for conjugated C=C bonds (alkene **5**), full conversion was achieved under 3 bar H₂ overnight (entry 4, Table 3.2). In agreement with this behavior, the extended conjugated substrate (*trans*-1,4-diphenylbuta-1,3-diene) **6** was fully hydrogenated concerning the non-aromatic C=C bonds (entry 5, Table 3.2). The more sterically hindered conjugated substrate 1,2,3,4,5-pentamethylcyclopentadiene (**7**) allowed the selective reduction of one of the two endocyclic C=C bonds working at 20 bar of H₂ pressure (entry 6, Table 3.2).

Internal aromatic alkynes (**8**, **9**) were fully reduced obtaining the corresponding alkane derivatives (entries 7-8, Table 3.2). At lower H₂ pressure (entry 9, Table 3.2), only the formation of the corresponding *Z*-alkene was observed, giving up to *ca.* 50% yield; longer reaction times led to the formation of 1,2-diphenylethane. However, the internal alkyl-substituted alkyne, 5-

decyne (**10**; entry 10, Table 3.2) gave mainly the corresponding internal alkene; at longer time (18 h), full hydrogenation was observed (entry 11, Table 3.2).

Table 3.2. Hydrogenation of alkenes and alkynes catalyzed by **PdB** in glycerol.^a

| Entry | Substrate | Product | <i>p</i> H ₂ (bar) | Conv. (yield) ^b (%) |
|-------|-----------|---------|-------------------------------|---------------------------------------|
| | | | | |
| 1 | | | 3 20 | >99 ^c >99 ^d |
| 2 | | | 20 (3) | 88 ^e [65 ^f] |
| 3 | | - | 20 | n.r. |
| 4 | | | 3 | >99 (99) ^g |
| 5 | | | 3 | >99 (98) ^g |
| 6 | | | 3 (20) | 86 (n.d) [>99 (n.d)] |

| | | | | |
|----|---|--|---|----------------------------|
| 7 |  |  | 1 | >99 (97) |
| 8 |  |  | 3 | >99 (99) |
| 9 |  |  | 1 | 50 (49) |
| 10 |  |  | 3 | >99 (90/10) ^{h,i} |
| 11 |  |  | 3 | >99 (96) ^h |

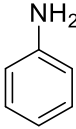
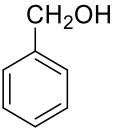
^a Results from duplicated experiments. Reaction conditions: 1 mmol of substrate (**2-10**) and 1 mL of the catalytic glycerol solution of **PdB** (10^{-2} mol L⁻¹, 0.01 mmol of total Pd); n.r. means no reaction; n.d. means not determined. ^b Determined by GC and GC/MS using decane as internal standard. ^c Dodecane/internal alkenes = 54/46. ^d Dodecane/internal alkenes = 55/45. ^e Ratio **3/3G/3H** = 12/70/18. ^f Ratio **3/3G/3H** = 35/43/22. ^g Isolated yield. ^h Cyclooctane as internal standard. ⁱ *cis*-5-decene/*n*-decane = 90/10.

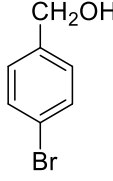
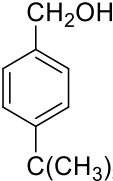
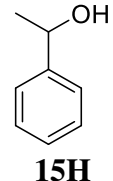
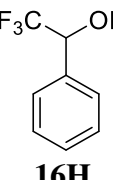
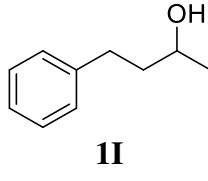
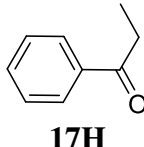
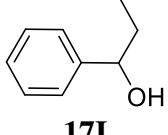
We were also interested in the hydrogenation of other organic functional groups, such as nitro and carbonyl derivatives (Table 3.3). As expected, nitrobenzene gave aniline in quantitative yield (entry 1, Table 3.3).⁴⁴ **PdB** was also an efficient catalyst for the reduction of carbonyl groups, coming from both aldehydes (**12-14**) and ketones (**15-17**). Work has been reported in literature concerning the hydrogenation of carbonyl group by palladium nanoparticles. Recently, Nindakova *et al.* has reported the study of enantioselective hydrogenation of ketones on Pd nanoparticles applied in the form of colloidal suspension prepared in the Pd(acac)₂(-)-cinchonidine-H₂ system.⁴⁵ Concerning the formyl groups, benzaldehyde derivatives exhibiting substituents inducing different electronic effects, were fully converted into the corresponding benzyl alcohols under smooth conditions (3 bar H₂; entries 2-4, Table 3.3). Aromatic ketones **15** and **16**, more challenging substrates, were hydrogenated to give the corresponding secondary alcohols, but under higher hydrogen

pressure (entries 5-6, Table 3.3). The non-conjugated ketone (which are thermodynamically less favored for hydrogenation) (**1H**) gave a moderate conversion to the corresponding secondary alcohol (**1I**) at 40 bar H₂ pressure (entry 7, Table 3.3). This is attributed to the fact that the entire π -system of dienes is involved in adsorption through di- π -coordination, which is more favorable than the d- σ mode of adsorption of a single double bond.⁴⁶ The 1-phenylprop-2-yn-1-one (**17**) mainly gave the saturated ketone (**17H**) with only 15% of the corresponding secondary alcohol (**17I**) (entry 8, Table 3.3). This reactivity behavior concerning the reduction of carbonyl groups follows the same trend than that reported recently by J. Dupont and co-workers using supported palladium nanoparticles on poly (ionic liquid) materials based on pyrrolidinium salts.¹⁰

Alkyl ketones (such as 3-pentanone and 2,2,4,4-tetramethyl pent-3-one) and alkyl aldehydes (like hexanal) were not reduced (up to 20 bar H₂). Similarly, benzonitrile and esters were not hydrogenated under harsh conditions.

Table 3.3. Hydrogenation of nitro and carbonyl groups catalyzed by **PdB** in glycerol.^a

| Entry | R ₁ | R ₂ | Product | Conv. (yield) ^b (%) |
|-------------------|-------------------------------|----------------|---|--------------------------------|
| 1 _{c, d} | NO ₂ (11) | H |  11H | >99 (99) |
| 2 | CHO (12) | H |  12H | 98 (95) |

| | | | | |
|----------------|--|----------------------------------|--|--------------------------|
| 3 | CHO (13) | Br |  <p>13H</p> | 99 (97) |
| 4 | CHO (14) | C(CH ₃) ₃ |  <p>14H</p> | 90 (89) |
| 5 _e | COCH ₃ (15) | H |  <p>15H</p> | >99 (98) _f |
| 6 _e | COCF ₃ (16) | H |  <p>16H</p> | >99 (97) |
| 7 _g | CH ₂ CH ₂ COCH ₃ (1H) | H |  <p>1H</p> | 40 (37) |
| | | |  <p>17H</p> | |
| 8 _e | COC≡CH (17) | H |  <p>17I</p> | >99 (85/15) _h |

^a Results from duplicated experiments. Reaction conditions: 1 mmol of substrate (**1H**, **12-18**) and 1 mL of the catalytic glycerol solution of **PdB** (10⁻² mol L⁻¹, 0.01 mmol of total Pd). ^b Determined by GC and GC/MS using decane as internal standard. ^c H₂ pressure 10 bar. ^d Reaction for 2 h. ^e H₂ pressure 20 bar. ^f Isolated yield. ^g H₂ pressure 40 bar. ^h **17H/17I** ratio.

After catalysis, the product extracted was analyzed by ICP-AES in order to detect leaching of palladium from the catalytic phase; fortunately, no leaching of Pd was detected. However, some aggregation was observed by TEM preserving the zero-valent PdNPs (Figures 3.11 and 3.12); the formation of aggregates may be the reason for the observed decrease of the catalytic activity and hence it was difficult to use the PdNPs for an efficient recycling (Fig. 3.13).

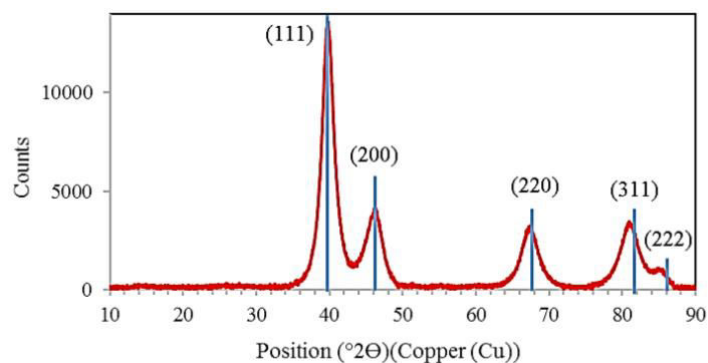


Figure 3.11. Powder-XRD of the **PdB** at solid state after catalysis.

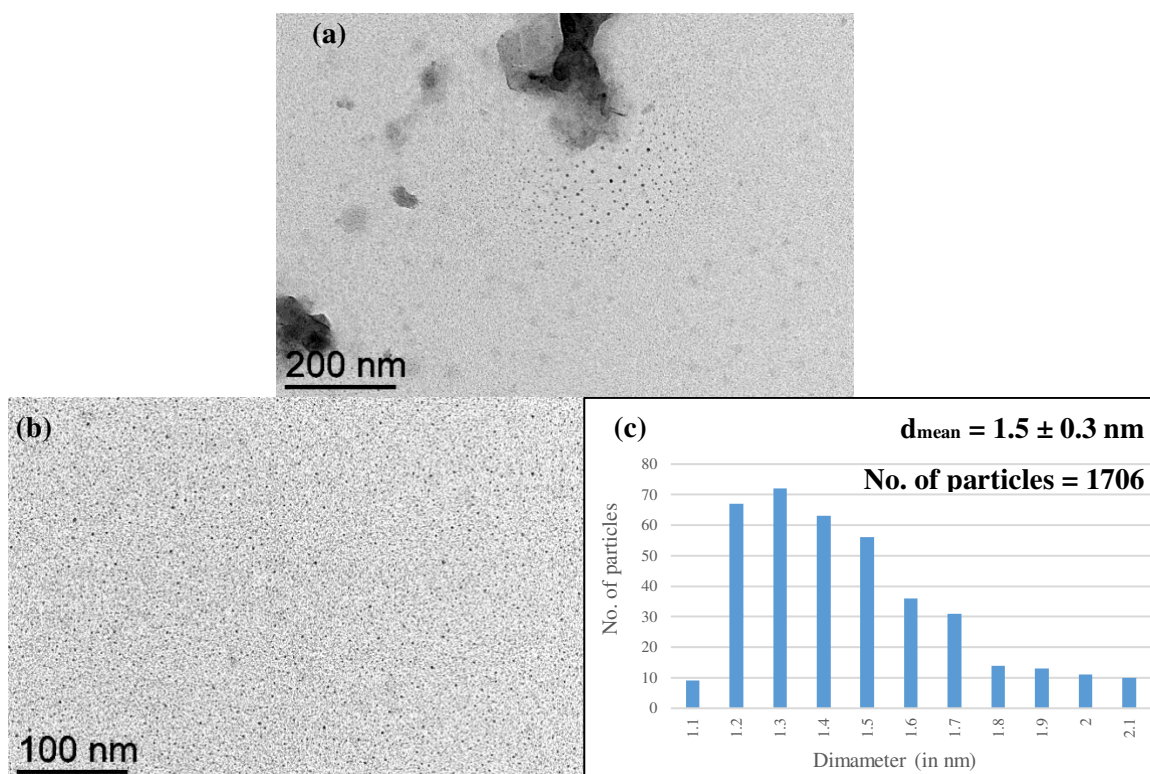


Figure 3.12. TEM analyses ((a), (b)) and mean size distribution (c) recorded in glycerol of **PdB** after catalysis.

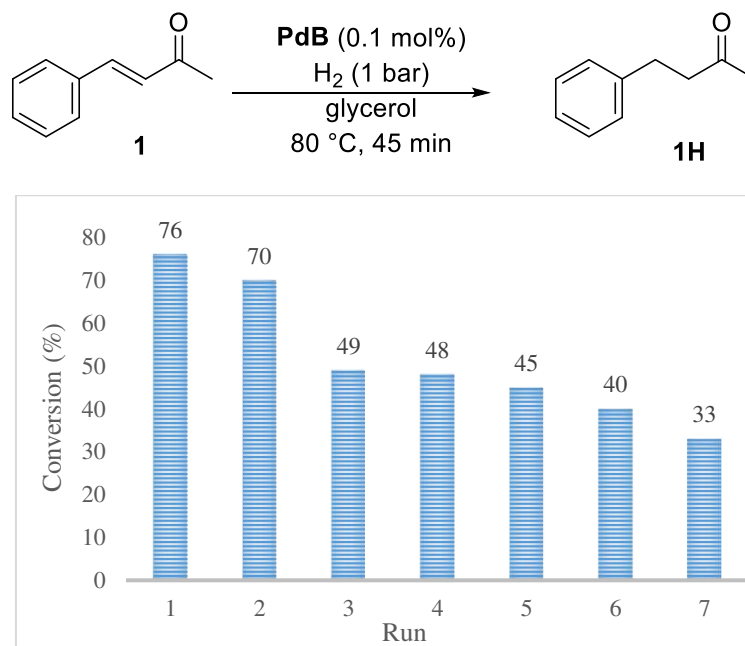


Figure 3.13. Hydrogenation reaction of **1** catalyzed by **PdB** in glycerol and the diagram showing the recycling of the catalytic phase.

3.3. Experimental Section

3.3.1. Methods and materials

Unless otherwise stated, all chemical reagents were obtained from commercial suppliers and used without further purification. All manipulations were performed using Schlenk techniques under argon atmosphere. Glycerol was dried under vacuum at 80 °C for 18 h prior to use. *N*-tosyl-alanine was prepared following previously reported methodology.⁴⁷ High-pressure reactions were carried out in a Top Industrie Autoclave. NMR spectra were recorded on a Bruker Advance 300 spectrometer at 293 K (300 MHz for ¹H NMR, 75.5 MHz for ¹³C NMR and 50.6 MHz for ¹⁵N). GC analyses were carried out on a GC Perkin Elmer Clarus 500 with ionization flame detector, using SGE BPX5 column composed by 5% phenylmethylsiloxane, coupled to a Perkin Elmer Clarus MS560 mass detector. TEM images of PdNPs dispersed in glycerol were obtained from a JEOL JEM 1400 instrument running at 120 kV. PdNPs size distributions and average diameters were determined from TEM images applying Image-J software associated to a Microsoft Excel macro. Powder X-ray diffraction analyses were collected on a XPert (Theta-Theta mode) Panalytical diffractometer with $\alpha(\text{Cu K}\alpha 1, \text{K}\alpha 2)=1.54060, 1.54443 \text{ \AA}$. Elemental and ICP-AES analyses were carried out at the “Service d’Analyse” of Laboratoire de Chimie de Coordination (Toulouse) using a Perkin Elmer 2400 series II analyser and an iCAP 6300 ICP Spectrometer. XPS measurements were

performed at room temperature with a SPECS PHOIBOS 150 hemispherical analyzer (SPECS GmbH, Berlin, Germany) in a base pressure of 5×10^{-10} mbar using monochromatic Al K α radiation (1486.74 eV) as excitation source.

3.3.2. Synthesis of palladium nanoparticles stabilized by choline-based derivatives in glycerol

0.05 mmol (14.1 mg) of [PdCl₂(cod)] and 0.85 mmol of choline-based derivative [117 mg for choline chloride (**A**); 294.5 mg for choline *N*-tosylalaninate (**B**)] were dissolved in 5 mL of glycerol and stirred under argon in a Schlenk flask at 80 °C for 18 h. Then, the resulting solution was washed with dichloromethane (3x5 mL) in order to remove any insoluble IL from glycerol phase. A black colloidal solution was then obtained.

3.3.3. Synthesis of palladium nanoparticles stabilized by choline tosylalaninate at solid state, PdB

After synthesis, PdNPs in glycerol were transferred to a centrifugation tube and 2 mL of ethanol were added. Centrifugation was carried out at 4500 rpm for 1 h and then the solution was separated by decantation. This process was repeated 3 times until complete removal of glycerol. The remaining black powder was then dried under vacuum at 80 °C overnight. Elementary analysis (palladium content determined by ICP-AES) for **PdB**: Pd 84.0%, C 7.55%, N 0.30%, H 0.40%.

3.3.4. General procedure for Pd-catalyzed hydrogenation in glycerol

In a Fisher–Porter bottle (working from 1 to 3 bar total pressure) or an autoclave (working from 3 to 20 bar total pressure), the appropriate substrate (1 mmol for 1 mol% of catalyst or 10 mmol for 0.1 mol% of catalyst) was added to 1 mL of preformed nanoparticles (2.85 mg of Pd) in glycerol under argon. The reaction mixture was put under vacuum and then pressurized with H₂ at the convenient pressure, heated up at 80 °C and stirred for the appropriate time; then cooled down to room temperature before extraction. Organic products were extracted from glycerol by a biphasic methodology, adding dichloromethane (5 × 3 mL); organic phases were collected and solvent removed under vacuum. Conversion and yields were determined by GC using decane as internal standard. The obtained products were characterized by GC-MS data and ¹H and ¹³C NMR and compared to literature reports to confirm spectral identity.

3.3.5. Characterization of organic compounds

4-phenylbutan-2-one (1H)₄₈ ¹H NMR (300 MHz, CDCl₃) δ 7.45 – 7.15 (m, 5H), 2.96 (d, *J* = 7.5 Hz, 2H), 2.83 (d, *J* = 7.7 Hz, 2H), 2.20 (s, 3H). ¹³C NMR (75 MHz, CDCl₃) δ 207.8, 141.0, 128.5, 128.3, 126.1, 45.1, 30.0, 29.7.

Dodecane (2H)₄₉ ¹H NMR (300 MHz, CDCl₃) δ 1.31 (s, 20H), 1.07 – 0.76 (m, 6H). ¹³C NMR (75 MHz, Chloroform-*d*) δ 32.1, 29.9, 29.5, 22.8, 14.2.

1-phenylcyclohexane (5H)₅₀ ¹H NMR (300 MHz, CDCl₃) δ 7.20 (d, *J* = 13.5 Hz, 5H), 2.45 (s, 1H), 1.59 (d, 10H). ¹³C NMR (75 MHz, CDCl₃) δ 148.2, 128.4, 126.9, 125.9, 44.7, 34.6, 27.1, 26.3.

1,4-diphenylbutane (6H)₅₁ ¹H NMR (300 MHz, CDCl₃) δ 7.56 – 6.95 (m, 10H), 2.63 (s, 4H), 1.67 (s, 4H). ¹³C NMR (75 MHz, CDCl₃) δ 142.6, 128.5, 125.7, 35.9, 31.2.

Propylbenzene (8H)₄₈ ¹H NMR (300 MHz, CDCl₃) δ 7.94 – 6.68 (m, 5H), 3.00 – 2.30 (t, 2H), 1.76 (m, 2H), 1.06 (t, 3H). ¹³C NMR (75 MHz, CDCl₃) δ 142.8, 128.3, 125.7, 38.2, 24.7, 13.9.

Bibenzyl (9H)₄₉ ¹H NMR (300 MHz, CDCl₃) δ 7.51 – 7.15 (m, 10H), 2.99 (s, 4H). ¹³C NMR (75 MHz, CDCl₃) δ 141.9, 128.5, 126.0, 38.0.

cis-stilbene (9I)₅₂ ¹H NMR (300 MHz, CDCl₃) δ 7.64 – 7.06 (m, 10H), 6.62 (s, 2H). ¹³C NMR (75 MHz, CDCl₃) δ 137.3, 130.3, 128.9, 128.3, 127.2.

n-decane (10I)₅₃ ¹H NMR (300 MHz, CDCl₃) δ 1.27 (s, 16H), 0.86 (s, 6H). ¹³C NMR (75 MHz, CDCl₃) δ 32.1, 29.8, 29.5, 22.8, 14.2.

Aniline (11H)₅₃ ¹H NMR (300 MHz, CDCl₃) δ 7.53 – 7.07 (m, 2H), 7.01 – 6.59 (m, 3H), 3.68 (s, 2H). ¹³C NMR (75 MHz, CDCl₃) δ 146.4, 129.2, 118.4, 115.1.

Benzyl alcohol (12H)₅₁ ¹H NMR (300 MHz, CDCl₃) δ 7.39 (m, 5H), 4.63 (s, 1H), 3.58 (s, 1H). ¹³C NMR (75 MHz, CDCl₃) δ 140.8, 128.4, 127.4, 126.9, 64.7.

4-bromobenzyl alcohol (13H)₅₃ ¹H NMR (300 MHz, CDCl₃) δ 7.65 – 6.97 (m, 4H), 4.69 (s, 2H). ¹³C NMR (75 MHz, CDCl₃) δ 139.8, 131.7, 128.7, 121.5, 64.7.

4-(tert-butyl)-benzyl alcohol (14H)₅₄ ¹H NMR (300 MHz, CDCl₃) δ 7.63 – 7.12 (m, 4H), 4.67 (s, 2H), 2.68 (s, 1H), 1.39 (d, 9H). ¹³C NMR (75 MHz, CDCl₃) δ 150.6, 138.0, 126.9, 125.5, 65.0, 34.6, 31.4.

Phenylethanol (15H)⁵¹ ¹H NMR (300 MHz, CDCl₃) δ 7.63 – 7.09 (m, 5H), 4.90 (d, 1H), 2.47 (s, 1H), 1.52 (d, 3H). ¹³C NMR (75 MHz, CDCl₃) δ 145.9, 128.5, 127.5, 125.44, 70.4, 25.2.

2,2,2-trifluoro-1-phenylethanol-1-ol (16H)⁵⁵ ¹H NMR (300 MHz, CDCl₃) δ 7.42 (d, *J* = 3.0 Hz, 5H), 5.01 (d, *J* = 6.8 Hz, 1H), 3.27 (s, 1H). ¹³C NMR (75 MHz, CDCl₃) δ 129.6, 128.7, 127.5, 72.9 (d, *J* = 31.9 Hz). ¹⁹F NMR (282 MHz, CDCl₃) δ -78.28 (d, *J* = 6.8 Hz).

4-phenylbutan-2-ol (11)⁵⁶ ¹H NMR (300 MHz, CDCl₃) δ 7.27 (m, 5H), 3.86 (m, 1H), 3.07 – 2.55 (m, 2H), 1.95 (s, 1H), 1.87 – 1.77 (m, 1H), 1.28 (d, 3H). ¹³C NMR (75 MHz, CDCl₃) δ 142.1, 128.4, 125.8, 67.5, 40.9, 32.2, 23.6.

3.4. Conclusions

To sum up, we efficiently prepared and fully characterized new palladium nanocatalysts, stabilized by environmentally friendly choline-based ionic liquids in glycerol. The counter anion of the choline derivative showed a non-innocent effect on the catalytic activity, probably due to the higher adsorption of chloride than tosyl-alaninate at the metallic surface,⁵⁷ and consequently hindering the interaction of reagents with palladium.

PdB was active for the hydrogenation of C-C multiple bonds and for C=O bond of aromatic aldehydes and aromatic ketones. It was found that it was more active for conjugated substrates as explained above in Section 3.2.2.⁵⁸ For non-conjugated substrates, such as internal alkyl alkynes, **PdB** was highly selective to the formation of the corresponding alkene. The organic products extracted from the catalytic glycerol phase did not contain palladium according to ICP-AES analyses, proving the efficient immobilization of PdNPs in the glycerol phase.

3.5. References

- (1) Favier, I.; Madec, D.; Gómez, M. Metallic Nanoparticles in Ionic Liquids - Applications in Catalysis. *Nanomater. Catal. First Ed.* **2012**, 203–249. <https://doi.org/10.1002/9783527656875.ch5>.
- (2) Suzuki, A. Carbon-Carbon Bonding Made Easy. *Chem. Commun.* **2005**, No. 38, 4759–4763. <https://doi.org/10.1039/b507375h>.
- (3) de Vries, J. G. Ligand-Free Heck Reactions Using Low Pd-Loading. *Chem. Commun.* **2004**, 4 (14), 1559–1563. <https://doi.org/10.1039/b406719n>.

- (4) Zapf, A.; Jackstell, R.; Rataboul, F.; Riermeier, T.; Monsees, A.; Fuhrmann, C.; Shaikh, N.; Dingerdissen, U.; Beller, M. Erratum: Practical Synthesis of New and Highly Efficient Ligands for the Suzuki Reaction of Aryl Chlorides (Chemical Communications (2004) (38-39) DOI: 10.1039/B311268n). *Chem. Commun.* **2004**, 10 (11), 1340.
- (5) Tang, D.; Sun, X.; Zhao, D.; Zhu, J.; Zhang, W.; Xu, X.; Zhao, Z. Nitrogen-Doped Carbon Xerogels Supporting Palladium Nanoparticles for Selective Hydrogenation Reactions: The Role of Pyridine Nitrogen Species. *ChemCatChem* **2018**, 10 (6), 1291–1299. <https://doi.org/10.1002/cctc.201702007>.
- (6) Concepción, P.; García, S.; Hernández-Garrido, J. C.; Calvino, J. J.; Corma, A. A Promoting Effect of Dilution of Pd Sites Due to Gold Surface Segregation under Reaction Conditions on Supported Pd-Au Catalysts for the Selective Hydrogenation of 1,5-Cyclooctadiene. *Catal. Today* **2016**, 259, 213–221. <https://doi.org/10.1016/j.cattod.2015.07.022>.
- (7) Cookson, J. The Preparation of Palladium Nanoparticles. *Platin. Met. Rev.* **2012**, 56 (2), 83–98. <https://doi.org/10.1595/147106712X632415>.
- (8) Chahdoura, F.; Mallet-Ladeira, S.; Gómez, M. Palladium Nanoparticles in Glycerol: A Clear-Cut Catalyst for One-Pot Multi-Step Processes Applied in the Synthesis of Heterocyclic Compounds. *Org. Chem. Front.* **2015**, 2 (4), 312–318. <https://doi.org/10.1039/c4qo00338a>.
- (9) Reina, A.; Pradel, C.; Martin, E.; Teuma, E.; Gómez, M. Palladium Nanoparticles Stabilised by Cinchona-Based Alkaloids in Glycerol: Efficient Catalysts for Surface Assisted Processes. *RSC Adv.* **2016**, 6 (95), 93205–93216. <https://doi.org/10.1039/c6ra19230k>.
- (10) Simon, N. M.; Abarca, G.; Scholten, J. D.; Domingos, J. B.; Mecerreyes, D.; Dupont, J. Structural, Electronic and Catalytic Properties of Palladium Nanoparticles Supported on Poly(Ionic Liquid). *Appl. Catal. A Gen.* **2018**, 562 (April), 79–86. <https://doi.org/10.1016/j.apcata.2018.06.001>.
- (11) Luza, L.; Rambor, C. P.; Gual, A.; Bernardi, F.; Domingos, J. B.; Grehl, T.; Brüner, P.; Dupont, J. Catalytically Active Membranelike Devices: Ionic Liquid Hybrid Organosilicas Decorated with Palladium Nanoparticles. *ACS Catal.* **2016**, 6 (10), 6478–6486. <https://doi.org/10.1021/acscatal.6b01813>.
- (12) Luza, L.; Gual, A.; Rambor, C. P.; Eberhardt, D.; Teixeira, S. R.; Bernardi, F.; Baptista, D. L.; Dupont, J. Hydrophobic Effects on Supported Ionic Liquid Phase Pd Nanoparticle Hydrogenation Catalysts. *Phys. Chem. Chem. Phys.* **2014**, 16 (34), 18088–18091. <https://doi.org/10.1039/c4cp03063j>.
- (13) Venkatesan, R.; Prechtel, M. H. G.; Scholten, J. D.; Pezzi, R. P.; MacHado, G.; Dupont, J.

- Palladium Nanoparticle Catalysts in Ionic Liquids: Synthesis, Characterisation and Selective Partial Hydrogenation of Alkynes to Z-Alkenes. *J. Mater. Chem.* **2011**, *21* (9), 3030–3036. <https://doi.org/10.1039/c0jm03557b>.
- (14) Umpierre, A. P.; Machado, G.; Fecher, G. H.; Morais, J.; Dupont, J. Selective Hydrogenation of 1,3-Butadiene to 1-Butene by Pd(0) Nanoparticles Embedded in Imidazolium Ionic Liquids. *Adv. Synth. Catal.* **2005**, *347* (10), 1404–1412. <https://doi.org/10.1002/adsc.200404313>.
- (15) Hu, Y.; Yang, H.; Zhang, Y.; Hou, Z.; Wang, X.; Qiao, Y.; Li, H.; Feng, B.; Huang, Q. The Functionalized Ionic Liquid-Stabilized Palladium Nanoparticles Catalyzed Selective Hydrogenation in Ionic Liquid. *Catal. Commun.* **2009**, *10* (14), 1903–1907. <https://doi.org/10.1016/j.catcom.2009.06.025>.
- (16) Dong, H.; Chen, Y. C.; Feldmann, C. Polyol Synthesis of Nanoparticles: Status and Options Regarding Metals, Oxides, Chalcogenides, and Non-Metal Elements. *Green Chem.* **2015**, *17* (8), 4107–4132. <https://doi.org/10.1039/c5gc00943j>.
- (17) Chahdoura, F.; Pradel, C.; Gómez, M. Copper(I) Oxide Nanoparticles in Glycerol: A Convenient Catalyst for Cross-Coupling and Azide-Alkyne Cycloaddition Processes. *ChemCatChem* **2014**, *6* (10), 2929–2936. <https://doi.org/10.1002/cctc.201402214>.
- (18) Chahdoura, F.; Pradel, C.; Gómez, M. Palladium Nanoparticles in Glycerol: A Versatile Catalytic System for C-X Bond Formation and Hydrogenation Processes. *Adv. Synth. Catal.* **2013**, *355* (18), 3648–3660. <https://doi.org/10.1002/adsc.201300753>.
- (19) Dang-Bao, T.; Pla, D.; Favier, I.; Gómez, M. Bimetallic Nanoparticles in Alternative Solvents for Catalytic Purposes. *Catalysts* **2017**, *7* (7). <https://doi.org/10.3390/catal7070207>.
- (20) Albericio, F.; Isidro-Ilobet, A.; Mercedes, A. Amino Acid-Protecting Groups. **2009**, 2455–2504.
- (21) Hirai, H.; Nakao, Y.; Toshima, N.; Adachi, K. Colloidal Rhodium in Polyvinyl Alcohol As Hydrogenation Catalyst of Olefins. *Chem. Lett.* **1976**, *5* (9), 905–910. <https://doi.org/10.1246/cl.1976.905>.
- (22) Zhang, Z.; Li, H.; Zhang, F.; Wu, Y.; Guo, Z.; Zhou, L.; Li, J. Investigation of Halide-Induced Aggregation of Au Nanoparticles into Spongelike Gold. *Langmuir* **2014**, *30* (10), 2648–2659. <https://doi.org/10.1021/la4046447>.
- (23) Yang, Q.; Wang, Z.; Bao, Z.; Zhang, Z.; Yang, Y.; Ren, Q.; Xing, H.; Dai, S. New Insights into CO₂ Absorption Mechanisms with Amino-Acid Ionic Liquids. *ChemSusChem* **2016**, *9* (8), 806–812. <https://doi.org/10.1002/cssc.201501691>.
- (24) Chahdoura, F.; Favier, I.; Gómez, M. Glycerol as Suitable Solvent for the Synthesis of Metallic

- Species and Catalysis. *Chem. - A Eur. J.* **2014**, *20* (35), 10884–10893. <https://doi.org/10.1002/chem.201403534>.
- (25) Favier, I.; Pla, D.; Gómez, M. Metal-Based Nanoparticles Dispersed in Glycerol: An Efficient Approach for Catalysis. *Catal. Today* **2018**, *310* (June 2017), 98–106. <https://doi.org/10.1016/j.cattod.2017.06.026>.
- (26) Root, L. J.; Stillinger, F. H. Short-range Order in Glycerol. A Molecular Dynamics Study. *J. Chem. Phys.* **1989**, *90* (2), 1200–1208. <https://doi.org/10.1063/1.456176>.
- (27) Patterson, A. L. The Scherrer Formula for X-Ray Particle Size Determination. *Phys. Rev.* **1939**, *56* (10), 978–982. <https://doi.org/10.1103/PhysRev.56.978>.
- (28) Jensen, H.; Pedersen, J. H.; Jørgensen, J. E.; Pedersen, J. S.; Joensen, K. D.; Iversen, S. B.; Sjøgaard, E. G. Determination of Size Distributions in Nanosized Powders by TEM, XRD, and SAXS. *J. Exp. Nanosci.* **2006**, *1* (3), 355–373. <https://doi.org/10.1080/17458080600752482>.
- (29) Jensen, H.; Joensen, K. D.; Jørgensen, J. E.; Pedersen, J. S.; Sjøgaard, E. G. Characterization of Nanosized Partly Crystalline Photocatalysts. *J. Nanoparticle Res.* **2004**, *6* (5), 519–526. <https://doi.org/10.1007/s11051-004-1714-3>.
- (30) Kumar Petla, R.; Vivekanandhan, S.; Misra, M.; Kumar Mohanty, A.; Satyanarayana, N. Soybean (&I≫Glycine Max&I≫) Leaf Extract Based Green Synthesis of Palladium Nanoparticles. *J. Biomater. Nanobiotechnol.* **2012**, *03* (01), 14–19. <https://doi.org/10.4236/jbnb.2012.31003>.
- (31) Hines, L. F.; Stille, J. K. Stereochemistry of Carbonylation of Some Diene-Palladium(II) Complexes and Their Corresponding Carbon-Palladium (II) σ -Bonded Oxymetallation Products. *J. Am. Chem. Soc.* **1972**, *94* (2), 485–490. <https://doi.org/10.1021/ja00757a027>.
- (32) Sedgwick, D. M.; Hammond, G. B. The History and Future Challenges Associated with the Hydrogenation of Vinyl Fluorides. *J. Fluor. Chem.* **2018**, *207* (January), 45–58. <https://doi.org/10.1016/j.jfluchem.2017.12.019>.
- (33) Kauffman, G. B. Johann Wolfgang Döbereiner's Feuerzeug. *Platin. Met. Rev.* **1999**, *43* (3), 122–128.
- (34) Williams, W. D. Döbereiner's Hydrogen Lighter. *Bull. Hist. Chem.* **1999**, *24*, 66–68.
- (35) Rönsch, S.; Schneider, J.; Matthischke, S.; Schlüter, M.; Götz, M.; Lefebvre, J.; Prabhakaran, P.; Bajohr, S. Review on Methanation - From Fundamentals to Current Projects. *Fuel*. 2016. <https://doi.org/10.1016/j.fuel.2015.10.111>.

- (36) Reese, M.; Marquart, C.; Malmali, M.; Wagner, K.; Buchanan, E.; McCormick, A.; Cussler, E. L. Performance of a Small-Scale Haber Process. *Ind. Eng. Chem. Res.* **2016**, *55* (13), 3742–3750. <https://doi.org/10.1021/acs.iecr.5b04909>.
- (37) Abatzoglou, N.; Dalai, A. K.; Gitzhofer, F. Green Diesel from Fischer–Tropsch Synthesis: Challenges and Hurdles. *Proc. 3rd IASME/ ...* **2007**, 223–232.
- (38) Mattson, B.; Foster, W.; Greimann, J.; Hoette, T.; Le, N.; Mirich, A.; Wankum, S.; Cabri, A.; Reichenbacher, C.; Schwanke, E. Heterogeneous Catalysis: The Horiuti–Polanyi Mechanism and Alkene Hydrogenation. *J. Chem. Educ.* **2013**, *90* (5), 613–619. <https://doi.org/10.1021/ed300437k>.
- (39) Yang, B.; Gong, X. Q.; Wang, H. F.; Cao, X. M.; Rooney, J. J.; Hu, P. Evidence to Challenge the Universality of the Horiuti–Polanyi Mechanism for Hydrogenation in Heterogeneous Catalysis: Origin and Trend of the Preference of a Non-Horiuti–Polanyi Mechanism. *J. Am. Chem. Soc.* **2013**, *135* (40), 15244–15250. <https://doi.org/10.1021/ja408314k>.
- (40) Ohno, S.; Wilde, M.; Mukai, K.; Yoshinobu, J.; Fukutani, K. Mechanism of Olefin Hydrogenation Catalysis Driven by Palladium-Dissolved Hydrogen. *J. Phys. Chem. C* **2016**, *120* (21), 11481–11489. <https://doi.org/10.1021/acs.jpcc.6b00987>.
- (41) López-Vinasco, A. M.; Guerrero-Ríos, I.; Favier, I.; Pradel, C.; Teuma, E.; Gómez, M.; Martin, E. Tuning the Hydrogen Donor/Acceptor Behavior of Ionic Liquids in Pd-Catalyzed Multi-Step Reactions. *Catal. Commun.* **2015**, *63*, 56–61. <https://doi.org/10.1016/j.catcom.2014.10.011>.
- (42) Liao, G.; Dong, W. H.; Yang, J. L.; Li, W.; Wang, J.; Mei, W. L.; Dai, H. F. Monitoring the Chemical Profile in Agarwood Formation within One Year and Speculating on the Biosynthesis of 2-(2-Phenylethyl)Chromones. *Molecules* **2018**, *23* (6). <https://doi.org/10.3390/molecules23061261>.
- (43) Jutz, F.; Andanson, J. M.; Baiker, A. A Green Pathway for Hydrogenations on Ionic Liquid-Stabilized Nanoparticles. *J. Catal.* **2009**, *268* (2), 356–366. <https://doi.org/10.1016/j.jcat.2009.10.006>.
- (44) Carturan, G.; Facchin, G.; Cocco, G.; Navazio, G.; Gubitosa, G. Hydrogenation of Nitrocompounds with Supported Palladium Catalysts: Influence of Metal Dispersion and Nitrocompound Nature. *J. Catal.* **1983**, *82* (1), 56–65. [https://doi.org/10.1016/0021-9517\(83\)90117-3](https://doi.org/10.1016/0021-9517(83)90117-3).
- (45) Nindakova, L. O.; Strakhov, V. O.; Kolesnikov, S. S. Hydrogenation of Ketones on Dispersed Chiral-Modified Palladium Nanoparticles. *Russ. J. Gen. Chem.* **2018**, *88* (2), 199–207. <https://doi.org/10.1134/S1070363218020044>.

- (46) S., C.; Matiadis, D.; Markopoulos, J.; Igglessi-Markopoulou, O. Homogeneous Chemoselective Hydrogenation of Heterocyclic Compounds – The Case of 1,4 Addition on Conjugated C-C and C-O Double Bonds of Arylidene Tetramic Acids. *Hydrogenation* **2012**. <https://doi.org/10.5772/48739>.
- (47) Sdira, S. Ben; Felix, C. P.; Giudicelli, A.; Seigle-ferrand, P. F.; Perrin, M.; Lamartine, R. J.; Academic, K. Synthesis and Structure of Lower Rim C-Linked N -Tosyl Peptidocalix [4] Arenes. **2003**, No. 13, 6632–6638. <https://doi.org/10.1021/jo034275j>.
- (48) Hayes, J. F.; Shipman, M.; Twin, H. Multicomponent Reactions Involving 2-Methyleneaziridines: Rapid Synthesis of 1,3-Disubstituted Propanones. *J. Org. Chem.* **2002**, 67 (3), 935–942. <https://doi.org/10.1021/jo016164v>.
- (49) Xu, X.; Cheng, D.; Pei, W. Iron-Catalyzed Homocoupling of Bromide Compounds. *J. Org. Chem.* **2006**, 71 (17), 6637–6639. <https://doi.org/10.1021/jo060673l>.
- (50) Chem, T. J. Synthesis and Isolation of 1-Cyclohex-1 , 2-Dien-1-Ylbenzene from 1- (2-Iodocyclohex-1-En-1-Yl) Benzene and 1- (2-Iodocyclohex-2-En-1-Yl) Benzene. **2007**, 31, 647–657.
- (51) Eisch, J. J.; Dutta, S. Carbon-Carbon Bond Formation in the Surprising Rearrangement of Diorganylzirconium Dialkoxides: Linear Dimerization of Terminal Olefins. *Organometallics* **2005**, 24 (14), 3355–3358. <https://doi.org/10.1021/om050256j>.
- (52) Belger, C.; Neisius, N. M.; Plietker, B. A Selective Ru-Catalyzed Semireduction of Alkynes to Z Olefins under Transfer-Hydrogenation Conditions. *Chem. - A Eur. J.* **2010**, 16 (40), 12214–12220. <https://doi.org/10.1002/chem.201001143>.
- (53) Patra, A. K.; Kundu, S. K.; Kim, D.; Bhaumik, A. Controlled Synthesis of a Hexagonal-Shaped NiO Nanocatalyst with Highly Reactive Facets {1-1-0} and Its Catalytic Activity. *ChemCatChem* **2015**, 7 (5), 791–798. <https://doi.org/10.1002/cctc.201402871>.
- (54) Dieskau, A. P.; Begouin, J. M.; Plietker, B. Bu₄N[Fe(CO)₃(NO)]-Catalyzed Hydrosilylation of Aldehydes and Ketones. *European J. Org. Chem.* **2011**, 3 (27), 5291–5296. <https://doi.org/10.1002/ejoc.201100717>.
- (55) Šterk, D.; Stephan, M.; Mohar, B. Highly Enantioselective Transfer Hydrogenation of Fluoroalkyl Ketones. *Org. Lett.* **2006**, 8 (26), 5935–5938. <https://doi.org/10.1021/ol062358r>.
- (56) Imura, S.; Manabe, K.; Kobayashi, S. Hydrophobic Polymer-Supported Catalyst for Organic Reactions in Water: Acid-Catalyzed Hydrolysis of Thioesters and Transprotection of Thiols. *Org. Lett.* **2003**, 5 (2), 101–103. <https://doi.org/10.1021/ol026906m>.

- (57) Favier, I.; Toro, M. Lou; Lecante, P.; Pla, D.; Gómez, M. Palladium-Mediated Radical Homocoupling Reactions: A Surface Catalytic Insight. *Catal. Sci. Technol.* **2018**, 8 (18), 4766–4773. <https://doi.org/10.1039/c8cy00901e>.
- (58) Garg, G.; Foltran, S.; Favier, I.; Pla, D.; Medina-González, Y.; Gómez, M. Palladium Nanoparticles Stabilized by Novel Choline-Based Ionic Liquids in Glycerol Applied in Hydrogenation Reactions. *Catal. Today* **2019**. <https://doi.org/10.1016/j.cattod.2019.01.052>.

Chapter 4

Catalytic Hydrogenation under
Carbon Dioxide and Extraction
of Products using Supercritical
Carbon Dioxide

4.1. Pd-catalyzed hydrogenation reactions under sub and supercritical carbon dioxide

4.1.1. Introduction

Catalytic hydrogenation is one of the most employed reactions in industrial applications.^{1,2} Hydrogenations are majorly catalyzed by noble metals like Ru, Pd, Pt etc. involving different solvents, such as water, alcohols, ionic liquids.^{3,4} The common factors influenced by solvents are 1) hydrogen solubility, which directly affects overall rates, 2) catalytic dissociation of molecular hydrogen, 3) solubility of reactants and products, and 4) competitive adsorption of solvent molecules on the active sites of the catalyst.⁵ Hydrogenation reactions are often limited due to the low solubility of hydrogen in the solvents currently used. Application of CO₂ in sub or supercritical states during hydrogenation can serve as a promotor for transporting hydrogen into the liquid phase and thus enhance the equilibrium concentrations of both reactants and products in the gaseous phase.^{6,7} For example, Brunner *et al.* investigated and calculated the phase equilibria of hydrogen, carbon dioxide, squalene, and squalane for the hydrogenation of squalene to squalane, showing that the additional application of scCO₂ enhances the equilibrium concentrations of squalene and squalane in the gaseous phase.⁶ Their results focused on planning of hydrogenation of squalene to squalane using supercritical carbon dioxide (scCO₂) as a modifier for solubility in both phases. Supercritical reaction media have been investigated for completely solubilizing hydrogen and thereby eliminating gas–liquid transport resistances in heterogeneous-catalyzed hydrogenations. Härräd and Møller showed that by employing supercritical conditions, reaction rates for hydrogenation of fats and oils (triglycerides) can go as high as 1,000 times compared to conventional methods, *i.e.* a multiphase, gas–liquid system at low pressures in which the hydrogen is contacted with a nickel-based catalyst that is suspended in the vegetable oil.⁸ Supercritical carbon dioxide (scCO₂), in this context, attracts a lot of attraction due its green properties and easy availability. ScCO₂ is chemically relatively inert (for example, it is resistant to free radical chemistry) and is a low-toxic aprotic solvent.^{7,9,10}

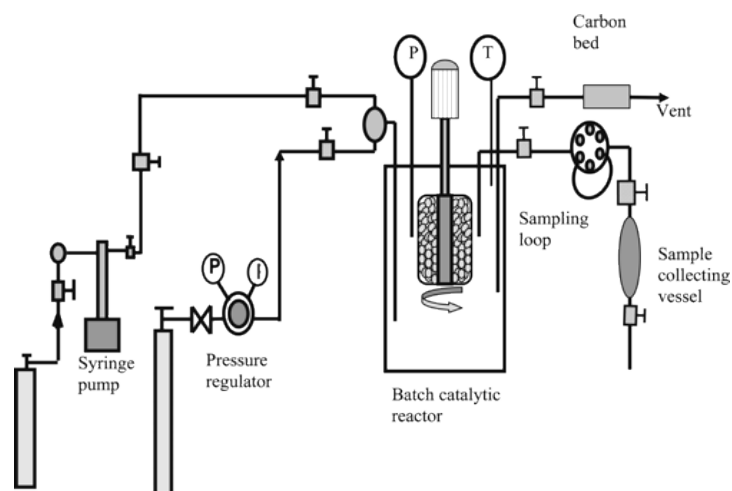


Figure 4.1. Schematic diagram of a laboratory-scale hydrogenation reactor under scCO_2 medium. (Open access)¹¹

Typically, during a hydrogenation process under scCO_2 , the starting material and molecular hydrogen are dissolved in scCO_2 giving one phase system. Consequently, at the end of the reaction, the supercritical mixture is returned to the gas phase due to the depressurization of the system and the products and any unreacted starting material can easily be collected as they separate from the gas phase (Figure 4.1).^{11,12} Bogel-Łukasik *et al.* reported that Rh and Ru catalyzed hydrogenation in a CO_2 -expanded liquid terpene is influenced by the phase equilibria which determines the fine changes in the liquid and the vapor phases composition, and the volume expansion of the liquid phase attributable to the presence of CO_2 (Figure 4.2).¹³

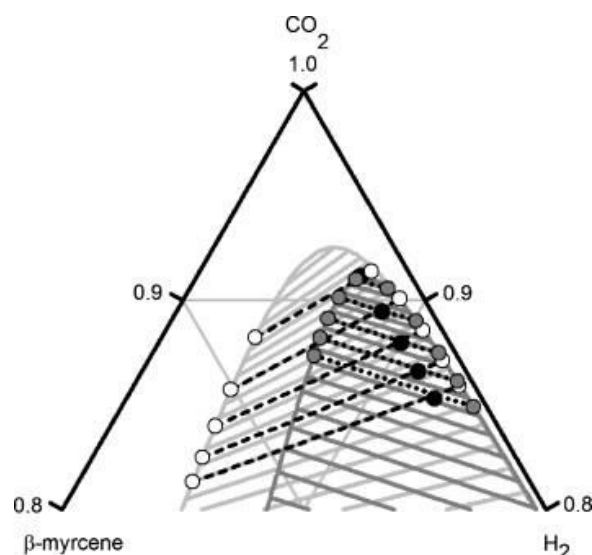
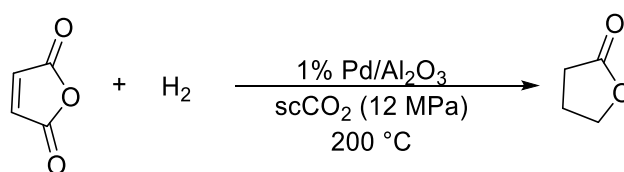


Figure 4.2. Predicted vapor–liquid equilibrium phase diagrams for CO₂ + β -myrcene + H₂ (light grey phase envelop) system at 12.5 MPa total pressure and 323.15 K. Filled circles (●) represent the overall initial composition of the reaction mixture. Dashed tie lines give the compositions of the liquid and the gas phase (○). Dotted tie lines and grey circles represent the compositions of the liquid and the gas phase for CO₂ + limonene + H₂ (dark grey phase envelop) system. (Reprinted from reference (13), Copyright 2010, with permission from Elsevier)

Supercritical CO₂ can also help to achieve better selectivity.^{11,14,15} Pillai *et al.* and Wang *et al.* showed that for the hydrogenation of maleic anhydride over palladium catalyst in scCO₂ higher selectivity of towards γ -butyrolactone (GBL) can be obtained as compared to conventional organic solvent system (Scheme 4.1).^{11,14,15}



Scheme 4.1. Hydrogenation of maleic anhydride.¹⁵

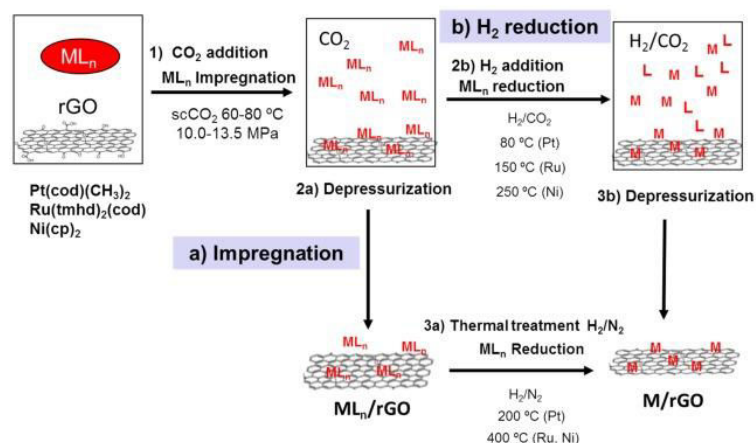


Figure 4.4 (a) Metal deposition on rGO by: (a) impregnation in scCO₂ and further reduction in H₂/N₂ and (b) reduction in H₂/CO₂. Reprinted from reference (21), Copyright 2016, with permission from Elsevier.

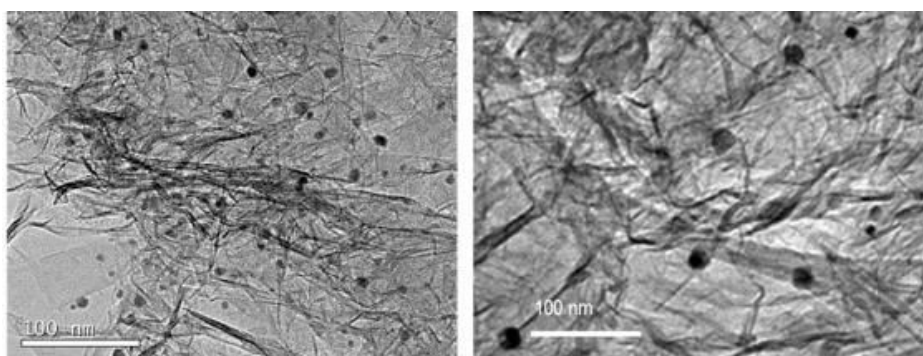


Figure 4.5 TEM images of Ni/rGO obtained in scCO₂ using: impregnation (left) and (b) H₂ reduction in scCO₂ (right). Reprinted from reference (21), Copyright 2016), with permission from Elsevier.

In this context, this chapter will serve to discuss about the effect of CO₂ on catalytic hydrogenation of nitrobenzene and 4-phenylbutan-2-one using tosylalaninate stabilized palladium nanoparticles in glycerol. The aim of this study was to increase the catalytic efficiency of the PdNPs used in this thesis. In other words, we want to achieve high conversion rates using lower amount of H₂.

4.1.2. Results and discussion

As discussed above, carbon dioxide (CO₂) has been known to increase the efficiency of hydrogenation by increasing the solubility of hydrogen into the system.^{9,22,23} The work in Chapter 3 (Section 3.2) described the system used for hydrogenation of various compounds

exhibiting different functional groups using palladium nanoparticles (PdNPs) as catalyst.²⁴ In the discussion below, we aim to use carbon dioxide to increase the efficiency of the PdNPs used in Chapter 3.

To study the effect of sub and supercritical CO₂ on hydrogenation the catalytic reduction of nitrobenzene to aniline was studied. This work was done under the supervision of Dr. A. M. Masdeu-Bultó at University Rovira i Virgili (Tarragona, Spain). Table 4.1 summarizes the results for the reduction of nitrobenzene with different pressure of carbon dioxide at 80 °C. Entry 1 shows the conversion of the substrate under 5 bar of H₂ in the absence of CO₂, obtaining a high conversion. Then, the effect of CO₂ was studied. As high amounts of CO₂ was introduced, formation of aniline decreased dramatically (entries 2 and 3, Table 4.1). The plausible explanation behind this decrease can be that as the amount of CO₂ increases, the partial pressure of H₂ ($p_{\text{H}_2} = 5$ bar, $p_{\text{CO}_2} = 235$ bar – 275 bar) in the system decreases which leads to low availability of H₂ for the reduction or in the other words, H₂ in the system is diluted due to high amounts of CO₂. Similar observations were reported by Olbrich *et. al.*, where they saw an indirect decrease of the hydrogenation of pyrolysis oil over nickel-based catalysts due to the lower partial pressure of hydrogen.²⁵ Following these observations, the pressure of the system was decreased and the reaction was done in non-supercritical conditions ($p_{\text{H}_2} = 5$ bar, $p_{\text{CO}_2} = 70$ bar) (entry 4, Table 4.2). These conditions led to full conversion of nitrobenzene. However, with this result it is not possible to conclude whether carbon dioxide is helping in increasing the efficiency of hydrogenation because the conversion in presence and absence of CO₂ is the same.

Table 4.1. Hydrogenation of 4-nitrobenzene in glycerol catalyzed by PdNPs stabilized by choline tosylalaninate.^a

| Entry | $p(\text{H}_2)$ (bar) | $p(\text{CO}_2)$ (bar) | Conversion (yield) ^b (%) |
|-------|--------------------------|---------------------------|--|
| 1 | 5 | 0 | 97 (93) |
| 2 | 5 | 235 | 45 (43) |
| 3 | 5 | 275 | 11 (n.d) |
| 4 | 5 | 70 | >99 (95) |

^a Results from duplicated experiments. Reaction conditions: 1 mmol of **1** and 1 mL of the corresponding catalytic glycerol solution of PdNPs (10⁻² mol L⁻¹, 0.01 mmol of total Pd). ^b Determined by GC and GC/MS using decane as internal standard. n.d = not determined.

From these results, it is clear that nitrobenzene is not an appropriate substrate for this study due to its easy reduction. Therefore, a more challenging substrate was chosen. 4-Phenylbutanone was then used as model substrate in order to study the reduction of a ketone group into a secondary alcohol, leading to the formation of 4-phenylbutan-2-ol (Table 4.2). In order to better observe the effect of the partial pressures of CO₂ and hydrogen, as well as the effect of total pressure on the conversion, reactions 1 to 7 were conducted at the same total pressure of 40 bar, the effect of an increase in total pressure is shown in entry 8 of table 4.2.

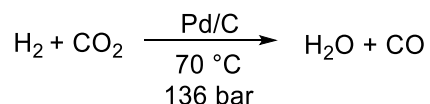
Table 4.2. Hydrogenation of 4-phenylbutanone in glycerol catalyzed by PdNPs stabilized by choline tosylalaninate.^a

| Entry | $p(\text{H}_2)$ (bar) | $p(\text{CO}_2)$ (bar) | Conv. (yield) ^b (%) |
|----------------|--------------------------|---------------------------|--------------------------------|
| 1 | 20 | 0 | 23 (21) |
| 2 | 30 | 0 | 26 (23) |
| 3 | 40 | 0 | 40 (37) |
| 4 | 10 | 30 | 37 (35) |
| 5 | 30 | 10 | 26(22) |
| 6 ^c | 10 | 30 | 40 (35) |
| 7 ^d | 10 | 30 | 11.5 (n.d) |
| 8 ^e | 10 | 30 | 44.3(41) |
| 9 | 40 | 40 | 45(40) |

^a Results from duplicated experiments. Reaction conditions: 1 mmol of **1** and 1 mL of the corresponding catalytic glycerol solution of PdNPs (10⁻² mol L⁻¹, 0.01 mmol of total Pd). ^b Determined by GC and GC/MS using decane as internal standard. ^c Reaction time 40 h. ^d Reaction time 7 h. ^e 2 mmol of substrate and 2 mL of the catalytic glycerol solution of PdNPs.

In the absence of CO₂ (entries 1 2 and 3, Table 4.2), we could reach 40% conversion under harsh conditions (40 bar H₂) and only 23% conversion under 20 bar H₂. We could clearly state the benefic effect of CO₂ when the reaction was carried out under the same total pressure (40 bar) but using four times less amount of hydrogen (entry 3 vs 4, Table 4.2). The conversion remains low under 30 bar H₂ and 10 bar CO₂ (entry 5). The reason for this is that when 10 bar CO₂ was probably not enough to increase the conversion that is initially obtained with 30 bar H₂ in the absence of CO₂ (entry 2). However, we were unable to increase the conversion beyond 40% (entries 6, 8-9) even when the reaction was run at longer time (40 h, entry 6) or with higher

catalytic load (2 mol%, entry 8) or higher pressure of H₂ and CO₂ (entry 9). We also did the reaction under the same conditions but at shorter time to confirm the saturation of the reaction, in other words, we wanted to see at what point the reaction reaches its maximum conversion. In entry 7, (Table 4.2) we could see that for a shorter time (7 h), the conversion was only 11%. The reason behind this behavior might be the catalyst deactivation after a certain time. One of the reasons can be associated to the formation of CO as a by-product of the reverse water-gas shift reaction even at low temperature (Scheme 4.2).^{12,26}



Scheme 4.2. Reaction showing formation of carbon monoxide as a product of the reverse water-gas shift reaction.^{12,26}

Another plausible explanation proposed for deactivation of palladium in the presence of CO₂ and hydrogen at high pressures is the formation of metal formate species, In other words, insertion of CO₂ between the metal and the dissociative adsorbed hydrogen can lead to the formation of metal formates, *e.g.* Pd-C(O)OH.^{12,27} Jessop had suggested that these formates are stable at high pressure but revert to CO₂ and H₂ when depressurized.²⁷

We were also interested in knowing the state of nanoparticles after catalysis (Figure 4.6). It is evident from Figure 4.6 (a & b) that CO₂ led to the agglomeration of PdNPs after catalysis. However, it was found that when more amount of H₂ was used, the PdNPs retained their dispersion (Figure 4.7(a)). It can be clearly seen that the presence of H₂ avoided the agglomeration and led to dispersed PdNPs. It was also observed that when PdNPs were exposed to H₂ for a longer time (even though the amount of H₂ was less) there was some inhomogeneous dispersion in the system after catalysis ((Figure 4.7(b)).

(a)

(b)

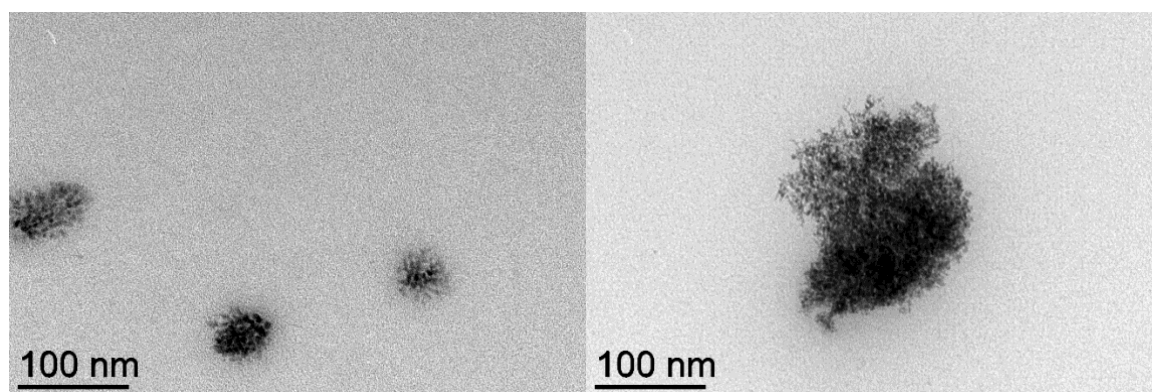


Figure 4.6. TEM micrographs of PdNPs after catalysis (a) 10 bar H₂ + 30 bar CO₂ at 80 °C for 18 h (b) 10 bar H₂ + 30 bar CO₂ at 80 °C for 7 h

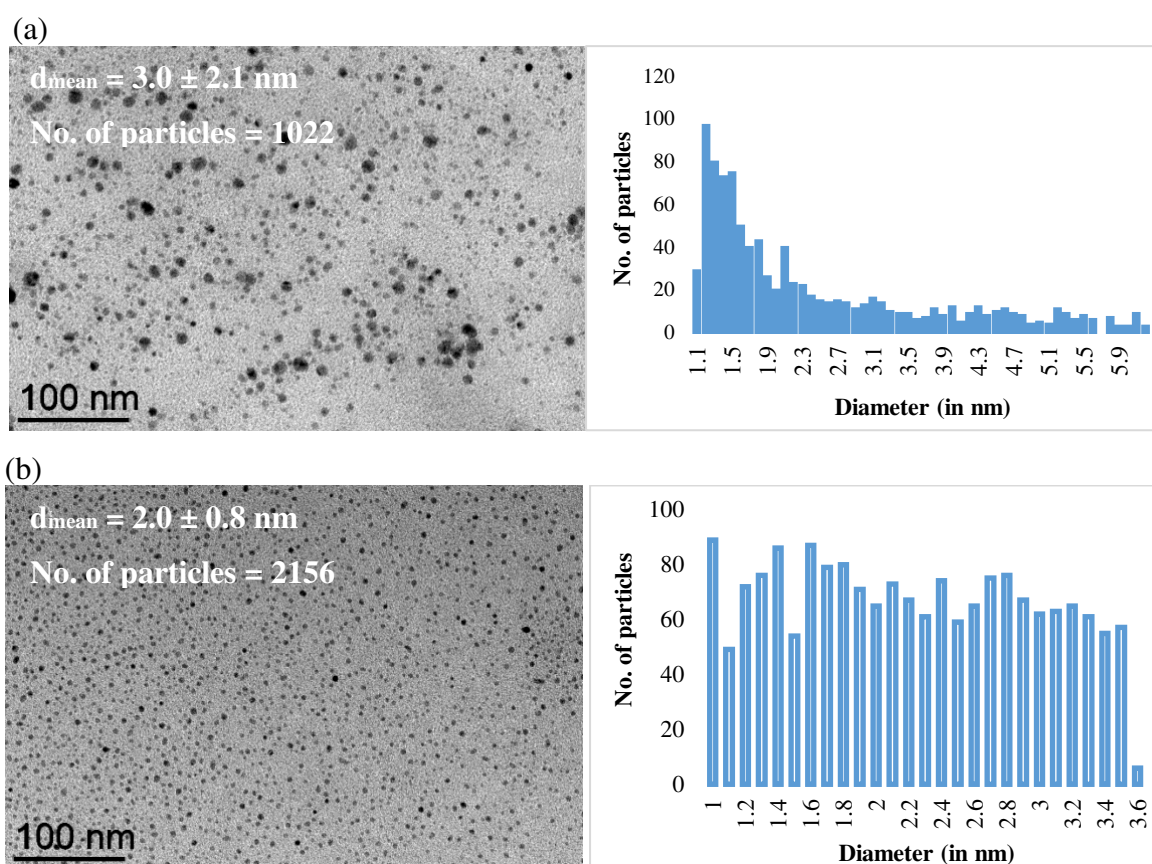


Figure 4.7. TEM micrographs and the respective size distribution of PdNPs after catalysis (a) 30 bar H₂ + 10 bar CO₂ at 80 °C for 18 h (b) 10 bar H₂ + 30 bar CO₂ at 80 °C for 40 h

To sum up the first part of this chapter, it can be said that carbon dioxide helped increasing the efficiency of the hydrogenation reactions. It should also be noted that it is not only the partial pressures of the individual gases but also the total pressure of the system that determines the conversion.

4.2. Extraction of organic products using supercritical carbon dioxide

4.2.1. Introduction

Supercritical fluid extraction (SCFE) is the extraction done with a fluid at temperatures and pressures near the critical point.²⁸ SCFs have “gas-like” viscosity and “liquid-like” density. Table 4.3 compares the density, viscosity and diffusivity of gas, SCF and liquid.²⁹ The low viscosity of SCF leads to fast diffusivity and therefore overcomes the problems of mass transfer. Additionally, the compressibility of an SCF is much larger than that of liquid that allows large changes in volume and density over a small change in the pressure.^{28,29} These properties make SCFs an excellent candidate for separation and extraction processes it is possible to vary the solubility by tuning the operational conditions.^{30–33} Even though SCFE is more expensive than the classic extraction techniques, it is widely adopted especially at industrial scale.^{34–36}

Table 4.3. Comparison of the densities, viscosities and diffusivity of gases, SCFs and liquids.²⁹

| Substance | Density (gmL ⁻¹) | Viscosity (cP) | Diffusivity (mm ² s ⁻¹) |
|-----------|------------------------------|----------------|--|
| Gas | 10 ⁻³ | 0.01 | 200 |
| SCF | 0.2-1.0 | 0.002-0.1 | 0.01-0.1 |
| Liquid | 1.0 | 0.3-2.0 | 0.001 |

Supercritical carbon dioxide is one of the most promising solvent used for extraction.^{37–40} It is nontoxic, nonflammable, and hugely available. Supercritical CO₂ has low dielectric constant (similar to hexane) that allows scCO₂ to dissolve mainly nonpolar low-molecular weight compounds.⁴¹ Additionally, when the extract is recovered in the separators, CO₂ is easily separated because of its high volatility (Figure 4.1).^{11,28} Use of scCO₂ for extraction after a catalytic reaction can effectively avoid the use of volatile organic solvents. Moreover, an additional product from the co-solvent can lead to the problems of cross contamination.⁴² Blanchard *et al.* investigated the feasibility of using scCO₂ for the separation of organic solutes from ionic liquids.⁴³ They doped 1-n-butyl-3-methylimidazolium hexafluorophosphate ([bmim][PF₆]) with 20 different organic solutes. They showed above 95% recovery of

numerous types of organic compounds, polar and nonpolar, aromatic and aliphatic, volatile and nonvolatile, with variety of chemical substituents from [bmim][PF₆] with scCO₂ (Figure 4.8).

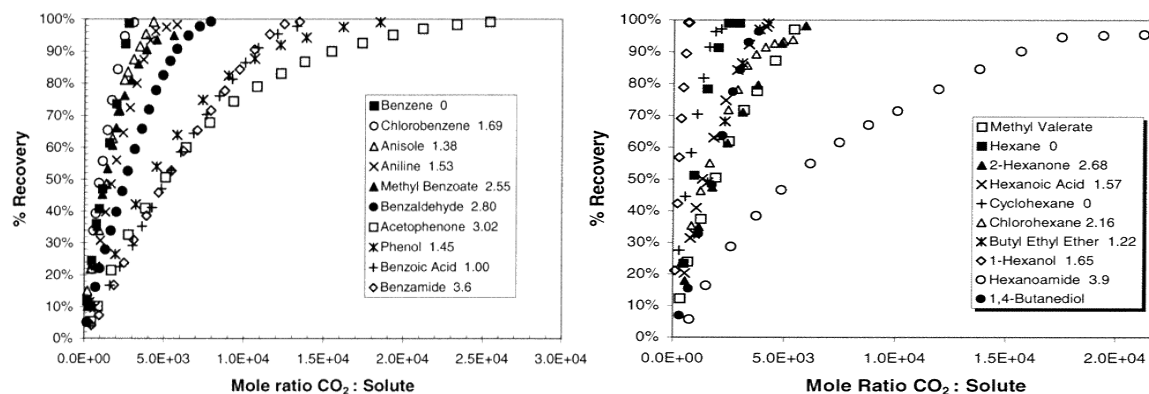
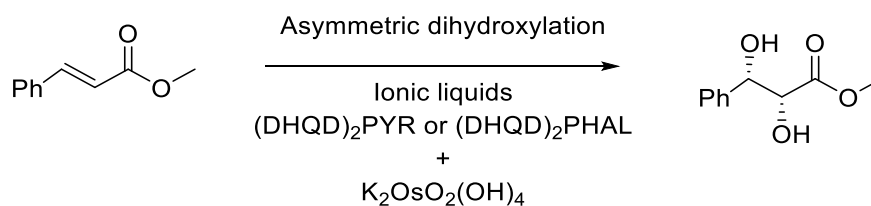
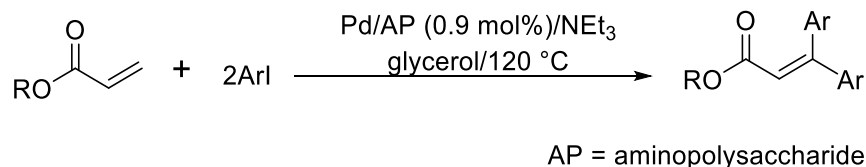


Figure 4.8. Extraction of aromatic (left) and aliphatic (right) solutes from [bmim][PF₆] with scCO₂ at 40 °C and 138 bar. Solute dipole moments (Debye) shown in figure. Reprinted (adapted) with permission from reference (43). Copyright 2001 American Chemical Society.

Distribution coefficient, K , is an important thermodynamic property to study the extraction of solutes.⁴³ K is the ratio of the solute mole fractions in the supercritical and IL phases, respectively. The distribution coefficient is determined by the non-ideality of the solute in the supercritical fluid and liquid phases. Since, [bmim][PF₆] does not dissolve appreciably in the CO₂, the supercritical phase is essentially organic solute and CO₂.⁴³ Serbanovic *et al.* did the extraction of products for their osmium-catalyzed asymmetric dihydroxylation of methyl trans-cinnamate in different ionic liquids (1-*n*-butyl-3-methylimidazolium hexafluorophosphate ([C₄mim]PF₆), 1-*n*-butyl-3-methylimidazolium tetrafluoroborate ([C₄mim]BF₄), 1-*n*-butyl-3-methylimidazolium bis(trifluoromethylsulfonyl)imide ([C₄mim][NTf₂]), 1-*n*-octyl-3-methylimidazolium hexafluorophosphate ([C₈mim]PF₆) and 1-*n*-butyl-2,3-methylimidazolium tetrafluoroborate ([bdmim]BF₄)) (Scheme 4.3). They found out that it is more advantageous to perform the product extraction by scCO₂ than by common organic solvents, because the extraction is more efficient and no contamination of osmium in the product was detected.⁴⁰ Delample *et al.* also used scCO₂ for the selective extraction of diarylated alkene from the glycerol-palladium phase in their Mizoroki-Heck coupling reaction (Scheme 4.4).⁴⁴



Scheme 4.3. Osmium-catalyzed asymmetric dihydroxylation of methyl trans-cinnamate in different ionic liquids.⁴⁰



Scheme 4.4. β,β -Diarylation of acrylate derivatives in glycerol.⁴⁴

In the frame of the present work, we carried out and optimized the extraction of phenylbutanone using supercritical carbon dioxide.

4.2.2. The Extractor

A SEPAREX SF200 pilot (Separex Company, Nancy, France) was used to carry out the extraction. Figure 4.9 (a and b) shows the real and the schematic diagram for the extractor, respectively. This apparatus consisted of a 200 mL contacting vessel that can be used as a reactor and/or liquid-fluid extractor. The introduction of CO₂ was done through a filter mesh screen from a commercial HPLC pump. This device allowed good dispersion of CO₂ in the glycerol based mixture. Additionally, a magnetic stirrer was added to improve the dispersion. A cascade of three 20-ml cyclonic separators is present at the contactor outlet. The pressure in each vessel can be adjusted by depressurization valves. A volumetric pump (Milton Roy, flow rate maximum 5 kg/h) was used to pump subcooled CO₂ in the system. The extractor was then heated to the desired temperature with the continuous flow of CO₂. Experiments can be carried out in open-loop or closed-loop configuration, in which case, after condensation, CO₂ was recycled at the head of the pump. Temperatures and pressures were controlled in each unit of the pilot, The limitation of the pressure is 300 bar and temperature is around 80 °C \pm 5.

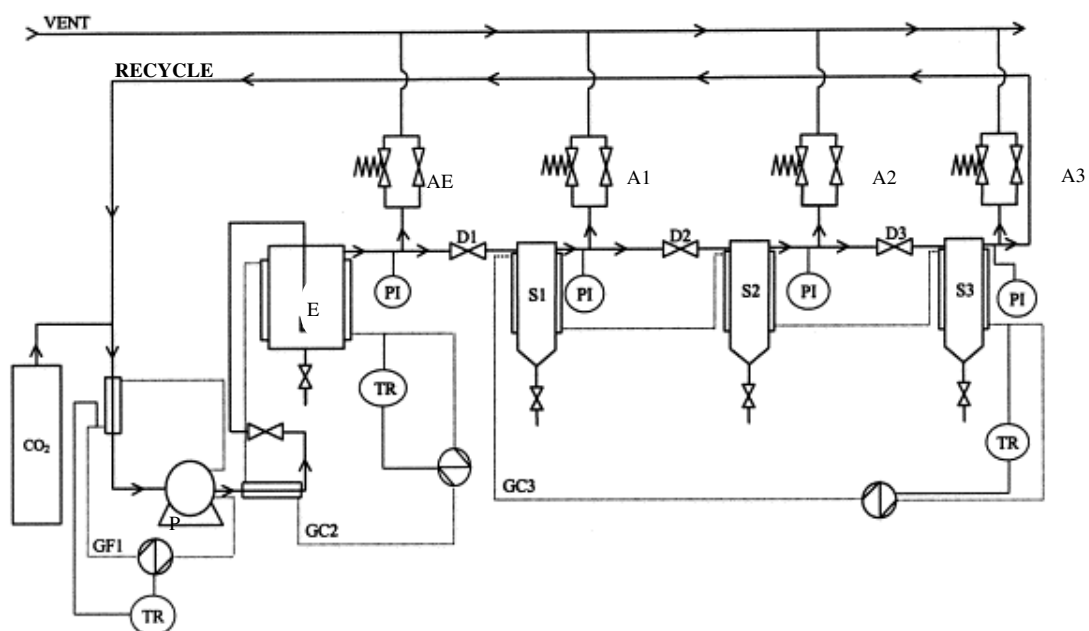
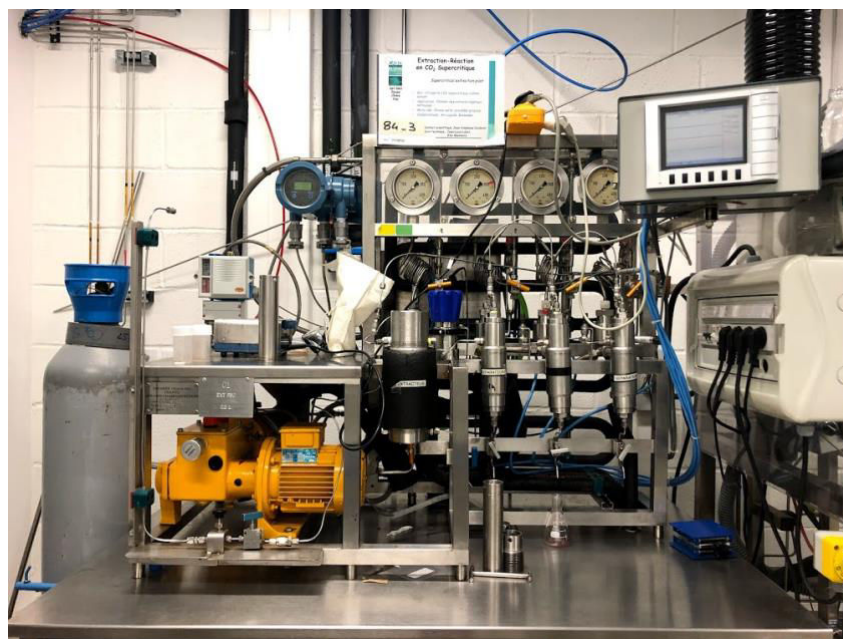


Figure 4.9 (a) SEPREX SF200 pilot. (b) Schematic diagram of Pilot SF200: E, extractor; S1, S2, S3: separators; GF1, cooling group; GC2, GC3: heating groups; PI, pressure indicator; TR, temperature regulator; D1, D2, D3: depressurization valves.

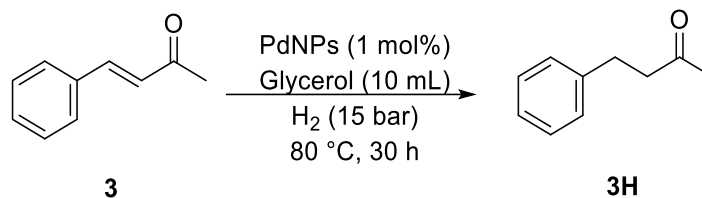
The extractor E and the three separators S1, S2 and S3 are connected in series. Temperatures are kept constant by a temperature control system that includes the GC2 and GC3 hot groups and "double envelopes" heat exchangers around E, S1, S2 and S3. In some extraction schemes, the separator S1 can also be cooled using the cold group GF1. The system is fed with liquid CO₂ contained in a pressure bottle CO₂ (pressure equal to the vapor pressure at room temperature). The CO₂ was maintained in the liquid state before and in the pump P using the

GF1 cold unit and was then raised beyond its critical temperature by means of a tubular heat exchanger before being introduced into the extractor E. The pressure in the extractor was kept constant using the pressure regulator (pressure relief valve) D1. The pressures in the separators S1 and S2 were maintained using the control valves D2 and D3. At the outlet of the extractor and each separator, a drain valve is placed (AE, A1, A2 and A3, respectively) for directing the solvent to the vent (in case of work in open circuit). It is also possible to work in closed (with CO₂ recycling) by closing the drain valves and opening the recycling valve R. In this case, the CO₂ passes through the recycling line. The symbols TI and PI are respectively temperature and pressure indicators. These indicators were connected to a recorder (Endress + Hauser) allowing the recording of these quantities over time. TRs are regulators of the temperature of the hot groups and the cold group. This installation also allows the use of co-solvents. They were introduced by the P-CS pump from the co-solvent tank R-CS, mixed and dissolved in CO₂ just before the extractor inlet.

4.2.3. Results and Discussion

As mentioned in Chapter 3, after catalysis the extraction of organic products was done by various volatile organic solvents like dichloromethane, cyclohexane, ethyl acetate, heptane etc. In order to replace the use of volatile organic solvents, the extraction of the products was done using scCO₂. For this purpose, the extraction of compounds involved in our benchmark reaction mentioned in Chapter 3 were. This reaction involves hydrogenation of 4-phenyl-but-3-en-2-one (**3**) to 4-phenyl butanone (**3H**) (Scheme 4.5). As a preliminary test, a mixture of the **3** and **3H** in glycerol was taken to carry out the extraction and determine the optimal conditions. It is important to study the extraction of both compounds, **3** and **3H**, mainly for those reactions exhibiting partial conversion. For a 200 mL extractor, 60 mL of glycerol were used in order to let the diffuser completely immerse in the solvent. 2 mmol (0.3 g) of **3H** was added to the glycerol and the conditions were set (entry 1, Table 4.4). The extraction was started with 125 bar of pressure and 40 °C as this is the condition where a decrease in viscosity is seen for our system (see Chapter 2, section 2.1.1, figure 2.7(a)). However, under these conditions, nothing was extracted. As the solubility increases with increasing temperature, the temperature was increased up until 80 °C preserving the pressure, but in this case as well, no significant product was extracted (entry 2; Table 4.4). Next, the amount of CO₂ was increased up to 200 bar. It was also thought that that amount of product in use might not be enough as compared to the volume

of the extractor, thus, the amount increased to 1 g (0.67 mmol). The volume of glycerol was also reduced to 40 mL in order to increase the solvent/product ratio. For these conditions, extraction was performed at two different temperatures 60 °C and 80 °C, extracting 17.6% and 24.7% of **1** for the two temperatures respectively (entries 3 and 4; Table 4.4).



Scheme 4.5. Hydrogenation reaction of 4-phenyl-but-3-en-2-one (**3**) to 4-phenyl butanone (**3H**)

Therefore, these conditions were explored in order to improve the extraction. Firstly, the amount used was doubled (2 g; 1.35 mmol of **3**) and the extraction was done again at 60 °C and 80 °C. The results at these conditions were significantly improved. At 60 °C, 42.5 % of **3** was recovered (entry 5, Table 4.4) and at 80 °C, 75% recovery was achieved (entry 6, Table 4.4). Since, using 2 g of **3** at 80 °C gave the best result so far after the pressure of the both the extractor and the separators was increased. Unfortunately, in this case no recovery was made (entries 7 and 8; Table 4.4). Therefore, the conditions in entry 6 were considered as the best. So far, extraction was done using the **3** (except for entries 1 and 2). Consequently, the optimized conditions in entry 6 were tried with **3H** and 70% of the product was extracted without any difficulty (entry 9, Table 4.4). The solubility of both 4-phenyl-but-3-en-2-one and 4-phenyl butanone is similar in scCO₂ since they are structurally close. Therefore, they are extracted in almost same amount under the same parameter. This similarity in their structure also makes it difficult to separate both **3** and **3H** during the extraction, as described below.

After achieving the maximum extraction of both **3** and **3H** separately, the extraction was done for the mixture **3** and **3H**. 1 g each of **3** and **3H** were mixed, making the total amount 2 g (same amount as used in entries 6 and 9.) Only 50% of the mixture was recovered with 65% selectivity towards the **3H** (entry 10, Table 4.4). It is to be noted that both the substrate and the product were extracted at the same time as a mixture and it was not possible to separate the two. The amount of both the compounds were further increased (entry 11, Table 4.4). The extraction improved by a factor of 15%, however, the ratio of **3** and **3H** was 1:1. The ratio of **3** and **3H** was determined by GC/MS using decane as an internal standard.

Table 4.4. Conditions applied to the SEPAREX extractor for extraction of 4-phenyl but-3-en-2-one (**3**) and 4-phenyl butanone (**3H**)^a

| Entry | Mass glycerol (mL) | Mass 3H (g) | Mass 3 (g) | T (°C) | Pressure in extractor E (bar) | Pressure in separator S1 (bar) | Pressure in separator S2 (bar) | Extracted mass (g)/(%) |
|----------------|--------------------|--------------------|-------------------|--------|-------------------------------|--------------------------------|--------------------------------|--|
| 1 _b | 60 | 0.3 | - | 40 | 125 | 30 | 8 | - |
| 2 _b | 60 | 0.3 | - | 60-80 | 125 | 30 | 8 | - |
| 3 | 40 | - | 1 | 60 | 200 | 50-60 | 20 | 0.176 (17.6%) |
| 4 | 40 | - | 1 | 80 | 200 | 50-60 | 20 | 0.247 (24.7%) |
| 5 | 40 | - | 2 | 60 | 200 | 50 | 22 | 0.850 (42.5%) |
| 6 | 40 | - | 2 | 80 | 203 | 55 | 17 | 1.5 (75%) |
| 7 | 40 | - | 2 | 80 | 253 | 45 | 16 | - |
| 8 | 40 | - | 2 | 80 | 253 | 100 | 40-60 | - |
| 9 | 40 | 2 | - | 80 | 200 | 52 | 15 | 1.4 (70%) |
| | | | | | | | | Total= 1.025 (50%) |
| 10 | 40 | 1 | 1 | 80 | 204 | 52 | 12 | 3H = 0.67 (65%) 3 = 0.36 (35%) |
| | | | | | | | | Total = 2.6 (65%) |
| 11 | 40 | 2 | 2 | 80 | 202 | 45-55 | 45-55 | 3H= 1.22 (47%) |

$$\mathbf{3} = 1.38$$

(53%)

^a Flow rate of CO₂ = 30 g/min. ^b Flow rate of CO₂ = 15 g/min. For each extraction, samples were collected at an interval of 5-10 minutes.

The conditions used in entry 11 were considered as the optimal conditions. The extraction with the system of our deep eutectic solvent, glycerol and choline tosylalaninate, was then performed under these conditions. 10 mL of DES with 10 mmol (1.5 g) each of **3** and **3H** were used. This scale was chosen because it was ten times the original scale used in our studies (see Chapter 3, Table 3.1). The mixture was then diluted with 30 mL of glycerol to make the total of 40 mL solvent. 73% of **3H** (1.095 g) and 90% of **3** (1.35 g) of the substrate were recovered. Additionally, the amount left in the mixture of DES and glycerol was extracted by dichloromethane using biphasic methodology (See Experimental Section 4.3.4) and quantified using GC/MS with decane as internal standard. It was found out that only 0.025% and 0.017% of **3** and **3H** respectively were left behind. It implies that rest of the mass was lost in the extractor that could not be recovered.

After this optimization, the extraction was applied to the catalytic system. A ten times scaled-up (starting material was 10 mmol, 1.5 g) reaction was done for the benchmark reaction (Scheme 4.5) and its products were extracted using scCO₂. 89% of **3H** was extracted using the condition of entry 11 from Table 4.3. Fortunately, no product **3H** was lost in the extractor. The extracted product was also analyzed by ICP-AES in order to detect extraction of palladium from the catalytic phase. No leaching of Pd was detected. Additionally, the TEM images of the PdNPs showed remains immobilized in the glycerol phase (Figure 4.10).

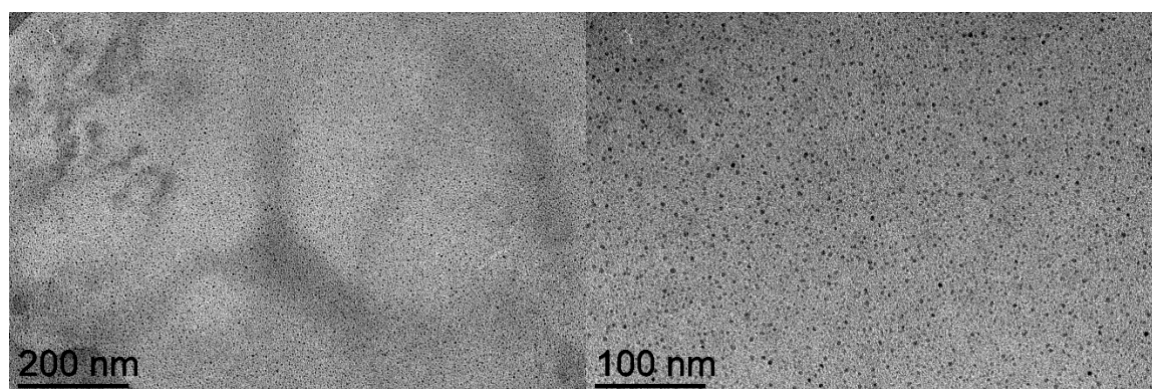


Figure 4.10. TEM of PdNPs after extraction.

Diffusion of constants of **3** and **3H** in the glycerol/choline tosylalaninate and CO₂ mixture at three different temperature with increasing pressures were calculated (Figure 4.11 and 4.12 respectively). The diffusion constant were calculated using Stokes-Einstein equation (Equation 4.1).⁴⁵

$$D = \frac{k_B T}{6\pi\eta R} \quad \text{Equation 4.1}$$

where, k_B is the Boltzmann constant ($= 1.38064852 \times 10^{-23} \text{ m}^2\text{kg s}^{-2}\text{K}^{-1}$), T is the temperature, η is the viscosity, these values were taken from the data obtained from measurements with molecular rotors (**MR1** and **DCVJ**), in section 2.4.1 and 2.4.2 of Chapter 2 of this thesis, and R is chosen to be the radius of a sphere of volume equal to the van der Waals volume of the diffusing molecule. R is calculated using Bondi method described by Zhao *et al.* (Equation 4.2).⁴⁶

$$\text{van der Waals volume (} V_{\text{vdw}} \text{)} = \sum \text{ all atom contributions} - 5.92N_B - 14.7R_A - 3.8R_{NR}$$

where, N_B is the number of bonds, R_A is the number of aromatic rings, and R_{NR} is the number of non-aromatic rings). N_B is the number of bonds present simply calculated by $N_B = N - 1 + R_A + R_{NR}$ (where N is the total number of atoms).

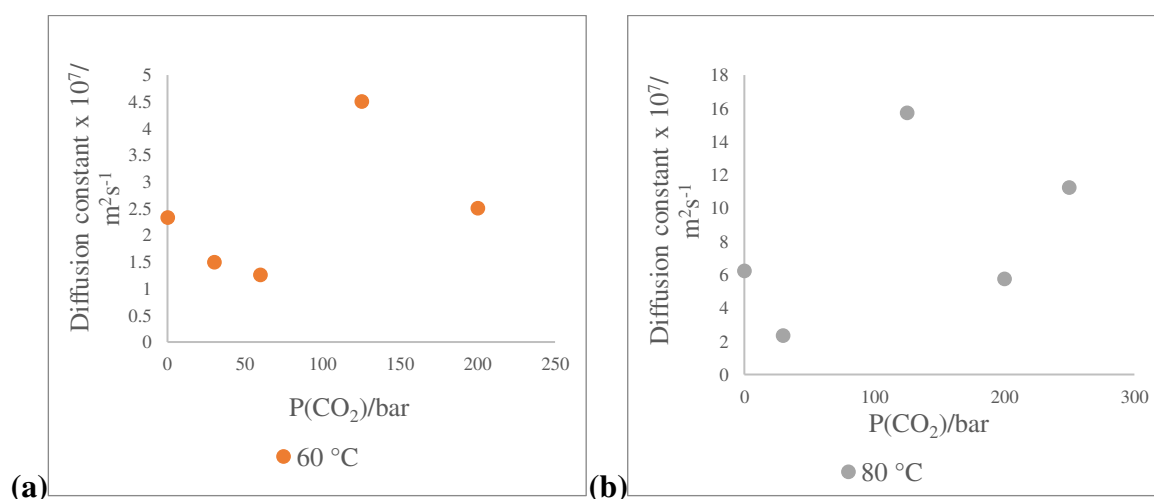


Figure 4.11. Diffusion constant of **3** in glycerol/choline tosylalaninate and CO₂ mixture at (a) 60 °C and (b) 80 °C.

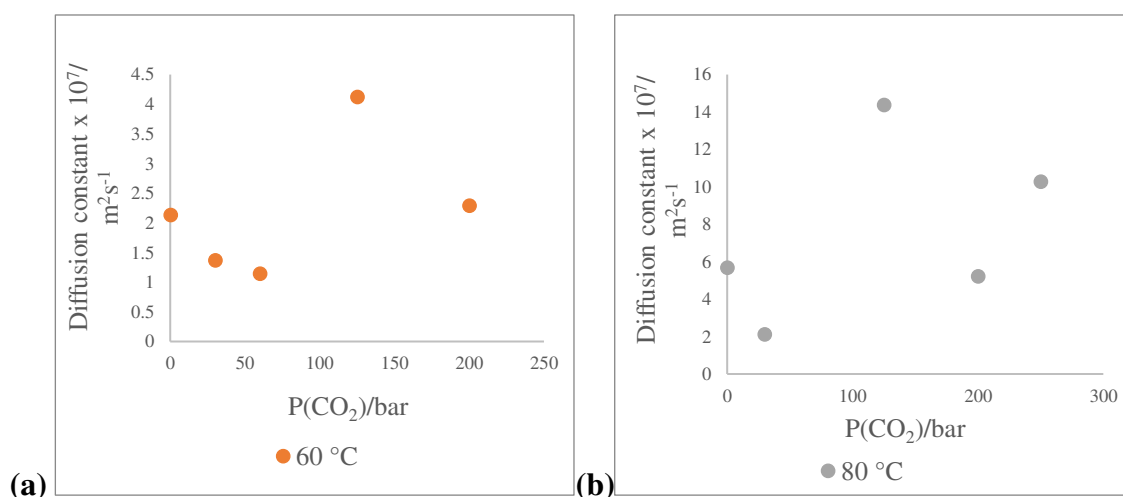


Figure 4.12. Diffusion constant of **3H** in glycerol/choline tosylalaninate and CO₂ mixture at (a) 60 °C and (b) 80 °C.

From data of diffusion constants in Figure 4. 10 and 4.11, large dispersion is obtained in the data calculated, which comes undoubtedly from the dispersion obtained in measurements of viscosity. As it has been discussed in chapter 2, improvement of viscosity measurements is needed by using fluorescence decay time and better experimental techniques.

Additionally, diffusion constants of **3** and **3H** in glycerol/choline tosylalaninate were calculated at increasing temperature while the pressure of CO₂ was kept to zero (Figure 4.13). As expected, the diffusion constant increased with increasing temperature due to the viscosity decrease with increasing temperature. This explains why the extraction efficiency increased with an increase in temperature.

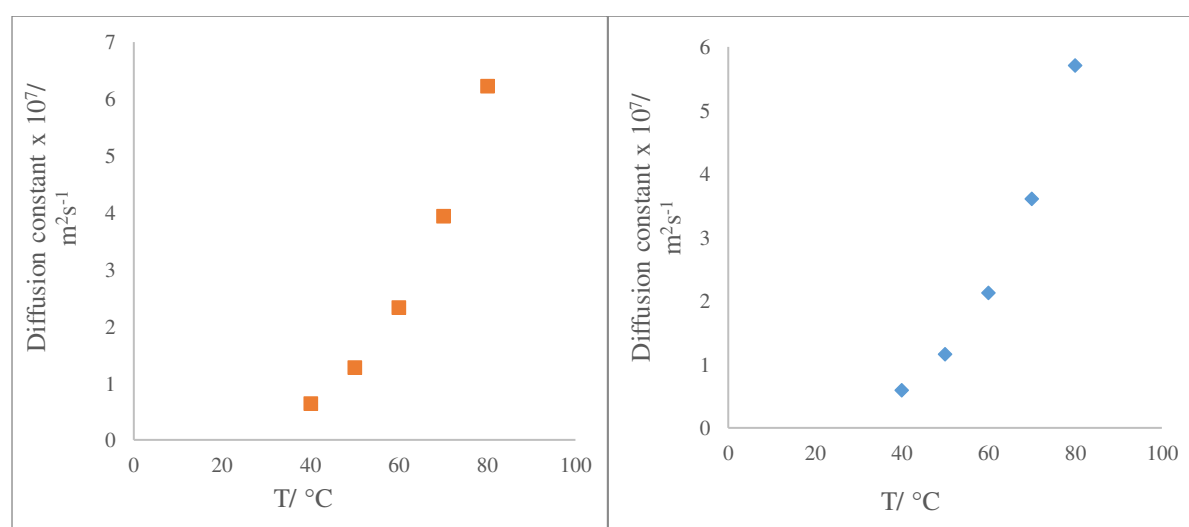


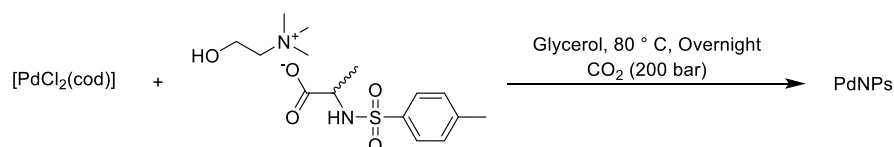
Figure 4.13. Diffusion constant of **3** (left) and **3H** (right) in glycerol/choline tosylalaninate with increasing temperature (P=0 bar).

4.3. Synthesis of palladium nanoparticles under scCO₂ and their catalytic activity

In section 4.2.3, where scCO₂ extraction of organic products is discussed, it is shown how PdNPs remain immobilized even after extraction (Figure 4.10). This observation envisaged the synthesis PdNPs in the presence of scCO₂. The idea was to check whether scCO₂ promotes the formation of more catalytically active nanoparticles.

4.3.1. Result and discussion

The synthesis of PdNPs was done following the methodology described in Chapter 3 (Section 3.1.2). The only modification during the synthesis was that it was done under 200 bar of CO₂ instead of atmospheric pressure of argon (Scheme 4.6). A black colloidal solution of PdNPs were obtained. The synthesized nanoparticles were observed under TEM in the glycerol phase (Figure 4.14). The PdNPs synthesized were so small (1.3 ± 0.3 nm) that it was difficult to observe them under low resolution TEM.



Scheme 4.6. Synthesis of choline tosylalaninate stabilized palladium nanoparticles in glycerol under scCO₂

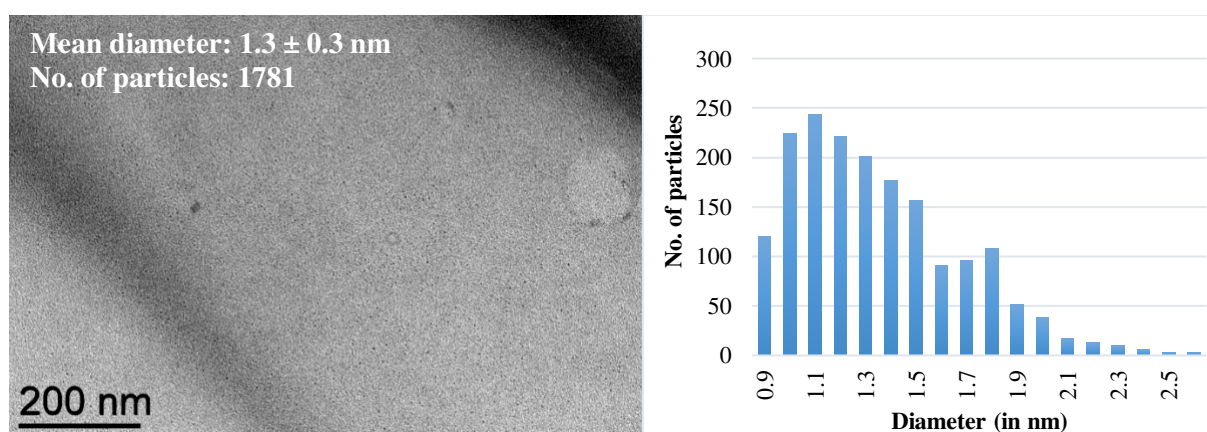
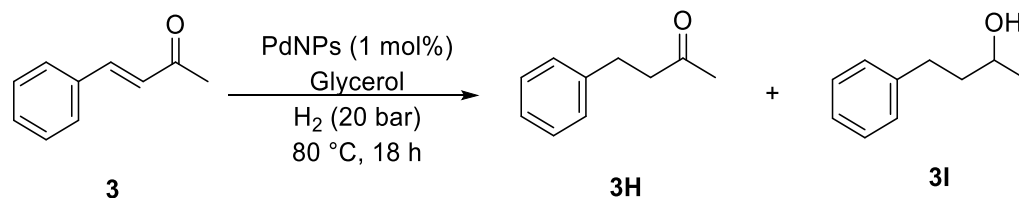


Figure 4.14. TEM images of PdNPs in glycerol with the corresponding size distribution diagram.

The catalytic activity of these nanoparticles was studied by hydrogenation of 4-phenyl-but-3-en-2-one (**3**) at 20 bar of H₂ (Scheme 4.7). Table 4.5 gives the comparison of hydrogenation of **3** using PdNPs synthesized in the absence (entry 1) and the presence (entry 2) of scCO₂.

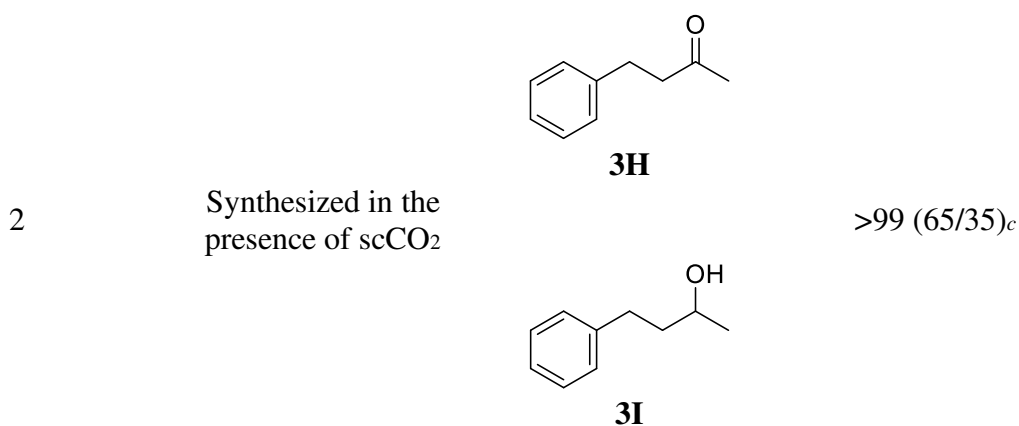


Scheme 4.7. Hydrogenation reaction of 4-phenyl but-3-en-2-one (**3**) to 4-phenyl butanone (**3H**) and 4-phenyl butan-2-ol (**3I**)

It was found the nanoparticles synthesized in the presence of scCO₂ were more active, favoring the hydrogenation of carbonyl group in addition to the exocyclic C=C bond. They showed a better selectivity (35%) towards reducing the carbonyl group present in **3** as compared to the PdNPs synthesized in absence of scCO₂ (18%) for the same reaction.

Table 4.5. Hydrogenation of 4-phenyl-but-3-en-2-one catalyzed by PdNPs stabilized by choline tosylalaninate in glycerol.^a

| Entry | PdNPs | Product | Conv. (selectivity) ^b (%) |
|-------|---|-----------------------------------|---|
| 1 | Synthesized in the absence of scCO ₂ | <p>3H</p> <p>3I</p> | >99 (82/18) ^h |



^a Results from duplicated experiments. Reaction conditions: 1 mmol of substrate **3** and 1 mL of the catalytic glycerol solution of **PdB** (10⁻² mol L⁻¹, 0.01 mmol of total Pd). ^b Determined by GC and GC/MS using decane as internal standard. ^c **3H/3I** ratio.

After catalysis, the product was extracted using biphasic extraction using dichloromethane and TEM was done for the catalytic phase (Figure 4.15). It was observed that the PdNPs synthesized under scCO₂ remain intact and no aggregation was observed. Unlike the case of the PdNPs that were synthesized in the absence of scCO₂, where the nanoparticles formed aggregates after extraction using biphasic conditions (Chapter 3, Section 3.2.2, Figure 3.12).

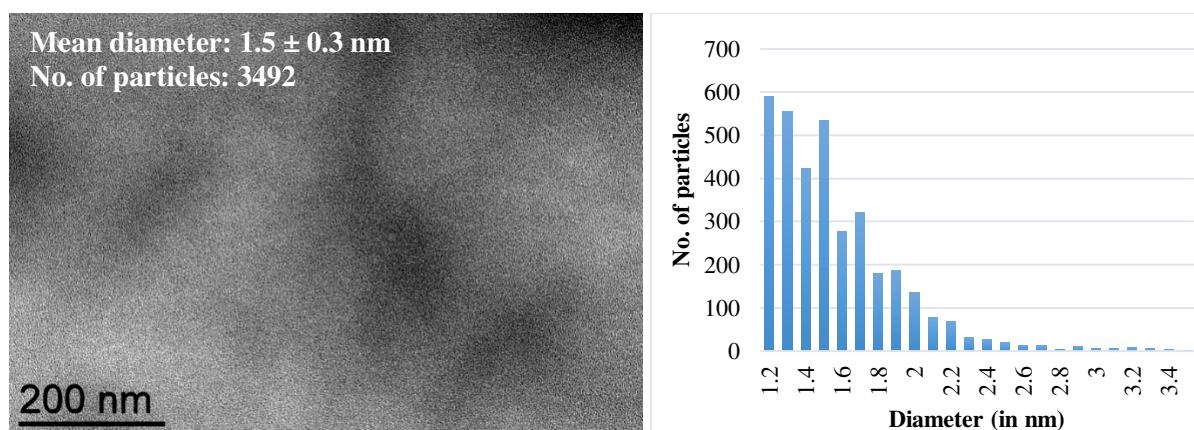


Figure 4.15. TEM images of PdNPs in glycerol after catalysis with the corresponding size distribution diagram.

Following the above results, it can be said that scCO₂ favors the formation of smaller and more catalytically active PdNPs. Since scCO₂ is known to trigger higher solubility of metal precursor in the glycerol/choline tosylalaninate system it leads forming smaller nanoparticles, which in return gives enhanced activity.⁴⁷ The synthesized PdNPs can be explored for other kind of catalytic reactions. Additionally, since no aggregates are formed after catalysis, these nanoparticles are promising candidates from recycling point of view.

4.4. Experimental section

4.4.1. Materials and methods

Unless otherwise stated, all chemical reagents were obtained from commercial suppliers and used without further purification. All manipulations were performed using Schlenk techniques under argon atmosphere. Glycerol was dried under vacuum at 80 °C for 18 h prior to use. Choline tosylalaninate was prepared following reported methodology. High-pressure reactions were carried out in a Top Industrie Autoclave. GC analyses were carried out on a GC Perkin Elmer Clarus 500 with ionization flame detector, using SGE BPX5 column composed by 5% phenylmethylsiloxane, coupled to a Perkin Elmer Clarus MS560 mass detector. TEM images of PdNPs dispersed in glycerol were obtained from a JEOL JEM 1400 instrument running at 120 kV. PdNPs size distributions and average diameters were determined from TEM images applying Image-J software associated to a Microsoft Excel Elemental ICP-AES analyses were carried out at the “Service d’Analyse” of Laboratoire de Chimie de Coordination (Toulouse) using a Perkin Elmer 2400 series II analyser and an iCAP 6300 ICP Spectrometer. A SEPAREX SF200 pilot (Separex Company, Nancy, France) was used to carry out the extraction.

4.4.2. General procedure for hydrogenation using choline tosylalaninate stabilized palladium nanoparticles under CO₂

In an autoclave of volume 100 mL (working from 5 to 350 bar total pressure), the appropriate substrate/nitrobenzene (1 mmol for 1 mol% of catalyst or 10 mmol for 0.1 mol% of catalyst) was added to 1 mL of preformed nanoparticles (1 mol%; 2.85 mg of Pd) in glycerol under argon. The reaction mixture was put under vacuum and then pressurized with H₂ and/or CO₂ at the convenient pressure, heated up at 80 °C and stirred for the appropriate time; then cooled down to room temperature before extraction. Organic products were extracted from glycerol by a biphasic methodology, adding dichloromethane (5 × 3 mL); organic phases were collected and solvent removed under vacuum. Conversion and yields were determined by GC using decane as internal standard. The obtained products were characterized by GC-MS data and ¹H and ¹³C NMR and compared to literature reports to confirm their spectral identity.

4.4.3. Procedure for extraction of organic products left in glycerol phase after using the extractor

Organic products were extracted from glycerol by a biphasic methodology, adding dichloromethane (10 × 15 mL); organic phases were collected and solvent removed under vacuum. Conversion and yields were determined by GC using decane as internal standard. The obtained products were characterized by GC-MS data and ¹H and ¹³C NMR and compared to literature reports to confirm spectral identity.

4.4.4. Characterization of organic compounds

Aniline (1H) ³⁴ ¹H NMR (300 MHz, CDCl₃) δ 7.53 – 7.07 (m, 2H), 7.01 – 6.59 (m, 3H), 3.68 (s, 2H). ¹³C NMR (75 MHz, CDCl₃) δ 146.4, 129.2, 118.4, 115.1.

4-phenylbutan-2-ol (2H) ⁴⁸ ¹H NMR (300 MHz, CDCl₃) δ 7.63 – 7.09 (m, 5H), 4.90 (d, 1H), 2.47 (s, 1H), 1.52 (d, 3H). ¹³C NMR (75 MHz, CDCl₃) δ 145.9, 128.5, 127.5, 125.44, 70.4, 25.2.

4-phenylbutan-2-one (3H) ⁴⁸ ¹H NMR (300 MHz, CDCl₃) δ 7.45 – 7.15 (m, 5H), 2.96 (d, *J* = 7.5 Hz, 2H), 2.83 (d, *J* = 7.7 Hz, 2H), 2.20 (s, 3H). ¹³C NMR (75 MHz, CDCl₃) δ 207.8, 141.0, 128.5, 128.3, 126.1, 45.1, 30.0, 29.7.

4.5. Conclusions

It can be concluded that carbon dioxide enables to increase the efficiency of hydrogenation in catalytic reactions. As mentioned above, the reason for increased conversion of the substrate to product is the increased solubility of hydrogen in the system in the presence of carbon dioxide. Increase in carbon dioxide content when the hydrogen pressure decreases brings the system closer to the critical pressure, where the liquid expands in volume. In these conditions, the higher solubility of hydrogen compensates for the lower partial pressure in the gas phase. The results obtained in the presence of carbon dioxide decreases the amount of hydrogen used by three times when the other parameters are kept the same.

It is important to note that it is not just the partial pressure of hydrogen that increases conversion but total pressure, and even more, partial pressure of carbon dioxide is a determining factor. A higher partial pressure of carbon dioxide increases conversion, even if partial pressure of hydrogen is lower, clearly showing that carbon dioxide increases the availability of hydrogen. Here, we showed that in the presence of CO₂, we could hydrogenate ketones in to

secondary alcohol using very less amount of H₂; ketones, in general, are harder to hydrogenate using PdNPs.^{49,50} However, the partial pressure of both the gases have to be carefully optimized as a large increase in the partial pressure of carbon dioxide can also result in dilution of hydrogen and cause a negative effect. In this context, CO₂ has emerged as an alternative medium for a variety of synthetic reactions. Application of CO₂ during hydrogenation can serve as a promotor for transporting hydrogen into the liquid phase and thus enhance the equilibrium concentrations of both reactants and products in the gaseous phase.^{6,7}

Depending on supports and reaction conditions, the recycling is efficient, but often deactivation catalyst issues appear, mainly due to both agglomeration of metal nanoparticles with the consequent specific surface decrease and poisoning by carbon monoxide adsorption, which can be *in situ* formed during the hydrogenation process. Curiously, metal nanoparticles constituted by first-row transition metals (Fe, Ni, Cu, Co...) have scarcely applied in hydrogenation under scCO₂ conditions.

In relation to the extraction of organic compounds by scCO₂, successful extraction of phenylbutanone was carried out from choline tosylalaninate stabilized palladium nanoparticles in glycerol, achieving up to 90% of the product. Neither glycerol nor the ionic liquid was extracted during this process. Furthermore, palladium nanoparticles also remains immobilized in the glycerol phase and were not detected in the extracted organic phase.

Additionally, scCO₂ helps in synthesis of more active metal nanoparticles by increasing by the solubility of metallic precursor in the glycerol/IL phase increases. This leads to formation of smaller palladium nanoparticles. The smaller nanoparticles possess better catalytic activity.

It is evident from the above experiments that supercritical carbon dioxide is a greener and effective alternative for the extraction of organic products after catalytic hydrogenation in IL. It eliminates the use of volatile organic solvents and avoids the risk of cross contamination. The removal of solvent (CO₂) is quite easy at end of the extraction by depressurization. Moreover, the supercritical fluid extraction is relatively fast due to the low viscosity, high diffusivity, and tunable solvent power of the scCO₂. However, one of the major disadvantage of using scCO₂ for extraction is its difficulty in extracting polar and ionic compounds.⁵¹ The polarity of scCO₂ can be changed by mixing it with another supercritical fluid or adding a co-solvent. For example, the coupling of scCO₂ and subcritical water is a very recent and promising alternative that has proved to extract non-polar analytes successfully.⁴¹

4.6. References

- (1) Balakos, M. W.; Hernandez, E. E. Catalyst Characteristics and Performance in Edible Oil Hydrogenation. *Catal. Today* **1997**, *35* (4), 415–425. [https://doi.org/10.1016/S0920-5861\(96\)00212-X](https://doi.org/10.1016/S0920-5861(96)00212-X).
- (2) Sedgwick, D. M.; Hammond, G. B. The History and Future Challenges Associated with the Hydrogenation of Vinyl Fluorides. *J. Fluor. Chem.* **2018**, *207* (January), 45–58. <https://doi.org/10.1016/j.jfluchem.2017.12.019>.
- (3) Jutz, F.; Andanson, J. M.; Baiker, A. A Green Pathway for Hydrogenations on Ionic Liquid-Stabilized Nanoparticles. *J. Catal.* **2009**, *268* (2), 356–366. <https://doi.org/10.1016/j.jcat.2009.10.006>.
- (4) Singh, U. K.; Vannice, M. A. Kinetics of Liquid-Phase Hydrogenation Reactions over Supported Metal Catalysts - A Review. *Appl. Catal. A Gen.* **2001**, *213* (1), 1–24. [https://doi.org/10.1016/S0926-860X\(00\)00885-1](https://doi.org/10.1016/S0926-860X(00)00885-1).
- (5) Subramaniam, B.; Chaudhari, R. V.; Chaudhari, A. S.; Akien, G. R.; Xie, Z. Supercritical Fluids and Gas-Expanded Liquids as Tunable Media for Multiphase Catalytic Reactions. *Chem. Eng. Sci.* **2014**, *115*, 3–18. <https://doi.org/10.1016/j.ces.2014.03.001>.
- (6) Brunner, G.; Saure, C.; Buss, D. Phase Equilibrium of Hydrogen, Carbon Dioxide, Squalene, and Squalane. *J. Chem. Eng. Data* **2009**, *54* (5), 1598–1609. <https://doi.org/10.1021/jc800926z>.
- (7) Budisa, N.; Schulze-Makuch, D. Supercritical Carbon Dioxide and Its Potential as a Life-Sustaining Solvent in a Planetary Environment. *Life* **2014**, *4* (3), 331–340. <https://doi.org/10.3390/life4030331>.
- (8) King, J. W.; Holliday, R. L.; List, G. R.; Snyder, J. M. Hydrogenation of Vegetable Oils Using Mixtures of Supercritical Carbon Dioxide and Hydrogen. *JAACS, J. Am. Oil Chem. Soc.* **2001**, *78* (2), 107–113. <https://doi.org/10.1007/s11746-001-0229-8>.
- (9) Jessop, P. G.; Ikariya, T.; Noyori, R. Homogeneous Catalysis in Supercritical Fluids Homogeneous Catalysis in Supercritical Fluids. *Technology* **1999**, *99* (January), 475–494. <https://doi.org/10.1021/cr970037a>.
- (10) Mayadevi, S. *Ijca* 51a(9-10) 1298-1305. **2012**, *51*, 1298–1305.

- (11) Pillai, U. R.; Sahle-Demessie, E. Hydrogenation of 4-Oxoisophorone over a Pd/Al₂O₃ Catalyst under Supercritical CO₂ Medium. *Ind. Eng. Chem. Res.* **2003**, *42* (26), 6688–6696. <https://doi.org/10.1021/ie030571a>.
- (12) Arunajatesan, V.; Subramaniam, B.; Hutchenson, K. W.; Herkes, F. E. Fixed-Bed Hydrogenation of Organic Compounds in Supercritical Carbon Dioxide. *Chem. Eng. Sci.* **2001**, *56* (4), 1363–1369. [https://doi.org/10.1016/S0009-2509\(00\)00359-6](https://doi.org/10.1016/S0009-2509(00)00359-6).
- (13) Bogel-Lukasik, E.; Wind, J.; Bogel-Lukasik, R.; Da Ponte, M. N. The Influence of Hydrogen Pressure on the Heterogeneous Hydrogenation of β -Myrcene in a CO₂-Expanded Liquid. *J. Supercrit. Fluids* **2010**, *54* (1), 46–52. <https://doi.org/10.1016/j.supflu.2010.01.011>.
- (14) Wang, Q.; Cheng, H.; Liu, R.; Hao, J.; Yu, Y.; Zhao, F. Influence of Metal Particle Size on the Hydrogenation of Maleic Anhydride over Pd/C Catalysts in ScCO₂. *Catal. Today* **2009**, *148* (3–4), 368–372. <https://doi.org/10.1016/j.cattod.2009.07.072>.
- (15) Pillai, U. R.; Sahle-Demessie, E. Selective Hydrogenation of Maleic Anhydride to γ -Butyrolactone over Pd/Al₂O₃ catalyst Using Supercritical CO₂ as Solvent. *Chem. Commun.* **2002**, *2* (5), 422–423. <https://doi.org/10.1039/b111047k>.
- (16) Tang, L.; Nguyen, V. H.; Shim, J. J. Supercritical CO₂ Mediated Synthesis and Catalytic Activity of Graphene/Pd Nanocomposites. *Mater. Res. Bull.* **2015**, *71*, 53–60. <https://doi.org/10.1016/j.materresbull.2015.06.043>.
- (17) Padmajan Sasikala, S.; Poulin, P.; Aymonier, C. Prospects of Supercritical Fluids in Realizing Graphene-Based Functional Materials. *Adv. Mater.* **2016**, *28* (14), 2663–2691. <https://doi.org/10.1002/adma.201504436>.
- (18) Türk, M.; Erkey, C. Synthesis of Supported Nanoparticles in Supercritical Fluids by Supercritical Fluid Reactive Deposition: Current State, Further Perspectives and Needs. *J. Supercrit. Fluids* **2018**, *134* (October 2017), 176–183. <https://doi.org/10.1016/j.supflu.2017.12.010>.
- (19) Wolff, S.; Crone, M.; Muller, T.; Enders, M.; Bräse, S.; Türk, M. Preparation of Supported Pt Nanoparticles by Supercritical Fluid Reactive Deposition: Influence of Precursor, Substrate and Pressure on Product Properties. *J. Supercrit. Fluids* **2014**, *95*, 588–596. <https://doi.org/10.1016/j.supflu.2014.08.034>.

- (20) Saquing, C. D.; Cheng, T. T.; Aindow, M.; Erkey, C. Preparation of Platinum/Carbon Aerogel Nanocomposites Using a Supercritical Deposition Method. *J. Phys. Chem. B* **2004**, *108* (23), 7716–7722. <https://doi.org/10.1021/jp049535v>.
- (21) Morère, J.; Sánchez-Miguel, E.; Tenorio, M. J.; Pando, C.; Cabañas, A. Supercritical Fluid Preparation of Pt, Ru and Ni/Graphene Nanocomposites and Their Application as Selective Catalysts in the Partial Hydrogenation of Limonene. *J. Supercrit. Fluids* **2017**, *120*, 7–17. <https://doi.org/10.1016/j.supflu.2016.10.007>.
- (22) Solinas, M.; Pfaltz, A.; Cozzi, P. G.; Leitner, W. Enantioselective Hydrogenation of Imines in Ionic Liquid/Carbon Dioxide Media. *J. Am. Chem. Soc.* **2004**, *126* (49), 16142–16147. <https://doi.org/10.1021/ja046129g>.
- (23) Bertucco, A.; Canu, P.; Devetta, L.; Zwahlen, A. G. Catalytic Hydrogenation in Supercritical CO₂: Kinetic Measurements in a Gradientless Internal-Recycle Reactor. *Ind. Eng. Chem. Res.* **1997**, *36* (7), 2626–2633. <https://doi.org/10.1021/ie960369q>.
- (24) Garg, G.; Foltran, S.; Favier, I.; Pla, D.; Medina-González, Y.; Gómez, M. Palladium Nanoparticles Stabilized by Novel Choline-Based Ionic Liquids in Glycerol Applied in Hydrogenation Reactions. *Catal. Today* **2019**, No. November 2018, 0–1. <https://doi.org/10.1016/j.cattod.2019.01.052>.
- (25) Olbrich, W.; Boscagli, C.; Raffelt, K.; Zang, H.; Dahmen, N.; Sauer, J. Catalytic Hydrodeoxygenation of Pyrolysis Oil over Nickel-Based Catalysts under H₂/CO₂ Atmosphere. *Sustain. Chem. Process.* **2016**, *4* (1), 1–8. <https://doi.org/10.1186/s40508-016-0053-x>.
- (26) Burgener, M.; Ferri, D.; Grunwaldt, J. D.; Mallat, T.; Baiker, A. Supercritical Carbon Dioxide: An Inert Solvent for Catalytic Hydrogenation? *J. Phys. Chem. B* **2005**, *109* (35), 16794–16800. <https://doi.org/10.1021/jp0521353>.
- (27) Jessop, P. G.; Leitner, W. Supercritical Fluids as Media for Chemical Reactions. *Chem. Synth. Using Supercrit. Fluids* **2007**, 1–36. <https://doi.org/10.1002/9783527613687.ch1>.
- (28) Díaz-Reinoso, B.; Moure, A.; Domínguez, H.; Parajó, J. C. Supercritical CO₂ Extraction and Purification of Compounds with Antioxidant Activity. *J. Agric. Food Chem.* **2006**, *54* (7), 2441–2469. <https://doi.org/10.1021/jf052858j>.
- (29) Cunico, L. P.; Turner, C. *Supercritical Fluids and Gas-Expanded Liquids*; Elsevier Inc.,

2017. <https://doi.org/10.1016/B978-0-12-805297-6.00007-3>.
- (30) Mukhopadhyay, M. Extraction and Processing with Supercritical Fluids. *J. Chem. Technol. Biotechnol.* **2009**, *84* (1), 6–12. <https://doi.org/10.1002/jctb.2072>.
- (31) Daintree, L. S.; Kordikowski, A.; York, P. Separation Processes for Organic Molecules Using SCF Technologies. *Advanced Drug Delivery Reviews.* 2008. <https://doi.org/10.1016/j.addr.2007.03.024>.
- (32) Camy, S.; Condoret, J. S. Modelling and Experimental Study of Separators for Co-Solvent Recovery in a Supercritical Extraction Process. *J. Supercrit. Fluids* **2006**. <https://doi.org/10.1016/j.supflu.2005.03.005>.
- (33) Demirbaş, A. Supercritical Fluid Extraction and Chemicals from Biomass with Supercritical Fluids. *Energy Convers. Manag.* **2001**. [https://doi.org/10.1016/S0196-8904\(00\)00059-5](https://doi.org/10.1016/S0196-8904(00)00059-5).
- (34) Munshi, P.; Bhaduri, S. Supercritical CO₂: A Twenty-First Century Solvent for the Chemical Industry. *Curr. Sci.* **2009**, *97* (1), 63–72. <https://doi.org/10.1002/chin.201011250>.
- (35) Beckman, E. J. Supercritical and Near-Critical CO₂ in Green Chemical Synthesis and Processing. *J. Supercrit. Fluids* **2004**, *28* (2–3), 121–191. [https://doi.org/10.1016/S0896-8446\(03\)00029-9](https://doi.org/10.1016/S0896-8446(03)00029-9).
- (36) Perrut, M. Supercritical Fluid Applications: Industrial Developments and Economic Issues. *Ind. Eng. Chem. Res.* **2000**, *39* (12), 4531–4535. <https://doi.org/10.1021/ie000211c>.
- (37) Rovetto, L. J.; Aieta, N. V. Supercritical Carbon Dioxide Extraction of Cannabinoids from Cannabis Sativa L. *J. Supercrit. Fluids* **2017**, *129*, 16–27. <https://doi.org/10.1016/j.supflu.2017.03.014>.
- (38) Chang, L. H.; Jong, T. T.; Huang, H. S.; Nien, Y. F.; Chang, C. M. J. Supercritical Carbon Dioxide Extraction of Turmeric Oil from Curcuma Longa Linn and Purification of Turmerones. *Sep. Purif. Technol.* **2006**. <https://doi.org/10.1016/j.seppur.2005.06.018>.
- (39) Erkey, C.; Madras, G.; Orejuela, M.; Akgerman, A. Supercritical Carbon Dioxide Extraction of Organics from Soil. *Environ. Sci. Technol.* **1993**, *27* (6), 1225–1231. <https://doi.org/10.1021/es00043a025>.

- (40) Serbanovic, A.; Branco, L. C.; Nunes Da Ponte, M.; Afonso, C. A. M. Osmium Catalyzed Asymmetric Dihydroxylation of Methyl Trans-Cinnamate in Ionic Liquids, Followed by Supercritical CO₂ Product Recovery. *J. Organomet. Chem.* **2005**, *690* (15), 3600–3608. <https://doi.org/10.1016/j.jorganchem.2005.04.025>.
- (41) Cabral, B. J. C.; Rivelino, R.; Coutinho, K.; Canuto, S. A First Principles Approach to the Electronic Properties of Liquid and Supercritical CO₂. *J. Chem. Phys.* **2015**, *142* (2). <https://doi.org/10.1063/1.4905256>.
- (42) Kroon, M. C.; Van Spronsen, J.; Peters, C. J.; Sheldon, R. A.; Witkamp, G. J. Recovery of Pure Products from Ionic Liquids Using Supercritical Carbon Dioxide as a Co-Solvent in Extractions or as an Anti-Solvent in Precipitations. *Green Chem.* **2006**, *8* (3), 246–249. <https://doi.org/10.1039/b512303h>.
- (43) Blanchard, L. A.; Brennecke, J. F. Recovery of Organic Products from Ionic Liquids Using Supercritical Carbon Dioxide. *Ind. Eng. Chem. Res.* **2001**, *40* (1), 287–292. <https://doi.org/10.1021/ie000710d>.
- (44) Delample, M.; Villandier, N.; Douliez, J. P.; Camy, S.; Condoret, J. S.; Pouilloux, Y.; Barrault, J.; Jérôme, F. Glycerol as a Cheap, Safe and Sustainable Solvent for the Catalytic and Regioselective β,β -Diarylation of Acrylates over Palladium Nanoparticles. *Green Chem.* **2010**, *12* (5), 804–808. <https://doi.org/10.1039/b925021b>.
- (45) Kaintz, A.; Baker, G.; Benesi, A.; Maroncelli, M. Solute Diffusion in Ionic Liquids, NMR Measurements and Comparisons to Conventional Solvents. *J. Phys. Chem. B* **2013**, *117* (39), 11697–11708. <https://doi.org/10.1021/jp405393d>.
- (46) Zhao, Y. H.; Abraham, M. H.; Zissimos, A. M. Fast Calculation of van Der Waals Volume as a Sum of Atomic and Bond. *J. Org. Chem.* **2003**, No. 13, 7368–7373. <https://doi.org/10.1021/jo034808o>.
- (47) Hart, A. E.; Akers, D. B.; Gorosh, S.; Kitchens, C. L. Reverse Micelle Synthesis of Silver Nanoparticles in Gas Expanded Liquids. *J. Supercrit. Fluids* **2013**, *79*, 236–243. <https://doi.org/10.1016/j.supflu.2013.02.014>.
- (48) Hayes, J. F.; Shipman, M.; Twin, H. Multicomponent Reactions Involving 2-Methyleneaziridines: Rapid Synthesis of 1,3-Disubstituted Propanones. *J. Org. Chem.* **2002**, *67* (3), 935–942. <https://doi.org/10.1021/jo016164v>.

- (49) Simon, N. M.; Abarca, G.; Scholten, J. D.; Domingos, J. B.; Mecerreyes, D.; Dupont, J. Structural, Electronic and Catalytic Properties of Palladium Nanoparticles Supported on Poly(Ionic Liquid). *Appl. Catal. A Gen.* **2018**, *562* (April), 79–86. <https://doi.org/10.1016/j.apcata.2018.06.001>.
- (50) Drahansky, M.; Paridah, M. .; Moradbak, A.; Mohamed, A. .; Owolabi, F. abdulwahab taiwo; Asniza, M.; Abdul Khalid, S. H. . We Are IntechOpen , the World ' s Leading Publisher of Open Access Books Built by Scientists , for Scientists TOP 1 %. *Intech* **2016**, *i* (tourism), 13. <https://doi.org/http://dx.doi.org/10.5772/57353>.
- (51) Luque de Castro, M. D.; Jiménez-Carmona, M. M. Where Is Supercritical Fluid Extraction Going? *TrAC - Trends Anal. Chem.* **2000**, *19* (4), 223–228. [https://doi.org/10.1016/S0165-9936\(99\)00228-9](https://doi.org/10.1016/S0165-9936(99)00228-9).

Summary, Conclusions and Perspectives

In this Thesis, we explored multiple aspects that included the synthesis and physico-chemical studies of a bio-based deep eutectic solvent (DES) in particular tuning its viscosity by using carbon dioxide, synthesis and characterization of palladium nanoparticles both in colloidal and solid state phases. Pd-catalyzed hydrogenation reactions including sub and supercritical carbon dioxide conditions, and extraction of organic products from catalytic DES solutions using supercritical carbon dioxide.

In the first part of the Thesis, we successfully synthesized choline derived amino acid based ionic liquid by a simple ion exchange reaction. However, protected amino acid (tosylalanine) was used since amino acids reacts with carbon dioxide leading to carbamate derivatives. The ionic liquid synthesized in this thesis was choline tosylalaninate (ChTs-ala). ChTs-ala along with glycerol in the ratio of 1:100 was used as deep eutectic solvent (DES). Since, DESs are highly viscous they hinder mass transfer and therefore, an attempt was made to lower the viscosity of this DES by using CO₂ in sub or supercritical conditions as a strategy to control solvent properties, in particular viscosity, in a word, to develop what has been called “Solvent Engineering”. To measure the viscosity of DES, in addition to the classical rheometer measurements which give bulk data information, an innovative *in-situ* method was applied using molecular rotors in order to determine the viscosity at a microscopic level. 9-(2,2-Dicyanovinyl)julolidine (DCVJ) and BODIPY-based molecular rotors were used for these measurements. Thus, molecular rotors permit to measure the microscopic viscosity in a system, which is one of the key parameters that controls the diffusion rate of molecular species and hence affects the reaction rates of diffusion-controlled processes on the microscopic level. It was observed that when the DES was pressurized with CO₂ the viscosity of the system increased initially. However, as the amount of CO₂ increased in the system, the viscosity of the DES started to decrease significantly. Therefore, it can be concluded that CO₂ can be used to control the viscosity of a choline tosylalaninate/glycerol system.

In the second part of the Thesis, the above-mentioned DES system was used to synthesize palladium nanoparticles (PdNPs). PdNPs were prepared from [PdCl₂(cod)] (cod = 1,5-cyclooctadiene) in a ChTs-ala and glycerol mixture, acting as stabilizer (ChTs-ala) and solvent (glycerol). The water present in ChTs-ala acted as a reducing agent. Taking advantage of the

Summary, Conclusions and Perspectives

low vapor pressure of DES, TEM analysis of colloidal PdNPs was carried out, without needing to be centrifuged. Well-dispersed PdNPs of mean size 1.7 ± 0.6 nm were obtained. Furthermore, PdNPs were isolated at solid state by centrifugation and their Powder-XRD (PXRD) analysis showed the absence of any Pd(II) crystalline species and only the presence of zero-valent nanoparticles exhibiting a face cubic center structure. The crystallite size found from the X-ray diffraction peaks (calculated by the Scherrer equation) was *ca.* 3.7 nm; differences in size between TEM and PXRD are frequently observed because the average crystallite size (PXRD) is not necessarily the same as the particle size (TEM). XPS analysis corroborated the absence of any amorphous oxidized palladium species. Additionally, XPS showed the presence of carbon, oxygen, chloride and nitrogen that confirms the presence of the ionic liquid even after isolation of nanoparticles; the presence of chloride probably comes from the metal precursor. This also explains that PdNPs at solid state could be re-dispersed in glycerol without formation of aggregates due to the presence of stabilizers.

The PdNPs system was highly active for catalytic hydrogenation reactions. It was observed that the catalyst was selectively active for conjugated C=C bonds and terminal C=C bonds under smooth conditions (1-3 bar H₂, 80 °C, 2-18 h, 1 mol% Pd), extracting the organic products after catalysis by addition of an immiscible organic soluble in relation to the catalytic phase, such as dichloromethane, ethyl acetate etc.. However, it was not possible to reduce isolated internal C=C bonds. Alkynes were also reduced using this system. Other functional groups like nitro and carbonyl groups could also be efficiently reduced using low catalytic load (1 mol%). After catalysis, no leaching of metal was observed in the extracted organic products (ICP analyses); however, the catalytic phase showed the formation of aggregates which can be the responsible of the reduced catalytic activity after the first catalytic run.

In the third part of the Thesis, sub and supercritical CO₂ conditions were used to improve the catalytic activity of the above synthesized PdNPs. Supercritical CO₂ was also used for the extraction of organic products by using a SEPARAX SF200 pilot. CO₂ is known to increase the efficiency of hydrogenation by increasing the solubility of hydrogen in the colloidal system. In other words, hydrogenation reactions are often limited due to the low solubility of molecular hydrogen in the solvents currently used. Application of sub and supercritical CO₂ conditions during the hydrogenation can serve as a promotor for transporting hydrogen into the liquid phase and thus to enhance the equilibrium concentrations of both reactants and products in the gaseous phase. For this purpose, the catalytic hydrogenation of nitrobenzene and 4-phenylbutan-2-one was studied. In the case of 4-phenylbutan-2-one, remarkable results were

Summary, Conclusions and Perspectives

obtained. In the absence of CO₂, the conversion of 4-phenylbutan-2-one into 4-phenylbutanol was 40% (40 bar H₂, 80 °C, 18 h, 1 mol% Pd). When CO₂ was used the same conversion was reached by using 4 times less H₂ (10 bar H₂, 30 bar CO₂, 80 °C, 18 h, 1 mol% Pd) at the same total pressure. These results clearly showed that CO₂ increases the availability of H₂ in the catalytic system.

Extraction of the obtained organic products after catalysis from the catalytic solution was also performed using scCO₂. The extraction conditions were optimized to achieve up to 90% extraction of organic products. It is also important to highlight that during the extraction process, neither glycerol nor ChTs-ala was extracted with the product. Additionally, scCO₂ did not lead to the aggregation of the PdNPs in the system (checked by TEM), remaining well dispersed in the glycerol phase. In addition, no traces of Pd nor the ionic liquid or glycerol were detected in the extracted products. This behavior leads us to conclude that scCO₂ can wisely be used for the extraction of selected organic products after a catalytic reaction, eliminating the use of volatile organic solvents and preserving the state of the catalyst.

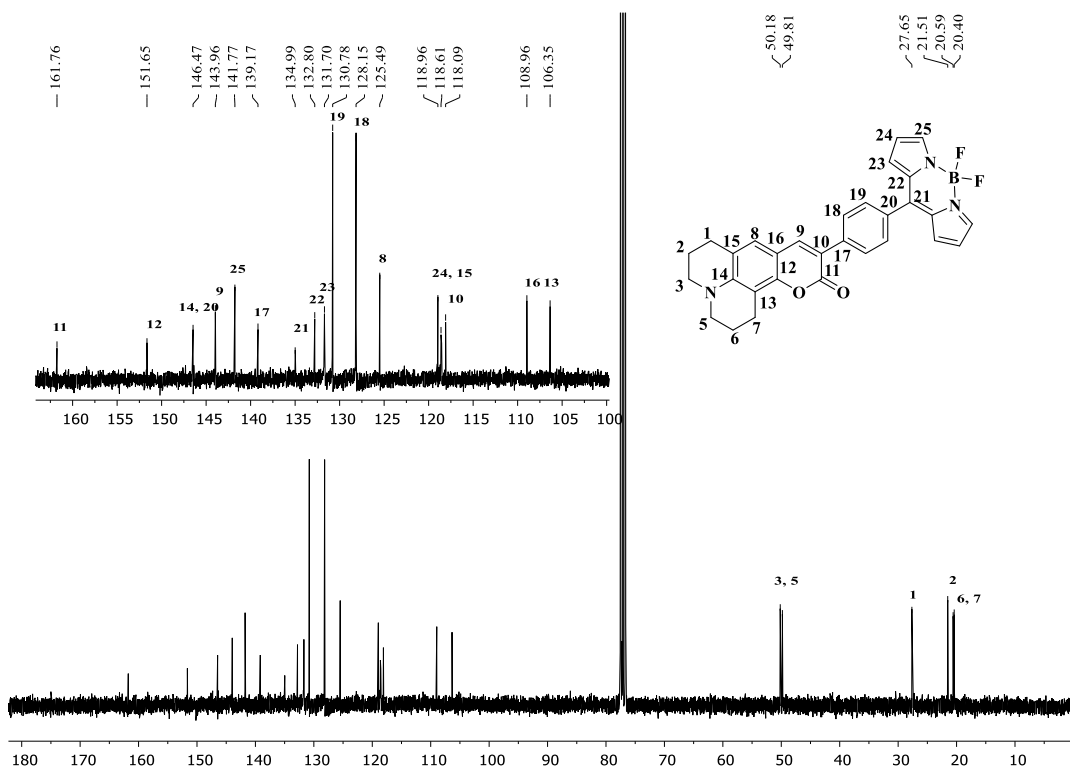
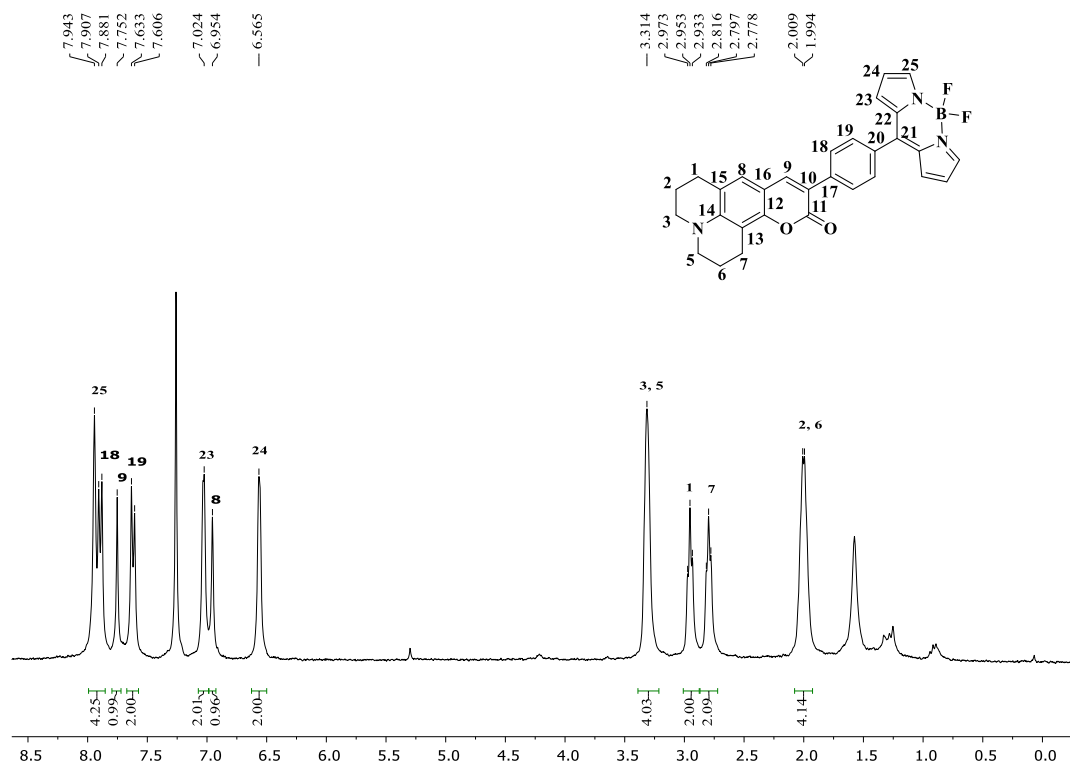
Some perspectives can be proposed from this work, as following indicated:

- Deep studies on physicochemical properties (such as density, polarity etc.) can be explored for DES and CO₂ systems, permitting a better knowledge of the medium and in consequence better conceive the synthesis of catalysts and their applications.
- Other physicochemical properties such as density, polarity etc. could be explored for the DES and CO₂ system with the aim of better characterize these media.
- Other molecular rotors can be synthesized and used as microviscosity probes, which would allow responding the main question arising from the use of this method: how bulk viscosity can be related to microviscosity?
- Taking advantage of the wide range of amino acids, different kind of choline based DES can be synthesized and explored for both solvent engineering and synthesis of metal nanoparticles. Applications in enantioselective hydrogenations can be envisaged, upon to fix the racemization of amino acids during their protection.
- The choline tosylalaninate/glycerol system can also be used in the synthesis of different kinds of metal-based nanoparticles, including those from earth-abundant metals (Cu, Ni, Fe, Co) and metal oxide and bimetallic nanoparticles. Once

Summary, Conclusions and Perspectives

synthesized the catalytic activity of these metal nanoparticles can be explored in the absence and presence of carbon dioxide.

Part 1: NMR characterization for MR1



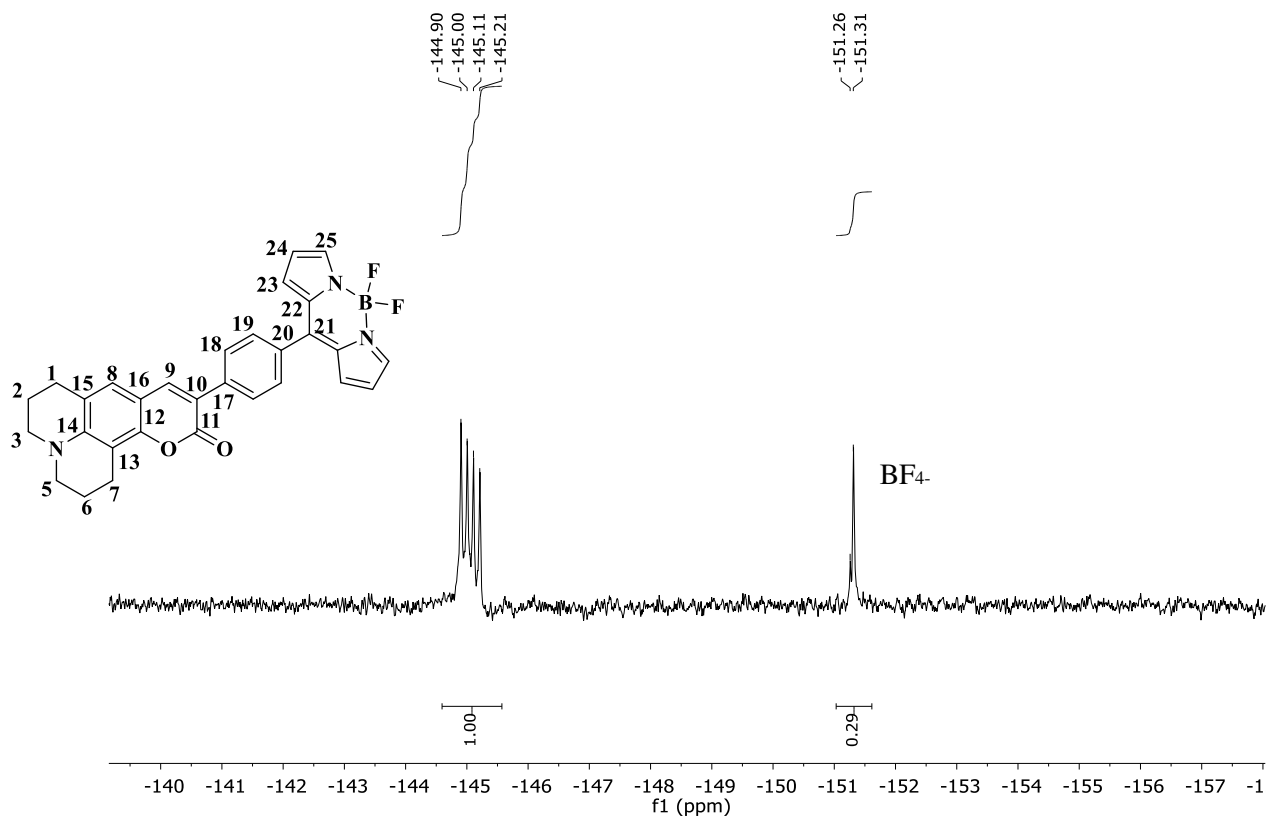


Figure A1.3. ^{19}F NMR spectrum of MR1 at 282 MHz in CDCl_3 .

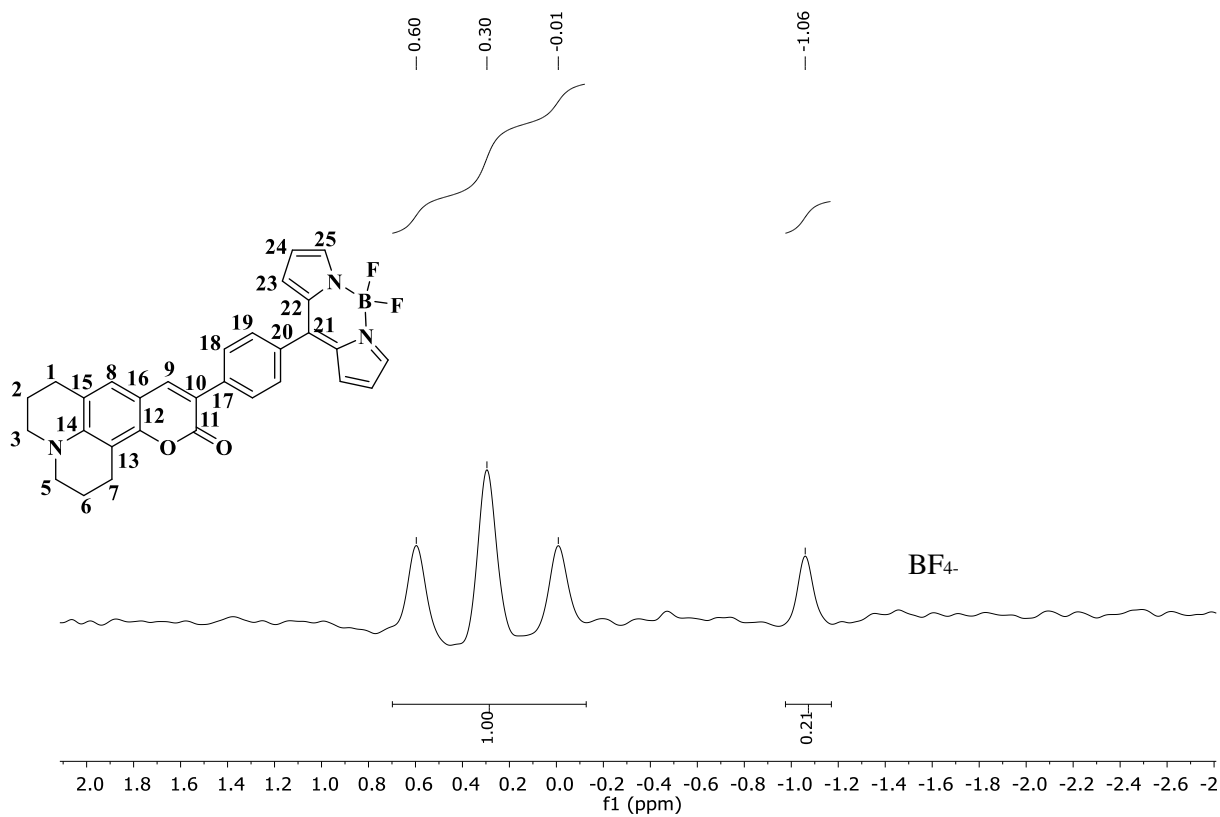


Figure A1.4. ^{11}B NMR spectrum of MR1 at 96 MHz in CDCl_3 .

Part 2: NMR characterization for MR2

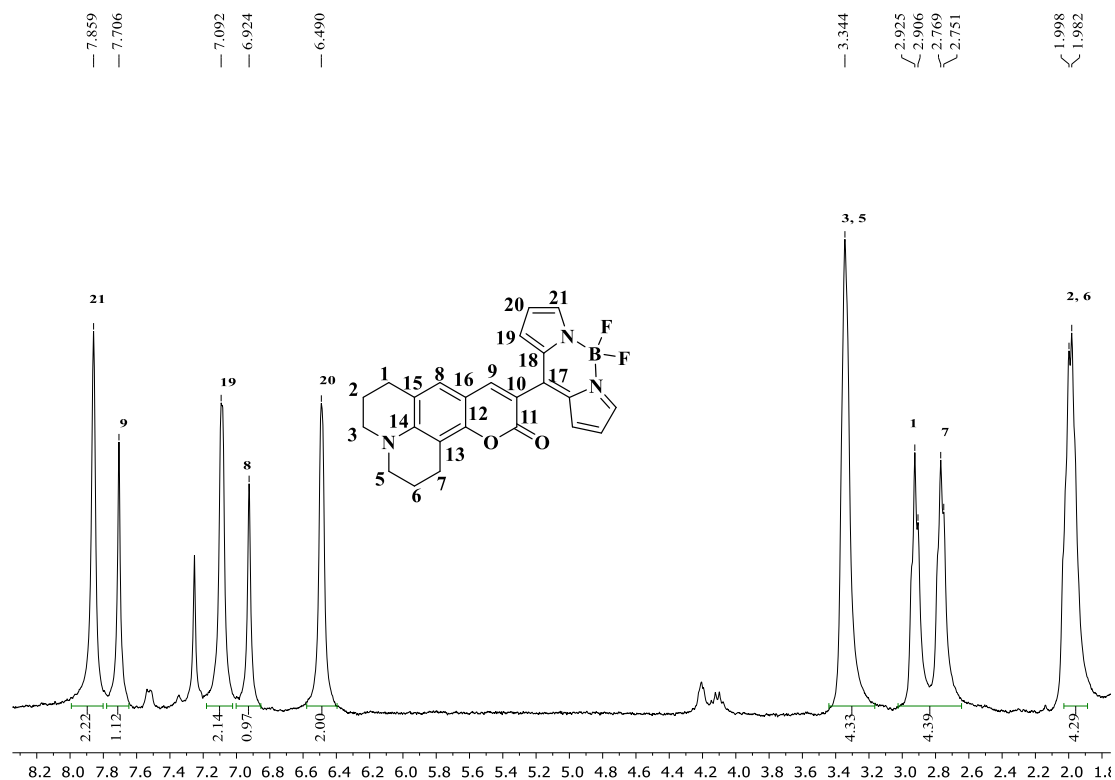


Figure A1.5. ^1H NMR spectrum of MR2 at 300 MHz in CDCl_3 .

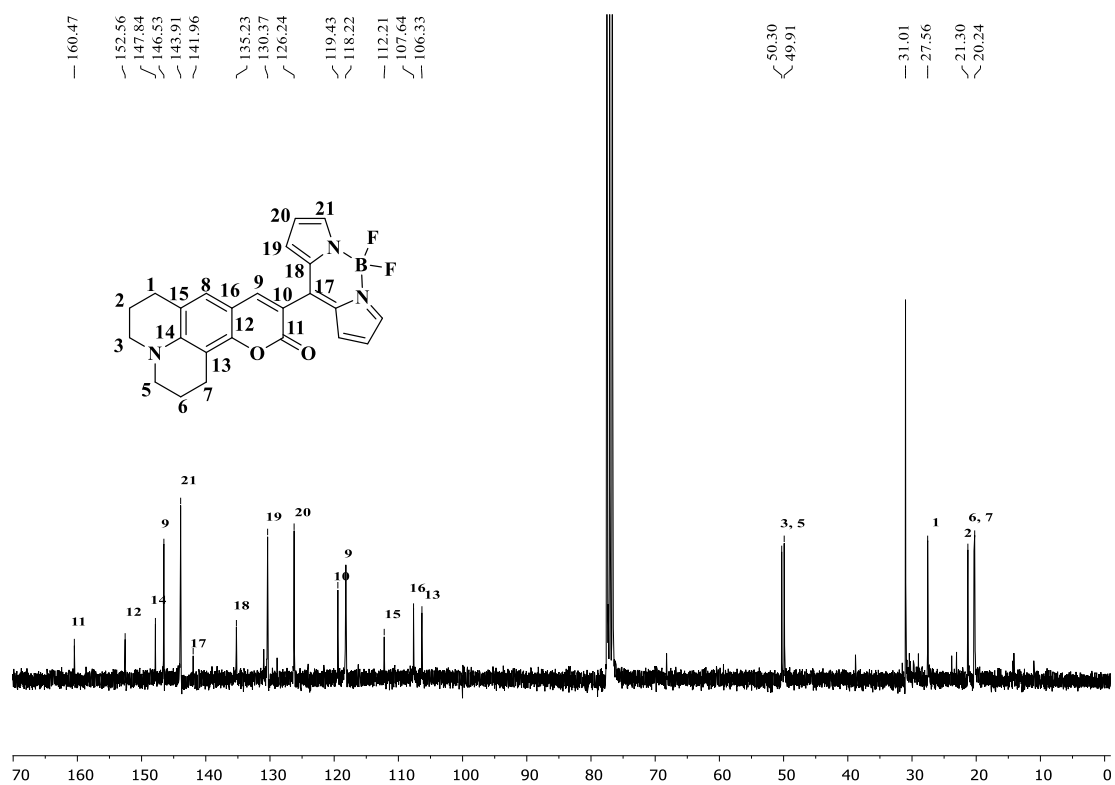


Figure A1.6. ^{13}C NMR spectrum of MR2 at 75 MHz in CDCl_3 .

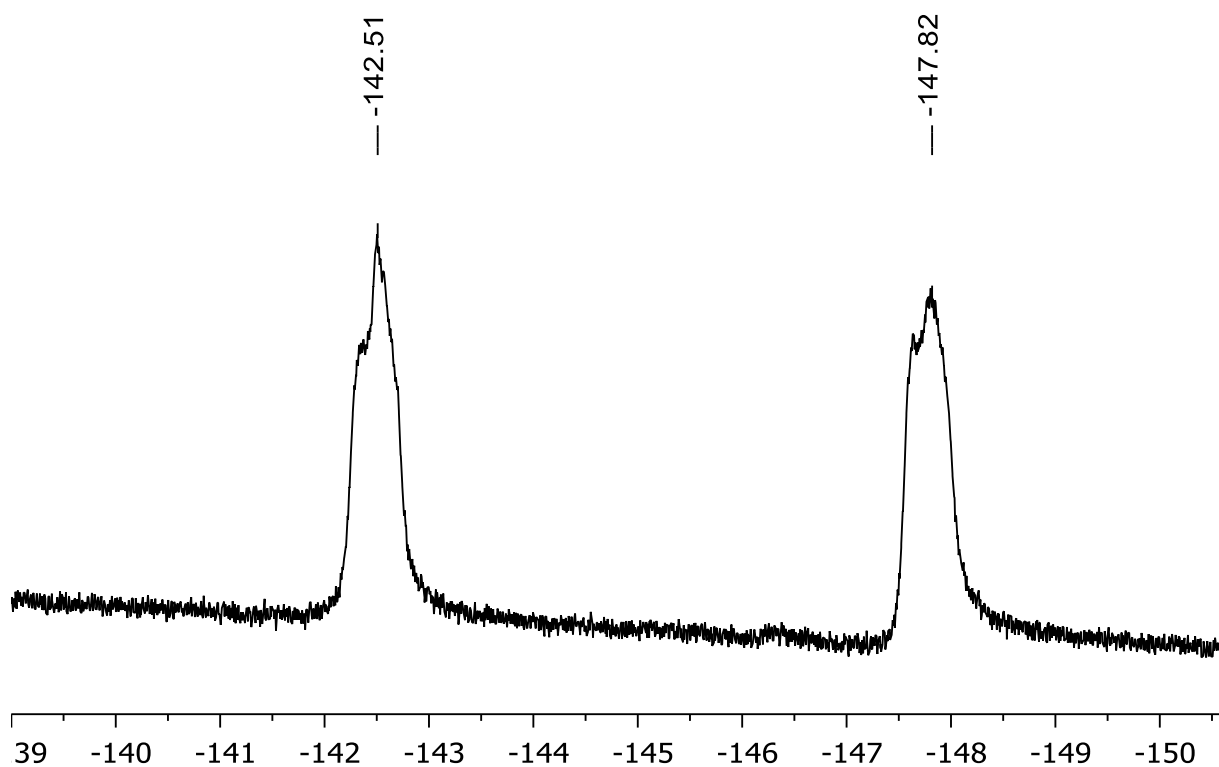


Figure A1.7. ^{19}F NMR spectrum of **MR2** at 282.4 MHz in CDCl_3 .

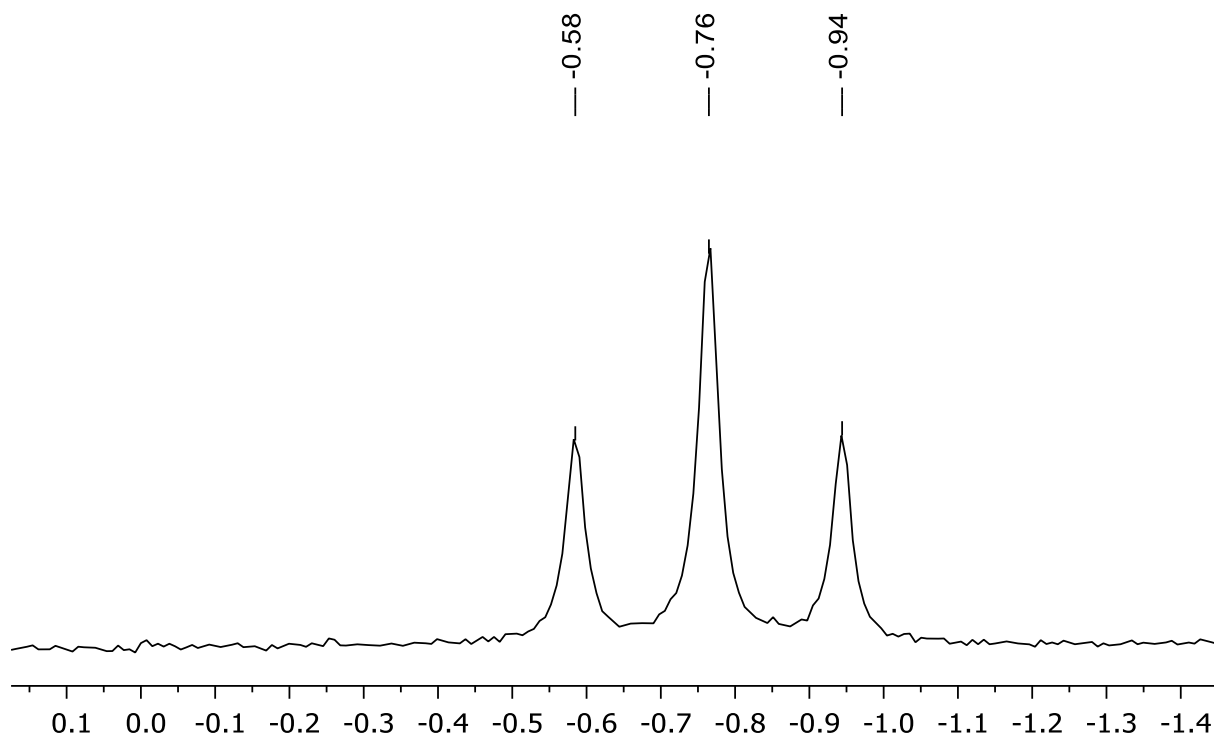
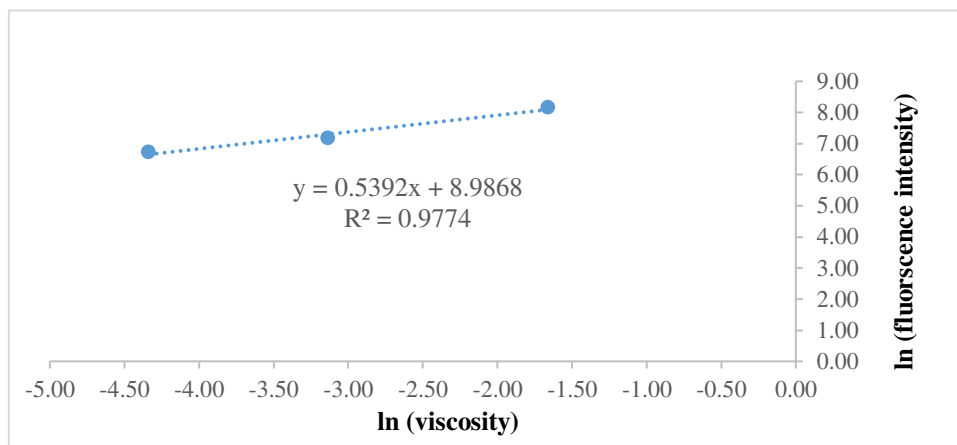
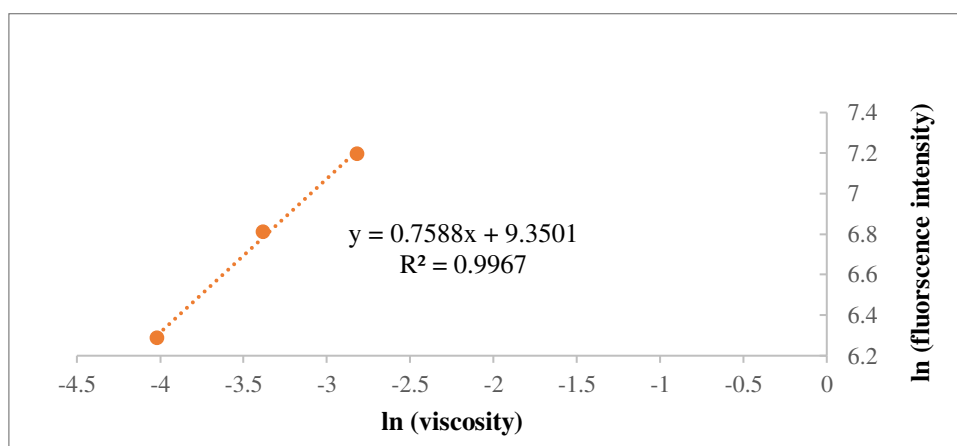
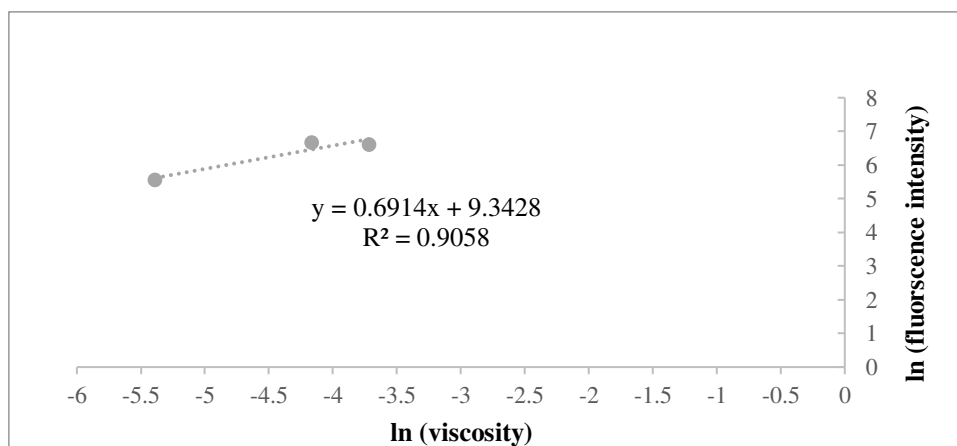


Figure A1.8. ^{11}B NMR spectrum of **MR2** at 160.4 MHz in CDCl_3 .

Part 1: Calibration curve of 9-(2,2-Dicyanovinyl)julolidine (DCVJ)**Figure A1.1.** Calibration curve of DCVJ at 40 °C**Figure A1.2.** Calibration curve of DCVJ at 60 °C**Figure A1.3.** Calibration curve of DCVJ at 80 °C

Part 2: Calibration curve of MR1

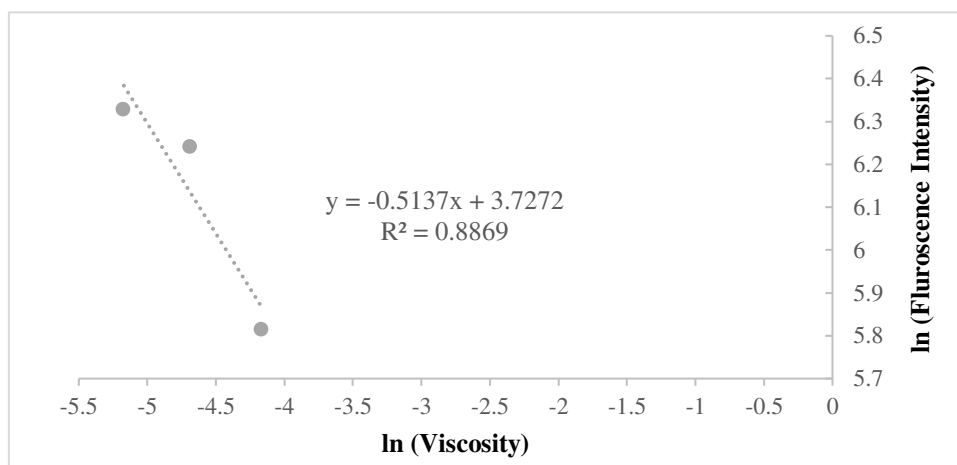


Figure A1.4. Calibration curve of MR1 at 80 °C

Here, it is observed that the calibration curve of the rotor **MR1** decreases with viscosity. The reason for this behavior is still uninvestigated.

Part 3: Calibration curve of MR2

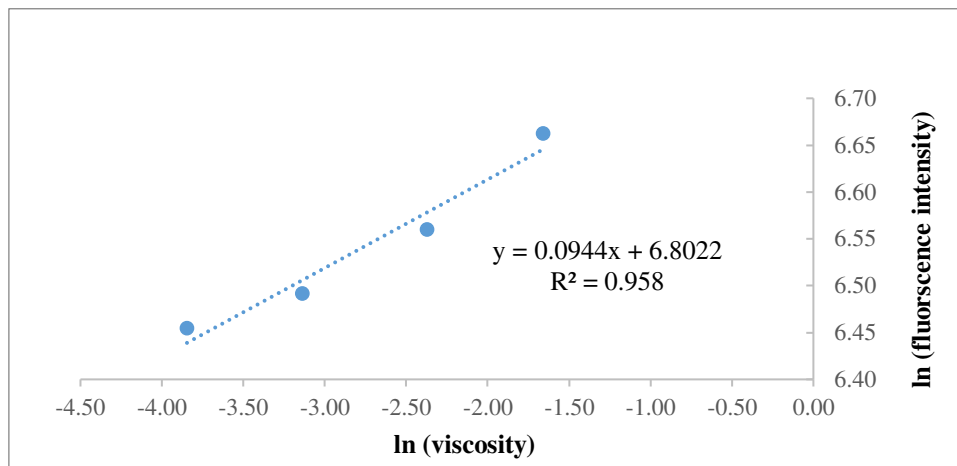


Figure A1.5. Calibration curve of MR2 at 40 °C

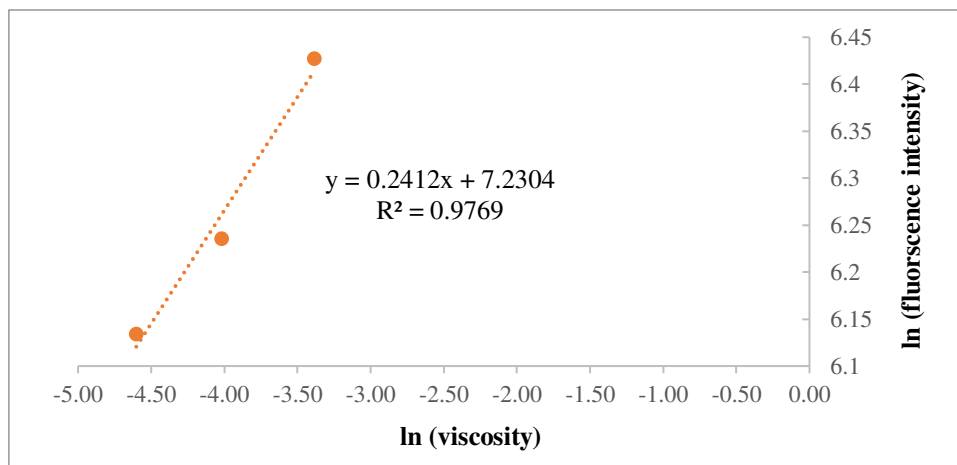


Figure A1.6. Calibration curve of MR2 at 60 °C

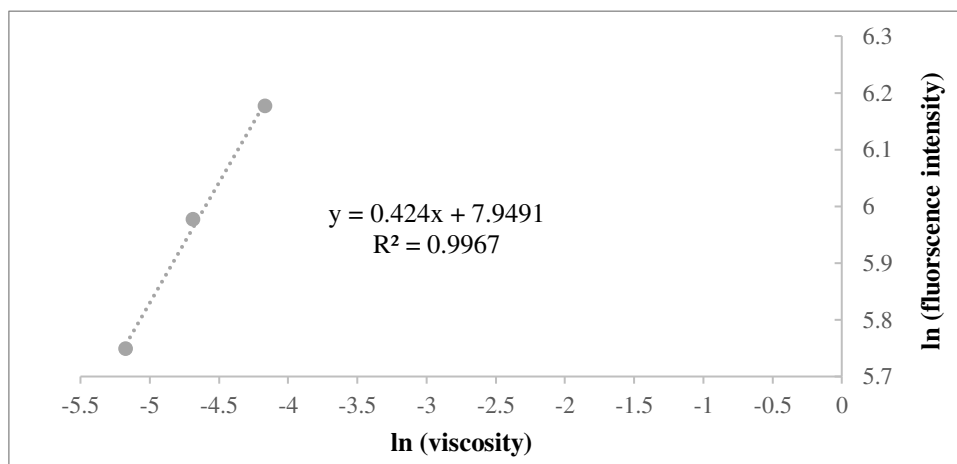


Figure A1.7. Calibration curve of MR2 at 80 °C

Bio-sourced ionic solvents and supercritical CO₂: design of sustainable processes for the synthesis of target molecules

Garima GARG, October 21st 2019, Toulouse

Supervisors: Yaocihuatl MEDINA-GONZALEZ and Montserrat GÓMEZ

This Thesis represents a multi-disciplinary project where aspects going from solvent engineering to catalysis using metal-based nanoparticles, are explored. In this project, solvent engineering has been applied to bio-based deep eutectic solvents (DES) synthesized from choline tosylalaninate and glycerol in an effort to decrease the solvent viscosity by using different amounts of carbon dioxide. In this context, molecular rotors were used as an innovative method to measure the viscosity, avoiding the use of expensive instrumentation and giving the possibility to access to the microviscosity of the system. Furthermore, DES have been applied for the synthesis of palladium nanoparticles, also acting as stabilizers, which were fully characterized. The as-prepared palladium nanoparticles were then used for catalytic hydrogenations of unsaturated C-C bonds, and nitro and carbonyl groups. Sub and supercritical CO₂ conditions have been applied to improve the efficiency of the palladium nanocatalysts in hydrogenation reactions and afterwards for the extraction of organic products. This work represents an effort to intensify a hydrogenation process in a highly viscous, non-volatile, biodegradable, and non-toxic DES by using CO₂ in order to decrease mass transfer limitations and to extract products from the reaction media.

Keywords: Biodegradable Ionic Solvents, Supercritical CO₂, Solvent Engineering, Catalysis, Metal Nanoparticles

Solvants ioniques biosourcés et CO₂ supercritique : conception des processus durable pour la synthèse de molécules cibles

Garima GARG, le 21^{er} octobre 2019 à Toulouse

Supervisors: Yaocihuatl MEDINA-GONZALEZ and Montserrat GÓMEZ

Cette thèse représente un projet multidisciplinaire qui explore des aspects allant de l'ingénierie des solvants à la catalyse à l'aide de nanoparticules métalliques. Dans le cadre de ce projet, l'ingénierie des solvants a été appliquée à des solvants eutectiques profonds (SEP) biosourcés synthétisés à partir de tosylalaninate de choline et de glycérol afin de diminuer leur viscosité en utilisant différentes quantités de dioxyde de carbone. Les rotors moléculaires ont été utilisés comme méthode innovante pour mesurer la viscosité, évitant ainsi l'utilisation d'une instrumentation coûteuse et donnant accès à la microviscosité du système. De plus, ce système a été appliqué à la synthèse de nanoparticules de palladium, jouant également un rôle de stabilisants, qui ont été entièrement caractérisées. Les nanoparticules de palladium bien dispersées ont été ensuite utilisées pour l'hydrogénation catalytique de liaisons C-C insaturées, de groupes nitro et carbonyle. Le CO₂ dans ses états sub- ou supercritique a été utilisé pour améliorer l'efficacité des nanoparticules de palladium dans les réactions d'hydrogénation catalytique et subséquentement pour l'extraction du produit après la réaction de catalyse. Ce travail représente un effort pour intensifier un procédé de déhydrogénation dans un milieu très visqueux, non volatil, biodégradable, biosourcé et non-toxique en utilisant du CO₂ 1) pour améliorer le transfert de matière et 2) pour extraire les produits de la réaction du milieu réactionnel.

Keywords: Solvants ioniques biodégradables, CO₂ supercritique, Ingénierie des solvants, Catalyse, Nanoparticules métalliques